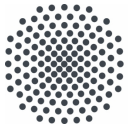

Universität Stuttgart

Renewable District Energy Systems with Formic Acid based Hydrogen Storage

Von der Fakultät Chemie der Universität Stuttgart zur Erlangung der Würde eines Doktors der Naturwissenschaften (Dr. rer. nat.) genehmigte Abhandlung

Vorgelegt von

Dipl.-Ing. Daniel Lust

aus Bietigheim-Bissingen

Hauptberichterin:	Prof. Dr. Ursula Eicker
Mitberichter:	Prof. Dr. Elias Klemm

Tag der mündlichen Prüfung: 28.07.2022

Hochschule für Technik Stuttgart
Zentrum für nachhaltige Energietechnik - zafh.net
In Kooperation mit
Institut für Technische Chemie, Universität Stuttgart

2022

Erklärung über die Eigenständigkeit der Dissertation

Hiermit erkläre ich, dass ich die vorliegende Arbeit mit dem Titel

Renewable District Energty Systems with Fomic Acid based Hydrogen Storage

selbstständig verfasst und keine anderen als die angegebenen Quellen und Hilfsmittel benutzt habe. Sämtliche Ausführungen, die anderen Schriften wörtlich oder sinngemäß entnommen wurden, sind als solche kenntlich gemacht.

Declaration of Authorship

I hereby declare that the present dissertation entitled

Renewable District Energty Systems with Fomic Acid based Hydrogen Storage

is entirely my own work expect where otherwise indicated. All statements taken verbatim or in spirit from other writings are identified as such.

Name: Daniel Lust

Singed:

Place, Date:

Acknowledgements

Writing a dissertation would not be possible without the help and continuous support of many people.
First of all, I would like to thank Prof. Dr. Bernd Plietker and Prof. Dr. Ursula Eicker for given me the opportunity to write this thesis. Further I would like to thank Prof. Eicker for her support throughout the years, either from Stuttgart or from Montreal, for always being helpful and for giving advice that really can change a stuck mind.
Furthermore, I would like to thank Prof. Dr. Elias Klemm for taking over the supervision of this work at half time, for introducing me to his research group and for supporting my research proposal based on this work.
I would also like to thank Prof. Dr. Jan Cremers for giving me the opportunity to start working and researching at HFT Stuttgart. Without this entry, I probably would never have met all the people which made this thesis possible.
Everyone working in a research environment could agree, that the funding of the work place could be a struggle at some times. Therefore, I would like to thank Dirk Pietruschka, Dietrich Schneider and Maximilian Haag from HFT Stuttgart for their never-ending support to get my job funded. I am not sure if this work would have been finished without their efforts.
In my opinion, having colleagues for professional exchange, heated discussions and mental support is essential for any success as well as for finding joy at work. In this case, I am very happy that Paul Rößner, Marcus Brennenstuhl, David Offtermatt, Hannes Marx and Tobias Erhart accompanied me throughout the process of writing this thesis.
This work would have never been possible without the help of my family. I would like to thank my parents, sister and brother-in-law for their support during my studies. My children Eric and Carla inspired me to finally finish this work. I sincerely hope that I know will have more free time to spend with them. The Lego "doctoral thesis writing robot", build by my son, may have helped too.
Finally, to my wife Anke: without your unconditional love, infinite understanding and inspiring calmness nothing would make sense.

Funding

This work is part of the joint graduate research training group 'Windy Cities' which was funded by the Ministry of Science, Research and Arts of Baden-Württemberg.

Contents

Nomenclature

Abbreviations

AEC	Alkaline Electrolysis Cell
CAPEX	Capital Expenditure
CCS	Carbon Capture and Storage
CCU	Carbon Capture and Utilization
CHP	Combined Heat and Power
DAC	Direct Air Capture
DACCU	Direct Air Carbon Capture and Utilization
DFAFC	Direct Formic Acid Fuel Cell
DFFC	Direct Formate Fuel Cell
DLFC	Direct Liquid Fuel Cell
DMFC	Direct Methanol Fuel Cell
EU	European Union
FC	Fuel Cell
FCV	Fuel Cell Vehicle
GDL	Gas Diffusion Layer
HER	Hydrogen Evolution Reaction
ICE	Internal Combustion Engine
INSEL	Integrated Simulation Environment Language

LOHC	Liquid Organic Hydrogen Carrier
MAPE	Mean Absolute Percentage Error
MEA	Membrane Electrode Assembly
MPL	Micro Porous Layer
OCV	Open Cell Voltage
OER	Oxygen Evolution Reaction
P2G	Power-to-Gas
P2H	Power-to-Heat
P2X	Power-to-X
PE	Polyethylene
PEMEC	Polymer Electrolyte Membrane Electrolysis Cell
PV	Photovoltaic
R&D	Research and Development
RES	Renewable Energy Sources
RWGSR	Reverse-Water-Gas-Shift-Reaction
SHE	Standard Hydrogen Electrode
SOC	State of Charge
SOEC	Solid Oxide Electrolysis Cell
V2G	Vehicle-to-Grid
WGSR	Water-Gas-Shift-Reaction

Physics Constants

F	Faraday constant	$96.485\,\mathrm{C\,mol^{-1}}$
R	Universal gas constant	$8.31\,\mathrm{J\,K^{-1}\,mol^{-1}}$
R_{s,CO_2}	Specific Gas Constant of Carbon Dioxide	$188.9\,\mathrm{J\,K^{-1}\,kg^{-1}}$

R_{s,H_2}	Specific Gas Constant of Hydrogen	4124.2 J K^{-1} kg^{-1}

Other Symbols

$[A]$	Concentration of species A	mol L^{-1}
α	Charge transfer coefficient	-
δ_m	Membrane thickness	m
$\dot{m}$	Mass flow rate	kg s^{-1}
$\dot{Q}$	Heat	J
η	Efficiency	-
λ	Membrane hydration factor	-
ν	Stoichiometric factor	-
∂z	Length element	m
Φ_{cat}	Volumetric catalyst fraction	-
ρ	Density	kg m^{-1}
σ_m	Membrane conductivity	-
A	Arrhenius constant, cross section	s^{-1}
C	Heat capacity	J
c	Concentration	mol L^{-1}
c_p	Specific heat capacity at constant pressure	J kg^{-1} K^{-1}
E_a	Activation energy	kJ mol^{-1}
E_{OCV}	Open cell voltage	V
E_{th}	Thermo-neutral voltage	V
G	Gibbs energy	J
H	Enthalpy	J mol^{-1}
I	Current	A

i	Current density	$\mathrm{A\,cm^{-2}}$
i_0	Exchange current density	$\mathrm{A\,cm^{-2}}$
i_L	Limit current density	$\mathrm{A\,cm^{-2}}$
k	Reaction rate slope	$\mathrm{s^{-1}}$
K_s	Acid dissociation constant	-
L	Length	m
M	Molar mass	$\mathrm{g\,mol^{-1}}$
m	Mass	kg
N	Number of elements	-
P	Power	W
p	Pressure	bar
Q	Nernst-Equation coefficient	-
R	Ohmic resistance	Ω
r	Reaction rate	$\mathrm{mol\,s^{-1}}$
S	Entropy	$\mathrm{J\,K^{-1}}$
T	Temperature	K
t	Time	s
u	Flow velocity	$\mathrm{m\,s^{-1}}$
V	Voltage, volume	V
W	Work (mechanical)	J
w	Specific work	$\mathrm{J\,kg^{-1}}$
Z	Compressibility factor	-
z	Number of transferred electrons	-

Kurzfassung

In zukünftigen Energiesystemen mit einem hohen Anteil fluktuierender Energieerzeugung durch Windkraft und Photovoltaik, wird Wasserstoff aus einer Elektrolyse eine zunehmend wichtige Rolle einnehmen. Die lokale Speicherung und der Transport von Wasserstoff sind jedoch technologisch herausfordernd. Eine vielversprechende Möglichkeit zur Wasserstoffspeicherung ist das Laden und Entladen eines Trägermoleküls, was oftmals eine drucklose Speicherung und die Verwendung bestehender Transportinfrastruktur erlaubt. Ameisensäure enthält 4.4 Gew.-% Wasserstoff, ist unter Umgebungsbedingungen flüssig und damit ein potentiell geeignetes Wasserstoffträgermolekül. Die zugrunde liegende Forschungsfrage dieser Arbeit ist, ob und unter welchen Voraussetzungen ameisensäurebasierte Wasserstoffspeicher für eine Anwendung als saisonaler Energiespeicher im Gebäudesektor geeignet sind.
Ein Ziel dieser Arbeit ist die Modellierung ameisensäurebasierter Wasserstoffspeichersysteme. Es werden drei Systeme beschrieben mit jeweils den folgenden Hauptkomponenten: eine reversible Wasserstoffbatterie, Flussreaktoren für die Hin- und Rückreaktion von Wasserstoff zu Ameisensäure und ein CO_2-Elektrolyseur für die direkte elektrochemische Reduktion von gasförmigem CO_2 mit Wasser zu Ameisensäure. Die entwickelten Modelle wurden mit experimentellen Daten oder Literaturwerten validiert. Weiterhin werden Verfahren zur Dimensionierung dieser Systeme, zur Betriebsführung und zur Integration in bestehende Energiesysteme gezeigt. In einer Fallstudie werden verschiedene Leistungsparameter der drei Systeme, wie Wirkungsgrad, Platzbedarf und Systemkomplexität, bewertet und einem Referenzsystem gegenübergestellt.
Es hat sich gezeigt, dass eine übertragbare, regelbasierte Dimensionierung der Systeme aufgrund der hohen Systemkomplexität unzureichend ist. Optimierungsverfahren, z.B. mit genetischen Algorithmen, könnten zu besseren Ergebnissen führen, setzen jedoch das Vorhandensein von Systemmodellen voraus. Die Fallstudie für ein Gebäudecluster hat ergeben, dass der CO_2-Elektrolyseur insgesamt das am besten geeignete System für eine Anwendung als Energiespeicher ist. Die Zugänglichkeit flüssiger Ameisensäure ernöglicht einen einfachen Energietransport und die Reaktion läuft unter moderaten Bedingungen ab. Der CO_2-Elektrolyseur wurde daraufhin detaillierter betrachtet und wesentliche Parameter für die Fallstudie optimiert. Durch hohe Überspannungen der Elektrolysezellen weist der CO_2-Elektrolyseur jedoch einen geringen Gesamtwirkungsgrad auf, wodurch in der betrachteten Fallstudie kein wirtschaftlicher Betrieb möglich ist. Auch die Erhöhung der Eingangsleistung durch die Hinzunahme von Kleinwindkraftanlagen hat nur einen geringen Einfluss auf die Gesamtperformance des Systems. Weiterer Forschungsbedarf zur hardwareseitigen Verbesserung des CO_2-Elektrolyseurs und zur Steuerung und Betriebsführung mit fluktuierender elektrischer Last ist demnach notwendig um den Wirkungsgrad zu erhöhen und einen wirtschaftlichen Einsatz des Systems als saisonaler Energiespeicher zu ermöglichen.

Abstract

In future energy systems with a high proportion of fluctuating energy generation from wind power and photovoltaics, hydrogen from electrolysis will play an increasingly important role. However, local storage and transport of hydrogen are technologically challenging. One promising option for hydrogen storage is charging and discharging a carrier molecule, which often allows pressureless storage and the use of existing transportation infrastructure. Formic acid contains 4.4 wt-% hydrogen and is liquid under ambient conditions, making it a potentially suitable hydrogen carrier molecule. The underlying research question of this work is whether and under what conditions formic acid-based hydrogen storage systems are suitable for application as seasonal energy storage in the building sector..

One objective of this work is to model formic acid-based hydrogen storage systems. Three systems are described, each with the following main components: a reversible hydrogen battery, flow reactors for the back-and-forth reaction of hydrogen to formic acid, and a CO_2 electrolyzer for the direct electrochemical reduction of gaseous CO_2 with water to formic acid. The developed models were validated with experimental data or literature values. Furthermore, procedures for sizing these systems, operation management and integration into existing energy systems are shown. In a case study, various performance parameters of the three systems, such as efficiency, space requirements and system complexity, are evaluated and compared to a reference system.

It has been shown that a transferable, rule-based dimensioning of the systems is insufficient due to the high system complexity. Optimization methods, e.g. with genetic algorithms, could lead to better results, but require the existence of system models. The case study for a building cluster showed that the CO_2 electrolyzer is overall the most suitable system for an energy storage application. The accessibility of liquid formic acid allows for easy energy transport and the reaction occurs under moderate conditions. The CO_2 electrolyzer was then considered in more detail and key parameters were optimized for the case study. However, due to high overvoltages of the electrolysis cells, the CO_2-electrolyzer has a low overall efficiency, which does not allow economical operation in the considered case study. Also, increasing the input power by adding small wind turbines has only a minor impact on the overall performance of the system. Further research is therefore needed to improve the hardware of the CO_2-electrolyzer and to control and operate it with a fluctuating electrical load in order to increase the efficiency and enable the system to be used economically as a seasonal energy storage system.

Chapter 1

Introduction

In this chapter the motivation for this thesis, along with related work different aspects for this thesis is presented. Furthermore, the research objectives, the methodology and the limits of this work are shown. The chapter closes with a description of the thesis' structure.

1.1 Motivation

The post-fossil era has began. In order to reach the climate goals of the Paris agreement to keep the global warming below 2°C, or preferably limit it to 1.5°C, the most extensive societal transformation since the industrial revolution is necessary. The combustion of fossil fuels must soon come to an end, which affects all sectors, including the production of electrical power. In 2020 Germany reached a renewable power production (mostly wind, photovoltaic (PV) and hydropower) of overall 45.3% [1]. In the next decades it is envisaged to increase the share of renewable energy sources (RES) to 65% in 2030 and finally to 100% in 2045 [2]. To match the overall annual energy demand in an energy system with fluctuating energy production, the installed power must be oversized. Although a large share of the overproduction could be compensated by the electrification of other sectors like mobility and heating and the following flexibility options like Vehicle-To-Grid (V2G) or Power-to-Heat (P2H), there will be an increased demand for seasonal electrical storage capacities. It is assumed that over the threshold of 80% renewable energy production, a massive use of storage technologies is necessary [3] to avoid grid damage in times of overproduction and to ensure supply safety in time of underproduction[1]. Figure 1.1 shows the key technical requirements for stationary energy storage systems. Besides the technical side, of course also economic factors must be be considered. If more and more energy sectors become electrified, there is an increasing need for an energy carrier, which could be better stored and transported

[1] A particularly feared period of underproduction is called 'Dunkelflaute' in German, meaning that no wind blows and no sun shines

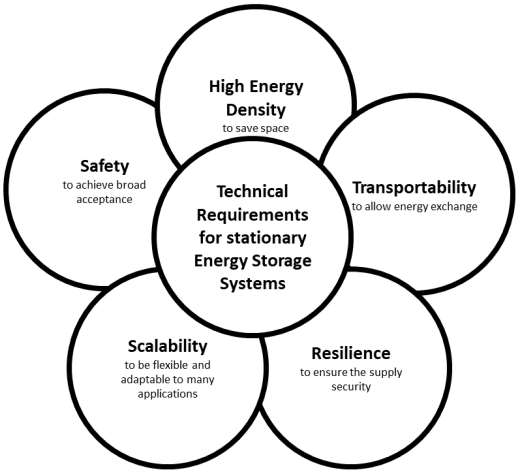

Figure 1.1: Technical requirements for energy storage systems

than electrons and which can be utilized in several sectors. Therefor, hydrogen will play a major role in fossil free energy systems, as it is a versatile energy carrier, which could be used to couple a broad range of sectors like industry, mobility and power. Besides the direct application in fuel cells or for combustion, hydrogen is an important raw product for the synthesis of synthetic natural gas (SNG) or large-chained hydrocarbons (e.g. kerosene) via Fischer-Tropsch-Synthesis. Consequently, most of the biggest economies in the world have released or are planning to release a hydrogen strategy. Japan was the first nation to publish a hydrogen strategy in 2017, followed by France (2018), South Korea and Australia (2019). In 2020 many more countries presented their hydrogen strategy, including Germany and the EU [4]. The hydrogen strategies differ from their alignment, as traditionally energy exporting nations (e.g. Australia) focus on the hydrogen production for the export, whereas energy importing countries (e.g. Japan, Germany) will increase their efforts in hydrogen utilization and diversifying the energy supply. However, a worldwide trade of hydrogen as an energy carrier requires efficient hydrogen transportation technologies, which is still an open field of research.

The intended role of hydrogen on the building and heating sector remains vague, as the direct electrification of heating systems (via heat pumps) is prioritized in most countries. Japan and South Korea explicitly name the building and heating sector a main target for their hydrogen goals. Other hydrogen strategies (including Germany and EU) initially assign a subordinate role to this sector. Hydrogen could be utilized in two different ways to generate heat: with fuel cells as a combined heat and power (CHP) plant or by the combustion in H2-ready gas boilers. If fuel cells are used a relevant amount of electrical power is generated, which could be used to power heat pumps during the winter season. Hydrogen in combination with fuel cell CHPs therefore can contribute to overcome the seasonal shift in

renewable power production with PV systems in summer and the largest power demand of heat pumps in winter. In a study commissioned by Viessmann Climate Solutions other possible advantages for the hydrogen utilization in this sector are mentioned. Among other things the need to supplement the direct electrification for buildings with a low level of energetic refurbishment (e.g. landmarked buildings) where heat pumps are inefficient is shown [5]. As for the worldwide transportation of hydrogen, also for its utilization in the building sector, the save, efficient and economical storage of hydrogen needs an acceleration of R&D efforts.

In order to reach sufficient energy densities for most applications hydrogen must not be stored under ambient conditions. In combination with its properties to built explosive atmospheres in air, its corrosivness for many material and the high diffusivity due to its small molecular size, hydrogen storage is a challenging task. On the other hand, for an application in the building sector, hydrogen storage should be safe, transportable and scalable. Technical possible options for hydrogen storage are widely discussed in literature. Four different storage options are relevant for stationary hydrogen storage:

- Large-scale storage in caverns
- Physical hydrogen storage: compression or liquefaction
- Metal hydrides
- Chemical storage in carrier molecules

All of the those options have specific disadvantages. Cavern storage relies on suitable geological conditions. Hydrogen liquefaction consumes about one third of the overall stored energy and must deal with boil-offs. Compressed hydrogen needs high-pressures with the resulting safety issues to achieve sufficient storage densities. Metal hydrides commonly have low gravimetric energy density and hence poor transportability. This work focuses on the on the fourth option: the hydrogenation and dehydrogenation of a carrier molecule. Figure 1.2 shows a simplified representation of this storage path.
Hydrogen produced via water electrolysis is used to hydrogenate a carrier molecule. This molecule could be stored and dehydrogenated on demand to release hydrogen. The released hydrogen could afterwards be used for energy conversion applications and the carrier molecule is free to be again hydrogenated.

Most of the promising hydrogen carriers discussed in literature are based on carbon compounds (except ammonia). For example Dibenzyltoluene, often referred to as 'liquid organic hydrogen carrier' (LOHC), is widely known as a possible hydrogen carrier molecule. Carbon with its property to being able to assume different oxidation states and its good availability

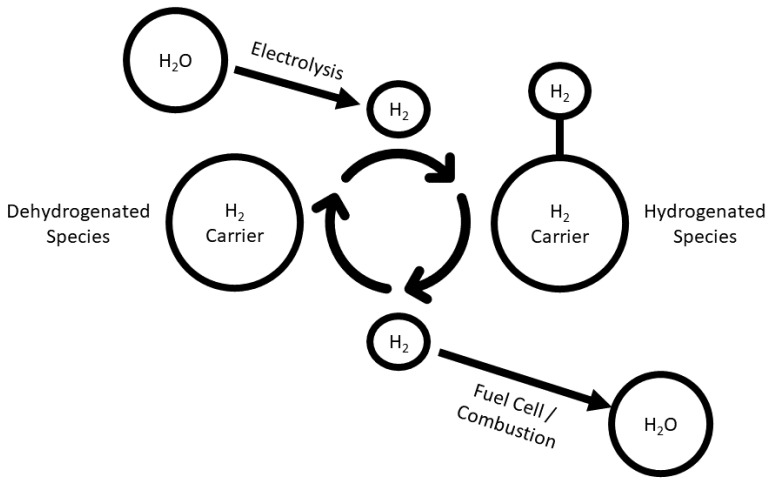

Figure 1.2: Simplified representation of hydrogen storage based on the hydrogenation and hydrogenation of a carrier molecule

as carbon dioxide makes it predestined for this application. In combination with technologies like direct air capture (DAC), which makes carbon dioxide available as a raw product directly from air, a closed carbon cycle is possible.

The first reduction step of the carbon atom in carbon dioxide decreases its oxidation state from +IV to +II. With two protons, formic acid (HCOOH) is created.

$$CO_2 + 2\,e^- + 2\,H^+ \longrightarrow HCOOH$$

With hydrogen as a proton source, this could be simplified as:

$$CO_2 + H_2 \rightleftharpoons HCOOH$$

Formic acid, or methanoic acid, is a non-toxic and non-flammable, carboxylic acid which is liquid under ambient conditions. It contains about 4.4 wt.-% of hydrogen. Besides the thermochemical reaction pathway, formic acid could also be produced via the direct electrolysis of carbon dioxide. These properties has brought formic acid in the focus of energy related research in recent years.

1.2 Related Work

In this section, the most important literature on which this work is based, is introduced.

Formic Acid as a hydrogen carrier molecule Willams, Crandall and Bloom suggested the electrochemical reduction of carbon dioxide to formic acid for energy storage purposes as early as 1978 [6]. Since then, formic acid was repeatedly discussed as a possible hydrogen storage molecule [7–9]. Also, the possibility of hydrogen storage as formate [10–12] or formic acid/formate blended solutions [13] are discussed in literature. A more general overview of hydrogen storage with formic acid among other methods is given by Dalebrook et al. [14] or Andersson & Grönkvist [15].

Thermochemical carbon dioxide reduction to formic acid The continuous production of formic acid from hydrogen and carbon dioxide in flow reactors in the absence of a base[2] is reported by Zhang et al. [16]. Weilhard et al. use buffering ionic liquids to avoid adding a base [17]. A two-step formic acid synthesis is described by Reymond et al. [18]. Reviews of catalysts for the carbon dioxide hydrogenation to formic aid are given by Sun et al. [19], Klankermayer et al. [20] and Alvarez et al. [21].

Catalytic carbon dioxide reduction to formic acid An important component for CO_2-electrolyzers are gas diffusion electrodes (GDE) to provide gaseous carbon dioxide at the electrolyzer cathode. The development and optimization of GDEs for the electrochemical reduction of carbon dioxide to formic acid is described by several research groups [22–25]. The design of a complete electrolyzer cell which is capable of operating at low pH values and thus produces formic acid rather than formate is published by [26–28]. To catalyze the cathode reaction, homogeneous or heterogeneous catalysts could be used. A profound review of molecular electrocatalysts for the conversion of CO_2 is given by Kinzel et al. [29]. Heterogeneous catalysts are e.g. evaluated by Lu et al. [30].

Formic Acid Dehydrogenation The formic acid decomposition to hydrogen and carbon dioxide with Pd catalysts is shown by [19, 31–33]. Hu et al. use a carbon supported Pt catalyst in a flow reactor for the dehydrogenation of formic acid [34]. The reactor design for this reaction with a heterogeneous Ru catalyst and a coupled PEM fuel cell is described by Yuranov et al. [35]. An evaluation of reported homogeneous catalyst for the formic acid decomposition is given by Guan et al. [36].

Modelling and Simulation The model of the CO_2-electrolyzer introduced in Chapter 5 is based on fundamentals which are also valid for modelling water electrolyzers. Models for PEM electrolyzers are described by [37–40]. A comprehensive description of PEM fuel cell modeling is given by Spiegel [41]. Fundamentals of reaction kinetics and chemical

[2] In the presence of a base formate rather than formic acid is produced

reactor modeling can also be found in literature (e.g. [42]). A model of a multi-phase non-isothermal flow reactor wit a fluidized bed is introduced by Orava et al. [43]. The simulation environment INSEL[3] in version 8 is used for modeling and simulating the formic acid bases hydrogen storage system. INSEL is an acronym for 'Integrated Simulation Environment Language'. It consists of a graphical model editor and the calculation sub-routines written in C++ or FORTRAN. The development of the INSEL environment was first described by Jürgen Schumacher [44].

Case Study A plus energy settlement located in the municipality of Wüstenrot ins southern Germany was chosen as a case study. For this district a profound data basis for buildings and energy systems is available, as several research projects already were executed with HFT Stuttgart and Wüstenrot as project partners (e.g. EnViSaGe[4], Sim4Blocks[5] or Smart2Charge[6]). The key parameters of the settlement, project results and relevant data are already published n several publications [45–48].

1.3 Research Objectives

This thesis aims at giving the reader a comprehensive overview of the utilization of formic acid as a hydrogen carrier molecule for energy storage applications in the building sector. It is intended to contribute to the transfer of this technology from lab scale to upscaled demonstration projects. The goal of this thesis is to develop models for formic acid based hydrogen storage systems and system integration concepts for derived energy systems in district scales. Therefor the following research objectives are addressed:

- Objective 1: How can the generation of formic acid from hydrogen and carbon dioxide or with direct CO_2-electrolysis be modeled? How can formic acid storage components be integrated into a larger energy system model with renewable energy sources, building loads and different energy conversion devices?

- Objective 2: How can these systems be dimensioned, controlled and integrated into existing energy systems?

- Objective 3: How can simplified models be used to evaluate the performance of these systems in an application scenario? How do formic acid based hydrogen storage systems perform, if applied to a building cluster with decentral heat pumps, PV systems and

[3] https://insel4d.ca/en/home_en.html
[4] http://www.envisage-wuestenrot.de/
[5] https://sim4blocks.eu/
[6] https://www.hft-stuttgart.de/forschung/projekte/aktuell/smart2charge

small wind turbines? Which system is most promising for an application in the building sector?

After a comprehensive literature review, the research objectives by modeling all relevant components and subsystems (e.g. controllers) as C++ code and combining them into system models. Therefor the simulation environment INSEL is used. All component models are validated against reported measurement data as far as possible. The INSEL simulation runs are combined with rule based dimensioning approaches via Python scripts to a contiguous workflow. Also, an automated dimensioning workflow using genetic algorithms is shown. For the evaluation of the system performance a combination of measured and simulated data for the energy systems (PV, small wind turbines) and energy demand (heating, household electricity) of ten existing buildings is used.

1.4 Structure of this Thesis

After the introduction (Chapter 1), useful theoretical knowledge is given in Chapter 2. Chapter 3 outlines existing technologies where the reduction of carbon dioxide to energy related products is already applied. This should help the reader to classify the later proposed systems in a larger context. Chapter 4 specifically treats the reduction of carbon dioxide to formic acid with two different production routes, the thermo-chemical formic acid production with reversible hydrogen batteries and flow reactors and the electrochemical formic acid production. Besides the description of usable catalysts, also possible reactor electrolysis cells designs are shown. The main part of this thesis begins with Chapter 5, where the development of all used component and system models is described. Where ever possible, the models are validated against literature data. In Chapter 6, four different systems for a formic acid based hydrogen storage system are introduced. Further, this chapter deals with system integration aspects, defines operation and control modes for the systems and introduces rules for the system dimensioning. Finally, the developed models are applied in a use case (Chapter 7). Simulation results of an simulated year, where all systems are applied to a building cluster, are evaluated and compared. Optimization steps, as well as economic aspects, are also carried out in Chapter 7. This work closes with a summary and suggestion for further research (Chapter 8).

Chapter 2

Theoretical Background

In this chapter, the necessary theoretical background for modelling formic acid based hydrogen storage systems is presented. First, the physical and chemical properties of all related substances, such as hydrogen, carbon dioxide and C1 substances are shown. Later on, the fundamentals of thermochemical and electrochemical carbon dioxide reduction are pointed out. This includes thermodynamcics, reaction kinetic considerations, the governing equations for ideal flow reactors and voltage-current-characteristics of electrochemical cells. This chapter closes with a consideration of formic acid decomposition to usable hydrogen.

2.1 Relevant Substances for Energy Storage related Carbon Dioxide Reduction

In this section different chemical elements and compounds are described which are relevant for Power-to-X (PtX) applications. Either as basic products like carbon dioxide, as intermediate substance (hydrogen) or final product (formic acid, methane)[1].

2.1.1 Hydrogen

Hydrogen is by far the most common element in the universe[2] An hydrogen atom consists of an proton and a surrounding electron. The hydrogen isotopes deuterium (^{2}H) and tritium (^{3}H) additionally contain one (^{2}H) or two (^{3}H) neutrons in their nucleus[3].

[1] Substances which are considered as generally available like water or by- products like oxygen are excluded

[2] Stars are formed out of hydrogen clouds when gravity reaches a critical point and nuclear fusion begins creating helium. First deuterium is formed from two hydrogen atoms, which is again reacting with hydrogen to ^{3}He. Two ^{3}He nucleons finally combine to ^{4}He.

[3] Several other hydrogen isotopes could be synthesized (up to ^{7}H), but are not stable and don't occur naturally

Under earth's environmental conditions hydrogen occurs in its molecular form, as gaseous H_2[4]. Table 2.1 shows some physical properties of hydrogen.

Table 2.1: Physical data of hydrogen

Melting Point	$-259\,°C$
Boiling Point	$-253\,°C$
Heat of Combustion	$-285.8\,kJ\,mol^{-1}$
Molecular Weight	$2.016\,g\,mol^{-1}$

Hydrogen's atomic appearance is important for several PtX processes as it is formed only from protons and electrons and is therefor often used as a proton source. Water electrolysis is based on the following reaction, called Hydrogen Evolution Reaction (HER):

$$2\,H^+ + 2\,e^- \longrightarrow H_2$$

The formation of hydrogen is also often an unwanted side-reaction. In electrochemistry this reaction is defined as the standard hydrogen electrode (SHE) with an assigned reduction potential of 0 V.

Hydrogen is used in many technical applications. Either as an direct energy carrier (fuel cells or combustion) or as an intermediate for further synthesis processes (e.g. methanation). Various applications where hydrogen is used for synthesis are discussed in Chapter 3.

2.1.1.1 Hydrogen Sources

Hydrogen could be provided by different sources, which is commonly represented by a color scheme (see Figure 2.1). Most important for technical applications are steam reforming with and without CCS, methane pyrolysis and water electrolysis with different power sources.

Steam Reforming Steam reforming is an important technical process to yield hydrogen. Natural gas reacts with steam to carbon monoxide and hydrogen over a nickel oxide catalyst.

$$CH_4(g) + H_2O(g) \rightleftharpoons CO(g) + 3\,H_2(g) \qquad \Delta H^{\ominus} = 206.2\,kJ\,mol^{-1}$$

The necessary reaction heat could be provided by partial oxidation of natural gas.

$$2\,CH_4(g) + O_2(g) \rightleftharpoons 2\,CO(g) + 4\,H_2(g) \qquad \Delta H^{\ominus} = -71\,kJ\,mol^{-1}$$

[4] Although most hydrogen on earth is bounded and very rare as pure gas

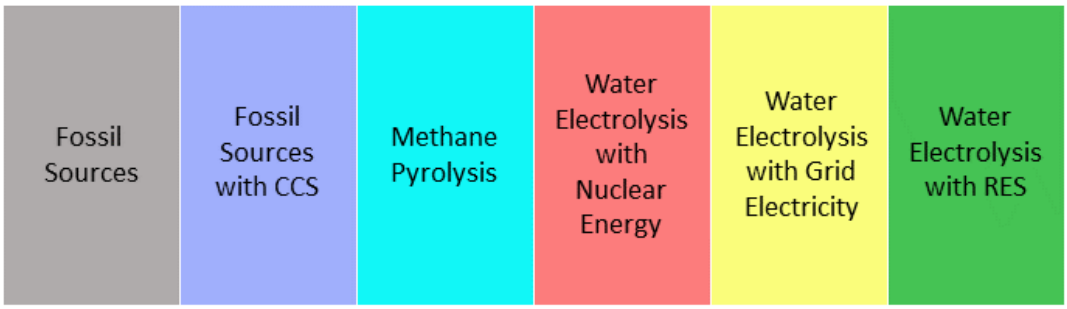

Figure 2.1: Hydrogen color scale

As steam reforming requires methane from fossil sources it is not a renewable way to produce hydrogen. Within the hydrogen color spectrum, hydrogen produced from steam reforming is labeled as 'grey hydrogen'. Blue hydrogen, on the other hand, means hydrogen from steam reforming with subsequent carbon capture and storage (CCS). Sometimes blue hydrogen is labeled as carbon neutral. However, Howarth and Jacobson [49] state, that the equivalent carbon emissions of blue hydrogen are even higher than those of the direct burning of natural gas, due to methane leakages and and the additional need for heat to run the steam reforming and carbon capture process. Steam reforming is also used in some commercially available home heating systems based on PEM fuel cells. This allows a direct operation of the fuel cell with natural gas from the gas grid.

Methane Pyrolysis Methane pyrolysis is a process where methane is splitted into its components carbon and hydrogen by thermal decomposition. It is not a sustainable process, as natural gas resources are needed, but no gaseous CO_2 is emitted to the atmosphere in this process. Hence it could be considered as a bridge technology towards green hydrogen (see Sánches-Bastardo et al [50]). Methane pyrolysis is reported with metal catalysts, like Ni, Co, Fe as well as carbon catalysts.

$$CH_4\,(g) \longrightarrow C(s) + 2\,H_2\,(g) \qquad \Delta H^{\ominus} = 37.7\,\mathrm{kJ\,mol^{-1}}$$

One major challenge is that high temperature of 700 to 900°C (for iron catalysts) and 800 to 1000°C (for carbon catalysts) are needed to run the process. The industrialization of the process is currently (as of 2021) under development [50]. Hydrogen from methane pyrolysis is generally labeled as turquoise hydrogen.

Water Electrolysis Water electrolysis means the splitting of water into its parts hydrogen and oxygen with electrical power in an electrolysis cell.

$$H_2O\,(l) \longrightarrow H_2\,(g) + \frac{1}{2}\,O_2\,(g) \qquad \Delta H^{\ominus} = 285.8\,\mathrm{kJ\,mol^{-1}}$$

It is a promising option for carbon neutral hydrogen generation, if driven by renewable energy sources. For more details on water electrolysis see Chapter 3. Hydrogen from water electrolysis is labeled as red (with nuclear energy), yellow (with grid energy) or green hydrogen (with renewable energy).

2.1.1.2 Safety aspects and material compatibility

In terms of hydrogen used for energy or mobile applications, safety aspects are always a concern. Hydrogen could react with oxygen when ignited (oxyhydrogen reaction). Under specific hydrogen concentration between 13.5 and 70 Vol-% in air, this reaction proceeds explosive [51]. For many people pictures of the Hindenburg disaster come to their minds, when confronted with Hydrogen for mobile applications. However most of the safety concerns could be controlled by state-of-the-art technology. Studies carried out for fuel cell vehicles (FCV) state, that FCV are safer than gasoline powered cars in accidents, even in tunnels. The greatest risks occur from hydrogen leakages within garages [51]. As hydrogen is odorless this issue could be handled by hydrogen sensors and automatic ventilation. For stationary high-pressure storage, the main risk is the bursting of the pressure vessel caused by heating (e.g. fire) or overfilling. These events could be prevented by using relief valves and thermal pressure relief devices (TPRD) which release the hydrogen in the vessel in case of overheating (melting fuse).

All materials with direct contact to hydrogen must be chosen carefully. This concerns for example pressure vessels but also sensors, gaskets or bolts. Atomic hydrogen tends to attack metallic materials at the boundaries of the metal structure. This effect is called hydrogen embrittlement and leads to cracks. High-alloy austentitic materials are often immune to hydrogen embrittlement.

2.1.2 Carbon Dioxide

Carbon dioxide has a negative image as "climate killer" and is some times even considered as a toxic substance. In fact carbon dioxide plays a large role in maintaining life on earth as it is the vector of the carbon cycle. The carbon dioxide additionally released to the atmosphere by the burning of fossil resources like coal or gasoline though acts as a catalyst of climate change. Therefor, the use of fossil fuels by mankind must end and technologies to capture

carbon dioxide from the atmosphere and use it as an resource must be developed. In this chapter the physical and chemical characteristics of carbon dioxide are evaluated and its role in nature described. Afterwards the technological usage of carbon dioxide is shown.

2.1.2.1 Physical and Chemical Properties

Carbon dioxide is under ambient conditions a inodorous gas. Its consists of a carbon and two oxygen atoms (see fig. 2.2) with a linear alignment.

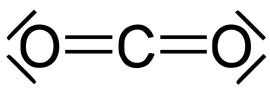

Figure 2.2: The molecular structure of carbon dioxide

Carbon dioxide is created by the reaction of carbon with oxygen:

$$C + O_2 \longrightarrow CO_2$$

The carbon dioxide which is released in the air by human technology is formed by the aerobic combustion of organic substances. For example the burning of methane:

$$CH_4 + 2\,O_2 \longrightarrow CO_2 + 2\,H_2O$$

In nature, carbon dioxide is created from cellular respiration, which provides energy to living creatures by the oxidation of glucose:

$$C_6H_{12}O_6 + 6\,O_2 \longrightarrow 6\,CO_2 + 6\,H_2O$$

In carbon dioxide, carbon exists in its highest possible oxidation state (+IV). This means that every reaction with carbon dioxide includes a reduction of the carbon atom by adding electrons. Carbon Dioxide is thermodynamically stable with an enthalpy of formation of about $\Delta H = -393\,\mathrm{kJ\,mol^{-1}}$.

Solubility of Carbon Dioxide in Water and Building of Carbonates For the reduction of carbon dioxide to formic acid, in most cases water is used as a solvent. Carbon dioxide could be dissolved in water, where it reversibly forms carbonic acid.

$$CO_2 + H_2O \rightleftharpoons H_2CO_3$$

Actually the solution does not contain many H_2CO_3 molecules, as 99% of the dissolved carbon dioxide is present in a physically dissolved form [52]. Carbonic acid has two dissociated forms leading to bicarbonate (HCO_3^-) and carbonate (CO_3^{2-}).

$$H_2CO_3 \rightleftharpoons H^+ + HCO_3^-$$

$$HCO_3^- \rightleftharpoons H^+ + CO_3^{2-}$$

The exact composition of the species concentrations depends on the pH value of the solution and could be looked up in Hägg's diagrams, with bicarbonate becoming the dominant species at a pH value above 6.5. For the reduction of carbon dioxide to formic acid, the formation of bicarbonates and carbonates is problematic, as this non-faradaic reaction, decreases the carbon selectivity for the formic acid production (e.g. see [28]). This is called the 'carbonate problem'. To counteract this, the pH value of the reaction solution should be kept low.

Carbon Dioxide and Carbon Monoxide equilibrium An important reaction for technical applications is the water-gas-shift-reaction (WGSR):

$$CO + H_2O \rightleftharpoons CO_2 + H_2 \quad \Delta H^{\ominus} = -42.2\,\mathrm{kJ\,mol^{-1}}$$

The mixture of carbon monoxide and hydrogen is called syngas and is used for many applications, such as Fischer-Tropsch-Synthesis or methanation. WGSR is used to decrease the amount of CO in the mixture and to generate hydrogen. At temperatures above 830°C, the equilibrium switches to the products. This reaction is referred to as Reverse-Water-Gas-Shift-Reaction (RWGSR).

$$CO_2 + H_2 \rightleftharpoons CO + H_2O$$

Similar to the WGSR, RWGSR is used to change the CO:H_2 ratio in the syngas.

2.1.2.2 Natural Occurrence

On earth, carbon dioxide occurs in different spheres. In the atmosphere, carbon dioxide is a trace gas, with a concentration of 417 ppm[5] in November 2021 [53]. A by far larger amount could be found in the hydrosphere, where carbon dioxide exists in a physically dissolved form and as bicarbonate and carbonate (see Section 2.1.2.1). Most of the carbon dioxide on earth is however bound in carbonate minerals of the lithosphere. Extraterrestrial carbon dioxide

[5]The increasing amount of carbon dioxide in earth's atmosphere through the burning of fossil fuels and other human factors (about 48% since the beginning of the Industrial Revolution [53]) is the most relevant factor of climate change. Carbon dioxide is a long-living species which absorbs and emits infrared light and therefor contributes to the greenhouse effect. High carbon dioxide concentrations in the atmosphere also leads to an acidification of the oceans.

could be found in the atmospheres of Mars and Venus where it is the dominating gas. It was also found on extrasolar bodies by Hubble Space Telescope [54].

2.1.2.3 Technical usable Carbon Dioxide Sources

To use carbon dioxide as a raw product for technical purposes a carbon dioxide source must be found. A common term used in this context is Carbon Capture and Utilization (CCU)[6]. In this section CCU technologies are classified into two categories[7]

- CCU from fossil sources, mainly power plant or industrial exhaust gases
- CCU from atmospheric CO_2 (Direct Air Carbon Capture and Utilization - DACCU)

In general the process of CCU is shown in figure 2.3.

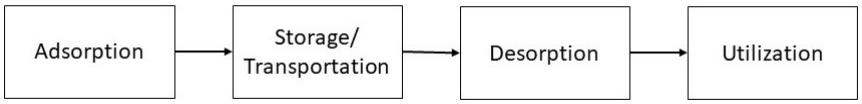

Figure 2.3: Schematic process of carbon capture and utilization

The first step (adsorption) corresponds to the actual CO_2 capture. This process could be divided into different sub-processes according to Figure 2.4. After the adsorption the captured CO_2 is chemically or physically bounded in a form as which it could be stored and distributed. To use the stored carbon dioxide, e.g. for the processing to fuels, a desorption must be executed releasing CO_2 for its utilization.
For a closed carbon cycle the integration of DACCU technologies are inevitable. Breyer et al. describe DAC as '*a key technology in the decades to come*' [55]. Nevertheless during a transition period CCU applications from fossil sources will contribute to decrease carbon dioxide emissions.

Carbon Dioxide Capture from fossil sources

General overviews of CCU technologies with fossil sources are given by Leung et al. [56] and Cuéllar-Franca et al. [57]. As follows only a brief overview is given.

[6] Besides CCU another term sometimes mentioned is CCS: Carbon Capture and Storage. CCS refers to technologies where CO_2 is captured and stored, e.g. in caverns or oceans, to reduce carbon emissions to the atmosphere but not further utilized. As this work focuses on the usage of carbon dioxide, CCS technologies are not further discussed

[7] Bioenergy Carbon Capture and Storage (BECCS) or Utilization (BECCU) are also not further described

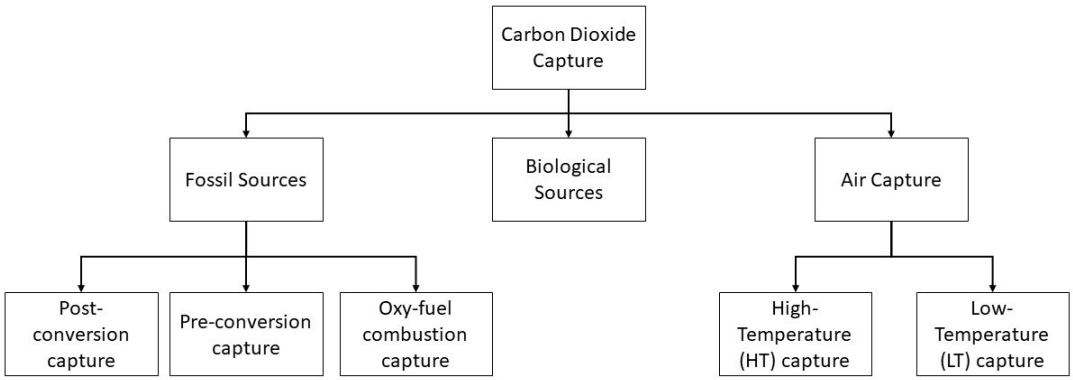

Figure 2.4: Carbon Capture Pathways

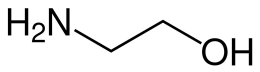

Figure 2.5: Molecular structure of monoethanolamine

Post-conversion capture

Post-conversion capture refers to technologies where CO_2 is separated from CO_2 rich exhaust gases from the combustion of fossil fuels. This could either be done by chemical sorbents or by physical measures such as membrane separation or solid sorbents. As chemical sorbents often amine-based (Monoethanolamine (MEA), Diethanolamine (DEA)) or alkaline compounds (e.g. NaOH) are used. Carbon dioxide capture with MEA (see fig. 2.5) is commonly used [57]. Gaseous CO_2 could be absorbed by MEA following to reaction paths [58]:

$$2\,R{-}NH_2 + CO_2 \longrightarrow RNH_3^+ + RNHCOO^-$$
$$R{-}NH_2 + CO_2 + H_2O \longrightarrow RNH_3^+ + HCO_3^-$$

Li et al. state that the desorption process consumes nearly 4.5 GJ of energy per ton CO_2 released from the solvent (pure MEA) [59].

Pre-conversion capture

Pre-conversion capture plays an important role for Internal Gasification Combined Cycle

(IGCC) power plants[8]. Carbon Dioxide is removed from the syngas. This is done by similar methods as for the post-conversion capture (e.g. MEA or physical methods).

Oxy-fuel combustion capture

Oxy-fuel combustion capture refers to a combustion process, where pure oxygen is used as an oxidant instead of air. As no nitrogen based combustion by-products come up, after water separation the exhaust stream is pure carbon dioxide. Nevertheless oxy-fuel combustion capture is of minor interest as an carbon dioxide source. This is because the aim of this technology is to recycle the carbon into the combustion process for a non-emission process (see [60, 61]).

Direct Air Capture of Carbon Dioxide (DAC)

To capture carbon dioxide air capture enables the possibility for a fully closed carbon cycle. Jennifer Wilcox describes the process in a TED-talk as a 'synthetic forest' [62], as like in plants CO_2-molecules are taken directly from the air and chemically bounded. A profound overview of DAC technologies including economic considerations is given Fasihi et al. [63]. At this point only a brief summary is given.

Direct air capture could be determined into tho different routes (see 2.4):

- Low-temperature (LT) DAC
- High-temperature (HT) DAC

LT-DAC

Solid sorbents are used for low-temperature DAC, mostly filters supported by amines, to capture CO_2 from the atmosphere. Air is blown through these filters until saturation is reached. The carbon dioxide molecules are released from the sorbent by heating up the system to about 100 °C. The released carbon dioxide gas occurs at a purity of more than 99 % [63]. A schematic overview of LT-DAC with a solid sorbent is shown in Figure 2.6.

HT-DAC

[8] Power plants where a solid fuel, e.g. waste or biomass is turned into a pressured gas (syngas) prior to its combustion

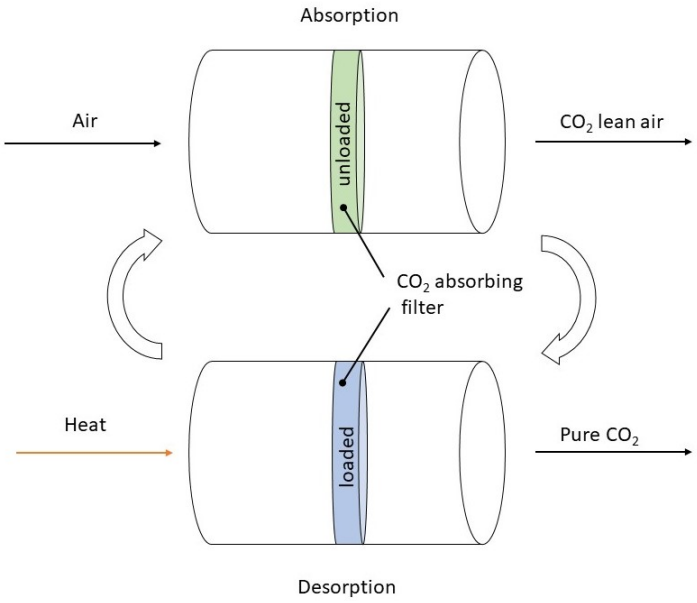

Figure 2.6: Low-temperature DAC with solid sorbent. Figure inspired by [63]

At high-temperature DAC technologies carbon dioxide is absorbed by an aqueous sodium hydroxide (NaOH)[9] solution leading to sodium carbonate (Na_2CO_3). In a second cycle NaOH is regenerated and solid calcium carbonate ($CaCO_3$)) formed from calcium hydroxide ($Ca(OH)_2$)). Heat is needed (about 900 °C) to release pure ($>$ 97 %) CO_2 from $CaCO_3$, which could afterwards be compressed, stored and utilized. The process is show in Figure 2.7.
Table 2.2 summarizes the energy demands for different DAC technologies[10]. Data is derived from Fasihi et al. [63].

Table 2.2: Energy Demand per $t_{CO_2}$of different realized DAC-Technologies

DAC-Technology	**Heat Demand [kWh/t_{CO_2}]**	**Electricity Demand [kWh/t_{CO_2}]**	**Project realization**
HT NaOH $Ca(OH)_2$	1420 - 2250	336 - 764	Carbon Engineering (Canada) [64]
LT amino-based	1500 - 2000	200 - 300	Climeworks (CH) [65]

[9] Potassium hydroxide (KOH) is also possible
[10] Electrical energy demand includes fans and CO_2 compression

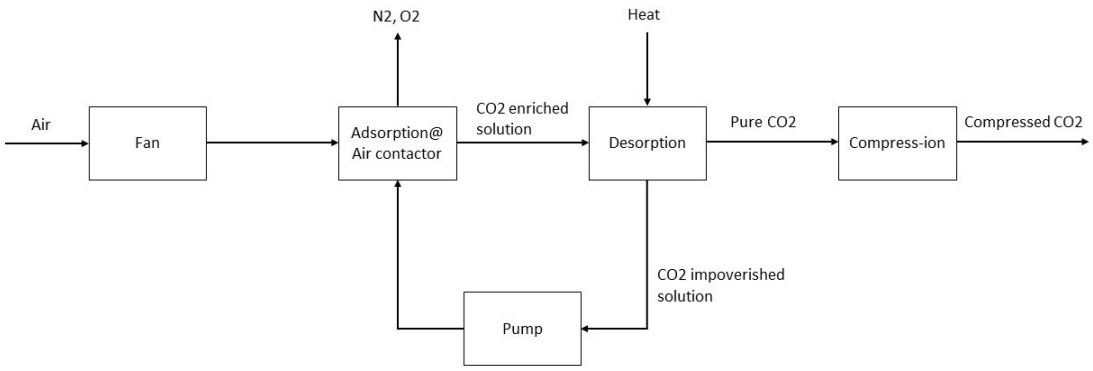

Figure 2.7: Generalized procedure of high-temperature Direct Air Capture of Carbon Dioxide in an aqueous solution

In summary. it could be said that DAC is a key technology for Power-to-X with carbon dioxide utilization to reach carbon neutrality. For a transition period until DAC is economical reasonable and technological mature, the capturing of carbon dioxide from exhaust gases (post-conversion capture) could be considered as the state-of-the-art carbon capture technology.

2.1.2.4 Technological use of carbon dioxide

Besides the reduction of carbon dioxide emissions it is also desirable to use carbon dioxide as a resource in order to supplement fossil fuels. As a part of syngas (mixture of CO, CO_2, H_2 and H_2O) carbon dioxide could be further processed to alkanes, to long-chained hydro-carbons or alcohols. These products could be blended to synthetic fuels. The key to climate neutrality of these fuels is the carbon dioxide source. If this synthetic fuels are burned afterwards in combustion engines or jet engines, carbon dioxide is in fact released back to the atmosphere. A closed carbon loop only occurs if the carbon dioxide is beforehand taken from the atmosphere rather than captured from exhaust gases from the combustion of fossil fuels. Besides the pathway with syngas, carbon dioxide could also be transformed to C1-compounds by the direct reduction of the carbon atom. Figure 2.8 shows the resulting substances after a 2, 4, 6 and 8 electron transfer.

In this work, the focus lays on the production of formic acid from carbon dioxide for a utilization as a hydrogen carrier. This and other technical relevant reactions with carbon dioxide used in a industrial scale are summarized in Table 2.3.

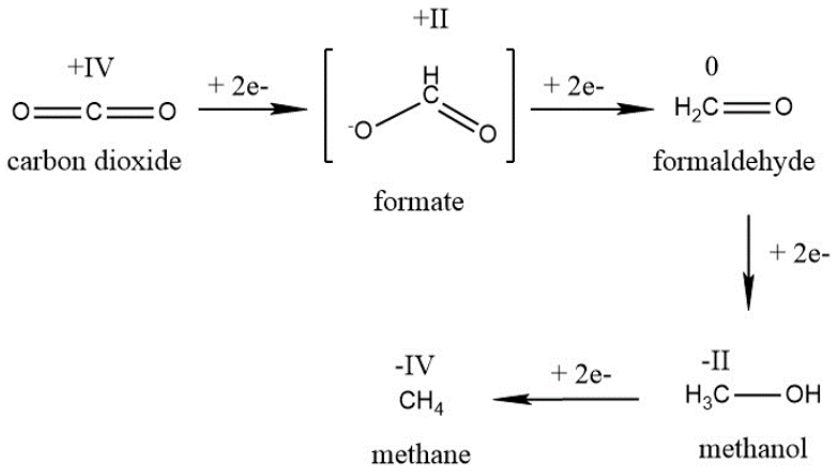

Figure 2.8: Carbon Dioxide reduction to C1-compounds

Table 2.3: Technical or biological important reactions with carbon dioxide

Reaction Type	**Product**	**Reaction equation**
Sabatier-Reaction (tec) / Methanogenesis (bio)	Methane	$CO_2 + 4\,H_2 \longrightarrow CH_4 + 2\,H_2O$
Methanol-Synthesis	Methanol	$CO_2 + 3\,H_2 \longrightarrow CH_3OH + H_2O$
Electrolysis	Formic Acid	$CO_2 + 2\,e^- + 2\,H^+ \longrightarrow HCOOH$
Electrolysis	Formaldehyde	$CO_2 + 4\,e^- + 4\,H^+ \longrightarrow HCHO + H_2O$
Electrolysis	Methanol	$CO_2 + 6\,e^- + 6\,H^+ \longrightarrow CH_3OH + H_2O$
Electrolysis	Methane	$CO_2 + 8\,e^- + 8\,H^+ \longrightarrow CH_4 + 2\,H_2O$
Photosynthesis (bio)	Glucose	$6\,CO_2 + 6\,H_2O \longrightarrow C_6H_{12}O_6 + 6\,O_2$
Urea-Synthesis	Urea	$2\ NH_3 + CO_2 \longrightarrow [H_2N{-}CO{-}O]NH_4$ $[H_2N{-}CO{-}O]NH_4 \longrightarrow H_2N{-}CO{-}NH_2 + H_2O$
Water-Gas-Shift	Syngas	$CO_2 + H_2 \rightleftharpoons CO + H_2O$

2.1.3 C1-Compounds

In this section, the physical and chemical properties of so called C1-compounds, which result from a reduction of the carbon atom on carbon dioxide, are shown. The molecular structures of formic acid, formaldehyde, methanol and methane are illustrated in Figure 2.9.

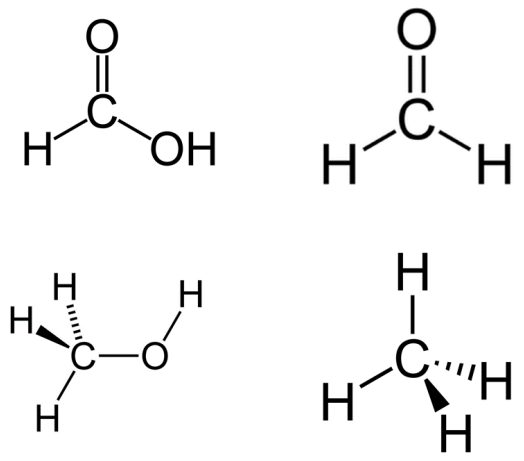

Figure 2.9: Molecular structure of C1-compounds: formic acid (top left), formaldehyde (top right), methanol (bottom left), methane (bottom right)

For technical applications important physical properties of the C1-compounds are summarized in Table 2.4.

Table 2.4: Physical properties of formic acid

Property	**Formic Acid**	**Formaldehyde**	**Methanol**	**Methane**
M [g mol^{-1}]	46.025	30.026	32.042	16.043
T_b [°C]	101	-19.1	64.7	-161.5
T_m [°C]	8.3	-92	-97.6	-182.4
ρ [kg m^{-3}]	1.22	-	0.79	-

As this work focuses on formic acid utilization for energy storage applications, subsequently specific properties of formic acid and formate are described.

2.1.3.1 Formic Acid and Formate

Under ambient conditions formic acid is a colorless liquid, which in nature in occurs in ants and bees. Formic acid is miscible with water and forms an azeotropic mixture.

Acidic Behavior Formic acid is a weak acid with a pK_s of 3.75. The pH value for formic acid in water could be calculated with Equation 2.1. Figure 2.10 shows the pH value for formic acid concentrations from 0.001 mol L^{-1} to 1 mol L^{-1}

$$pH = -log\left[\frac{1}{2}\cdot\left(-K_s + \sqrt{K_s^2 + 4\cdot K_s\cdot c}\right)\right] \tag{2.1}$$

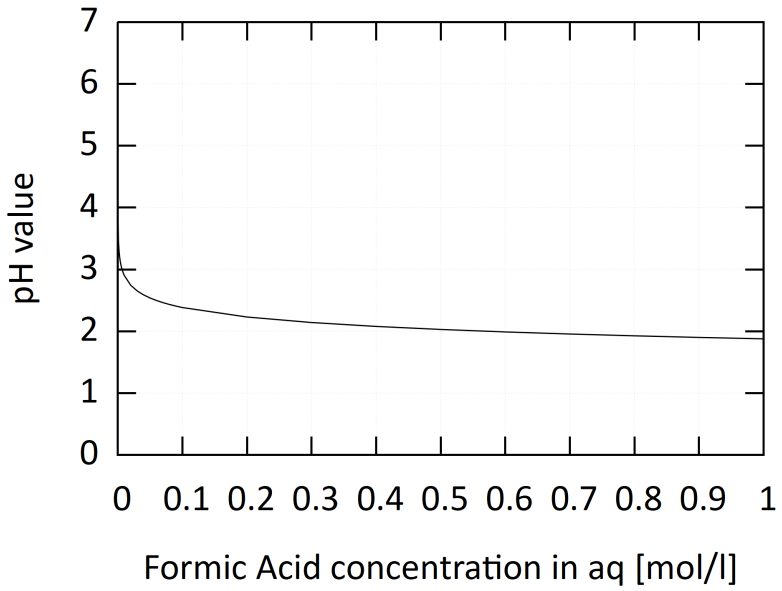

Figure 2.10: pH value for a specific formic acid concentration in water

The deprotonation of formic acid leads to the formate-ion $HCOO^-$.

$$HCOOH \rightleftharpoons H^+ + HCOO^-$$

With cations like Na^+ or K^+ the formate-ion builds salts.

Production In industrial processes formic acid is produced from methanol. In a first step methanol reacts with carbon monoxide to methyl formate.

$$CH_3OH + CO \longrightarrow HCOOCH_3$$

The second reaction step is a hydrolysis of methyl formate, where formic acid and methanol is produced.

$$HCOOCH_3 + H_2O \longrightarrow HCOOH + CH_3OH$$

Application Formic acid has a wide range of possible applications. Most of the worldwide consumed formic acid is used as a preservative and leather production. It is also used for rubber production, soldering or as a medicine against warts. Formic acid could be used for

power and heat production in formic acid fuel cells. BASF sells formate salts as a deicing agent for airports and roads.

Material Compatibility Caused by the acidity of formic acid metals in direct contact tend to corrosion. However, formic acid is compatible to the most common plastics (e.g. PE) at all concentrations. Specific stainless steels could also be used for formic acid storage.

2.2 Fundamentals of thermochemical Carbon Dioxide Reduction

A thermochemical reaction is characterized by the fact that the necessary activation energy of the reaction is provided as heat. For starting the reaction, heat in the equivalent of the activation energy must be available. Afterwards, the reaction runs permanently in the direction of the products when the Gibbs free energy at the reaction conditions is less than zero. For the carbon dioxide hydrogenation, this is only the case in the presence of a base or for dissolved substances [21].

2.2.1 Reaction Kinetics of Carbon Dioxide Reduction

The reaction of carbon dioxide with hydrogen to formic acid could be modeled as a second-order reaction.

$$\mathrm{A} + \mathrm{B} \longrightarrow \mathrm{C}$$

Assuming that both reactants A and B are present with identical concentrations, the reaction rate could be expressed as follows:

$$\frac{d[A]}{dt} = -k \cdot [A]^2 \tag{2.2}$$

Where k is the reaction slope. In an integrated form this results in:

$$\frac{1}{[A]} = \frac{1}{[A]_0} + k \cdot t \tag{2.3}$$

For the synthesis of formic acid the concentration of reactant A could be replaced with the concentration of gaseous hydrogen.

$$c_{H_2}(t) = \frac{c_{H_2,0}}{1 + c_{H_2,0} \cdot k_1 \cdot t} \tag{2.4}$$

For an ideal gas, the concentration of the species is related to the partial pressure according

to Equation 2.5.

$$c_{H_2} = \frac{p_{H_2}}{R \cdot T} \tag{2.5}$$

For the computation of the species concentrations Equation 2.2 could be expresses as:

$$\Delta[A] = -k \cdot [A]^2 \cdot \Delta t \tag{2.6}$$

Finally, at each time step the concentration of species A is given as:

$$[A](t + \Delta t) = -k \cdot [A](t)^2 \cdot \Delta t + [A](t) \tag{2.7}$$

The reaction slope k must be determined from experimental data. Its temperature dependency is considered with the Arrhenius equation:

$$k = A \cdot e^{\frac{-E_a}{R \cdot T}} \tag{2.8}$$

With the factor A being a temperature dependent constant for the reaction and E_a is the activation energy. If k_0 at the temperature T_0 is known, the reaction slope k_1 at the temperature T_1 could be calculated with Equation 2.9.

$$\ln \frac{k_0}{k_1} = -\frac{E_a}{R} \left(\frac{1}{T_0} - \frac{1}{T_1} \right) \tag{2.9}$$

2.2.2 The ideal Flow Reactor

In one of the system variants described later in this work, a flow reactor is provided for the synthesis of formic acid from hydrogen and carbon dioxide. The change of the the species concentration over time could be calculated for an ideal axial flow reactor according to Equation 2.10 [42].

$$\frac{\partial c_i}{\partial t} = -u_z \cdot \frac{\partial c_i}{\partial z} + \sum_{j=1}^{M} \nu_{i,j} \cdot r_j \tag{2.10}$$

With u_z being the flow velocity in z-direction and the sum representing all chemical reactions taking place in the reactor with the stochiemetric coefficient ν and the reaction rate r. The length increment ∂z is calculated from the reactor length $L_{reactor}$ and the number of numerical elements N.

$$\partial z = \frac{L_{reactor}}{N} \tag{2.11}$$

If a stationary flow could be assumed, Equation 2.10 simplifies as follows:

$$0 = -u_z \cdot \frac{\partial c_i}{\partial z} + \sum_{j=1}^{M} \nu_{i,j} \cdot r_j \tag{2.12}$$

The differential equation is computed by replacing the differential with differences. Also, it is assumed that all possibly occurring side reactions could be neglected.

$$c_i(z + dz) = c_i(z) + \frac{\nu_i \cdot r}{u} \cdot dz \tag{2.13}$$

For each species the final mass flow is calculated with the concentration at the reactor end $z = L_{reactor}$, with the molar mass M_i and the reactor cross section $A_{reactor}$:

$$\dot{m}_{i,out} = c_i(L_{reactor}) \cdot A_{reactor} \cdot u_z \cdot M_i \tag{2.14}$$

2.3 Fundamentals of the electrochemical Carbon Dioxide Reduction

In contrast to the thermochemical reaction path, the energy for the electrochemical carbon dioxide reduction is provided by an electrical field. The Gibbs free energy in this case determines the minimum voltage needed to run the electrolysis process.

2.3.1 Electrochemical Reaction Paths of the Carbon Dioxide Reduction

To most important intermediate species in the electrochemical carbon dioxide reduction is the radical anion $\cdot CO_2^-$ which is formed by transferring an electron to carbon dioxide.

$$CO_2 + e^- \rightleftharpoons \cdot CO_2^-$$

There are three different pathways for further reaction of the radical anion.

1. Dimerization with another radical anion to oxalate:

   $$\cdot CO_2^- + \cdot CO_2^- \longrightarrow (COO)_2^{2-}$$

2. Forming of carbonate and carbon monoxide with CO_2:

   $$\cdot CO_2^- + CO_2 + e^- \longrightarrow CO + CO_3^{2-}$$

3. Forming of formate in the presence of water:

   $$\cdot CO_2^- + H_2O + e^- \longrightarrow HCOO^- + OH^-$$

By Kinzel et al. this pathway is called the 'outer-sphere one-electron transfer for carbon dioxide activation' [29]. The drawback of this reaction path is that a high energy input is needed to bend the otherwise straight CO_2 molecule. The catalyst in this pathway works

as an electron carrier. In contrast to the outer-sphere transfer, there is also an inner-sphere electron transfer. Organometallic complexes could be used for this reaction path, which is determined by the fact that the CO_2 molecule is bound directly to the catalyst. It could be further subdivided into a path of an electron transfer to CO_2 through the molecular complex and a path of an electron transfer through a hydride intermediate [29].

Electron transfer through the complex:

$$[L_mM]^n + e^- \longrightarrow [L_mM]^{n-1} + CO_2 \longrightarrow [L_mM(CO_2)]^{n-1} + 2\,H^+ + e^- \longrightarrow \text{products}$$

Electron transfer through a hydride:

$$[L_mM]^n + e^- \longrightarrow [L_mM]^{n-1} + H^+ \longrightarrow [L_mMH]^{n-1} + CO_2 + H^+ + e^- \longrightarrow \text{products}$$

The inner-sphere reaction path takes advantage of the coordination of CO_2 to the metal, which lowers the overall energy demand for the electron transfer.

2.3.2 Thermodynamic of the electrochemical Carbon Dioxide Reduction

The open circuit voltage (OCV), which is necessary to maintain an electrolysis process from a thermodynamical point of view (without any losses) could be calculated as follows:

$$E_{OCV} = \frac{-\Delta G}{2F} \tag{2.15}$$

With the Gibbs free energy ΔG definied as:

$$\Delta G = \Delta H - T \cdot \Delta S \tag{2.16}$$

The irreversible share $T \cdot \Delta S$ represents the amount of energy which is provided by the heat from the surrounding matter. Higher temperatures mean, that the gibbs energy and thus the open circuit voltage of the electrolysis is reduced. If the OCV is calculated with $T \cdot \Delta S = 0$ the thermal neutral voltage E_{th} results.

$$E_{TH} = \frac{-\Delta H}{2F} \tag{2.17}$$

E_{TH} stands for the voltage needed for the electrolysis if the energy provided by heat is also covered by the electrical energy. Above this voltage the electrolysis process actually produces heat. Figure 2.11 shows the course of open cell voltage and the thermo-neutral voltage over the temperature. The OCV decreases with increasing temperature, as more and more heat

is available from the environment to run the electrolysis process. Above E_{th} the process always produces heat.

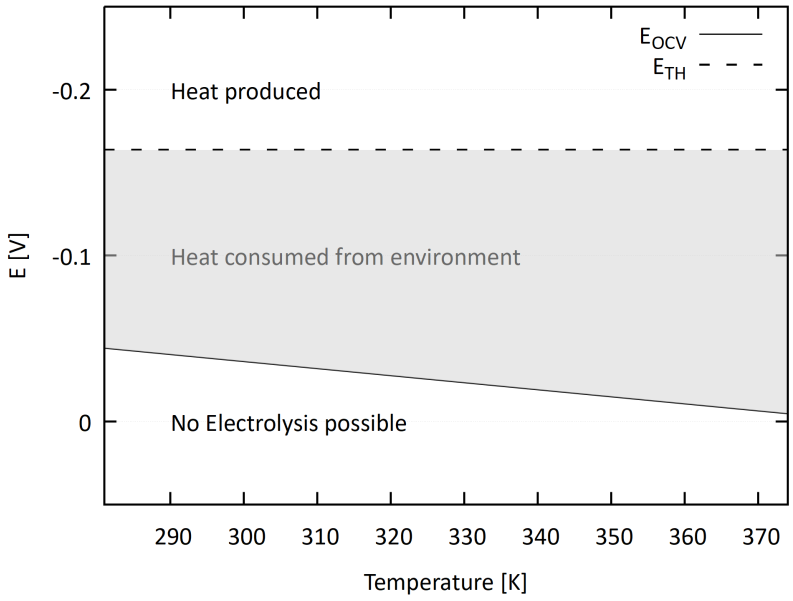

Figure 2.11: E_{OCV} and E_{TH} for the reaction $CO_2 + 2\,e^- + 2\,H^+ \longrightarrow HCOOH$ at ambient pressure and pH 0

The change of the OCV at different reaction conditions could be analyzed using the Nernst equation, taking the concentrations of the dissolved reduced and oxidized substances into account:

$$E_{OCV} = E^0 + \frac{RT}{zF} \cdot \ln\left(\frac{[ox]}{[red]}\right) \tag{2.18}$$

Through the Nernst equation, also the pH dependency of the half cell voltage could be determined, if the concentration of protons is added to the oxidized or reduced species respectively. For the cathode reaction of the carbon dioxide reduction to formic acid, Equation 2.18 is modified as follows:

$$E_{OCV} = E^0 + \frac{RT}{zF} \cdot \ln\left(\frac{[CO_2][H^+]^2}{[HCOOH]}\right) \tag{2.19}$$

Figure 2.12 shows the ph dependency of the cell voltage of the carbon dioxide reduction to formic acid (cathode) and water splitting at the anode.
Table 2.5 summarizes the open circuit voltages for the electrochemical CO_2 reduction at the cathode in an aqueous solution under standard conditions (pH 7, 25°C, 1 atm). With this

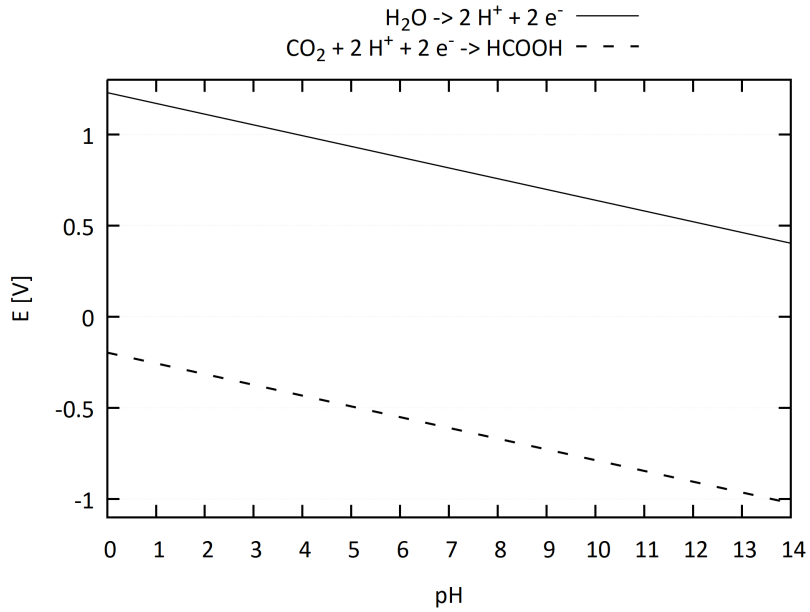

Figure 2.12: Pourbaix-Diagram for water splitting (anode) and carbon dioxide reduction to fromic acid (cathode)

data a Frost-Diagram of the carbon dioxide reduction could be drawn (see Figure 2.13), with the cumulative free energy ($z \cdot E$) on the y-axis.

From the Frost diagram it could be seen that formic acid is located on a minimum between CO_2^- and HCHO, which means that the formation of formic acid is thermodynamically favored. However, also CO lays on a minimum. As the carbon monoxide production is an unwanted side reaction, this reaction route must be suppressed kinetically.

The overall cell voltage result from the sum of the cathode and the anode half cell volt-

Table 2.5: Cathode reactions of electrochemical carbon dioxide reduction and open circuit voltages (from [66])

Cathode reaction	E_{OCV} **in aq. @pH7**
$CO_2 + e^- \longrightarrow CO_2^-$	$-1.9\,V$
$CO_2 + 2\,e^- + 2\,H^+ \longrightarrow CO + H_2O$	$-0.53\,V$
$CO_2 + 2\,e^- + 2\,H^+ \longrightarrow HCOOH$	$-0.61\,V$
$CO_2 + 4\,e^- + 4\,H^+ \longrightarrow HCHO + H_2O$	$-0.48\,V$
$CO_2 + 6\,e^- + 6\,H^+ \longrightarrow CH_3OH + H_2O$	$-0.38\,V$
$CO_2 + 8\,e^- + 8\,H^+ \longrightarrow CH_4 + 2\,H_2O$	$-0.24\,V$

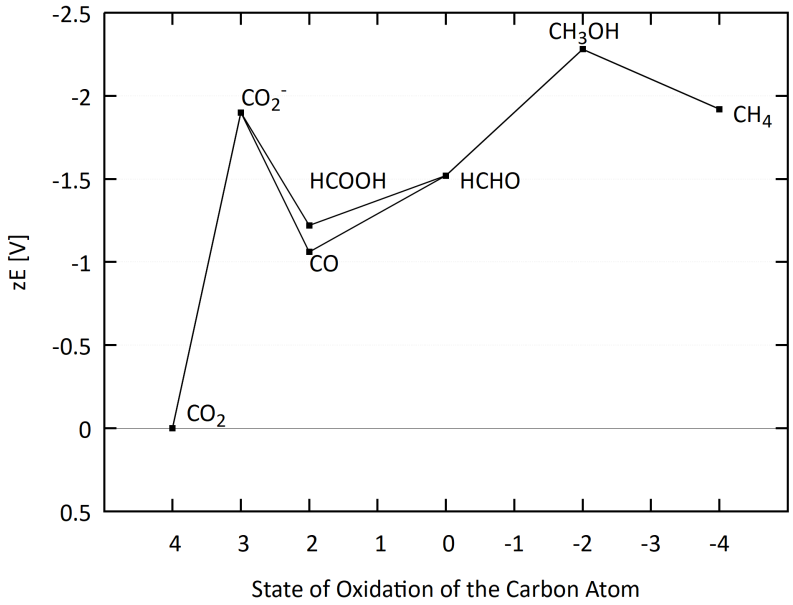

Figure 2.13: Frost-diagram for the carbon dioxide reduction at pH7

ages. Possible anode reactions for the electrochemical carbon dioxide reduction are water splitting or hydrogen deprotonation (see Table 2.6).

Table 2.6: Anode reactions

Anode reaction	E_{OCV} **in aq. @pH7**
$H_2 \longrightarrow 2\,H^+ + 2\,e^-$	$-0.413\,V$
$H_2O \longrightarrow 2\,H^+ + 2\,e^- + \frac{1}{2}\,O_2$	$0.816\,V$

2.3.3 Modelling of the Voltage Characteristic

The open circuit voltage described in section 2.3.2 is the least electrical potential which has to be provided in order to start the electrolysis process. However, in reality voltage losses caused by several chemical and physical phenomena add to the OCV. All in all the voltage of an electrolysis process is calculated with the open cell voltage E_{OCV}, the activation losses V_{act}, the ohmic losses V_{ohm} and the transportation losses V_{trans} as follows:

$$V = E_{OCV} + V_{act} + V_{ohm} + V_{trans} \tag{2.20}$$

2.3.3.1 Activation Losses

The activation losses come from the energy which is needed to break the chemical bonds of the involved species. Hence it is mainly depending on the used catalyst as well as on reaction conditions (e.g. cell temperature). Activation losses are dominant at low current densities. Generally they are modeled according to Equation 2.21 and Equation 2.22 [37]. The basic form of these equations is known as Butler-Volmer-equation.

$$V_{act,an} = \frac{RT_{an}}{\alpha_{an}F} sinh^{-}1\left(\frac{i}{2i_{0,an}}\right) \tag{2.21}$$

$$V_{act,cat} = \frac{RT_{cat}}{\alpha_{cat}F} sinh^{-}1\left(\frac{i}{2i_{0,cat}}\right) \tag{2.22}$$

The charge transfer coefficient α and the exchange current density i_0 are the main parameters which define these equations. Values for α could be found in literature and often tend to be around 0.5. Although α is an important parameter for electrode kinetics is is hard to be defined exactly. Guidelli et al. [67] proposed a definition in an IUPAC recommendation in 2014. The exchange current density is defined as the current flowing at equilibrium. A higher exchange current density means that the reaction is easier to start. In literature the exchange current density i_0 varies over a large amount of values, as the exact value is hard to determine. Most authors use i_0 to fit their model to experimental data [37]. The temperature dependency of the exchange current density could be calculated with an Arrhenius equation [39]:

$$i_0 = i_{0,ref} \cdot e^{\frac{E_a}{R} \cdot \left(\frac{1}{T} - \frac{1}{T_{ref}}\right)} \tag{2.23}$$

In the case of carbon dioxide electrolysis the modeling of the activation losses should be carried out carefully to reach an appropriate model accuracy as they are considered to dominate the voltage losses due to the low expected current densities. Also the differences of various catalysis systems could most likely be evaluated at the activation losses.

2.3.3.2 Ohmic Losses

The ohmic losses of an electrochemical reaction are determined by the electrical resistance of the conducting materials. It could be approximated by the sum of the total resistance R_{tot} of the current collectors and the resistance of the membrane. R_{tot} could be determined from an equivalent circuit model or used as a fitting parameter for experimental data.

$$V_{ohm} = R_{tot} \cdot i \cdot A + \frac{\delta_m}{\sigma_m} \cdot i \tag{2.24}$$

For modeling the conductivity σ_m of the membrane, often an empirical equation is used (see [37]):

$$\sigma_m = (0.005139 \cdot \lambda - 0.00326) \cdot e^{\left(1268 \cdot \left(\frac{1}{303} - \frac{1}{T_{cell}}\right)\right)} \tag{2.25}$$

The conductivity depends on the water content of the membrane, therefor the hydration factor λ is used. Different approaches for the calculation of λ are described in literature (see [38] and [68]). Values range from $\lambda = 7$ (dry) to $\lambda = 14$ (good hydration) and $\lambda = 22$ (bathed) (see [69]).

2.3.3.3 Mass Transport Losses

Transportation losses become dominant at higher current densities and are caused by mass transport limitations. The modeling of this phenomenon could be done with different approaches. A more detailed approach is based an Fick's Law of diffusion. This approach becomes more and more complex for multiphase flows, as they occurre in CO_2 electrolyis. According to Garcia-Valverde et al. [39] the transportation losses could be modeled by extending the Butler-Volmers equation with a term which considers another parameter: the limit current density i_l.

$$V_{trans} = \frac{RT}{\alpha F} \cdot sinh^{-}1 \left(\frac{\frac{i}{i_0}}{1 - \frac{i}{i_L}} \right) \tag{2.26}$$

The limit current density could also be used as a fitting parameter, if experimental data is available.

2.4 Fundamentals of Formic Acid Decomposition

The decomposition of formic acid to hydrogen and carbon dioxide is modeled as a first-order reaction.

$$\mathrm{A} \longrightarrow \mathrm{B} + \mathrm{C}$$

This means that the reaction rate only depends on the concentration of reactant A.

$$\frac{d[A]}{dt} = -k \cdot [A] \tag{2.27}$$

The solution of this differential equation is:

$$[A] = [A]_0 \cdot e^{-k \cdot t} \tag{2.28}$$

For a better computation of the time dependent species concentration Equation 2.27 is

expressed as:

$$[A](t + \Delta t) = -k \cdot [A](t) \cdot \Delta t + [A](t) \tag{2.29}$$

If the reaction slope k of the formic acid dehydrogenation is determined from experimental data at Temperature T, the reaction slope at any temperature could be calculated from Equation 2.9.

Chapter 3

Energy Conversion with chemical CO_2 Reduction: A Technological Overview

In this chapter a overview of different technologies based on the electrochemical or thermochemical reduction of carbon dioxide is given. The field of application of this technology is the conversion of electrical energy to chemical energy (P2X) for long term storage, transportation or mobile applications. The production of hydrogen via water electrolysis plays an decisive role in this context as hydrogen is in all catalytic reactions described in this chapter used as an reducing agent. Also, water electrolysis could be seen as a role model for the electrochemical reduction of carbon dioxide. Formic acid based energy storage, such as Carbon-Dioxide-Electrolysis, which in later chapters further described, is classified within the context of those P2X technologies. The chapter closes with some thoughts on storage and transportation aspects of P2X products as well as a consideration of the re-conversion of P2X products through fuel cells and combustion to electrical power and heat. The focus of the re-conversion lays on the stationary electricity and heat supply. Nevertheless sector coupling possibilities to mobile or industrial applications are shortly mentioned.

3.1 Water Electrolysis

The production of hydrogen through water electrolysis is a key technology for P2X applications, as hydrogen plays multiple roles in P2X processes:

- As a fuel for hydrogen powered cars with fuels cells (FCV)
- For re-electrification and heat generation in stationary fuel cells (CHP)

- For blending into the natural gas grid
- For industrial applications (e.g. ammonia synthesis)
- As a part of syngas for the processing of methane and other hydrocarbons
- As a proton donor for electrochemical reduction reactions, e.g. the reduction of carbon dioxide to formate

Due to this versatility hydrogen is often considered as an important energy carrier for all kinds of future applications and the driver for a fossil carbon free society.
Water electrolysis is an electrochemical process with a two electron transfer ($z = 2$), where water is split into its parts oxygen and hydrogen. In general this process could be described through the following chemical reaction:

$$H_2O\,(l) \longrightarrow H_2\,(g) + \frac{1}{2}\,O_2\,(g) \qquad \Delta H^{\ominus} = 285.83\,\mathrm{kJ\,mol^{-1}}$$

However the individual half cell reactions differ from cell type to cell type (see Table 3.1 and Figure 3.2). Water electrolysis is an endothermic reaction where energy must be provided. In this case by electrons which are driven by an electrical potential. If electrical power from renewable energy sources are used, the hydrogen production via water electrolysis is fully carbon neutral. Under standard conditions water electrolysis requires an open circuit voltage of $E_{OCV} = 1.229\,\mathrm{V}$ and a thermo-neutral voltage of $E_{th} = 1.48\,\mathrm{V}$. Nevertheless, the Gibbs-free energy of the water electrolysis depends on the partial pressures of each species at the cathode and anode as well as the temperature (see equation 3.1).

$$\Delta G = \Delta H - T_{cell}\Delta S + RT_{cell}\ln\left(\frac{p_{H_2}p_{O_2}^{0.5}}{p_{H_2O}}\right) \tag{3.1}$$

The changes of the Gibbs-free energy causes derivations of the open circuit voltage according to equation 3.2.

$$E_{OCV} = \frac{-\Delta G}{zF} \tag{3.2}$$

As hydrogen for technical applications is often used pressurized and state-of-the-art electrolyzers often allow pressurization directly at the system, the change of the E_{OCV} must be considered (see Figure 3.1).
Water electrolysis could be carried out in different kinds of electrochemical cell. Currently three different types of water electrolysis cells are mostly used:

- Alkaline Electrolysis Cell (AEC): is the most mature electrolysis type. A sulfuric acid is used for load (OH^-) transportation. AECs are known as limited dynamic and hence less suitable for direct coupling with renewable energy sources.

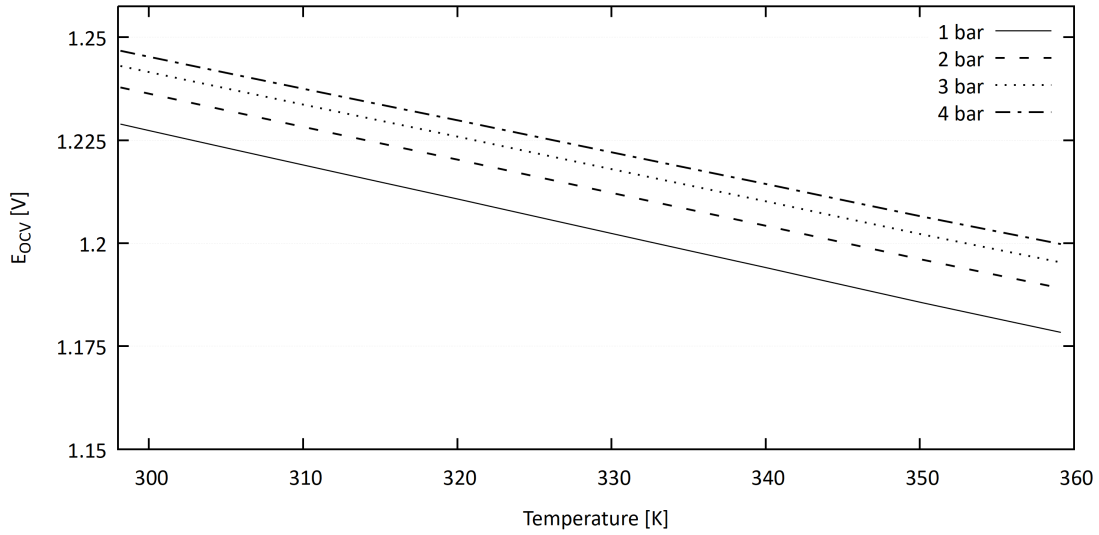

Figure 3.1: Change of E_{OCV} for water electrolysis with the hydrogen partial pressure

- Polymer Electrolyte Membrane Electrolysis Cell (PEMEC): uses a solid polymer membrane for load separation and transport of cations (H^+). PEMECs are highly dynamic with fast responses to load changes and the possibility of short overloading. Some drawbacks currently are the necessary use of noble metals (Pt, Pd) as catalysts and the membrane degradation.
- Solid Oxide Electrolysis Cell (SOEC): often named as high-temperature electrolysis as the operating temperature lays way above AECs or PEMECs (about 800 °C). Uses a ceramic material as electrolyte and O_2^- anions for load transportation. SOECs are usually very robust against additives (e.g. CO), but are least developed of the mentioned cell types as the high temperatures are challenging for the used materials.

Figure 3.2 shows a simplified cell design of the three above mentioned cell types.
The main difference lays in the electrolyte (load transport). Hence different half cell reactions could be formulated for each cell type (see Table 3.1).
For all types of water electrolyzers simulation models in various levels of detail and for different simulation tools are described in literature. Milewski et al. [70] show to different approaches for modeling an AEC. First with detailed estimation of the different electrochemial losses and second with the use of an equivalent electrical circuit. Both models are compared with experimental results and show average error of below 3 %. Carmo et al. [37] give a profound general overview of PEMEC modelling, where as Yigit et al. [40] show how to implement a detailed PEMEC model into Simulink. An important characteristic of PEMECs is its dynamic behavior. This is especially important, if the coupling with highly fluctuating energy sources

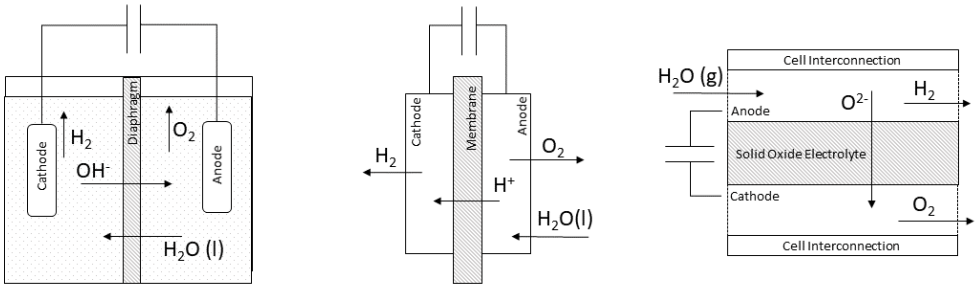

(a) AEC (b) PEMEC (c) SOEC

Figure 3.2: Schematic overview of different water electrolysis cell designs

Table 3.1: Half cell reactions of different water electrolysis cell types

	Anode	**Cathode**
AEC	$2\,OH^- \longrightarrow \frac{1}{2}\,O_2 + H_2O + 2\,e^-$	$2\,H_2O + 2\,e^- \longrightarrow 2\,OH^- + H_2$
PEMEC	$H_2O \longrightarrow 2\,H^+ + 2\,e^- + \frac{1}{2}\,O_2$	$2\,H^+ + 2\,e^- \longrightarrow H_2$
SOEC	$O_2^- \longrightarrow \frac{1}{2}\,O_2 + 2\,e^-$	$H_2O + 2\,e^- \longrightarrow H_2 + O_2^-$

should be investigation by simulations. Guilbert and Vitale [71] introduce a model of this behavior by approximating the capacitive characteristic of a PEMEC with the equivalent electrical scheme shown in Figure 3.3.

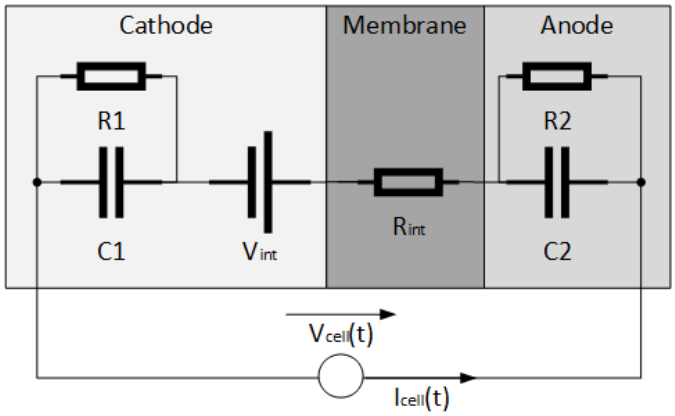

Figure 3.3: Equivalent electrical scheme to predict the capacative behavior of a PEMEC. Adapted from [71]

Udagawa et al. [72] describe a model of a planar SOEC stack at steady-state conditions and its electrochemcial performance at different current densities and temperatures. The use of a two-dimensional model of a SOEC using computational fluid dynamics (CFD) to predict the cell performance is shown by Ni [73]. An extensive technological comparison between AECs, PEMECs, and SOECs is given by Schmidt et al. [74]. For system integration aspects it should be again remarked that one main challanges of water electrolysis arises when electrolyzers are operated with intermitting loads from renewable energy sources. From the mentioned technologies PEMECs perform best under such circumstances [75] as they have the shortest system response and cold-start time [74]. SOEC is the least commercial ready technology, but is a promising options for the future as the design allows a reverse operation (fuel cell mode) and the Co-electrolysis of water and carbon dioxide to syngas (see Section 3.2).

3.1.0.1 Catalysis and Cell Design of PEMECs

From this point on only PEMECs are described more detailed to allow a comparison with the later introduced CO_2-electrolysis cell which also uses a polymer electrolyte membrane as an electrolyte.

Figure 3.4 shows the design of a so called membrane electrode assembly (MEA) of a PEMEC. It consists of the following parts:

- Bipolar plates: provide water at the anode and purge the products at both anode and cathode. Acts as cell closing and interconnect two cells.
- Current collector: provides electrons needed for the reduction reaction at the cathode and collects electrons freed by the oxidation at the anode. It conducts the reactants to the catalyst layer and connects anode and cathode electrical. Mostly designed as a gas diffusion layer (GDL) where gaseous substances are present or as micro porous layer (MPL) in case of present liquids.
- Catalyst Layer: carries the immobilized catalyst and conducts the released protons to the membrane. The catalyst mostly are nano particles embedded in an supporting structure.
- Membrane: as membrane material often modified Teflon, known under the trading name Nafion, is used. The membrane separates the load and conducts protons from the anode to the cathode.

The catalyst which are widely used for the oxygen evolution reaction (OER) is Ir supported by IrO_2, where as for the hydrogen evolution reaction (HER) mostly platinum on a carbon structure (Pt/C) is used. With this catalyst combination a performance in state-of-the-art

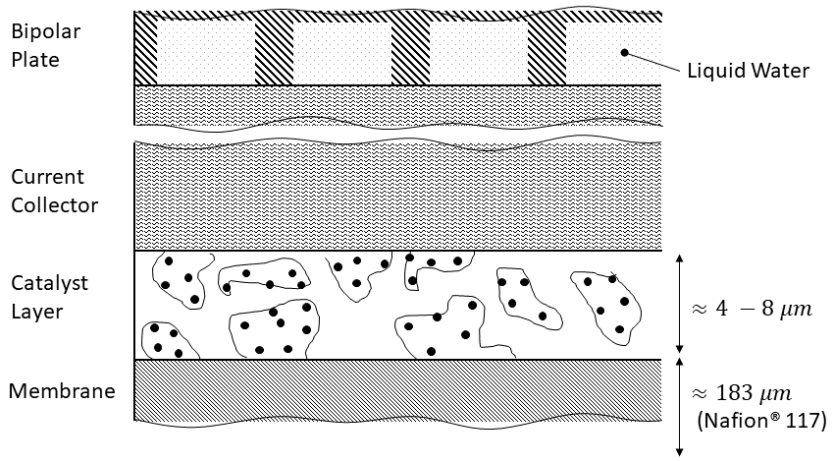

Figure 3.4: Microscopic view of a PEMEC anode MEA (not to scale)

PEMECs of 0.6 - 2.0 A/cm^2 at 1.8 V to 2.2 V is achieved.An overview of the development of cell voltages for different catalysts throughout the history of PEMECs is given by Carmo et al. [37] and Shiva Kumar et al. [76].Future developments concerning the catalyst are the use of cheaper (non-noble) catalysts and the overall reduction of the catalyst loading by better carrier structures which allow more efficient proton conduction and an increased active area. Such measures will make PEMECs more profitable.

3.1.0.2 Water Electrolysis System Design and Control

To drive the electrolysis process DC current is needed. Thus for grid connected systems appropriate arrangements for the current conversion must be set. Figure 3.5 shows an example for a grid connected electrolysis system. Electrical power is provided by PV and wind turbines. A connected battery could be used to minimize phases of deactivation.

To match specific input power specifications several cells are connected to a stack. It is very common to connect N cells in series, hence the voltage of the overall stack U_{stack} is given by the sum of the individual cell voltages U_i.

$$U_{stack} = \sum_{i=1}^{N} U_i \tag{3.3}$$

With a given stack voltage the input current could be determined.

$$I_{IN} = \frac{P_{IN}}{U_{stack}} \tag{3.4}$$

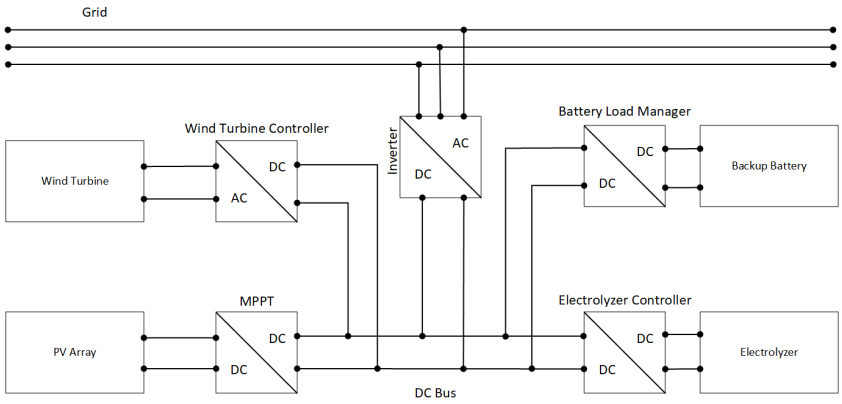

Figure 3.5: Example for a grid connected electrolysis system with wind turbine, PV and backup battery

Again N stacks could be connected (in parallel) if the input current is still too high.

$$I_{stack} = \frac{I_{IN}}{N_{stack}} \tag{3.5}$$

Figure 3.6 shows how the voltage and the current distribute for cells connected in series to a stack and several stacks connected in parallel.

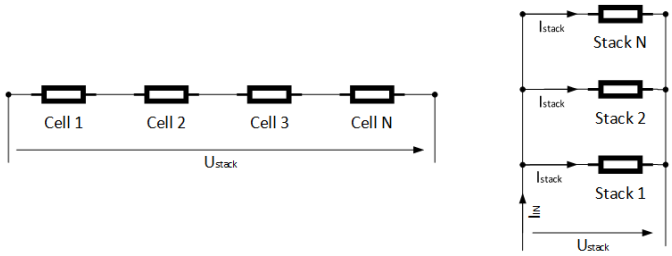

Figure 3.6: Voltage and current distribution for serial cell connection and parallel stack connection

An important aspect to evaluate the operation of an electrolysis system is its utilization factor UF_{EL} which is introduced by Papadopoulos et al [77][1].

$$UF_{EL} = \frac{\text{Actually Produced } H_2}{\text{Idealy Produced } H_2} = \frac{\text{Actually Produced } H_2}{H_2 \text{ production rate [kg/h] x 8760 [h]}} \tag{3.6}$$

This factor describes the share of the produced amount of hydrogen by the electrolysis system compared to theoretically achievable hydrogen amount with a 24/7 operation at

[1] orginally the symbol U_{EL} was used by Papadopulos et al. Here UF_{EL} is used to avoid confusion with the voltage U

ideal conditions. It is a useful factor to evaluate the performance of an integrated system and to determine the optimal dimensions of connected subsystems, e.g. battery storage. For comparison aspects and to get a feeling for the performance of PEMEC stacks, table 3.2 summarizes typical stack sizes, electrical characteristics and flow rates of stacks from one specific manufacturer for a large power spectrum. The specifications for the cell area and the current show a maximal current density of $3\,A/cm^2$.

Table 3.2: PEMEC Stack Parameters for a wide range of input power by the manufacturer Giner ELX [78]

Peak Electrical Power [kW]	**Cell Area [cm^2]**	**Number of Cells [-]**	**Voltage [V]**	**Current [A]**	**H_2 flow rate [Nm^3/h]**
0.285	50	1	1.9	15 - 150	0.054
1.4	50	5	9.7	15 - 150	0.27
24.3	300	14	27	90 - 900	5
146.7	300	84	163	90 - 900	30
490.9	1250	65	130.9	375 - 3750	100

3.1.1 Realization of Water Electrolysis Projects

Currently many water electrolysis pilot plants are operational with all kind of electrolysis cell types. A good overview of current water electrolysis projects in Europe is given by Wulf et al. [79]. The technology readiness level of the different cell types range from 6 - 7 for AECs and PEMECs to 5 for SOECs [79]. The installed power ranges from several kilo watt up to 600 MW for a planned alkaline electrolysis plant in France (for the year 2025). Nevertheless Smolinka et al. [80] state that about 1 to 5 GW installed electrolysis power is needed by the year 2030 the match the demand of Germany alone. The capital expenditure (CAPEX) for PEMECs today for a predicted performance of ($1\,Nm^3\,h^{-1}$)is about 7000 €, for AECs about 4000 € and SOECs about 8800 € [80]. The CAPEX is expected to drop significantly till 2050 especially for SOECs.

3.2 High Temperature Carbon Dioxide and Water Co-Electrolysis

Co-Electrolysis means the simultaneous conversion of water and carbon dioxide to hydrogen and carbon monoxide ($\rightarrow$ syngas) in solid oxide electrolysis cells (SOEC). The production of syngas is an important aspect of P2X, if hydrogen is not aimed to be the final product, but further thermo-chemical processing (see Sections 3.3, 3.4 and 3.5) is planned. A deeper

inside into Co-Electrolysis with SOECs is given by Zheng et al. [81], Graves et al. [82] and Wang et al. [83]. Figure 3.7 shows the working principle of Co-Electrolysis in SOECs.

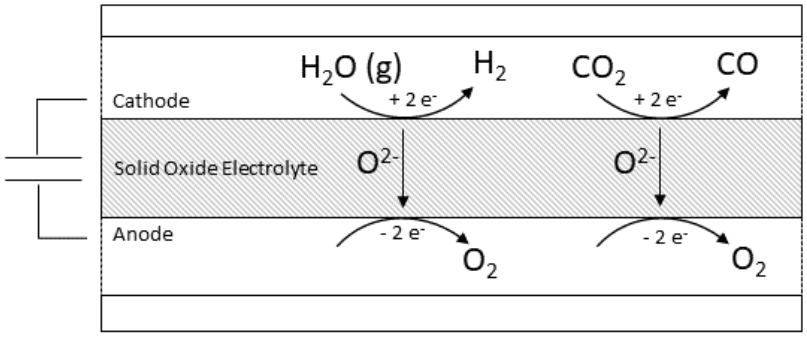

Figure 3.7: Schematic overview of CO_2 and water Co-electrolysis in a solid oxide electrolysis cell

At the cathode water is activated by two electrons, splitting into hydrogen and O_2^-. It is not fully understood if CO is formed after an electrochemical activation of carbon dioxide or by a water gas shift (WGS) reaction. According to Graves et al. [82] it is assumed that because of the high temperatures above 850 °C CO is mainly produced from RWGS.

Water splitting:

$$H_2O + 2\,e^- \longrightarrow H_2 + O_2^-$$

Electrochemical CO_2 reduction:

$$CO_2 + 2\,e^- \longrightarrow CO + O_2^-$$

Reverse water gas shift:

$$CO_2 + H_2 \longrightarrow CO + H_2O$$

Oxygen is released at the anode, where O_2^- is oxidized to O_2, releasing two electrons.

$$O^{2-} \longrightarrow \frac{1}{2}\,O_2 + 2\,e^-$$

The electrolyte is made of Yttria-stabilized zirconium (YSZ), which is a ceramic material of zirconium dioxide (ZrO_2) with added yttrium oxide (Y_2O_3) to be stable at room temperature. At the cathode Ni particles are added as catalyst (Ni-YSZ). Anodes are mostly made of a LSM-YSM[2] composite. Co-Electrolyzers are currently researched by several groups.

[2]LSM: lanthanum strontium manganite

Reytier et al. [84] describe an achieved current density of $-0.8\,\mathrm{A\,cm^{-2}}$ at 1.15 V (operation temperature: 800 °C). With an inlet gas composition of 0.65 H_2O, 0.25 CO_2 and 0.1 H_2 a conversion rate of 52 % is measured. This leads to a syngas production of $0.34\,\mathrm{Nm^3\,h^{-1}}$ at 80 A. Alenazey et al. [85] also achieved a current density of $-0.8\,\mathrm{A\,cm^{-2}}$ at cell voltages lower than 1.4 V. They noted a linear increase of CO with the current density, assuming that at least some CO_2 is converted through an electrochemical mechanism. Also more and more demonstration plants of high-temperature Co-Electrolysis plants are operational. Sunfire GmbH realized a 10 kW Co-electrolyzer capable of producing $4\,\mathrm{Nm^3\,h^{-1}}$. It is currently tested at the Karlsruhe Institute of Technology (KIT) in combination with carbon dioxide air capture and subsequent Fischer-Tropsch-Synthesis for synthetic fuel production [86, 87](see also Section 3.5). The project Reticus by Evonic and Siemens uses CO2-to-CO-Electrolysis to produce syngas in a first step. Afterwards syngas is fermented to alcohols like butanol and hexanol [88].

3.3 Methanation

Methanation refers to the production of methane from hydrogen and carbon monoxide or carbon dioxide. In general two possible process routes are available: biological or thermo-chemical. In this section only the thermo-chemical production is considered.

Methane is used for many technical applications, as it is the main part of natural gas. It is mostly used for power and heat generation through combustion, but is also applied in the mobility sector (gas engines). Hence methane today is an important energy carrier, but is is also a very potent greenhouse gas if released to the atmosphere purely[3] and the burning of fossil methane increases the overall amount of carbon dioxide in the atmosphere.

If carbon dioxide is used to produce synthetic methane, often referred as synthetic natural gas (SNG), a closed carbon loop is possible. This makes SNG interesting for a fast reduction of carbon dioxide emissions of different sectors, a all existing infrastructure (gas pipelines, cavern storage, gas turbines) could be re-used without any restrictions.

The formation of methane is possible from syngas (CO-methanation) and also directly from a CO_2 and hydrogen mixture (CO_2-methanation), also called Sabatier-Reaction.

[3] This effect is visible at the thawing of permafrost soil due to increased temperatures in the arctic. The thawing releases bounded methane in the atmosphere which itself accelerates global warming (see https://climate.nasa.gov/news/2785/unexpected-future-boost-of-methane-possible-from-arctic-permafrost/)

CO-methanation:

$$CO + 3\,H_2 \rightleftharpoons CH_4 + H_2O \qquad \Delta H^{\ominus} = -206\,\mathrm{kJ\,mol^{-1}}$$

Sabatier-Reaction:

$$CO_2 + 4\,H_2 \rightleftharpoons CH_4 + 2\,H_2O \qquad \Delta H^{\ominus} = -164\,\mathrm{kJ\,mol^{-1}}$$

The existence of CO and CO_2 is also related to each other by the water gas shift reaction (WGS) and the reverse water gas shift reaction (RWGS).

$$CO_2 + H_2 \rightleftharpoons CO + H_2O \qquad \Delta H^{\ominus} = 41\,\mathrm{kJ\,mol^{-1}}$$

The equilibrium of the involved species water, hydrogen, carbon monoxide, carbon dioxide and methane changes with the reaction conditions. To catalyze the reaction mostly nickel is used. The reaction kinetic is famously described by Xu and Froment [89, 90].

The reactor itself is mostly put into practice as a multi-stage adiabatic fixed bed reactor, which have a high TRL of 9 [91] and represents the simplest reactor design. Challenges with this reactor type arise with the occurring of temperature hot spots. Many other reactor types for the methanation are currently researched, e.g. cooled fixed bed reactors (polytropic reactors) or fluidized bed reactors.

The working principle of an adiabatic fixed-bed methanation reactor system is shown in figure 3.8.

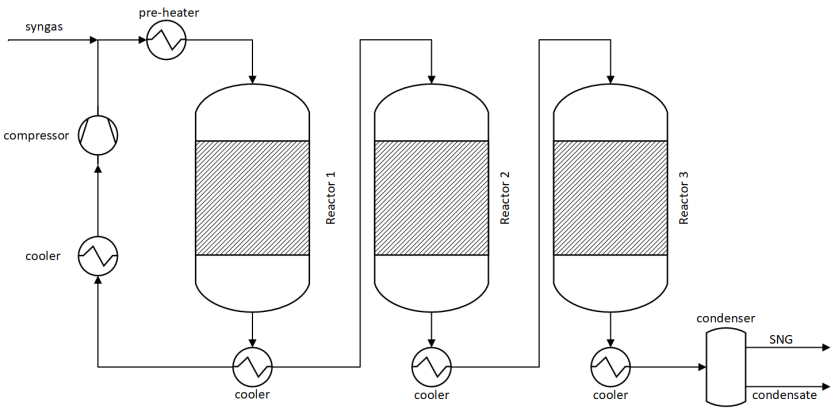

Figure 3.8: Schematic view of an adiabatic fixed-bed methanation reactor system (adapted from [91])

Adiabatic fixed-bed reactors are operated at a pressure of about 10 to 30 bar.

Concerns for the integration of methanation reactors into an energy systems are that a steady feed of hydrogen and carbon dioxide must be provided. As a hydrogen source water electrolysis is the most obvious option. As today carbon dioxide separated from biogas is the most prominent CO_2 source for methanation. Currently operational methanation plants with water electrolysis have an average power of 380 kW per facility and reach an efficiency of about 41% (electricity-to-methane) [92].

Reviews of current methanation projects are given by Roesch et al. [91] and Thema et al. [92]. An example for a very large project is the MAN power-to-gas plant for Augsburg. An alkaline electrolysis system with 4 MW nominal electrical power input is combined with an methanation plant capable of producing 150 kg of methane per hour [93]. At the lower end of the plant size spectrum, the integration of methanation systems into residential buildings is also possible. Such systems allow the storage of excess electrical energy from PV and demand driven reconversion to electricity and heat[4].

3.4 Methanol Synthesis

Methanol (CH_3OH) is also a very versitile energy carrier as it could be used for fuel cells (Direct Methanol Fuel Cell) or for blending liquid fuels. Currently EU regulations allow 3% of added methanol to gasoline, but fully methanol fueled vehicles are also possible. Methanol is also used in the chemical industry or further synthesis to liquid fuels (Dimethylether, Methanol-to-gasoline (MtG)[5]). Just like methanation, methanol synthesis can take place via a CO_2 or a CO process route.

CO_2 process route:

$$CO_2 + 3\,H_2 \rightleftharpoons CH_3OH + H_2O \qquad \Delta H^{\ominus} = -40.9\,\mathrm{kJ\,mol^{-1}}$$

CO process route:

$$CO + 2\,H_2 \rightleftharpoons CH_3OH \qquad \Delta H^{\ominus} = -90.7\,\mathrm{kJ\,mol^{-1}}$$

[4] https://www.carboncommentary.com/blog/2017/7/24/exytron-the-worlds-first-power-to-gas-system-with-integrated-co2-collection-and-reuse

[5] Methanol-to-gasoline process was developed in the 1970s by Mobil. In a first step DME is synthesized from MeOH. Afterwards DME and MeOH are dehydrated and form light olefins which oligomerize into higher olefins (up to C_{11}) [94]

Again RWGS plays a role for converting CO_2 to CO

$$CO_2 + H_2 \rightleftharpoons CO + H_2O \qquad \Delta H^{\ominus} = 41\,\mathrm{kJ\,mol^{-1}}$$

The methanol synthesis takes place at reaction temperatures of 200 °C to 300 °C at a pressure of about 100 bar. For the catalysis mostly copper and zinc oxides (CuO-ZnO-Al_2O_3) are used. For a deeper inside into the catalysis and thermodynamics of the methanol synthesis see Hus et al. [95]. The reactor system assembly, shown in figure 3.9, resembles the structure of a methanation system. The product gas must be recycled into the reactor as it still contains a high share of CO_2 due to low yields of methanol. The condensed product is finally distillated to get pure methanol. For reactor modeling aspects see Arab et al. [96] and Adji et al. [97].

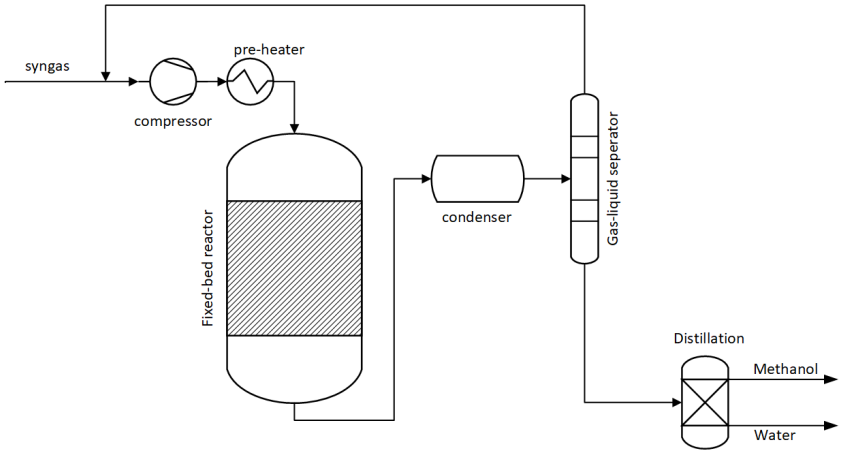

Figure 3.9: Schematic view of a fixed-bed methanol synthesis reactor system (inspired by [98])

There are currently some ongoing projects targeting at renewable methanol synthesis. The EU project Methanol-from-CO2 (MefCO2) was finalized in June 2019[6]. It realized a demonstration plant which is able to produce about 1 ton of methanol per day and capturing 1.5 tons of CO_2 per day from exhaust gases. An example for a commercially operated methanol synthesis plant is the system from Carbon Recylcing International in Iceland. It produces methanol with CO_2 from industrial emission gases and hydrogen from a 6 MW electrolysis plant, leading to a production rate of 4000 tons of methanol per year.

It is also possible to synthesize methanol directly from carbon dioxide through an electro-

[6] http://www.mefco2.eu/

chemical process route.

$$CO_2 + 6\,e^- + 6\,H^+ \longrightarrow CH_3OH + H_2O$$

Electrochemical methanol synthesis is however still far from practical application according to Albo et al. [99].

3.5 Fischer-Tropsch-Synthesis

The Fischer-Tropsch(FT)-synthesis is a chemical process to gain a mixture of hydrocarbons (alkanes, alkenes, alcohols) from syngas.

$$CO + 2\,H_2 \longrightarrow (-CH_2-) + H_2O \qquad \Delta H^{\ominus} = -152\,\mathrm{kJ\,mol^{-1}}$$

This process is usually done witch CO as the carbon source. If a carbon dioxide rich syngas is used for the FT-synthesis, CO must be produced from RWGS. The challenges arising with CO_2 as carbon source for FT-sythesis is described by Kaiser et al. [100]. FT-synthesis was developed in the 1920s. With the beginning of massive oil drilling after WW2, the FT-Synthesis was not further developed as it was no longer economical reasonable. Nevertheless FT-Synthesis could play a bigger role in the near future as the burning of fossil fuels must be drastically reduced to reach climate goals, but for some applications eg. commercial aviation, alternatives are not on the horizon. For carbon dioxide neutrality the syngas must be produced renewable, either from biogas reforming or Co-Electrolysis. As catalysts mostly iron or cobalt are used [101]. The reaction temperature reaches from 200 °C to 300 °C at pressures of 10 to 60 bar. The product output depends on the chain length of the synthesized hydrocarbons and follows an Anderson-Schulz-Flory distribution:

$$W_n = n \cdot \alpha^{n-1}(1-\alpha)^2 \tag{3.7}$$

Where n represents the amount of chained carbon atoms in the product and α the probability of propagation, leading to W_n, which is the weight fraction of the product with chain length n. Figure 3.10 shows the plotted sum of weight fractions for gasoline ($n = 5-11$), kerosene ($n = 10-16$) and diesel ($n = 12-18$) over α. The factor α could be controlled by changing reaction conditions and by the choice of the catalyst [102].
Figure 3.11 shows a simplified flow diagram for the FT-process. As reactor technologies often fluidized-bed reactor (high-temperature FT-synthesis) or fixed-bed reactors (low-temperature FT-synthesis) are chosen. The individual liquid fuels are gained from the product mixture by subsequent hydrocracking.
Existing or planned FT-plants are mostly large scale HT applications with production rates up

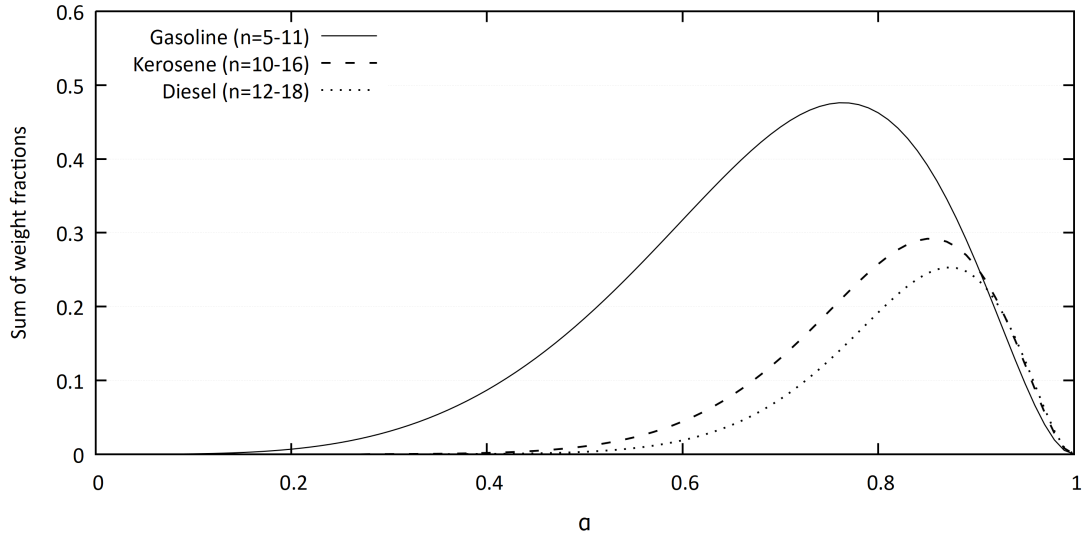

Figure 3.10: Sum of weight fractions over α for gasoline, kerosene and diesel

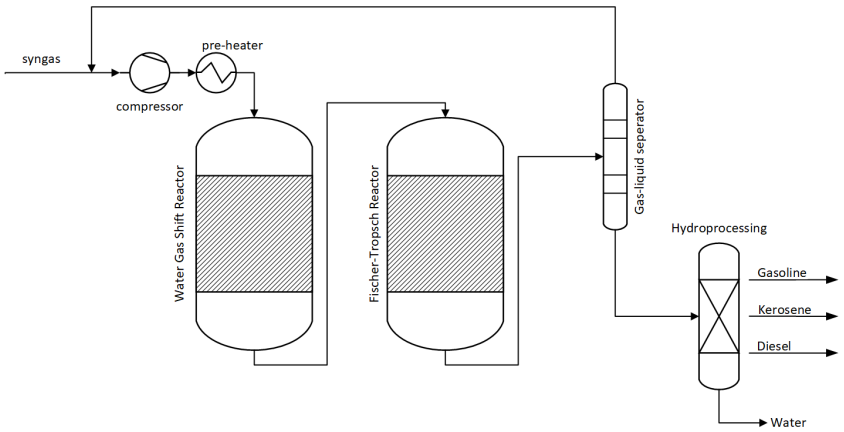

Figure 3.11: Simplified flow diagram for a Fischer-Tropsch process

to 1400000 bpd[7] [103]. The currently used reactor technology is not suitable for decentralized small or medium scale applications. However, according to Guettel et al. [103] new reactor technologies like microstructured or membrane reactors could make FT-synthesis suitable for downsized applications. FT-synthesis is also suitable for a coupling with electrolysis. Especially a coupled syngas production from Co-Electrolysis is offering interesting energy conversion options. In a simulation study by Becker et al. [104] such a coupled system of a SOEC for syngas production and FT synthesis was investigated. The overall system efficiency was found to be 54.8 %. One research project including FT-synthesis is the project P2X,

[7]barrels of oil per day

which is supervised by the Karlsruhe Institute of Technology (KIT). It investigates a combined system of carbon dioxide direct air capture, co-electrolysis, FT-synthesis and hydrockracking. The system is able to produce 10 L of fuel per day and a theoretical efficiency of 60% [87]. All in all large scale implementation FT-synthesis could contribute to a fast reduction of carbon dioxide emissions especially in the mobility sector with state-of-the-art combustion engines (E-fuels). Nevertheless promising alternatives to combustion engines (fuel cells, batteries) arise in all sectors (except aviation). Hence it should be considered to use valuable FT-synthesis products for applications without arising technological replacements for the combustion of liquid hydrocarbons.

3.6 Systems with other carbon based P2X products

Theoretically many different carbon based products are available through P2X. As a supplement to the above introduced technologies which were identified as most relevant, two further P2X systems will be introduced briefly at this section: the electrochemical ethanol synthesis and DME synthesis.

Ethanol ($CH_3{-}CH_2{-}OH$) is currently already used as a fuel additive. In the EU an blending of 5% ($\rightarrow$ E5) or 10% ($\rightarrow$ E10) is common. An electrochemical conversion of carbon dioxide to ethanol by a twelve electron transfer is reported by Song et al. [105].

$$2\,CO_2 + 9\,H_2O + 12\,e^- \longrightarrow C_2H_5OH + 12\,OH^-$$

A carbon nanospike electrode (CNS) with Cu nanoparticles was therefor used. The catalyst showed a higher activity for CO_2 reduction than for H_2 evolution[8].

Dimethylether (DME, see Figure 3.12) is a non-toxic liquid and regarded as alternative fuel for mobile applications. Catizzone et al. [106] are giving an overview of CO_2 recycling to DME.

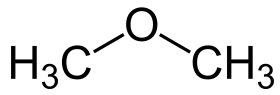

Figure 3.12: Dimethylether (DME) molecular structure

The synthesis of DME from CO_2 rich syngas (CO_2-to-DME) mostly includes methanol as

[8]The catalyst was commercially licensed in 2019 and the product named Electric Ethanol™(http://www.reactwell.com/services-and-products/ethanol/)

intermediate.

$$CO_2 + 3\,H_2 \rightleftharpoons CH_3OH + H_2O$$

$$2\,CH_3OH \rightleftharpoons CH_3OCH_3 + H_2O \qquad \Delta H^{\ominus} = -23.4\,\mathrm{kJ\,mol^{-1}}$$

A promising future option is a one-step DME synthesis from CO_2 and H_2 with zeolites [106]

3.7 Storage and Transportation of Power-to-X-Products

One of the main advantages of P2X compared to pure electrification is that its products, either gaseous or liquid, could easily be stored even over long periods of time. Most often the necessary infrastructure already exists. Methane could be stored and distributed via the gas grid and intercontinentally shipped as LNG. All liquid products could be stored in tanks and transported on tank cars. One exception regarding storage ability is hydrogen, for which more complex storage and transportation technologies must be applied due to its high diffusivity, its low volumetric energy density and non.existent infrastructure. These characteristics require hydrogen to be stored e.g. as compressed gas. In this section different technologies for hydrogen storage are presented. Later in this work, formic acid based hydrogen storage is introduced as a promising alternative to state-of-the-art hydrogen storage.

3.7.1 Hydrogen Storage

Hydrogen storage is always considered as a major hurdle towards an effective hydrogen infrastructure [14]. Following, a brief summary of chosen hydrogen storage methods are given[9].

3.7.1.1 Physical Hydrogen Storage

Compressed Hydrogen The state-of-the-art hydrogen storage technology is the compression of gaseous hydrogen in a range of 17 bar up to 700 bar for automotive systems[10]. Compression is necessary due to the relative low volumetric energy density of uncompressed hydrogen, which is especially disadvantageous for mobile applications. The compression itself consumes about 20% of the energy amount stored in the compressed hydrogen volume [107]. Problems arise because hydrogen as a small molecule has a high diffusivity through all kinds of materials leading to losses. Also the storage of gas at 700 bar includes safety issues (bursting of the pressure vessel). If the compression of hydrogen is considered isothermal[11] and

[9] This selection aims at giving a fast overview and does not claim to be complete. Many more hydrogen storage options are thinkable and currently discussed

[10] Even higher pressures are required for fueling stations

[11] Approximately true for stepwise compression

the ideal gas law (Equation 3.9) is supposed to be valid, the compression work could be calculated as follows[12]:

$$dW = \int_1^2 V \cdot dp \tag{3.8}$$

$$p \cdot V = m \cdot R_s \cdot T \tag{3.9}$$

For a given storage device, the gas volume is assumed to be constant. Therefor, from these two equations results the following equation for the needed work for a compression from pressure level p_1 to pressure level p_2:

$$dW = m \cdot R_s \cdot T \int_1^2 \frac{1}{p} \cdot dp$$

Truncating the equation by the mass leads to the specific compression work w needed per kg hydrogen:

$$dw = R_s \cdot T \int_1^2 \frac{1}{p} \cdot dp$$

Solving the integral finally leads to the following equation:

$$dw = R_s \cdot T \cdot \ln\left(\frac{p_2}{p_1}\right) \tag{3.10}$$

At higher pressures or higher temperatures the ideal gas law is no longer valid. The compressibility factor Z corrects the differences between ideal and real gas behavior.

$$dw = ZR_s \cdot T \cdot \ln\left(\frac{p_2}{p_1}\right) \tag{3.11}$$

Z could be calculated with a polynomial fitting described by Zheng et al. [108] with data from NIST. The results for a hydrogen compression at 298 K are shown in Figure 3.13 for hydrogen as an ideal gas and corrected with Z.
Besides safety issued other concerns are the design and material choice for high pressure hydrogen tanks. Although high-pressure storage is the de facto standard for automotive applications, for stationary applications lower pressures are chosen[13]. On overview of high-pressure hydrogen storage is given by Zheng et al. [110].

High compression ratios from atmospheric pressure to storage pressure, require multi-stage

[12] Note that using the ideal gas law is only a rough approximation for the specific energy needed for compression, but could be considered as adequate for low pressures. Especially for higher pressures above 100 bar other models for the equation of state are more accurate

[13] around 20 bar to 200 bar e.g. for hydrogen filling stations [109]

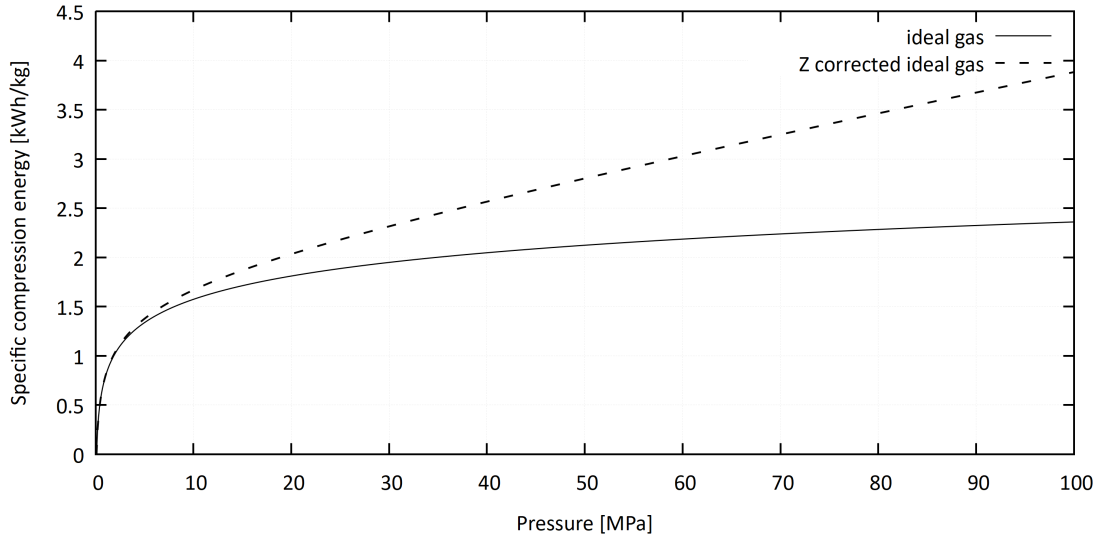

Figure 3.13: Specific energy needed for hydrogen compression at 298 K

compressors. Linde uses a 5 step ionic-liquid piston compressor for hydrogen compression up to 90 MPa. It is used for hydrogen fueling stations and consumes about 2.7 kWh/kg for 70 MPa fueling [111]. Another possibility for hydrogen compression are electrochemical hydrogen compressors (EHC), e.g. developed by HyET [112]. Advantages of this technology ist that it has no moving parts and could also be used to separate hydrogen from a gas mixture. In this sense high H_2 purity is achieved with N_2 and CH_4 as contaminant [113]. Figure 3.14 shows the working principle of an EHC. It could be seen from this illustration that EHCs are based on PEM cells.

Liquified Hydrogen The second physical hydrogen storage option, after compression, is liquefaction. Hydrogen must be cooled to 20 K to be stored as a liquid (LH_2). It is used if large energy densities are needed, e.g. LH_2 is used as a rocket propellant[14]. For shipping hydrogen over long distances liquefaction is also an option. The specific energy consumption for liquefaction is about 13- 15 kWh/kg [114].

3.7.1.2 Chemical Hydrogen Storage

Besides the physical storage of hydrogen as compressed gas or liquefied hydrogen it is also possible to store hydrogen by forming chemical bounds. In this section two chemical H_2 storage options are mentioned: metal hydrides and hydrogen storage in molecules.

[14]Today LH_2 is often replaced by RP-1, a kerosene variation, which has a higher density and does not require cooling

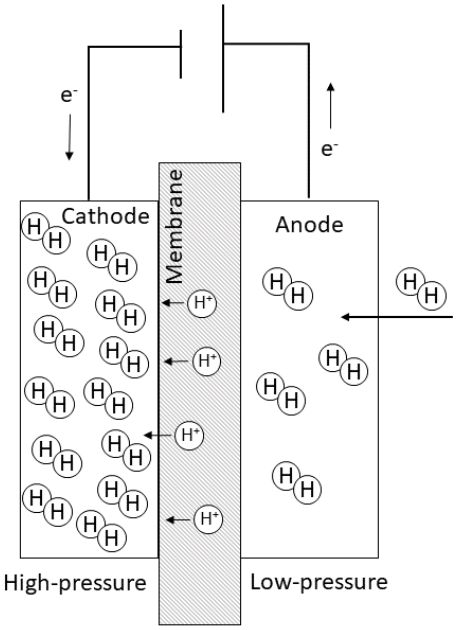

Figure 3.14: Electrochemical Hydrogen Compression

Metal hydrides Metal hydrides are compounds of hydrogen and metals. They allow a safe and high-density hydrogen storage. Also newer developments show that metal hydrides are also a possible hydrogen compression technology. Up to 200 bar are possible by directly converting thermal energy into hydrogen compression [115]. One metal compound which is suitable for hydrogen storage is sodium aluminium hydride $NaAlH_4$. The unloading and loading reaction could be described as follows:

$$3\,NaAlH_4 \rightleftharpoons Na_3AlH_6 + 2\,Al + 3\,H_2$$

$$Na_3AlH_6 \rightleftharpoons 3\,NaH + Al + \frac{3}{2}\,H_2$$

For the first reaction the specific enthalpy for the hydrogen absorption is $\Delta H_{abs} = -35.2\,\mathrm{kJ\,mol^{-1}}$ and $\Delta H_{des} = 38.4\,\mathrm{kJ\,mol^{-1}}$ for the desoprtion [115] and $\Delta H_{abs} = -46.1\,\mathrm{kJ\,mol^{-1}}$ and $\Delta H_{des} = 47.6\,\mathrm{kJ\,mol^{-1}}$ for the second reaction. Most metal hydrid systems need temperatures above 100 °C to release hydrogen.

Hydrogen storage in molecules Storing hydrogen in molecules offers some advantages as the produced compounds are often long-term stable, which is important for seasonal storage, and most often are liquid under ambient conditions which make them are easy

to handle and transportable. This form of hydrogen storage requires a hydrogenation and dehydrogenation reaction of a carrier molecule (hydrogen carrier) as shown in figure 3.15. After dehydrogenation the released hydrogen could be used in all kinds of technical hydrogen applications. A carrier molecule should have a high weight percent (wt%) of bounded hydrogen and be able to release hydrogen under moderate conditions.

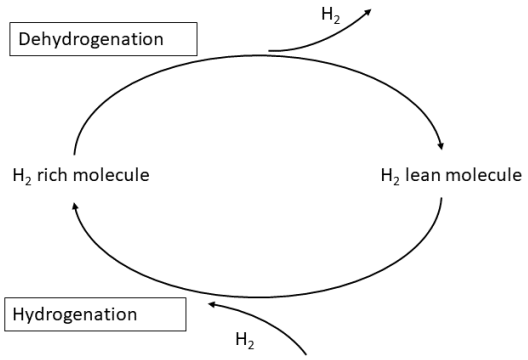

Figure 3.15: Hydrogenation and dehydrogenation of a hydrogen carrier

One compound discussed for the use as a hydrogen carrier is the focus of this thesis: formic acid. Formic acid has a hydrogen content of 4.4 wt%. It is further discussed in Chapter 4. Wasserscheid et al. describe a hydrogen system based on so called liquid organic hydrogen carriers (LOHC) [116–118]. In this case the carrier molecule is dibenzyltoluene (DBT). Loaded DBT has an hydrogen content of about 6.2 wt% which corresponds to an energy content of approximately 2.05 kW h kg^{-1} [119]. Figure 3.16 shows the hydrogenation and dehydrogenation of DBT. To make a dehydrogenation reaction redundant, it is investigated to use LOHCs directly in SOFCs for a combined heat and power generation [120].

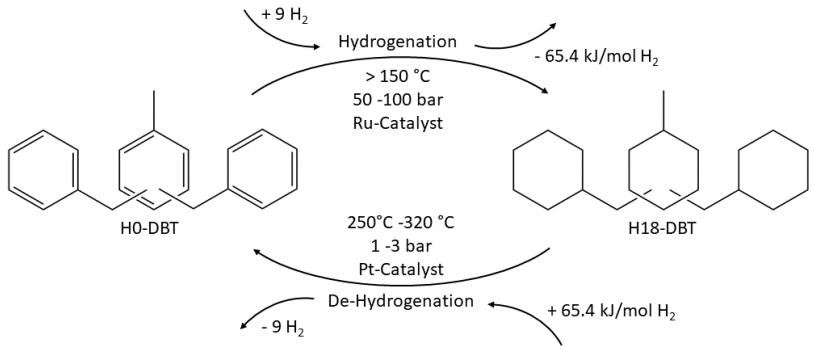

Figure 3.16: Hydrogenation and de-hydrogenation of Dibenzyltoluene (adopted from [119])

3.7.1.3 Hydrogen blended into the Gas Grid

A different hydrogen storage and distribution option, especially for stationary P2G applications, is blending hydrogen into the existing natural gas network. In this way the use of expensive local H_2 storage technologies is not required. The gas grid itself represents a huge energy storage capacity. In Germany all in all 47 underground gas caverns show a capacity of 230 TWh, the gas network pipes additional 130 TWh [121]. However some restrictions of the gas composition in the grid exist. According to a study from the NREL [122] these restrictions are bases on:

- Safety
- Material durability
- Leakage
- Impact on end-user systems

In Germany the threshold for hydrogen within the gas grid produced via electrolysis is by law at 5 vol-%[15] [123]. An increase to 10 vol% is planned. However the DIN 51624 states that the limit of hydrogen in tanks of gas engine vehicles is at 2 vol-%. It also seems that storing hydrogen rich gas in underground cavern is problematic due to increased growth of sulfate reducing bacteria and hence is limited to 5 vol-% [123]. The limits for H_2 blending are summarized in Figure 3.18. Another issue is that gas turbine manufactures must work on improvements to allow higher hydrogen concentrations in the fuel gas. The most relevant disadvantage of blending hydrogen into the natural gas grid is that the relative savings of carbon dioxide emissions do not correspond linearly to the share of hydrogen in the gas mixture (see Figure 3.17). This effect is caused by the lower heating value of hydrogen compared to natural gas, which leads to a overall increased gas consumption to match the same amount of heat.
For now there is no agreement of the hydrogen allowed in the gas grid for the European Union [124]. In many member countries no hydrogen blending is allowed at all. The EU funded project HyLAW[16] aims at removing legal barriers and adjust regulations of hydrogen blending throughout the participating countries. Concerncing the United States the NREL state that a hydrogen concentration of 5 to 15 vol-% is feasible with some improvements in the gas infrastructure (e.g. pipeline materials and end-user devices) [122].
A profound overview over current H_2 blending projects, as well as economic and modeling aspects is given by Quarton et al. [125].

[15] Unlimited for synthetic Methane
[16] https://www.hylaw.eu/

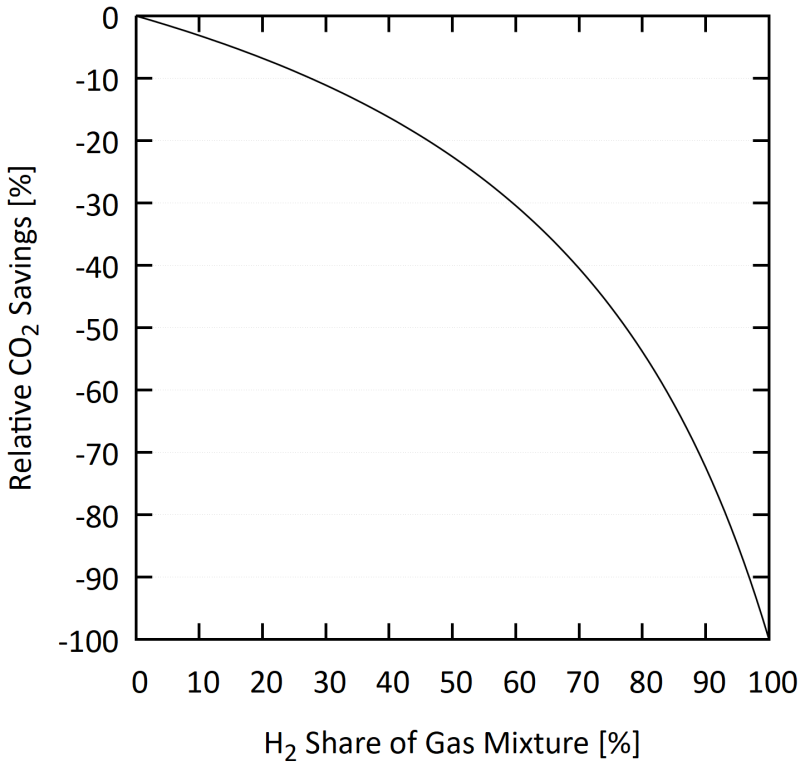

Figure 3.17: Relative savings of carbon dioxide emission based on the share of hydrogen in the gas grid

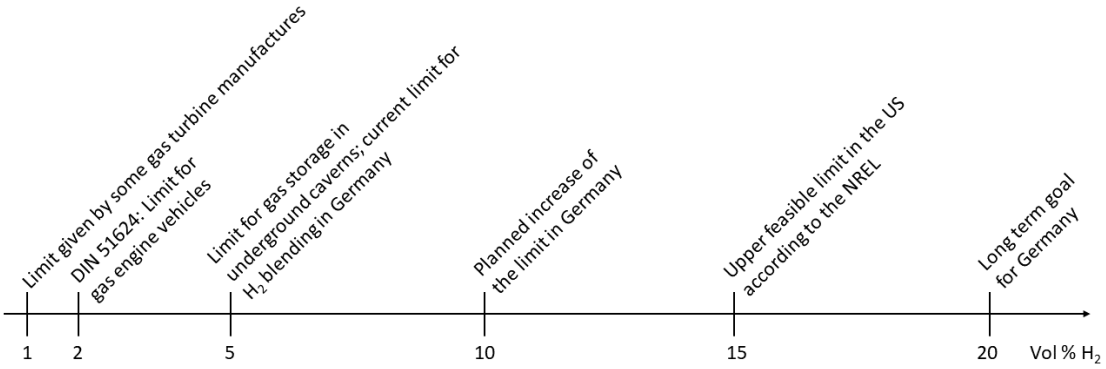

Figure 3.18: Limits for Hydrogen Blending to the Natural Gas Network (data derived from [123] and [122])

3.7.1.4 Comparison of Hydrogen Storage Options

Table 3.3 summarizes the most common methods for hydrogen storage. As high pressure hydrogen storage could be considered as state-of-the-art it is later on used in this work for a reference system. The main focus of this thesis lays on the utilization of formic aid as a molecular hydrogen carrier. Other hydrogen storage technologies are not further considered.

Table 3.3: Comparison of hydrogen storage technologies

Hydrogen Storage Technology	**Implementation Obstacles**
High Pressure Storage (25 to 80 MPa)	Explosion hazard may lead to acceptance issues
Liquefied Hydrogen (-253 °C)	High energy losses for hydrogen liquefaction, costly infrastructure
(Metal) Hydrides	Low gravimetric energy density, poor transportability
Feeding into the natural gas grid (up to 20 vol.-%)	Hydrogen is present as a gas mixture, for many applications (e.g. fuel cell) not suitable
Feeding into a pure hydrogen grid	New construction of network infrastructure or major adjustments to existing gas networks required
Molecular Hydrogen Carriers (LOHC, Methanol, Formic Acid)	Low TRL, possibly insufficient dynamic

3.8 Re-conversion of P2X products

The purpose of P2X is to decarbonize heat and power generation, mobility as well as industries. In this sense, P2X products, which are not used for industrial processes, must be reconverted to heat, electricity or propulsion. Therefor two fundamental concepts are possible: the smooth, but technological challenging route is the electrochemical re-conversion in fuel cells. The more approved but 'dirtier' route is the burning of P2X products in all kinds of combustion devices. As the focus of this work lays on the usage of PtX for stationary energy conversion, the following descriptions refer to stationary applications. Nevertheless where suitable some remarks on mobile applications are made. The direct utilization of P2X products include e.g. the synthesis of ammonia with hydrogen (Haber process; see the following reaction equation) or the use of formate as a de-icing agent for airports and roads.

$$N_2 + 3\,H_2 \longrightarrow 2\,NH_3 \qquad \Delta H^{\ominus} = -91.8\,\mathrm{kJ\,mol^{-1}}$$

3.8.1 Fuel Cells

Fuel cells are basically the reverse technology compared to electrolysis. The fuel, basically a reducing agent, e.g. hydrogen, is oxidized (without combustion) and donates electrons, which are able to do electrical work when conducted through an external electrical circuit. The application area of fuel cells include domestic heating units, backup power systems, mobile applications and portable applications[17]. Figure 3.19 shows the general working principle of a fuel cell. The fuel is feed to the anode and an oxidizer to the cathode. Through a catalytic reaction electrons are released, move through an electrical circuit and do electrical work.

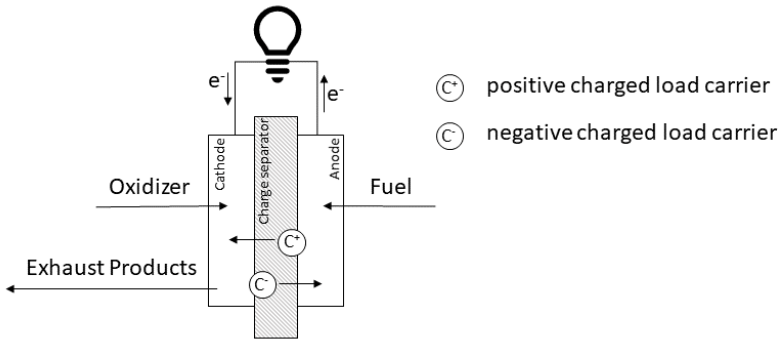

Figure 3.19: General working principle of a fuel cell

As for electrolysis cells (see sec. 3.1) the most prominent fuel cell types are:

- Alkaline Fuel Cell (AFC)
- Polymer Electrolyte Membrane Fuel Cell (PEMFC)
- Solid Oxide Fuel Cell (SOFC)

As a fuel feed for fuel cells, several P2X products are suitable, which is described in the subsequent sections.

3.8.1.1 Hydrogen Fuel Cells

The general reaction equation of a hydrogen fuel cell is:

$$H_2 + \frac{1}{2} O_2 \longrightarrow H_2O$$

[17]Some more uncommon applications for fuel cells include the powering of hearing aids and the generation of electricity with glucose from human blood [126, 127]

This equation directly shows one often discussed advantage of H_2 fuel cells: the only (local) emission is water[18]. Regarding the mobility sector, the operation of fuel cell vehicles hence contribute to a improvement of the air quality as no nitrogen oxides are emitted. Large stationary hydrogen fuel cell stacks are discussed for balancing load fluctuations in the electricity grid. Medium or small stacks on the other hand could be operated as home heating systems. Such H_2 fuel cell home heating system are more and more commercialized. State-of-the-art PEMFC systems gain the needed hydrogen by steam reforming of natural gas (see Section 2.1.1.1). Thereby it is necessary to be aware of a thorough carbon monoxide removal, as CO poisons the membrane of PEMFCs[19]. Compared to gas boilers FCs produce heat and electricity combined and hence allow more options for the integration into the building energy concept.

3.8.1.2 Fuel cells using liquid C1-substances

Besides the already mentioned hydrogen fuel cells, several other P2X products could be reconverted with fuel cells and are currently under investigation. A common term for such fuel cells is 'Direct Liquid Fuel Cell' (DLFC). Table 3.4 summarizes some DLFCs for the liquid C1-substances methanol, formic acid and formate[20]. Storage and handling of gaseous hydrogen could be avoided through the usage of liquid C1-fuels. Also liquid fuels usually have higher volumetric energy densities[21]. Drawbacks include the complex catalysis, issues with fuel crossover and unproven long-term durability [128]. As today, DLFCs are hardly a comercial ready option for large scaled heat and power generation. Profound reviews of DLFCs are given by Ong et al. [128] and Demirci [129].

Table 3.4: Fuel cells for C1-substances

Fuel Cell Type	**Fuel**	**Electrolyte**	**Reference**
Direct Methanol Fuel Cell (DMFC)	CH_3OH	PEM	[130]
Formic Acid Fuel Cell (DFAFC)	HCOOH	PEM	[131], [132], [133], [134]
Direct Formate Acid Fuel Cell (DFFC)	K^+HCOO^-, Na^+HCOO^-	AEM[22]	[135], [136], [137], [138]

[18] Note that for a fair comparison, the emissions released through hydrogen production must be taken into account. For a fully carbon free process hydrogen must be produced through water electrolysis with renewable energy sources (Green Hydrogen)

[19] Other fuel cell types, especially SOFCs are much more tolerant to CO in the fuel gas stream

[20] There also exist fuel cells types for higher hydrocarbons (e.g. ethanol) and nitrogen based compounds (e.g. hydrazine). As these substances are not part of this work see [128] for more details

[21] MeOH: 4820 $W\,h\,L^{-1}$ vs H_2: 180 $W\,h\,L^{-1}$. Source: [128]

Direct Methanol Fuel Cells (DMFC) are the most common DLFCs. At the anode currently most often Pt-Ru is used to catalyse the following reaction [128]:

$$CH_3OH + H_2O \longrightarrow CO_2 + 6\,H^+ + 6\,e^-$$

Pt is known to be a good catalyst for the oxygen reduction at the cathode.

$$\frac{1}{2}\,O_2 + 2\,H^+ + 2\,e^- \longrightarrow H_2O$$

Overall this lead to the following reaction and cell potential for the DMFC:

$$2\,CH_3OH + 3\,O_2 \longrightarrow 4\,H_2O + 2\,CO_2 \qquad E^0 = 1.213V$$

It is described in literature that open circuit voltages of 0.59 V an maximum current densities of 299 mA cm^{-2} could be achieved with DMFCs. Further, a peak power density of 23 mW cm^{-2} is reported [128].

Direct Formic Acid Fuel Cell (DFAFC) use state-of-the-art Pd/C catalyst to catalyze the following FAFC anode reaction:

$$HCOOH \longrightarrow CO_2 + 2\,H^+ + 2\,e^-$$

The cathode reaction could be described as a reduction of oxygen to water.

$$\frac{1}{2}\,O_2 + 2\,H^+ + 2\,e^- \longrightarrow H_2O$$

Anode and cathode reaction combined lead to the following overall FAFC reaction equation:

$$HCOOH + \frac{1}{2}\,O_2 \longrightarrow CO_2 + H_2O \qquad E^0 = 1.4V$$

Rice et el. [133] operate a DFAFC at 60 °C with a Pt catalyst. They report a current density of 134 mA cm^{-2} and a power density of 48.8 mW cm^{-2}. OCVs of 0.7 V are reported. Chang et al. [139] describe a Pd-Ni_2P catalyst for the oxidation of formic acid at a DFAFC anode reaching a power density of 550 mW cm^{-2}. The DFAFC was operated at 30 °C with a 3M FA solution. The power density of this setup is about 3.5 times higher than with a Pd/C catalyst.

Direct Formate Fuel Cell (DFFC) differ from DMFCs and FAFCs, as the charge is transported through OH^- anions rather than protons H^+. This requires the use of an anion

conducting membrane.
The anode reaction of a DFFC states that formate and OH^- react to carbonate and water.

$$HCOO^- + 3\,OH^- \longrightarrow CO_3^{2-} + H_2O + 2\,e^- \qquad E^0 = -1.05V$$

At the cathode oxygen and water are forming OH^-.

$$\frac{1}{2}\,O_2 + H_2O + 2\,e^- \longrightarrow 2\,OH^- \qquad E^0 = 0.40V$$

Overall this lead to the following reaction equation for DFFCs:

$$HCOO^- + \frac{1}{2}\,O_2 + OH^- \longrightarrow CO_3^{2-} + H_2O \qquad E^0 = 1.45V$$

Usually the catholyte consists of a mixture of NaOH and NaCOOH or KOH and KCOOH. As a catalyst for the anode reaction Pt or Pd based electrocatalysts are used. DFFC reach a state-of-the-art power density of about $591\,mW\,cm^{-2}$ at an operation temperature of 60 °C [135].

3.8.2 Combustion of PtX Products

Methane could be reconverted to heat an power by combustion. Compared to hydrogen, it has a high heating value (see Figure 3.20). Methane could be used as a fuel for many different devices: from small scaled gas boilers to large combined cycle gas turbines (CCGT) for power plants. Never developments include the so-called oxy-fuel combustion, where pure oxygen instead of air is used as an oxidizer. In this case, a 50 MW demonstration facility by NET power in Texas uses a closed cycle with supercritical CO_2, heated by the combustion of natural gas and oxygen, to drive a turbine (Allam cycle). As pure CO_2 is produced through the combustion it could be easily stored or used as a resource [60, 61, 140].

To maintain grid stability in times with low yields from renewable energy sources the combustion of natural gas is, for now, unavoidable. This underlines the importance of water electrolysis and methanation as natural gas could be replaced by carbo-neutral SNG. Another approach to decarbonize gas power plants but keeping its balancing capability would be the application of hydrogen fueled gas turbines. In the mobility sector, the combustion of hydrocarbons will also still play an important role in the foreseeable future. Especially for aviation, an alternative to liquid fuels for jet engines is not on the horizon, due to the need of a propulsion system with a high energy density. To decrease carbon dioxide emissions in aviation, the use of kerosene from FT-synthesis (with CO_2 from air), maybe blended with other carbon sources like alcohols, plant parts or vegetable oils, is an promising option [141].

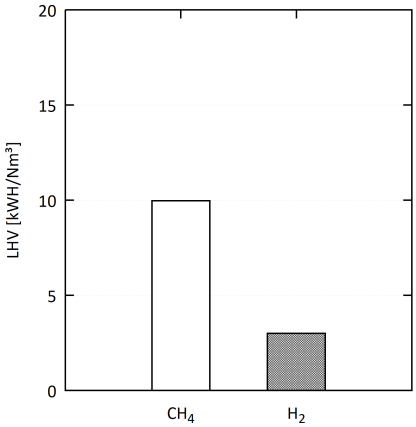

Figure 3.20: Lower heating value of methane and hydrogen

A comparable approach is also thinkable for cars or trucks with internal combustion engines (ICE). The use of gasoline or diesel from FT-synthesis blended with additives. Nevertheless for non-aviation applications, more efficient technologies (fuel cells, battery electric vehicles) are available.

3.9 Classification of Formic Acid within PtX technologies

The focus of this work lays on the utilization of formic acid as an energy carrier. In Chapter 4, three different reaction paths for formic acid are introduced: reversible hydrogen batteries, flow reactors and CO_2-electrolyzers. In this section, these reaction processes and formic acid as an energy carrier are classified an compared to the PtX processes and products described in this chapter.

Table 3.5 summarizes the PtX technologies presented in this Chapter and completes the listing with formic acid based reactions as an anticipation of the following chapters.
In this list, the reversible hydrogen battery stands out as the initial substance and the end product is the same (hydrogen). In this context, the reversible hydrogen battery could rather be included in the list of specific hydrogen storage technologies, rather than PtX. The CO_2-to-FA flow reactor can most likely be compared to methanation, methanol synthesis or FT synthesis. All those technologies use a carbon dioxide or carbon monoxide and hydrogen mixture as a initial substances and use thermal energy to drive the reaction. The CO_2-to-FA electrolysis cpuld be compared to PEM electrolysis and HT-Co-electrolysis as those technologies utilize electrical energy for the chemical process. However the CO_2-to-FA electrolysis is the only presented technology which provides a liquid product under moderate reaction

Table 3.5: Summary of PtX reaction pathways

Process	**Provided Energy**	**Initial Substance**	**Product**	**Product State**	**T [°C]**	**P [bar]**	**TRL**
PEM electrolysis	electrical	H_2O	H_2	gaseous	50 - 70	< 30	9
HT-Co-electrolysis	electrical	CO_2,H_2O	syngas	gaseous	800	≈ 13	6
Methanation	thermal	CO,CO_2,H_2	methane	gaseous	200 - 550	10 -30	9
Methanol synthesis	thermal	CO,CO_2,H_2	methanol	liquid	200 - 300	100	8
FT synthesis	thermal	CO,CO_2,H_2	gasoline etc	liquid	200 - 300	10 - 60	8
Rev. H_2 battery	thermal	H_2	H_2	gaseous	100	140	3
CO_2-to-FA flow reactor	thermal	CO_2,H_2	FA	liquid	70	100	6
CO_2-to-FA electrolysis	electrical	CO_2,H_2O	FA	liquid	30 - 70	1	5

conditions. This feature combined with the direct utilization of electrical energy brings this technology in the focus of a possible energy related application.

Table 3.6 lists the presented substances in this chapter with their main application and the described reaction path. In this context formic acid is mainly considered as a hydrogen carrier.

Table 3.6: Application and reaction path of the presented PtX products

Substance	**Main Application**	**Presented PtX Path**
Hydrogen	fuel cells, syngas production	water Electrolysis
Syngas	further synthesis of PtX products	Co-Electrolysis
Methane	gas engines, gas boiler, gas turbine	from syngas
Methanol	fuel additive, fuel cell, hydrogen carrier	from syngas
Ethanol	fuel additive	CO_2-Electrolysis
Gasoline	internal combustion engine	FT-Synthesis (syngas)
Kerosene	jet engine	FT-Synthesis (syngas)
DME	liquid fuel (diesel substitute)	from syngas
Formic Acid	hydrogen carrier (fuel cell, chemical industry, de-icing)	CO_2-Electrolysis, flow reactor

In the subsequent chapters only formic acid and hydrogen are further considered for the introduced systems.

Chapter 4

Carbon Dioxide Reduction to Formic Acid or Formate

Many currently used energy carriers are based on carbon compounds, such as natural gas, crude oil or coal. Hydrogen, besides electrification, will play a significant role at replacing these energy carriers and transforming energy systems towards green house gas neutrality. However, the large-scale use of hydrogen faces some disadvantages, such as safety and storage issues. In future energy systems carbon compounds may still be needed for specific applications (e.g. high-temperature process heat, aviation) or are used as a hydrogen carrier. If carbon dioxide extracted from the air is used a raw product to synthesise such compounds in technical processes, a closed carbon cycle could be achieved. The chain of carbon reduction from carbon dioxide to methane could be simplified as follows:

$$CO_2 \longrightarrow HCOOH \longrightarrow CH_2O \longrightarrow CH_3OH \longrightarrow CH_4$$

The focus of this work lays on the first step of carbon reduction: carbon dioxide to formic acid or formate. and an application of formic acid as a hydrogen carrier molecule. In general, the reaction equation for the reduction of carbon dioxide to formic acid looks as follows:

$$CO_2 + 2\,H^+ + 2\,e^- \longrightarrow HCOOH$$

A pair of electron is added to the carbon atom reducing it oxidation state from +IV to +II. To balance the electrical load also two protons must be added leaving HCOOH as a final product. The electrons could be transferred by two different approaches. Either from a reducing agent, like a hydrogen molecule ($H_2 \longrightarrow 2\,H^+ + 2\,e^-$) or by an electron source (cathode). This differentiation is subsequently labeled by 'catalytic carbon reduction' (CCR) and 'electrochemical carbon reduction' (ECR). Figure 4.1 shows a schematic comparison of

the two process routes.

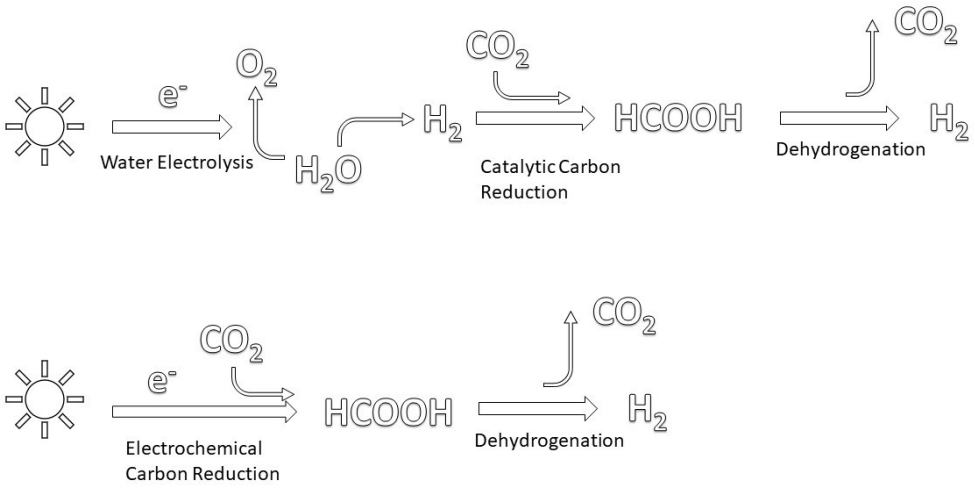

Figure 4.1: Catalytic and electrochemical carbon reduction

One major difference between the two options is that for the CCR a electron spending substance has to be provided. If hydrogen is used, CCR could be considered as a chemical hydrogen storage system, as the reverse reaction (formic acid dehydrogenation) releases usable hydrogen.

$$CO_2 + H_2 \rightleftharpoons HCOOH$$

If water electrolysis is used to generate hydrogen from renewable energy sources and the carbon dioxide is extracted from air, this process is a completely carbon neutral way for a long-term energy storage application. In an ECR process electrons could directly be used from a renewable energy source. The intermediate step via water electrolysis could therefor be saved.

This chapter begins with a presentation of the possible application of formic acid as a hydrogen carrier molecule. Afterwards both process routes of carbon dioxide to formic acid are shown. For both routes, the reactor components, usable catalysts and reactor design are discussed. Also, the processing of the reaction product for an energy application and the hydrogen generation from formic acid is shown.

4.1 Application of Formic Acid as a Hydrogen Carrier

The long-term storage of hydrogen is a technical challenge. A comparison of different hydrogen storage technologies for seasonal energy storage applications are carried out in Section 3.7.1.4. Molecular hydrogen carriers overcome some drawbacks compared to other hydrogen storage options. In general they avoid the large-scale storage of pressurized gases and show a good transportability and scalability. Formic acid is a non-flammable, non-toxic liquid under ambient conditions a could therefor be stored non-pressurized. As a liquid it could easily be transported using existing infrastructure, such as tank trucks. This allows an interregional and intercontinental trade and exchange of excess energy produced by renewable energy sources.

Formic acid contains 4.4 wt.-% of hydrogen. In most technical applications formic acid is not available as a pure substance, but in aqueous solution or as formate. Figure 4.2 shows the volumetric density of pure formic acid, different formic acid concentrations in aqueous solution and formate compared to pressurized hydrogen, other molecular hydrogen carriers and lithium ion batteries.

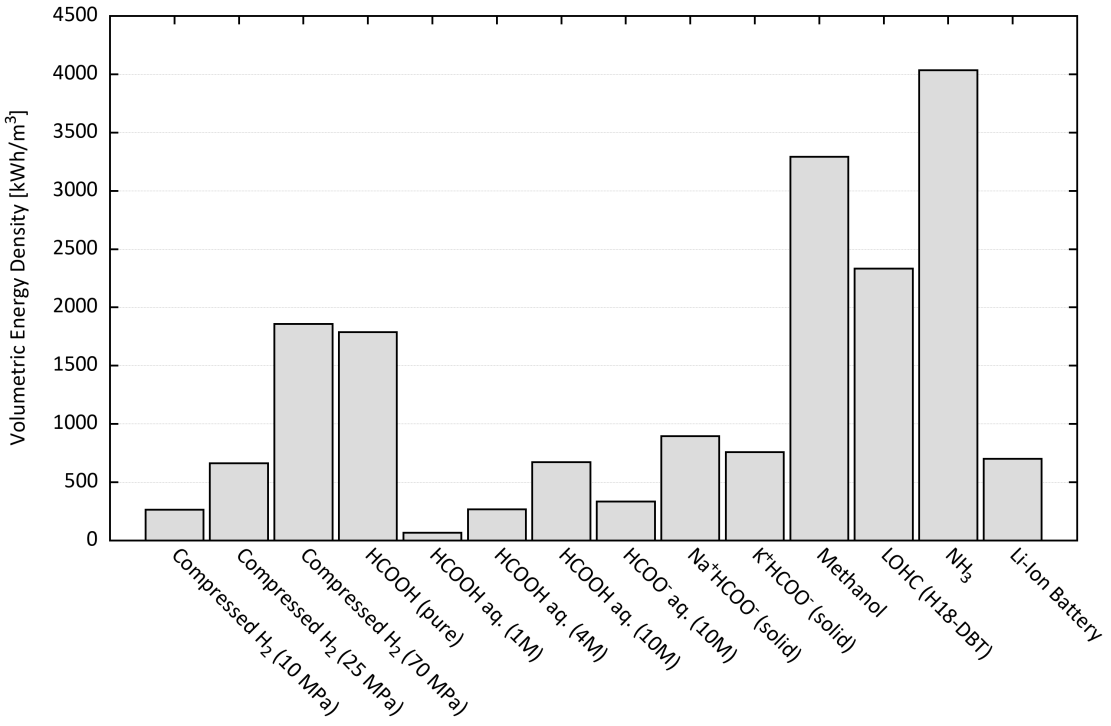

Figure 4.2: Volumetric energy density of formic acid compared to compressed hydrogen and other hydrogen carriers

At a concentration of 10M, the energy density of an aqueous formic acid solution is in the range of pressurized hydrogen at 25 MPa and lithium ion batteries, which makes it suitable for an energy storage application. For a comparable energy density as pressurized hydrogen at 10 MPa, a formic acid concentration of 4M is needed. This concentration could be considered as the lower bound of technical usability. Lower concentrations, as well as formate solutions, are insufficient for storage applications with regard to the energy density. From this bar chart it it also visible that other possible hydrogen carrier molecules, such as LOHC, Methanol and especially ammonia show superior energy densities compared to formic acid. However, in favor of formic acid is that it could be produced electrochemically with a two-electron transfer reaction.

Figures 4.3 and 4.4 shows the energy output of 1 m^3 of pure and 4 molar formic acid in comparison to a 1 m^3 pressurized hydrogen system at 30 MPa. The hydrogen from decomposed formic acid or an pressure device is used in a PEM fuel cell with en electrical and thermal efficiency of 40% (see [142]). The efficiency of the decomposition is based on values published by Müller et al. [9]. For pure formic acid the efficiency of decomposition is much higher compared to aqueous solutions and an overall h_{FA}-to-electricity-efficiency of 33% could be assumed.

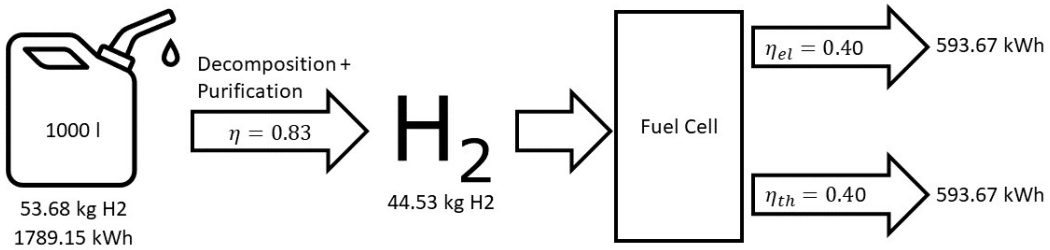

Figure 4.3: Energy content of 1000 l pure formic acid

The 4M formic acid solution contains about 8 kg of hydrogen with an energy content of 266.64 kWh. After decomposition and hydrogen utilization in a fuel cell, about 57.59 kWh of electricity and heat could be used. This corresponds to an overall h_{FA}-to-electricity-efficiency of 22%. According to Müller et al. [9] the efficiency of formic acid decomposition could be increased by recovering heat from the process.

Compared to pure and 4M formic acid 1 m^3 of pressurized hydrogen at 30 MPa contains about 24 kg of hydrogen, which is nearly completely available for an utilization (except leakage). With an specific energy demand of 2.25 kW h kg^{-1} (see Figure 3.13) about 53.75 kWh are needed for compression. With this system an h_{H_2}-to-electricity-efficiency of 32% is reached which equals the efficiency of the pure formic acid system.

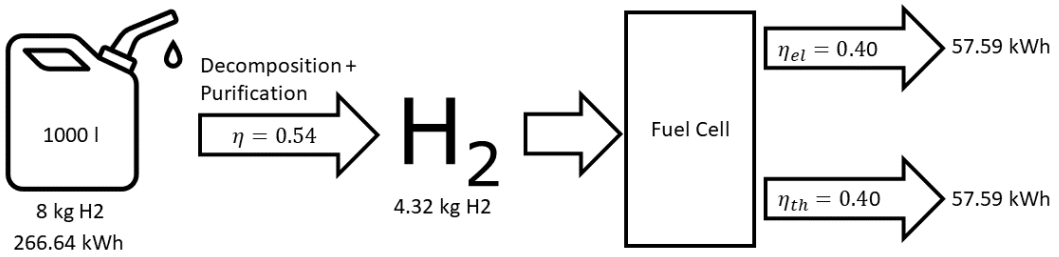

Figure 4.4: Energy content of 1000 l 4M formic acid

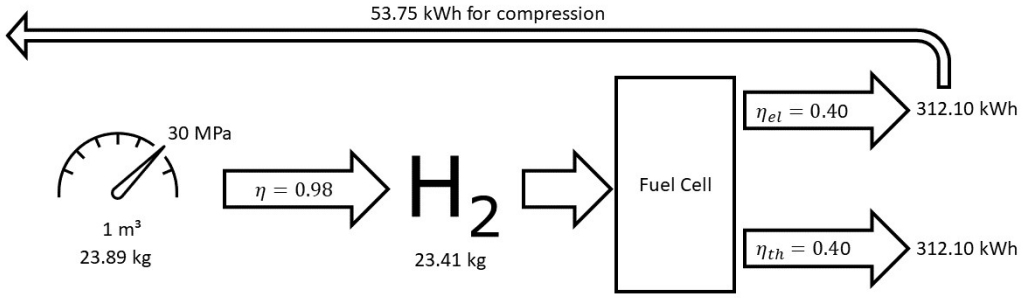

Figure 4.5: Energy content of 1 m^3 hydrogen at 30 MPa

Table 4.1 summarizes the hydrogen content, possible electricity output from a fuel cell and the overall efficiency from the lower heating volume of the stored hydrogen equivalent to the produced electricity for a stored volume of 1 m^3 respectively.

Table 4.1: Hydrogen content and overall efficiency of 1 m^3 pure formic acid, 4M aqueous formic acid solution and compressed hydrogen (30 MPa)

System	H_2 Content	Energy Output	Efficiency
Pure Formic Acid	53.68 kg	593.67 kWh	33%
4M Formic Acid	8 kg	27.73 kWh	10%
Compressed Hydrogen (30 MPa)	23.89 kg	312.1 kWh	32%

From these consideration it could be derived that, although a gravimetric hydrogen content of 4.4% for formic acid seems to to be low, formic acid could be considered as a suitable carrier molecule, if concentrations above 4M could be reached. The beneficial properties of formic acid as an energy carrier could traced back to its liquid state, even under ambient conditions. Lower concentrations and formate solutions, however, can not compete with other energy storage options, such as compressed hydrogen. A competitive concentration of

an aqueous formic acid solution would be around 10M.

4.2 Catalytic Carbon Dioxide Reduction to Formic Acid or Formate

Two different options of the catalytic carbon dioxide reduction to formic acid are considered in this section:

- The reversible hydrogen storage in formic acid, so called hydrogen batteries
- A two-process pathway with carbon dioxide hydrogenation and formic acid dehydrogenation in flow reactors

Both pathways presuppose the provision of gaseous hydrogen, e.g. from water electrolysis (see Figure 4.1).

4.2.1 Reversible Hydrogen Storage in Formic Acid - Hydrogen Battery

Figure 4.6 shows the general principle of a hydrogen battery. Gaseous hydrogen is provided for hydrogenation reaction of carbon dioxide to formic acid. The reverse reaction, dehydrogenation of formic acid, again releases gaseous hydrogen.

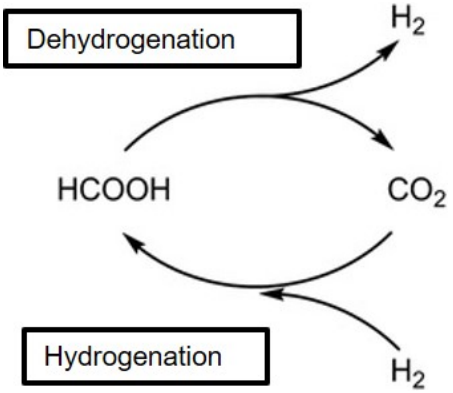

Figure 4.6: Principle of a reversible hydrogen battery

In most the systems described in literature, formic acid is not present in a pure form but bounded to amines such as DBU. Pressure and heat are needed to maintain the hydrogenation reaction. A pressure release and simultaneous heating triggers the dehydrogenation reaction. The hydrogen batteries could be used as a stationary energy storage system embedded in an energy system with water electrolysis and a fuel cell. One of the main advantages of using formic acid as an hydrogen carrier, good transportability, is limited by using an hydrogen battery. In this setup, only FA loaded DBU or 'battery cells' as a whole could be transported.

4.2.1.1 Catalysts for the reversible Hydrogen Storage in Formic Acid

Hsu et al. [143] describe a hydrogen battery based on a ruthenium complex catalyst (see Figure 4.7).

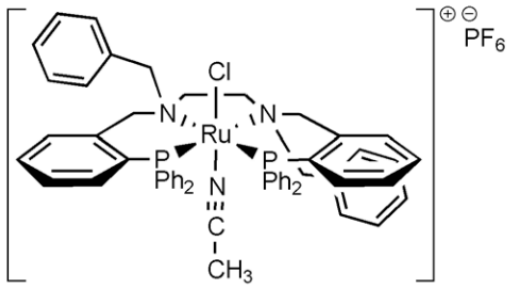

Figure 4.7: Ru complex used by the Plietker research group [143]

Both the hydrogenation and dehydrogenation process of this systems are operated at 100 °C. For the hydrogenation an inital pressure of 140 bar was applied. The dehydrogenation is executed at ambient pressure conditions. There was no CO contamination detected in the released hydrogen, which is important for the utilization of hydrogen in PEM fuel cells. Overall five complete loading and unloading cycles are documented with this battery.

Other Ru-complexes applied in hydrogen batteries are reported by Boddien et al. [144], Filonenko et al. [145] and Czaun et al [146].

4.2.1.2 Hydrogen Battery Design

Based on the hydrogen battery systems described in literature, a possible system design is shown in figure 4.8. This system could be described as a heated autoclave with a gas and a liquid phase.

The liquid phase consists of a base (DBU) and an homogeneous catalyst. Hydrogen from prior water electrolysis is mixed with carbon dioxide, compressed and induced in the reactor. Under pressure and a reaction temperature at 100 °C formic acid loaded DBU is formed in the liquid phase. If the DBU in the solution is fully loaded with formic acid, the reactor could be cooled down to ambient temperature. The release of hydrogen from the amine base could be controlled by again increasing the temperature above 100 °C. After separating the carbon dioxide, the hydrogen gas could be used in fuel cells. It is assumed that in this setup carbon dioxide is recycled and again mixed with hydrogen.

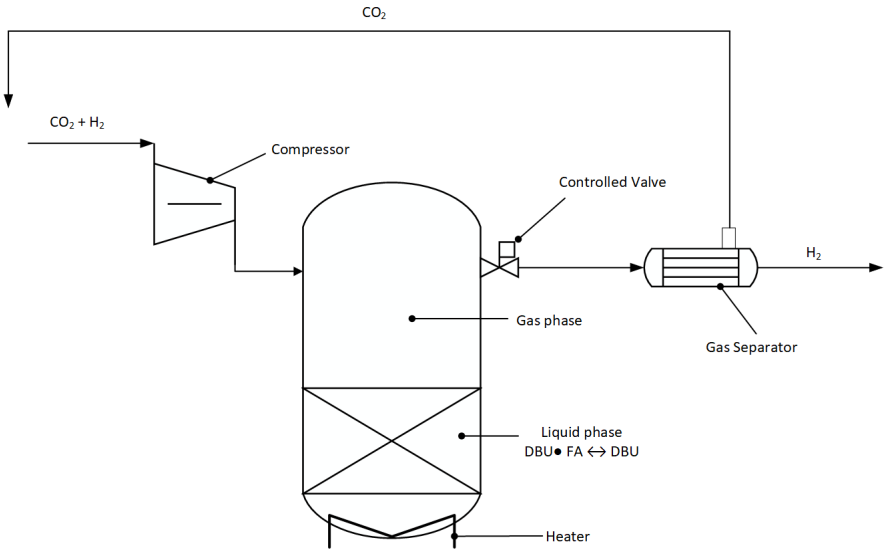

Figure 4.8: Design of a reversible hydrogen battery

4.2.2 Carbon Dioxide Hydrogenation to Formic Acid in a Flow Reactor

Compared to the hydrogen battery, a system with flow reactors is more complex, as it requires an individual reactor for the hydrogenation and the dehydrogenation reaction, as well as formic acid storage tanks. However, the divided setup has the advantage that formic acid could be extracted or supplied between the reactors. Figure 4.9 shows a possible system design.

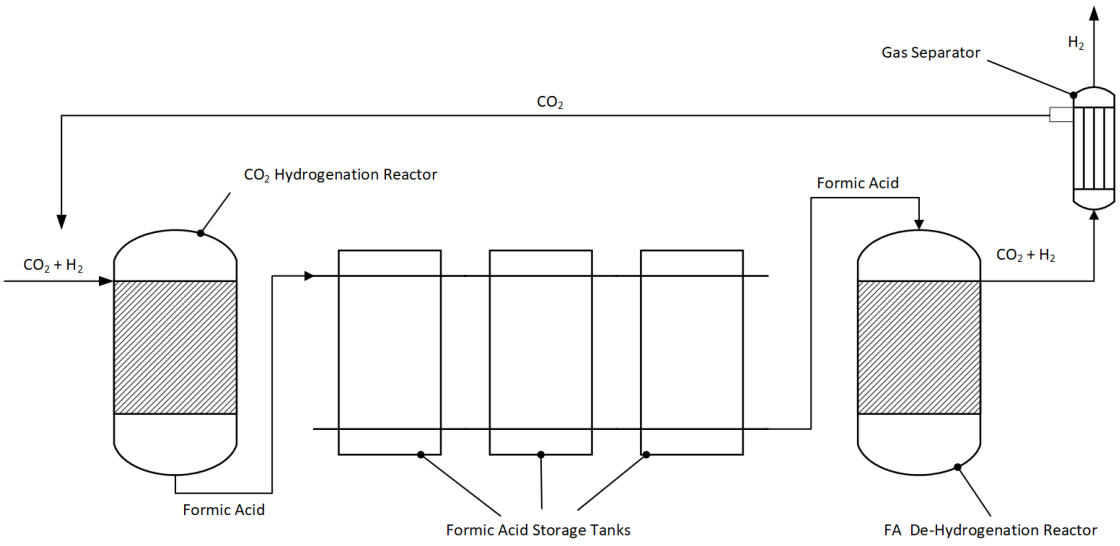

Figure 4.9: Design of a flow reactor system

A mixture of gaseous carbon dioxide and hydrogen must be provided to the hydrogenation reactor from which liquid formic acid could be derived and stored in tanks. Carbon dioxide is recycled after an gas separation process from the dehydrogenation reactor exhaust gas. Further details about the dehydrogenation reactor is given in Section 4.5. The purified hydrogen could afterwards be utilized in fuel cells.

4.2.2.1 Catalysts for the hydrogenation of carbon dioxide to formic acid in a flow reactor

The hydrogenation reaction, which leads to formic acid in a continuous flow is shown below.

$$CO_2(g) + H_2(g) \longrightarrow HCOOH(l) \quad \Delta G^{\ominus} = 32.9\,kJ\,mol^{-1} \quad \Delta H^{\ominus} = -31.2\,kJ\,mol^{-1}$$

The endergonic reaction is not favored under ambient conditions. Therefor it is a common approach to run the hydrogenation reaction in the presence of a base. However, this leads to the formation of formate instead of formic acid, which means lower energy densities. By using water the reaction also becomes exergonic, but the catalysts used so far show low activities [147].

$$CO_2(aq) + H_2(aq) \longrightarrow HCOOH(aq) \quad \Delta G^{\ominus} = -4\,kJ\,mol^{-1}$$

In general, two possible catalyst systems could be applied for such systems: homogeneous catalysts and heterogeneous catalysts. Zhang et al. [16] describe a system capable of continuously producing formic acid from carbon dioxide in a aqueous environment. A homogeneous catalyst ($RuCl_2(PTA)_4$) was used and kept in the system by separating formic acid with a semipermeable membrane. The activity of the catalyst could be enhanced by increasing the pressure or temperature. A TOF of 232 h^{-1} is shown. Finally, a 10 day run (70 °C, 10 MPa) with a TON of 35,000 and a final formic acid concentration of 2.5M was reported.

Weilhard et al. [17] use a buffering ionic liquid for the hydrogenation of carbon dioxide with a Ru-complex in a base-free environment. By adding a Lewis base ($Sc(OtF)_3$) a TON $> 8 \cdot 10^5$ and a TOF $> 2 \cdot 10^4$ h^{-1} is reported with a catalyst concentration of 0.28 μM. Overall a formic acid concentration of 0.32M is achieved with this system.

4.2.2.2 Reactor Design

If the catalyst of the reaction is available in an immobilized form, the reaction could be executed in a two-phase fixed-bed flow reactor. Figure 4.10 shows a possible layout for such a reactor type.

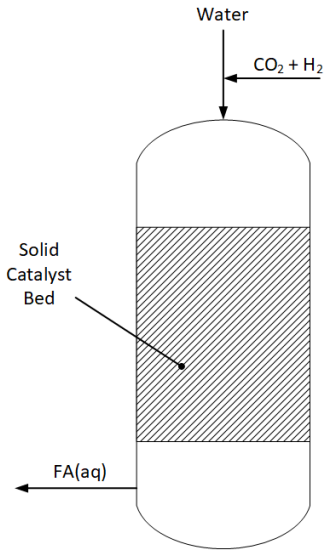

Figure 4.10: Possible reactor design for a carbon dioxide to formic acid flow reactor

Water and a CO_2/H_2-mixture is provided at the reactor inlet. After the reaction took place in the reactor bed, formic acid in aqueous solution and possible unreacted gas leaves the reactor at the outlet.

4.3 Electrochemical Carbon Dioxide Reduction to Formic Acid or Formate

As already shown in Figure 4.1, the electrochemical pathway of carbon dioxide to formic acid does not request gaseous hydrogen. The reaction takes place in electrochemcical cells, with water splitting at an anode and carbon dioxide reduction (CO_2RR) at the cathode. A two electron transfer to the carbon atom is necessary to reduce its oxidation state from +IV to +II. The overall reaction could be describes as follows

$$CO_2\,(g) + H_2O\,(l) \longrightarrow HCOOH\,(aq) + \frac{1}{2}\,O_2$$

In this section, only the electrochemcial reaction under acidic conditions are regarded as formic acid is the preferred product for energy storage applications, compared to formate, which would be created under alkaline conditions.

4.3.1 Cathode Reaction

The cathode reduction could be describes as follows with a standard potential in aqueous solution at pH 7:

$$CO_2\,(g) + 2\,H^+ + 2\,e^- \longrightarrow HCOOH\,(aq) \qquad E^0 = -\,0.61\,V$$

The reaction mechanism of the CO_2RR is describes in literature e.g. by Lee et al. [148]. Carbon dioxide molecules are adsorbed from the gas phase at the catalyst surface layer. If one electron is transferred a carbon dioxide radical is formed. Paired with one proton, a adsorbed formate is created at the catalyst layer. The second step of the reaction includes again an electron transfer, releasing a formate radical into aqueous solution. Finally, with another proton, formic acid is formed.

$$CO_2\,(g) \longrightarrow CO_2(ad)$$

$$CO_2(ad) + e^- \longrightarrow \cdot CO_2(ad)^-$$

$$\cdot CO_2(ad)^- + H^+ \longrightarrow \cdot HCOO(ad)$$

$$\cdot HCOO(ad) + e^- \longrightarrow \cdot HCOO\,(aq)^-$$

$$\cdot HCOO\,(aq)^- + H^+ \longrightarrow HCOOH$$

However, two possible side reaction may occur at the cathode, which are thermodynamically favored. The formation of carbon monoxide:

$$CO_2\,(g) + 2\,H^+ + 2\,e^- \longrightarrow CO\,(g) + H_2O\,(l) \qquad E^0 = -\,0.106\,V$$

And the hydrogen evolution reaction (HER):

$$2\,H^+ + 2\,e^- \longrightarrow H_2\,(g) \qquad E^0 = 0.00\,V$$

To maximize the formic acid output of this reaction, occurring side reactions must be suppressed. This could be done by choosing catalysts which kinetically favor the creation of the desired product and by maintaining the reaction conditions (temperature, cell potential) within the boundaries at which high product yields are detected. An overview of the selectivity of catalyst for the CO_2RR is given by Feaster et al. [149].

4.3.1.1 Electrolycatalysts for the carbon dioxide reduction reaction

In general two possible catalyst types for the CO_2RR are usable:

- Heterogeneous catalysts, e.g. Sn or Pt electrodes
- Homogeneous catalysts, e.g Ru complexes

Both catalyst types come with some advantages and disadvantages. Some characteristic properties of both catalyst types are outlined in Table 4.2.

Table 4.2: Comparison of homogeneous and heterogeneous catalyst for the CO_2RR

Homogeneous Catalysts	**Heterogeneous Catalysts**
highly selective and flexible as ligands and their position are selected	generally not very selective, side reactions occur
expensive, little proven	resilient, cheap, proven
catalyst must be separated from the product	relatively high activation losses

For the heterogeneous catalysis a wide range of possible sp and d metals are described in literature (see Lu et al. [30]), with sp metal oxides such as SnO_2 or Bi_2O_3 nanoparticles on a carrier structure (carbon black) are most common. Within the possible d metal electrocatalysts for the CO_2RR is Pt, Pd, Ag and Au.

For the homogeneous catalysis of the CO_2RR, a series of transition metal complexes (e.g. Ru, Re or Mn complexes) could be utilized. Molecular catalysts are capable of achieving a high selectivity but must be either separated from the product after the electrolysis or be immobilized on a carrier structure. A review of different molecular catalysts for the electrochemical reduction of carbon dioxide is given by Kinzel et al. [29].

4.3.2 Anode Reaction

At the anode of electrochemical cell for the CO_2RR under acidic conditions, water is split into protons, electrons and oxygen. The anode reaction and usable catalysts are well known from water electrolysis and proven.

$$H_2O \longrightarrow 2\,H^+ + 2\,e^- + \frac{1}{2}\,O_2 \qquad E^0{=}1.229\,V$$

For the anode reaction Ir based catalysts such as IrO_2 nanoparticles are most common.

4.3.3 Cell Design

Electrochemcial cells for the CO_2RR usually consist of a cathode and an anode, a membrane and a compartment at the cathode side of the membrane where the liquid products are discharged.

Gas Diffusion Electrodes In a continuous cell operation, the cathode must be designed as a gas diffusion electrode (GDE). GDEs allow a sufficient transport of gaseous reactants, in this case carbon dioxide, and thereby higher current densities. Usually, GDEs consists of a porous material (e.g. a carbon matrix) where the catalyst is dispersed (see Figure 4.11).

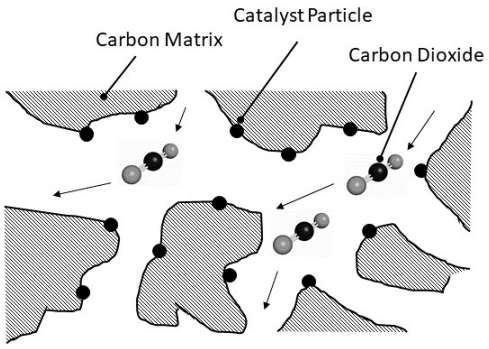

Figure 4.11: Schematic design of a GDE for a CO_2RR

GDEs must be designed in a way at which they provide a sufficient reactive area, but at the other hand the transport of reactants and products through the porous material must be ensured. When high current densities are applied, mass transport limitations often reduce the cell performance. The optimization of a GDE for the CO_2RR with hydrogen oxidation at the anode is described by Kopljar et al. [23]. Up to 400 mA cm^{-2} and a faraday efficiency of 75% for formate as a product were achieved with a dry deposited GDE loaded with SnO_2 nanoparticles.

Membrane Depending on the cell setup (acidic or alkaline) two different types of membranes could be used: cation exchange membrane[1] (CEM) or anion exchange membrane (AEM).
The most common material for CEMs is Nafion™, which conducts protons but not anions or electrons. However, a cross-over of substances is possible. By changing the membrane thickness, the substance cross-over could be reduced at the cost of higher cell voltages caused by the mechanical resistance of the material. AEMs on the other hand prevent the diffusion of cations but conduct anions such as OH^-. An AEM material for the electrochemical conversion of carbon dioxide, Sustanion™by Dioxide Materials, is described by Yang et al. [26].

[1]Also referred as proton exchange membranes (PEM)

Cell Assembly For a real application with water splitting at the anode, it maintain the operation at low pH-values in order to ensure that formic acid rather than formate is produced. Oßkopp et al. [28] introduce a cell assembly with a zero gap anode and a cation exchange membrane (see Figure 4.12). With this setup, a steady value of pH 3 is reported after an initial phase. 97% of the consumed carbon dioxide is found in formic acid or carbon monoxide (3% unwanted bicarbonates). It is reported that with this cell setup a FE of formic acid of 81% could be reached at 200 A cm^{-2}.

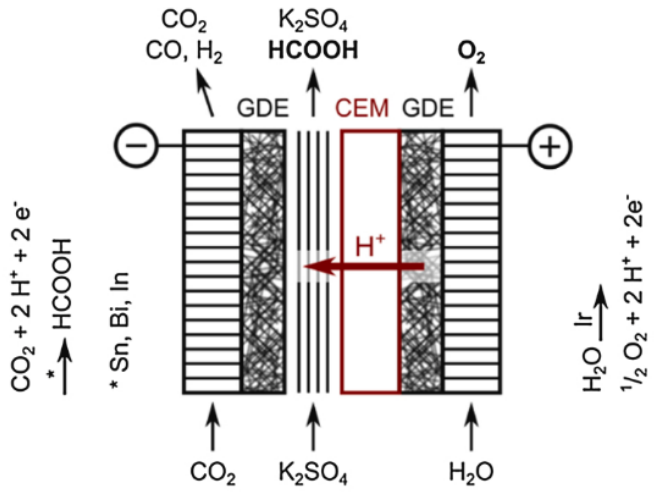

Figure 4.12: Zero Gap Anode (ZGA) cell for the CO_2RR. Source: [28]

A different cell assembly with three compartments separated by a CEM and an AEM is described by Yang et al. [27] (see Figure 4.13). Anions formed at the cathode ($HCOO^-$ and OH^-) are able to pass the AEM and combine with protons from the anode in the center compartment to formic acid and water. The center compartment is filled with an acidic ion exchange resin. Nafion 324 is used as a CEM and Sustanion as the AEM material. For the catalysis of the cathode reaction Bi_2O_3 nanoparticels are added to the GDE.
With this setup a long-term stability of over 1,000 h at a current density of 250 A cm^{-2} (3.6 to 3.7 V) is reported. Overall formic acid concentrations of up to 2.8 M could be achieved with a FE of 73% to 91.3%.

4.3.4 Stack Design

For the upscaling of the electrolyzer to a relevant power for energy storage applications, the active cell area must be increased to industrial scales. Also several cells must be connected to a stack. Therefor, the flow plates shown in Figure 4.12 and Figure 4.13 must be designed in two different versions: end plates and bi-polar plates. Figure 4.14 shows a possible stack

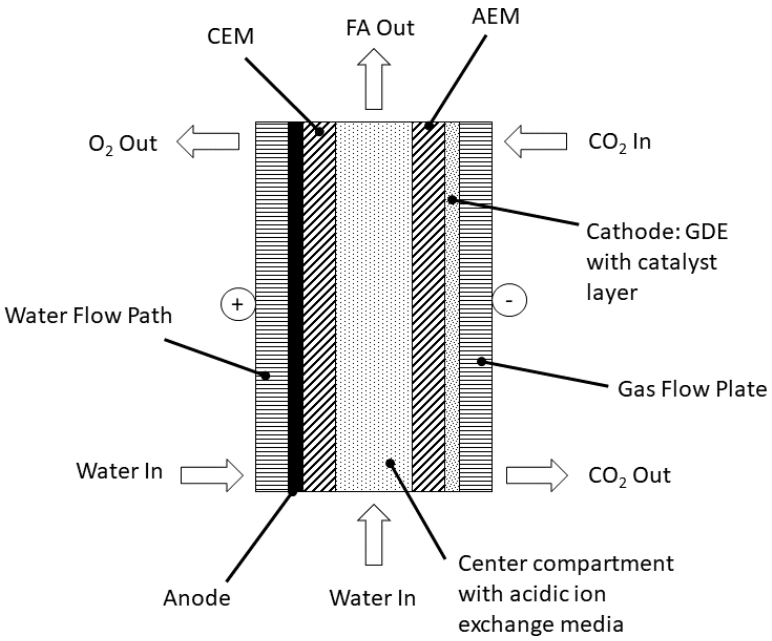

Figure 4.13: Three compartment electrolyzer with AEM and CEM (figure derived from [27])

layout with three cells based on Figure 4.13. The connection to an electrical power source must be provided at the anode and the cathode of the end cells. The internal cells must be electrically connected through the bipolar plates.

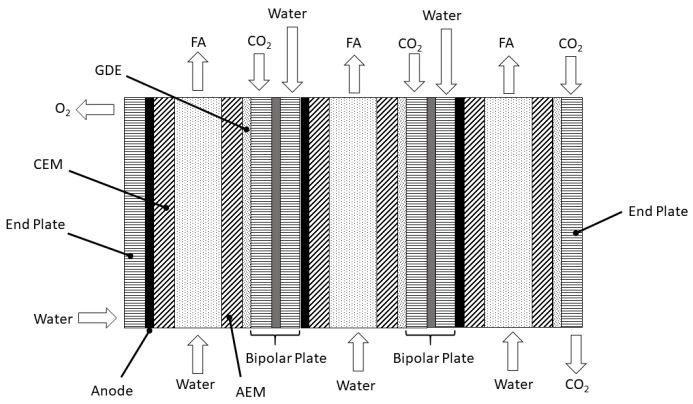

Figure 4.14: Stack Layout for a CO_2 Electrolyzer

The flow of liquid product (in this case an aqueous formic acid solution) could be designed either as a parallel or a serial flow (see Figure 4.15).

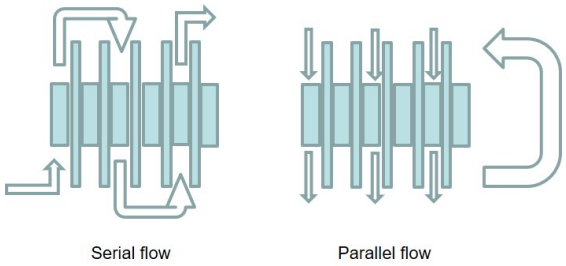

Figure 4.15: Serial and parallel flow of the liquid product

In a parallel flow, the liquid in and outflow in the center department is separated for each cell. To reach higher concentrations, the product could be recirculated. In a serial flow setup, the outflow of one cell enters the next cell. Therefor, the product concentration increases from cell to cell and the re-circulation may be saved, However, a serial setup could lead to electrical imbalances, as the cell voltage depends on the product concentration.

4.4 Product Processing

As the reported formic acid concentrations from CO_2 electrolysis are rather low (e.g. 0.4 M [28], 2.8 M [27]), the produced formic acid must be further treated and concentrated to reach formic acid concentrations suitable for an energy storage application (in the range of 10 M, see Figure 4.2). As formic acid and water are a azeotropic mixture, it could not be separated by a simple distillation. Two different processes for the concentrating of formic acid are described in this section: electrodialysis and azeotropic distillation.

Electrodialysis The electrodialysis is a chemical process at which ions could be transferred from a compartment with lower concentration to a compartment with a higher concentration. An electrical field an ion exchange membranes are needed for this process. Figure 4.16 shows the working principle of an electrodialysis for an formic acid/ water mixture. Through the application of an electrical potential, cations (H^+) and anions ($HCOO^-$) are forced at the opposite direction. In the middle compartment, they recombine to formic acid and thereby increase the concentration in this compartment.
Zhang et al. [16] describe the utility of electrodialysis after the formic acid production in a flow reactor. The process increases the formic acid concentration from 0.04 M to 2.5 M with an FE of 63% for one compartment.

The influence of concentration ratios and applied current densities for the electrodialysis of a formic acid solution is investigated by Luo et al. [150]. At a current density of $50\,A\,cm^{-2}$

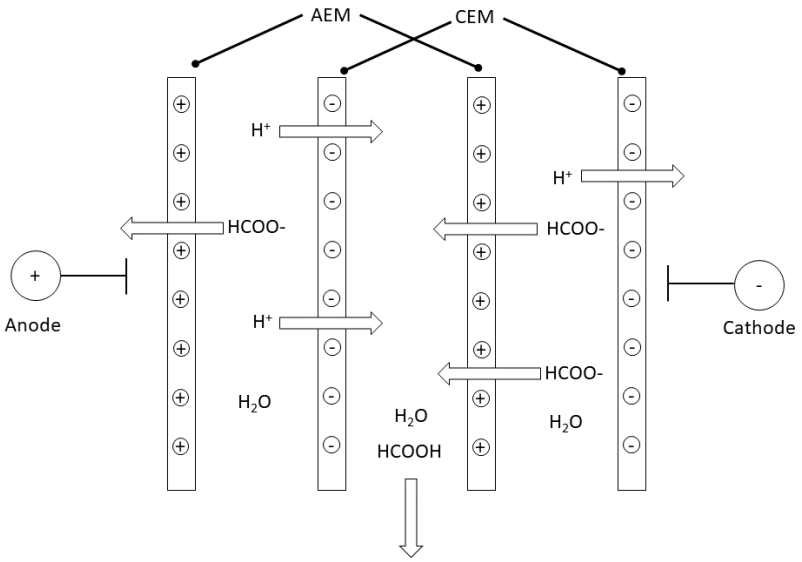

Figure 4.16: Principle of formic acid electrodialysis (Figure based on [16])

and an initial formic acid concentration of 5.96 M a maximum concentration ratio of 1.17 is reported. At a low initial concentration of 0.84 M a ratio of 1.7 is achieved at 25 A cm^{-2}.

Azeotropic Distillation (pressure-swing distillation) The pressure-swing distillation (PSD) aims at separating a binary formic acid/ water mixture by the use of two distillation columns operated at different pressures. This setup takes advantage of the fact that the composition of the azeotrop is sensitive to pressure changes [151]. The system described by Mahida et al. [151] is operated at 1.961 bar and 0.267 bar. Pure water could be extracted from the first distillation column, pure formic acid from the second. The remaining mixture is recirculated to the first column. It is reported, that with this setup about 57% of pure formic acid could be extracted from the azeotropic mixture.

With a single-stage azeotropic distillation, Kaczur et al. [152] report a final formic acid concentration of 85.8% from initial 20%. They operate the distillation at a pressure of 3.3 bar and a temperature of about 150°C.

4.5 Formic Acid Dehydrogenation

If formic acid is used as a hydrogen carrier, hydrogen must be released from formic acid in order to be used in fuel cells or combustion engines. This process is called formic acid

dehydrogenation. Below the reaction equation or this process is shown.

$$HCOOH\,(l) \longrightarrow H_2\,(g) + CO_2\,(g) \quad \Delta G^{\ominus} = -32.9\,kJ\,mol^{-1} \quad \Delta H^{\ominus} = 31.2\,kJ\,mol^{-1}$$

For a utilization in low-temperature PEMFCs, the fuel must not be contaminated with carbon monoxide. The dehydrogenation process should therefor suppress the dehydration of formic acid, which leads to the formation of carbon monoxide.

$$HCOOH\,(l) \longrightarrow H_2O\,(l) + CO\,(g) \quad \Delta G^{\ominus} = -12.4\,kJ\,mol^{-1} \quad \Delta H^{\ominus} = 29.2\,kJ\,mol^{-1}$$

It is also necessary to allow a controlled generation of hydrogen in this process for the demand driven operation of a subsequent fuel cell. Various homogeneous and heterogeneous catalyst are reported to catalyse the formic acid dehydrogenation.

Mihet el al. [33] use a heterogeneous Pd based catalyst for the formic acid decomposition. A hydrogen yield of 63.3% after 24 h from a 0.5 M formic acid solution at room temperature is reported. The reaction rate could be adjusted by the amount of used Pd and by changing the reaction temperature. However, the temperature only affects the reaction rate at the beginning and has little influence on the final hydrogen yield. Formic acid decomposition with heterogeneous catalysts are also reported in some other studies [19, 31, 32, 34, 35].

The application of homogeneous catalysts for the formic acid dehydrogenation is reviewed by Guan et al. [36]. They also introduce the concept of catalyst on-cost number to evaluate economic aspects. From this point of view a Ir complex in aqueous solution with a TOF of 1,900 h^{-1} at 60°C is assumed to has the potential for the utilization in stationary applications.
Table 4.3 summarizes the reported data of some heterogeneous and one homogeneous catalysts for a formic acid dehydrogenation.

Table 4.3: Comparison of reported catalysts for the formic acid dehydrogenation

Catalysts	**Temp. (°C)**	**TOF (h^{-1})**	**H_2 Yield (%)**	**Source**
Pd/TC	25	32.7	63.3	[33]
Pd/TC	40	67.9	54.4	[33]
Pd/TC	60	218.8	60.1	[33]
$PdMn_{0.6}$	25	610	-	[19]
$PdMn_{0.6}$	55	6860	-	[19]
Ru-TPPTS/PS	105	270	-	[35]
Ir complex in H_2O	60	1,900	-	[36]

Chapter 5

Modeling and simulation

The chemical reduction of carbon dioxide to formic acid allows new ways of hydrogen storage. Formic acid contains about 4.4 wt% Hydrogen, is long term stable and non toxic. Hydrogen could be released from formic acid by a dehydrogenation reaction and afterwards used in fuel cells or as a basic product for the industry. If the hydrogen is produced by electrolysis from renewable energy sources, and the carbon dioxide is either extracted from the air or a closed carbon loop is achieved, this process could be considered as carbon neutral. The storage of hydrogen as a molecule instead of physical storage (high-pressure, liquefaction) offers novel opportunities for seasonal energy storage and could be a supplement for batteries in an integrated energy system. Three different formic acid based hydrogen storage pathways are considered, which are already introduced in Chapter 4:

- A reversible hydrogen battery as described by Plietker et al. Gaseous hydrogen from prior water electrolysis reacts with carbon dioxide linked at a DBU base to formic acid. The Gaseous hydrogen could be released by the reverse reaction.
- Two flow reactors for the hydrogenation of carbon dioxide and the dehydrogenetion of formic acid. In this setup formic acid is stored in an external storage tank.
- The electrochemical pathway, which could also be called "Carbon Dioxide Electrolysis". Two electrons are transferred in an electrochemical reaction to carbon dioxide. With the addition of two protons, formic acid is formed. Hence, no gaseous hydrogen is needed, which decreases the system complexity (water electrolysis becomes no longer necessary) and safety. Hydrogen could be released from formic acid with a dehydrogenation flow reactor.

In this chapter, firstly the novel component models for the three described systems are introduced. They are complemented with models for a PEM Electrolyzer, high-pressure hydrogen storage (compressor and high-pressure tank) and a Fuel Cell. The component models are

combined to energy system models based on the systems described in chapter 5. All models are prepared to be used in the INSEL simulation environment. Finally, in this chapter, the overall dimensioning and simulation workflow, as applied in Chapter 7, is described.

This chapter aims at answering the first research objective of this thesis:

- How can the generation of formic acid from hydrogen and carbon dioxide or with direct CO_2-electrolysis be modeled?
- How can formic acid storage components be integrated into a larger energy system model with renewable energy sources, building loads and different energy conversion devices?

5.1 Novel Component Models for Formic Acid based Hydrogen Storage

The models for formic acid based hydrogen storage developed in this chapter should be used to evaluate the system performance if applied in the building sector. In order to asses the system as a seasonal storage technology, the simulation duration should at least be one year. However, to develop control strategies (second research objective of this thesis) requires the representation of the dynamic behavior of the components, at least in a minute scale. These requirements results in a long simulation period on the one hand and the necessity of a short time step on the other hand. Multi-dimensional modelling methods, such as CFD are too computationally intensive for this purpose. Models based on monthly energy balance do not allow conclusion about the system dynamic with fluctuating loads. Furthermore, the developed component models must be capable for the combination to system models with additional components, such as batteries or controllers, leading to a high system complexity. Especially for the design of system models, graphical programming languages, such as Simulink, Modelica or INSEL are commonly used. For this work, INSEL was chosen as a programming language for the system models, as it provides the most interfaces to other models and workflows developed in the research group. C++ is used as the programming language for the component models to allow an easy transfer of the developed models to other simulation environments. Subsequently, the dynamic models to simulate formic acid based hydrogen storage are described.

5.1.1 Reversible Hydrogen Storage in Formic Acid - Hydrogen Battery

The model for the reversible hydrogen battery is based on reported experimental data by Hsu et al [143]. For this model the following simplifications were made:

- Possible change of activation energy because formic acid is linked to DBU is neglected, due to insufficient experimental data.
- CO_2 input is considered as gaseous (experimental data with dry ice), as this would be a more practical approach for a real system application.
- The heat capacities of the reactor and the substances are neglected, as the heating and the cooling times are assumed to be short compared to the simulation duration.

5.1.1.1 Reaction Kinetic Model

The reversible hydrogen storage based on formic acid consists of two reactions. The forward reaction (carbon dioxide hydrogenation) is be modeled as a second order reaction, where as the backward reaction (formic acid dehydrogenation) has characteristics of a first-order reaction. The fundamentals of the governing equation of each reaction type are shown in Chapter 2.

Initial Conditions The initial conditions which are further used to calculated the reaction rate are given by the Hsu et al. [143] (see Table 5.1).

Table 5.1: Reported initial conditions of the reversible hydrogen battery [143]

Parameter	Symbol	Value
Autoclave volume	V [l]	0.1
Catalyst load	m_{cat} [mg]	56.8
Reaction temperature	T_{react} [°C]	100
Initial hydrogen pressure (room temp.)	$p_{H_2,0}$ [bar]	70
Initial gas pressure (reaction temp.)	p_{init} [bar]	140

With the initial hydrogen pressure, the hydrogen concentration at ambient temperature is calculated.

$$c_{H_2,0} = \frac{p_{H_2,0}}{R \cdot T_{amb}} \tag{5.1}$$

The hydrogen partial pressure at reaction temperature is calculated as follows:

$$p_{H_2,init} = c_{H_2,0} \cdot R \cdot T_{react} \tag{5.2}$$

From the difference of the gas pressure at reaction temperature and the hydrogen partial pressure results the carbon dioxide pressure caused by sublimated dry ice.

$$p_{CO_2,init} = p_{init} - p_{H_2,init} \tag{5.3}$$

And finally the starting amount of carbon dioxide is calculated.

$$c_{CO_2,0} = \frac{p_{CO_2,init}}{R \cdot T_{react}} \tag{5.4}$$

Carbon Dioxide Hydrogenation The reaction equation shows that one mol of formic acid is formed from one mol of carbon dioxide and one mol of hydrogen.

$$CO_2 + H_2 \longrightarrow HCOOH \qquad \Delta H^{\ominus} = -31.2\,\mathrm{kJ\,mol^{-1}}$$

The concentration of hydrogen at each time step could be calculated using equations 5.5, with the slope of the forward reaction k_1 over the regarded interval.

$$c_{H_2}(t) = \frac{c_{H_2,0}}{1 + c_{H_2,0} \cdot k_1 \cdot t} \tag{5.5}$$

Equation 5.5 is transformed to its derivative form in Equation 5.6.

$$c_{H_2}(t + \Delta t) = c_{H_2}(t) - k_1 \cdot c_{H_2}(t)^2 \cdot \Delta t \tag{5.6}$$

The concentration of formic acid at each time step is determined by the difference of the hydrogen concentration, as every mol of hydrogen contributes to one mol of formic acid (no side reactions assumed).

$$c_{FA}(t + \Delta t) = c_{FA}(t) + (c_{H_2}(t) - c_{H_2}(t + \Delta t)) \tag{5.7}$$

And finally, the carbon dioxide concentration is according to Equation 5.8 calculated from the differences of the formic acid and the carbon dioxide concentration at the previous time step.

$$c_{CO_2}(t + \Delta t) = c_{CO_2}(t) - c_{FA}(t) \tag{5.8}$$

With the formic acid concentration at each time step and the concentration of DBU in the solvent, the loading state of the battery could be calculated as in Equation 5.9.

$$SOC(t) = \frac{c_{FA}(t)}{c_{DBU}} \tag{5.9}$$

The model assumes that all of the consumed hydrogen contributes to form formic acid and no side reactions occur. The reaction rate slope k_1 of the carbon dioxide hydrogenation is a fitting parameter and derived from experimental data, so that the decrease of the gas phase pressure over time is aligned to the reported experimental results, which state that after 2.5 h the gas phase pressure has decreased to 100 bar. Out of it, k_1 is determined to

be $1.15 \times 10^{-5}\,\mathrm{L\,mol^{-1}\,s^{-1}}$. Figure 5.1a shows the evolution of the gas phase pressure over time and the development of the species concentrations over time are shown in Figure 5.1b.

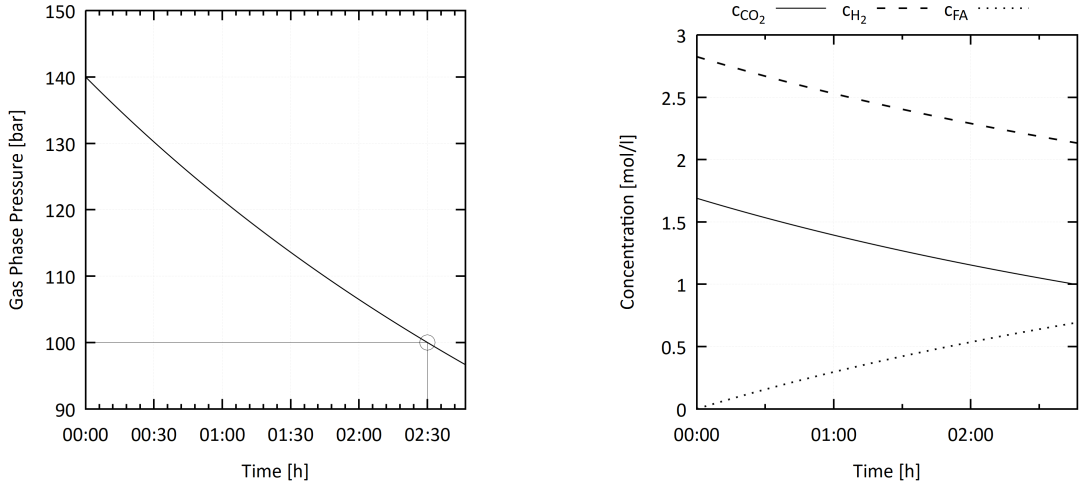

(a) Gas Phase Pressure

(b) Concentrations

Figure 5.1: Carbon Dioxide Hydrogenation

Finally, the linearized reaction rate r_1 of the forward reaction in the interval from 0 to 2.5 h results from Equation 5.10.

$$r_{H2tFA} = \frac{-\Delta c_{H_2}}{\Delta t} = \frac{-\Delta c_{CO_2}}{\Delta t} = -7.1 \times 10^{-5}\,\mathrm{mol\,L^{-1}\,s^{-1}} \tag{5.10}$$

With a catalyst load of 56.8 mg and a reaction volume of 0.1 L follows a reaction rate with regard to the catalyst mass of:

$$r_{H2tFA} = -7.1 \times 10^{-5}\,\mathrm{mol\,L^{-1}\,s^{-1}} \cdot \frac{0.1\,\mathrm{L}}{56.8 \times 10^{-6}\,\mathrm{kg}} = -0.125\,\mathrm{mol\,kg^{-1}\,s^{-1}} \tag{5.11}$$

Formic Acid Dehydrogenation At the decomposition of formic acid, one mol of hydrogen one mol of carbon dioxide is produced from one mol of formic acid.

$$\mathrm{HCOOH} \longrightarrow \mathrm{CO_2} + \mathrm{H_2} \tag{1}$$

This reaction could be modeled as a first-order reaction. The concentration of formic acid at each time-step is given by the differential equation Equation 5.12.

$$c_{FA}(t) = c_{FA,0} \cdot e^{-k_2 \cdot t} \tag{5.12}$$

In its derivative form the differential equation writes as follows:

$$c_{FA}(t + \Delta t) = c_{FA}(t) - k_2 \cdot c_{FA}(t) \cdot \Delta t \tag{5.13}$$

The initial formic acid concentration $c_{FA,0}$ results from the amount of produced formic acid at the carbon dioxide hydrogenation reaction. It is reported by Hsu et al. that at a reaction temperature of 100 °C after 2.5 hours 22 bar of produced gas was measured (see Figure 5.2a), which leads to a reaction slope k_2 of $7.88 \times 10^{-5}\,\mathrm{s}^{-1}$. Figure 5.2b shows the resulting curve of the species concentration for the reported dehydrogenation reaction.

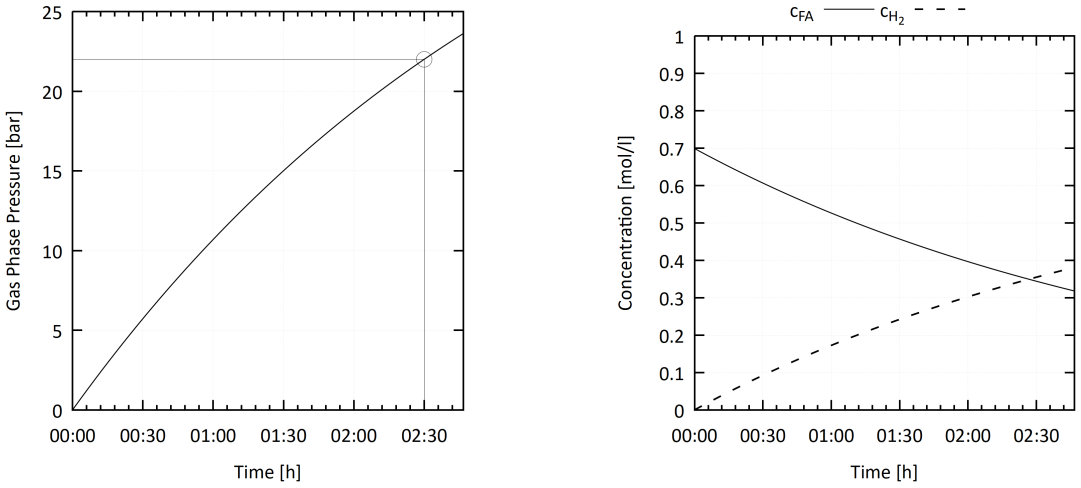

(a) Gas Phase Pressure (b) Concentrations

Figure 5.2: Formic Acid Dehydrogenation

The linearized reaction rate over the regarded interval of the formic acid dehydrogenation is calculated as follows:

$$r_{FAtH2} = \frac{-\Delta c_{FA}}{\Delta t} = 3.94 \times 10^{-5}\,\mathrm{mol\,L^{-1}\,s^{-1}} \tag{5.14}$$

Like in Equation 5.11 this reaction rate could be expressed with regard to the catalyst mass.

$$r_{FAtH2} = 3.94 \times 10^{-5}\,\mathrm{mol\,L^{-1}\,s^{-1}} \cdot \frac{0.1\,\mathrm{L}}{56.8 \times 10^{-6}\,\mathrm{kg}} = -0.07\,\mathrm{mol\,kg^{-1}\,s^{-1}} \tag{5.15}$$

The reactions rates of the forward and backward reaction are summarized in Table 5.2.

Table 5.2: Reaction rates for the reversible hydrogen battery

Reaction	Reaction Slope	Reaction Rate [$\mathrm{mol\,kg^{-1}\,s^{-1}}$]
Carbon Dioxide Hydrogenation	$1.15 \times 10^{-5}\,\mathrm{L\,mol^{-1}\,s^{-1}}$	-0.125
Formic Acid Dehydrogenation	$7.88 \times 10^{-5}\,\mathrm{s^{-1}}$	0.07

5.1.1.2 INSEL Block for the Reversible H2 Battery

The INSEL Block of the Reversible H2 Battery uses five inputs during the simulation run, which are shown in Figure 5.3. The parameters used to determine the component design are shown on the right side of Figure 5.3.

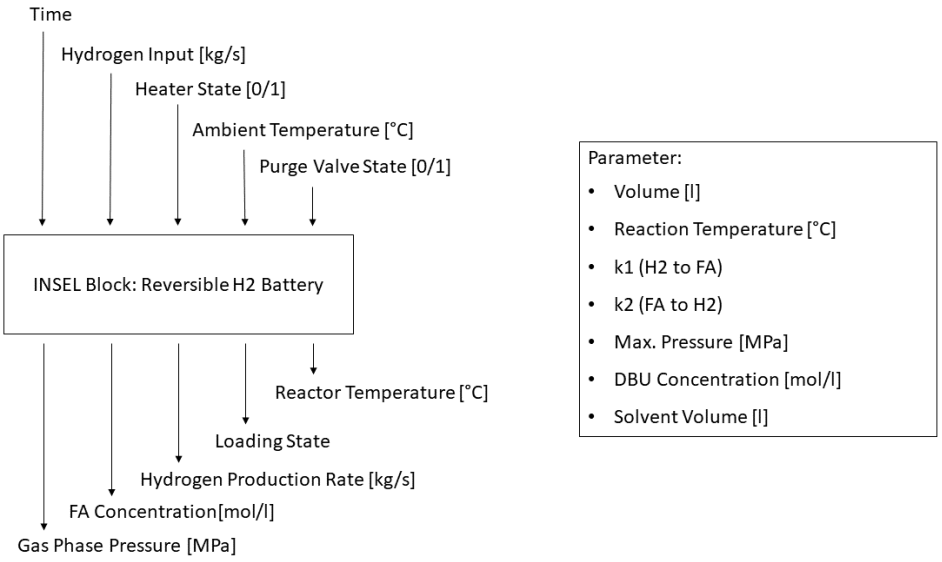

Figure 5.3: Reversible H2 Battery: INSEL block overview

The heater and the purge valve work as actors to control the operating mode of the system. All in all four operating states are possible:

- Hydrogen Filling: The reactor is filled with gaseous hydrogen from a hydrogen source (e.g. an electrolyzer). Heater is turned off and purge valve is closed.
- Hydrogenation: The reactor is filled with hydrogen. Heater is turned on and purge valve is closed. Formic acid is produced. Simultaneous hydrogen inflow is possible.
- Dehydrogenation + Hydrogen Release: Heater is turned on and purge valve is opened. Hydrogen is produced from formic acid and released

- Hydrogen Release: Heater is turned off, purge valve is open. Hydrogen is released.
- Idle: Heater is turned of and purge valve is closed. No hydrogen inflow or outflow.

Figure 5.4 shows a test run of an INSEL simulation of the reversible H2 Battery Block, which shows all possible operating modes. The reactor is filled with hydrogen for one hour. Afterwards the reactor stays idle for two hours. At hour three, the heater is turned on, which causes a pressure increase and starts the hydrogenation reaction. During the hydrogenation reaction, the pressure drops and the concentration of formic acid increases. At about 8:30 hours the heater is turned off, which brings the reactor again into idle mode. After 15 hours from the beginning of the experiment, the heater is turned on and the purge valve is opened. This effects an immediate loss of pressure and the dehydrogeneation reaction begins. Gaseous hydrogen leaves the reactor at the specified production rate.

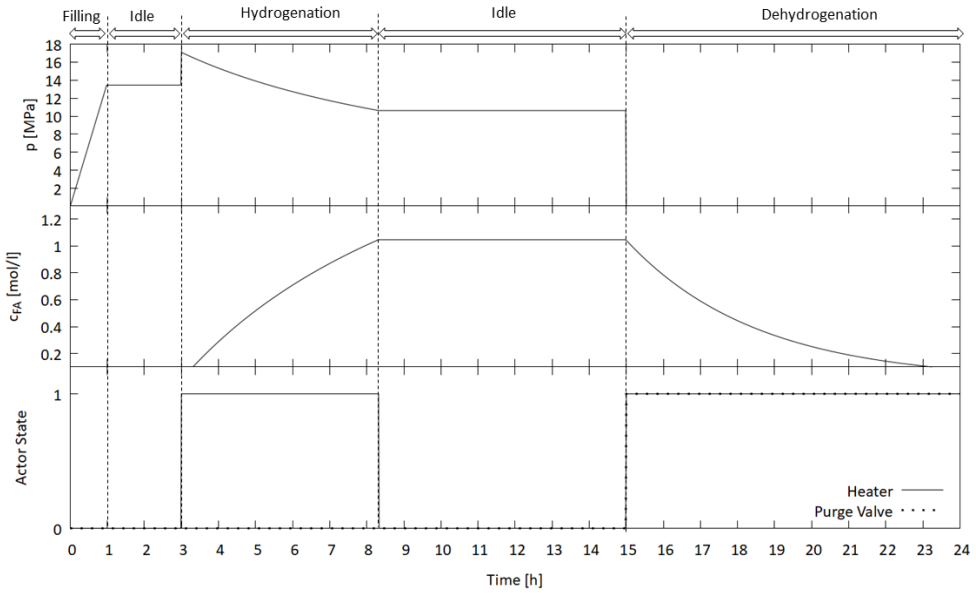

Figure 5.4: Reversible H2 Battery: INSEL test run

5.1.2 Flow Reactor

The flow reactor differs from the hydrogen battery, as the carbon dioxide hydrogenation and the formic acid dehydrogenation are separated in two different reactors. This approach allows the supply or removal of formic acid for distribution purposes. In the following sections flow reactor models for each reaction are introduced. The reaction slopes are adopted from the Reversible Hydrogen Battery assuming the usage of the same catalyst in an immobilized

form. However, the reaction slopes are parameterized in the component model and could be changed if other catalysts should be applied.

5.1.2.1 H2tFA - Flow reactor model

The reaction kinetic model developed with experimental data for the Ru based homogeneous catalyst is further used in a steady-state fixed-bed flow reactor model. This reactor type, compared to a batch reactor, allows a continuous formic acid production. The following simplifications are made:

- The reaction is assumed to be steady-state, due to slow reaction rates.
- The catalyst is immobilized and equally distributed in the reactor bed.
- Any produced gaseous formic acid is condensed after it leaves the reactor and is available in its liquid form for storage.
- The transport of the produced formic acid from the reaction area is guaranteed.
- The reaction temperature is kept constant due to uniform reactor cooling.
- The equilibrium constant of the water-gas-shift reaction lays clearly on the product side (CO_2 and H_2) at the reaction temperature. No CO or H_2O is produced.
- Pressure losses along the reactor length are neglected.

Figure 5.5 shows the flow diagram of the reactor model. As the reactor is designed to be coupled with an electrolyzer, the inflow of hydrogen is defined as an input variable, depending on the electrolyzer output. The individual calculation steps are described subsequently.

Carbon Dioxide Demand The demand of carbon dioxide inflow results from the assumption that the reaction is operated at stoichiometric equality between hydrogen and carbon dioxide with the molar masses M_{H_2} and M_{CO_2} of each species. Therefor, the carbon dioxide demand is calculated as follows:

$$\dot{m}_{CO_2,in} = \dot{m}_{H_2,in} \cdot \frac{M_{CO_2}}{M_{H_2}} \tag{5.16}$$

Initial Conditions The reactor length is divided into length increments dx for the main loop.

$$dx = \frac{L}{N} \tag{5.17}$$

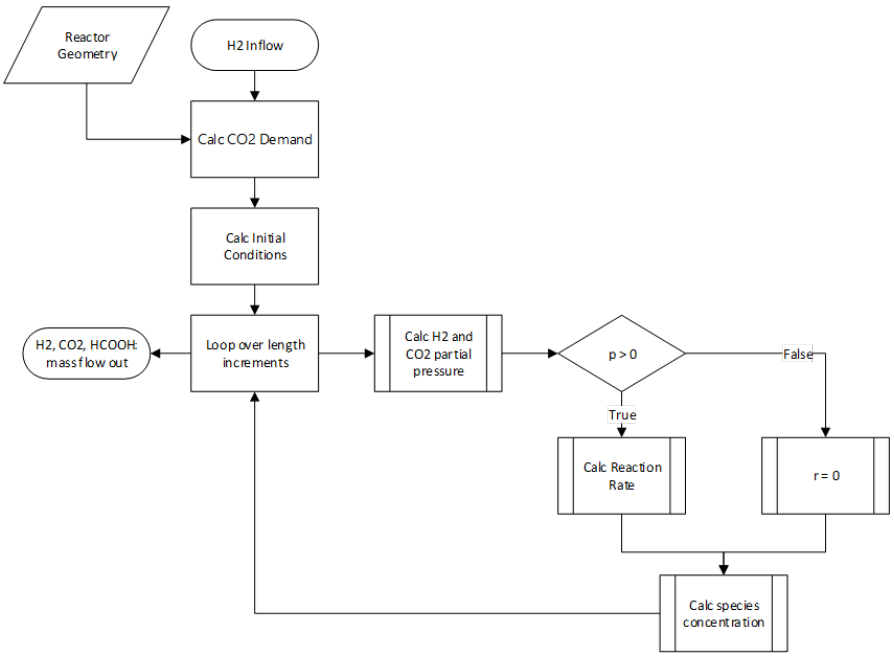

Figure 5.5: Hydrogen to formic acid flow reactor model: flow diagram

To maintain stoichiometric equality between hydrogen and carbon dioxide, the initial partial pressures are assumed to be equal.

$$p_{H_2,in} = p_{CO_2,in} = 0.5 \cdot p_{in} \tag{5.18}$$

With the mass flow $\dot{m}$, the individual gas constant R_s, the reaction temperature T_{react} and the partial pressure results the initial hydrogen volume flow.

$$\dot{V}_{H_2,in} = \frac{\dot{m}_{H_2,in} \cdot R_{s,H_2} \cdot T_{react}}{p_{H_2,in}} \tag{5.19}$$

And accordingly the initial carbon dioxide volume flow is calculated.

$$\dot{V}_{CO_2,in} = \frac{\dot{m}_{CO_2,in} \cdot R_{s,CO_2} \cdot T_{react}}{p_{CO_2,in}} \tag{5.20}$$

With the reactor cross section A and the overall initial volume flow the flow velocity u could be calculated.

$$A = \frac{\pi \cdot d^2}{4} \tag{5.21}$$

$$u = \frac{\dot{V}_{H_2,in} + \dot{V}_{CO_2,in}}{A} \tag{5.22}$$

Finally, the initial concentration of each species is calculated with the partial pressure and the reaction temperature using the ideal gas law.

$$c_{H_2,in} = \frac{p_{H_2,in}}{R \cdot T_{react}} \tag{5.23}$$

$$c_{CO_2,in} = \frac{p_{CO_2,in}}{R \cdot T_{react}} \tag{5.24}$$

Main loop At each length increment the pressure of each species i is calculated.

$$p_i = c_i \cdot R \cdot T_{react} \tag{5.25}$$

With the reactor length L and the number of numerical parts N, the length of one increment is

$$\Delta x = \frac{L}{N} \tag{5.26}$$

The reaction rate at each reactor length increment is calculated as follows with a conversion factor of 10^{-3} ($\mathrm{mol\,L^{-1}}$ to $\mathrm{mol\,m^{-3}}$).

$$r = k \cdot c_{H_2}(x) \cdot c_{CO_2}(x) \cdot 10^{-3} \tag{5.27}$$

If the partial pressure of H_2 or CO_2 is less or equal to zero, meaning that all of the reactants are consumed, the reaction rate is also set to zero. With the reaction rate r and the time in each increment $\tau = dx/u$ the concentrations at the subsequent increments could be calculated:

$$\begin{pmatrix} c_{H_2}(x+\Delta x) \\ c_{CO_2}(x+\Delta x) \\ c_{FA}x+\Delta x) \end{pmatrix} = \begin{pmatrix} c_{H_2}(x) \\ c_{CO_2}(x) \\ c_{FA}(x) \end{pmatrix} + \begin{pmatrix} -r \\ -r \\ r \end{pmatrix} \cdot \tau \tag{5.28}$$

Outflow After the final length increment is reached, the outflow of each species is calculated with the final partial pressure.

$$\dot{m}_{H_2,out} = \frac{p_{H_2,final} \cdot \dot{V}_{H_2,in}}{R_{s,H_2} \cdot T_{react}} \tag{5.29}$$

$$\dot{m}_{CO_2,out} = \frac{p_{CO_2,final} \cdot \dot{V}_{CO_2,in}}{R_{s,CO_2} \cdot T_{react}} \tag{5.30}$$

The resulting formic acid outflow results from the overall inflow minus the outflows of hydrogen and carbon dioxide (mass conservation).

$$\dot{m}_{FA,out} = \dot{m}_{in} - \dot{m}_{H_2,out} - \dot{m}_{CO_2,out} \tag{5.31}$$

H2tFA Flow Reactor - INSEL Block The inputs, outputs and the parameters needed to run the INSEL Block of the H2tFA Flow Reactor are shown in Figure 5.6.

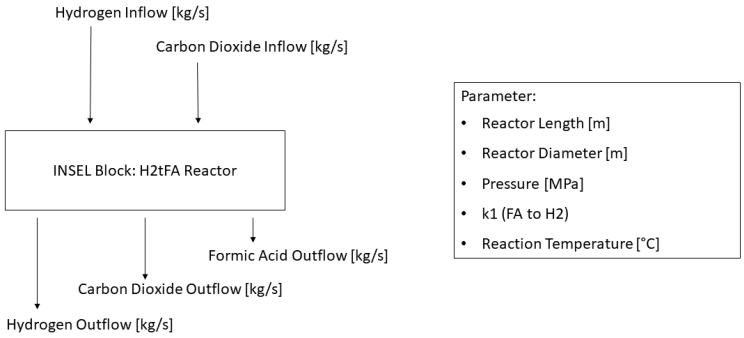

Figure 5.6: Hydrogen to formic acid flow reactor model: INSEL block inputs, outputs, parameters

A test run was executed with one reactor ($L = 19m, D = 0.5m$) at reaction conditions of 14 MPa and 110 °C. For 9,000 seconds the external hydrogen flow is constant at 2.4×10^{-4} kg s^{-1}, after 9,000 s only recirculating hydrogen is fed to the reactor. Carbon dioxide is at all times fed stoichiometrically to the reactor. The produced formic acid is filled into a 1,000 l tank after condensation. Figure 5.7 shows the resulting hydrogen flows and the filling level of the reactor for an simulation run of 14,000 seconds.

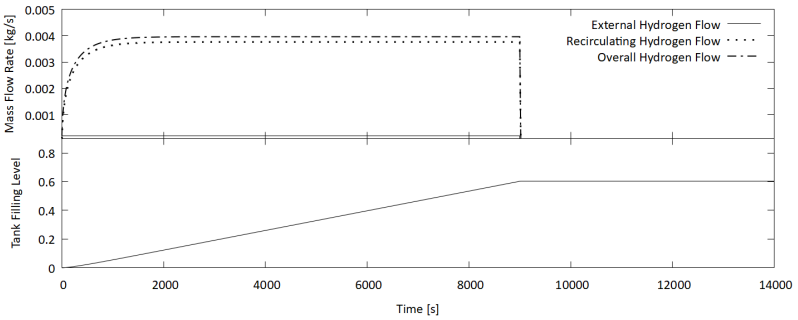

Figure 5.7: Hydrogen to formic acid flow reactor model: INSEL block test

5.1.2.2 FAtH2 - Flow reactor model

The formic acid to hydrogen reactor is designed as a multi-phase fluidized bed reactor. Liquid formic acid is continuously fed to the reactor and the gaseous products hydrogen and carbon dioxide are immediately removed from the reactor. However, the modeling of a transient multi-phase multi-dimensional reactor with heat transfer requires advanced numerical methods, such as CFD, to solve the governing partial differential equations. A profound introduction the modeling of a FAtH2 reactor using multi-physics simulation tools us given by Cendula et al. [43]. As the application of CFD methods are not suitable for the application in complex system models with long simulation durations, a simplified model is introduced in this section. As, in this case, as the reactor design itself is not in focus of this work, the following simplifications are applied:

- The reactor is assumed to be steady-state.
- The reaction is isothermal with a uniform temperature distribution over the reactor.
- The pressure dependency of the reaction is neglected.
- The reaction rate dependents linearly on the catalyst density.
- In this reactor setup, the reaction rate is solely controlled by the reaction temperature.

Reaction Rate According to Cendula et al. [43], the reaction rate could be determined with the following equation:

$$r = A \cdot \Phi_{cat} \cdot \frac{\rho_{FA} \cdot \Phi_{FA}}{M_{FA}} \cdot e^{\left(-\frac{E_a}{R \cdot T_{react}}\right)} \tag{5.32}$$

With A being the frequency factor of the Arrhenius equation, Φ_{cat} the volumetric fraction of the catalyst, the density ρ_{FA} and molar mass M_{FA} of formic acid, the volumetric fraction of formic acid $\Phi_{FA} = 1 - \Phi_{cat}$ (all gaseous products are assumed to immediately leave the reactor), the activation energy E_a and the reaction temperature T_{react}.

Mass Flows The mass flow in kg s^{-1} of hydrogen, carbon dioxide, as well as the mass flow demand of formic acid in order to keep the amount of formic acid in the reactor balanced, is calculated with the reaction rate r, the volume of the reactor $V_{reactor}$ and the molar mass of each species.

$$\dot{m}_{H_2} = r \cdot V_{reactor} \cdot M_{H_2} \tag{5.33}$$

$$\dot{m}_{CO_2} = r \cdot V_{reactor} \cdot M_{CO_2} \tag{5.34}$$

$$\dot{m}_{FA} = r \cdot V_{reactor} \cdot M_{FA} \tag{5.35}$$

FA-to-H2 Reactor - INSEL Block The inputs, outputs and needed parameters to run the INSEL Block of the FA-to-H2 reactor are shown in Figure 5.8. The reaction is controlled by the temperature, which is used as a single input.

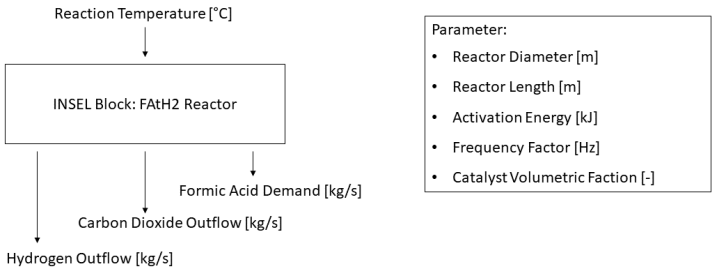

Figure 5.8: FAtH2 reactor INSEL block: inputs, outputs and parameters

The outflow of both gaseous products which depends on the applied temperature is validated against literature data reported by Laurenczy et al. [35] (see Figure 5.9).

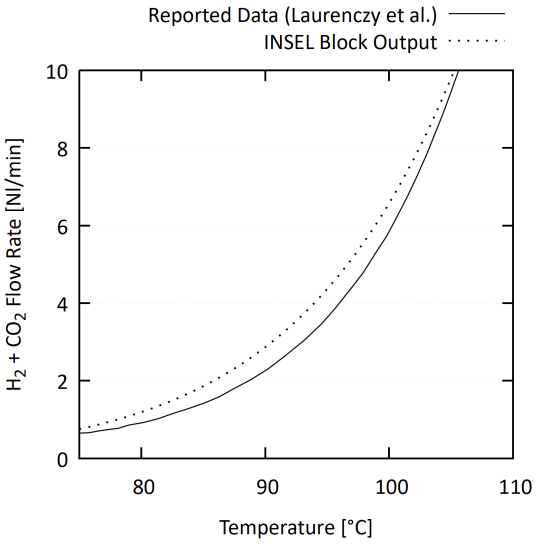

Figure 5.9: Formic Acid to hydrogen reactor model: validation against literature data

5.1.3 Electrochemical Formic Acid Production - Carbon Dioxide Electrolysis

In the following section the model of the electrochemcial formic acid production, the CO_2-electrolysis is presented. The fundamental equations of the electrolysis are comparable to other electrolysis technologies, such as water electrolysis and must be adapted to the electrolysis of carbon dioxide to formic acid. However, there exist some differences. The model must take possible side reactions, such as the formation of carbon monoxide or hydrogen (HER) into account. The following simplifications were applied:

- The limit current density and the Faraday efficiency are modeled empirically based on measurement data.
- Effects due to changes of the pH value are neglected, due to insufficient experimental data.
- Cathode an anode have the same characteristic parameters, such as ohmic resistance.

5.1.3.1 Electrochemical Model

The open-cell voltage (OCV) of the electrolyzer is modelled with a Nernst-Equation and the standard electrode potential $E^0 = -0.61V$.

$$E_{OCV,cat} = E^0_{cat} - \frac{R \cdot T}{z \cdot F} \cdot \ln Q \tag{5.36}$$

The coefficient Q consists of the the concentrations of each species in solution as well as the carbon dioxide partial pressure.

$$Q = \frac{[HCOOH]}{p_{CO_2} \cdot [H^+]} \tag{5.37}$$

The cathode halt-cell potential was modelled by an extended Butler-Volmers equation, which takes the limit current density into accout.

$$V_{cat} = E_{OCV,cat} + \frac{R \cdot T}{\alpha_{cat} \cdot F} \cdot asinh \left(\frac{\frac{i}{i_{e,cat}}}{1 - \frac{i}{i_{l,cat}}} \right) + i \cdot R_{ohm} \tag{5.38}$$

Changes in the exchange current density due to different operating temperatures are considered with an Arrhenius-equation. Where $i_{ref,cat}$ is a reference exchange current density at the temperature T_{ref}. E_a is the activation energy of the cathode reaction.

$$i_{e,cat} = i_{ref,cat} \cdot e^{\frac{-E_{a,cat}}{R} \cdot (\frac{1}{T} - \frac{1}{T_{ref}})} \tag{5.39}$$

For the modelling of temperature dependency of the limit current density an exponential equation with two parameters a and b was applied. The fitting of the parameters to experimental data is shown in Section 5.1.3.5.

$$i_{l,cat} = a \cdot e^{b \cdot T} \tag{5.40}$$

The anode reaction V_{an} is modelled similar to the cathode reaction. Values for the standard potential, the activation energy, the charge transfer coefficient and the reference exchange current density are taken from literature. It is assumed that the limit current density and the ohmic resistance equals the values for the anode reaction. The open cell voltage for the anode is calculated as follows:

$$E_{OCV,an} = E^0_{an} - \frac{R \cdot T}{z \cdot F} \cdot \ln Q \tag{5.41}$$

With the quotient Q, where the activity of water a_{H_2O} is assumed to be approximately one.

$$Q = \frac{p^{0.5}_{O_2}}{a_{H_2O}} \approx p^{0.5}_{O_2} \tag{5.42}$$

The overall cell voltage is finally composed of the anode and cathode half cell reactions:

$$V_{cell} = V_{cat} + V_{an} \tag{5.43}$$

With the equations from the electrochemical model, the specific voltage-current characteristic of the CO_2-electrolyzer could be determined. Figure 5.11a shows the voltage-current curve against measurement data.

5.1.3.2 Thermal Model

The change of the cell temperature over time is modelled with a differential equation which balances the heat from an external heater $\dot{Q}_{heat}$, the reaction heat $\dot{Q}_{reaction}$ and the heat losses to the environment $\dot{Q}_{loss}$. In this equation C represents the overall heat capacity of the system.

$$\frac{\partial T}{\partial t} C = \dot{Q}_{heat} + \dot{Q}_{reaction} - \dot{Q}_{loss} \tag{5.44}$$

The heating power $\dot{Q}_{heat}$ could be determined with equation 5.45 using the mass flow $\dot{m}$ and the specific heat capacity c_p of the heat carrier. T_{in} refers to the temperature of the medium at the electrolyzer inflow, T_{out} at the outflow respectively.

$$\dot{Q}_{heat} = \dot{m} \cdot c_p \cdot (T_{in} - T_{out}) \tag{5.45}$$

To calculate the reaction heat, it is assumed that the occurring cell potential above the thermo-neutral voltage contributes to the heating of the cell.

$$\dot{Q}_{reaction} = (V_{cell} - V_{th}) \cdot I \tag{5.46}$$

Losses the the environment due to radiation and convection are modelled with the following equation, where K and m are fitting parameters to experimental data.

$$\dot{Q}_{loss} = K \cdot (T_{cell} - T_{amb})^{1+m} \tag{5.47}$$

The fitting of K and m to measurement data is shown in Section 5.1.3.5.

5.1.3.3 Formic Acid Production Model and Carbon Dioxide Demand

The formic acid production rate of the electrolysis is determined by the Faraday efficiency η_{FA}, which states how much of the electrical current is actually used to form formic acid. It it assumed that η_{FA} changes with the reaction temperature and the current density, both in a second order polynomial dependency. The polynomial coefficients $a_{x,y}$ must be determined experimentally.

$$\eta_{FA}(T, i) = a_{0,0} + a_{1,0} \cdot T + a_{0,1} \cdot i + a_{1,1} \cdot T \cdot i + a_{2,0} \cdot T^2 + a_{0,2} \cdot i^2 \tag{5.48}$$

With the Faraday efficiency η_{FA}, the electrical current I and the molar mass of formic acid M_{FA} the gravimetric production rate of formic acid could be calculated as follows:

$$\dot{m}_{FA,out} = \frac{I}{z \cdot F} \cdot \eta_{FA} \cdot M_{FA} \tag{5.49}$$

Accordingly, the demand of carbon dioxide could be specified with the molar mass of carbon dioxide M_{CO_2}:

$$\dot{m}_{CO_2,demand} = \frac{I}{z \cdot F} \cdot M_{CO_2} \tag{5.50}$$

5.1.3.4 Integration of the CO_2-electrolyzer model into INSEL

Figure 5.10 shows the inputs, outputs and the parameters of the INSEL block of the CO_2-electrolyzer. The charge transfer coefficient α, the reference exchange current density $i_{e,0}$, the activation energy E_a and the standard potential E_0 must be determined for the cathode and anode separately.

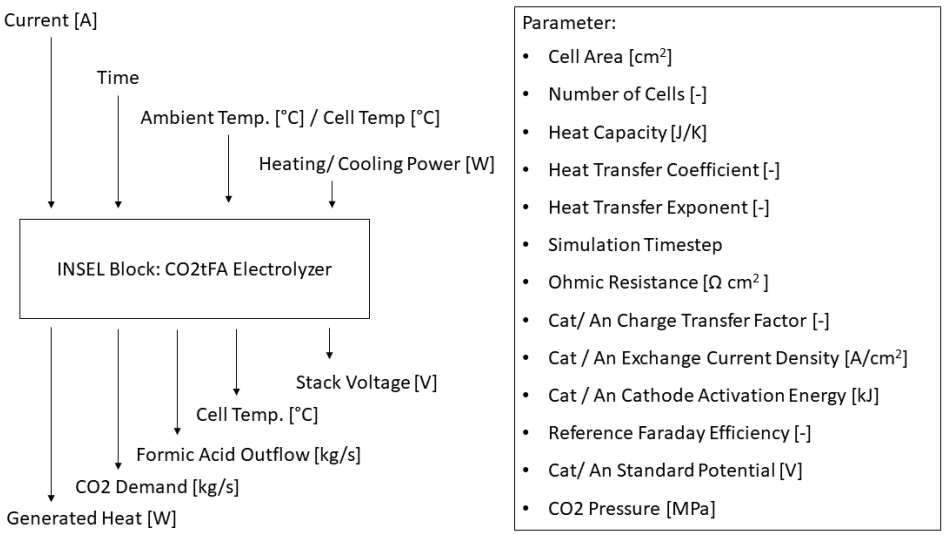

Figure 5.10: CO_2-electrolyzer INSEL BlocK: inputs, outputs, parameters

5.1.3.5 CO_2-Electrolyzer Model Validation

In the following section, the electrochemcical model, the Faraday efficiency and the thermal model of the electrolyzer are validated against measurement data.

Voltage-Current-Characteristics The electrochemical model, which is used in the INSEL block of the CO_2-electrolyzer was validated against measured data for the cathode voltage at specific current densities. Experiments were executed using a cathode with a GDE and a heterogenous Sn catalyst. The data was provided by the Institute of Chemical Technology of the University of Stuttgart. Table 5.3 shows the values for the parameters α_{cat}, $i_{ref,cat}$, $E_{a,cat}$ and R_{ohm} as fitted to the experimental data.

Table 5.3: Voltage-current characterization - fitting parameters

Parameter	Value
α_{cat}	0.4
$i_{ref,cat}$	$1 \times 10^{-8}\,\mathrm{A\,cm^{-2}}$
$E_{a,cat}$	$90\,\mathrm{kJ\,mol^{-1}}$
R_{ohm}	$0.1\,\Omega\,\mathrm{cm^2}$

With the fitting parameters, the voltage-current characteristic of the CO_2-electrolyzer could

be calculated. Figure 5.11a shows the results of the voltage-current characteristic with fitted parameters for 20 °C and 70 °C. For the voltage-current characteristic the mean absolute percentage error (MAPE) was calculated in order to evaluate the deviation of the model from the measurement data. The MAPE is calculated as 1.76 % for the the 35 °C curve and 1.27 % for the 70 °C curve respectively.

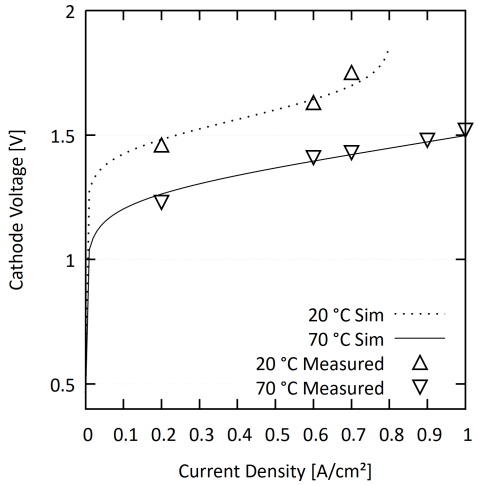

(a) Measured cathode voltage against simulated data

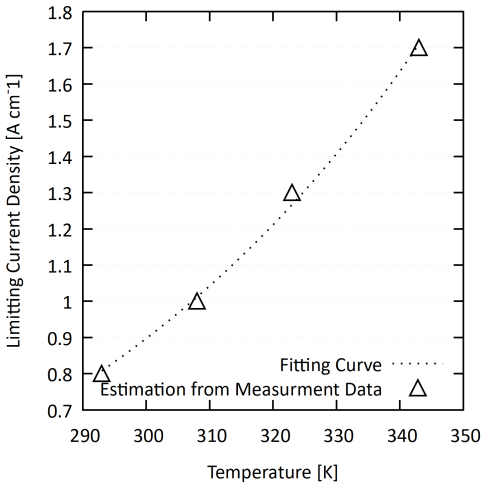

(b) Fitting Curve for the limit Current Density

Figure 5.11: CO_2-electrolyzer model validation

Figure 5.11b shows the fitting curve for the limit current density i_l. The MAPE for i_l is not determined separately as the limit current density is also included in the voltage-current submodel.

Faraday Efficiency - Fitting Parameters The polynomial coefficients $a_{x,y}$ of Equation 5.48 were fitted to match experimental data of the Faraday efficiency of the formic acid production η_{FA}. The Matlab Curve Fitting application was used to determine the polynomial coefficients. The resulting coefficients are summarized in Table 5.4.
Figure 5.12 shows the measured values and the fitting curve for η_{FA} over the current density at 35 °C and 50 °C. The MAPE was calculated to evaluate the derivation for of the model from the measurement data. For the Faraday efficiency at 35 °C the MAPE is 8.69 % and 2.7 % at 50 °C. The accuracy of the model for the Faraday efficiency is lower than for the voltage-current model. The empirical model needs more and higher resolution data to determine the polynomial parameters precisely. An improvement of this model should therefor either be based on better data or the empirical model should be changed with a physical model of the Faraday efficiency.

Table 5.4: Faraday efficiency: fitting parameters

Parameter	Value
$a_{0,0}$	-719
$a_{1,0}$	5.228
$a_{0,1}$	-0.08906
$a_{1,1}$	0.0003979
$a_{2,0}$	-0.008492
$a_{0,2}$	-4.622e-5

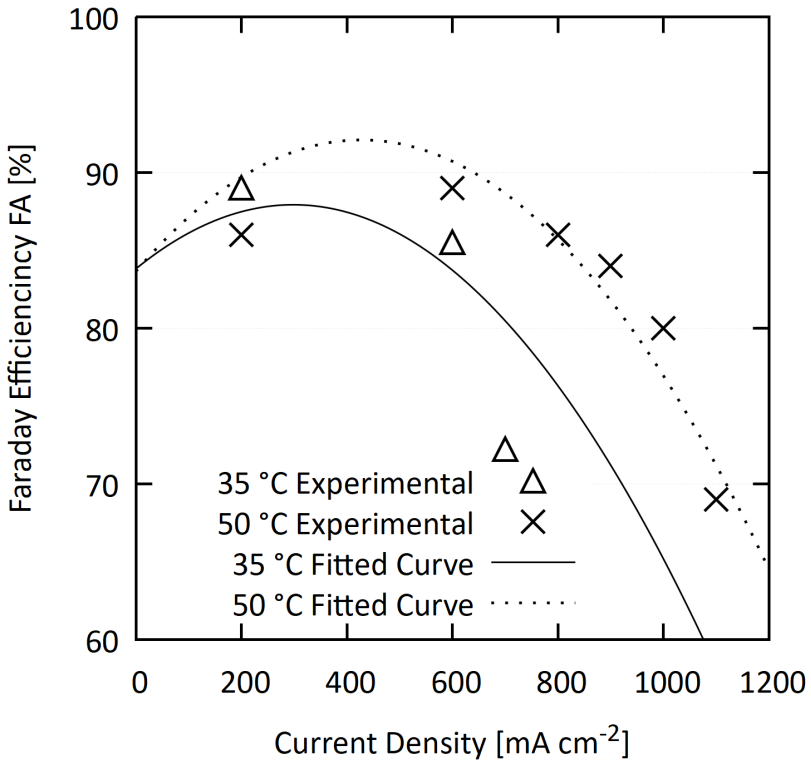

Figure 5.12: Measured vs fitted data for the Faraday efficiency η_{FA} of the CO_2-electrolyzer

Thermal characteristics - Heat capacity and heat losses To validate the thermal model described by Equation 5.44 and determine the heat capacity C, as well as the parameters of the cool down curve K and m, an experiment was carried out at the CO_2-electrolyzer test rig. The measurement variables used for the thermal characterization are shown in Figure 5.13.

For this experiment, water was used a heat carrier. The water was heated up by a thermostat

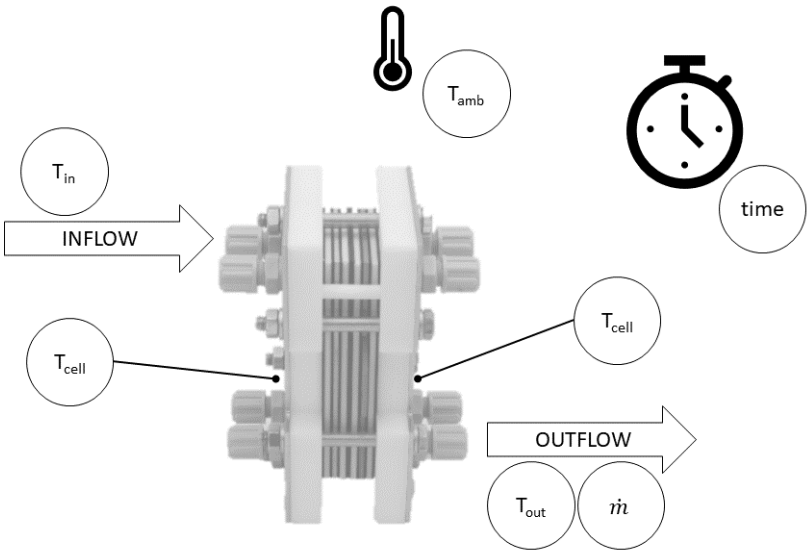

Figure 5.13: Measurement variables of the experimental setup for the thermal characterization of the CO_2-electrolyzer

and afterwards pumped through the cell. With a temperature setpoint of 90 °C, the cell was heated up for 30 min with a constant pump power, without an active electrolysis process ($\dot{Q}_{reaction} = 0$). After the heat up time, the cell was cooled down passively to ambient conditions. All temperatures where measured by thermocouples. The mass flow was determined indirectly by measuring the volume of water flowing through the cell in 30 s. The experiment parameters are summarized in Table 5.5.

Table 5.5: Thermal Characerization - Experiment Parameters

Parameter	**Value**
Heat Carrier	Water
Temperature Setpoint	90 °C
Heating Time	30 min
Mass Flow Rate	0.0117 kg s^{-1}

The INSEL model of the CO_2-electrolyzer was used to solve the differential equation of the thermal model (Equation 5.44) and the parameters C, K and m were fitted to the experimental data. The parameter fitting leads to the values shown in Table 5.6.

Table 5.6: Thermal model: parameter fitting

Parameter	Value
C	2679
K	1.64
m	0.19

Figure 5.14 shows the measured cell temperature as well as the simulation results with fitted parameters. The MAPE of the fitted model is 0.13 %.

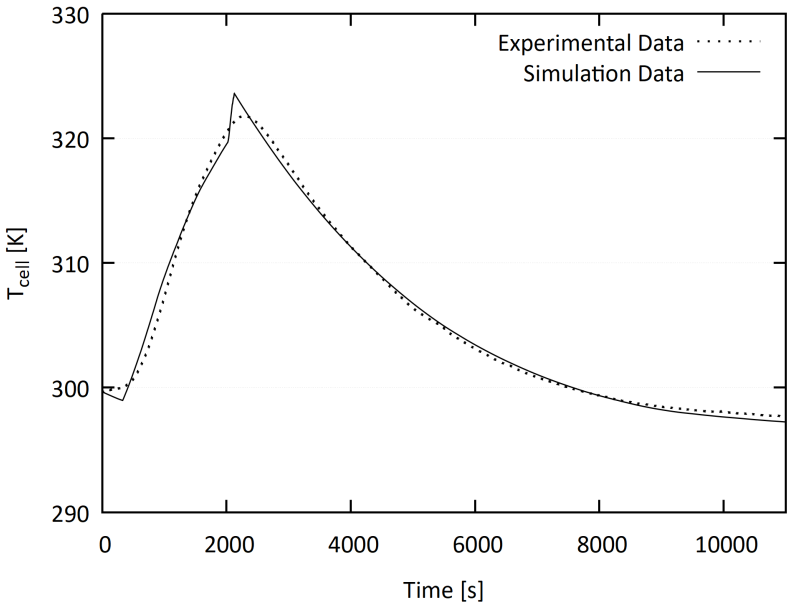

Figure 5.14: Experimental data and simulation results for active heating up and passive cool down of the CO_2-electrolyzer

Compared to the cool down curve, the heating up of the cell shows more discrepancy. Especially at the start and the end of the heating phase. It is assumed that the deviation is caused by the simplifications of the model where the inertia of the fluid is not regarded. Another potential source of error is that the water mass flow is not measured continuously during the experiment. As fluctuations are occurring most likely because of temperature differences and the existence of air bubbles in the pipes, the heating power $\dot{Q}_{heat}$ is not determined exactly at every measurement point. These effects however are short termed compared with the larger time scales for the planned CO_2-electrolyzer operation. It must be noted that the fitting of the model parameters were executes with a single-cell laboratory setup of the CO_2-electrolyzer. In order to simulate an upscaled system, the parameters must

be adapted to measured data of a CO_2-electrolyzer stack.

5.1.4 Auxiliary Components

In this section, auxiliary components needed for the implementation of the previous described component models into system models are described. A formic acid storage tank and a FA-to-H2 reactor controller.

5.1.4.1 Formic Acid Storage Tank

The storage tank for formic acid is modelled as a simple 'bucket'. At each time step the mass of formic acid in the tank is calculated based on the balance of the inflow $\dot{m}_{FA,in}$ and outflow $\dot{m}_{FA,out}$ of formic acid.

$$m_{FA}(t) = m_{FA}(t - \Delta t) + (\dot{m}_{FA,in} - \dot{m}_{FA,out}) \cdot \Delta t \tag{5.51}$$

With the stored formic acid at each time step filling level S_{FAtank} is determined.

$$S_{tank}(t) = \frac{m_{FA}(t)}{\rho_{FA} \cdot V_{tank}} \tag{5.52}$$

Additionally, the formic acid storage tank model allows the enabling of refills, if external formic acid deliveries are regarded for the investigated use case (e.g. for off-grid applications). Therefor, the lower bound of the filling level must be determined at which an external refill is triggered.

5.1.4.2 FA-to-H2 Reactor Controller

The controller of the FAtH2-Reactor provides a temperature setpoint for the reactor, which depends on the hydrogen demand of a subsequent fuel cell. The temperature is used as an input for the INSEL Block of the FAtH2-Reactor (see Figure 5.8). Equation 5.53 shows the dependency of the hydrogen output of the reactor from the reactor volume and the reaction temperature (see also Equation 5.12). The parameters a and b are used as fitting parameters.

$$\dot{m}_{H_2}(V, t) = a \cdot V \cdot e^{b \cdot \frac{1}{T}} \tag{5.53}$$

The hydrogen outflow of the reactor at different temperatures and different reactor volumes are determined with the INSEL Block described in Section 5.1.2.2. Figure 5.15 shows a surface plot of the hydrogen outflow.
A curve fitting with Equation 5.53 was executed to determine the fitting parameters a and b. The resulting parameters are shown in Table 5.7.

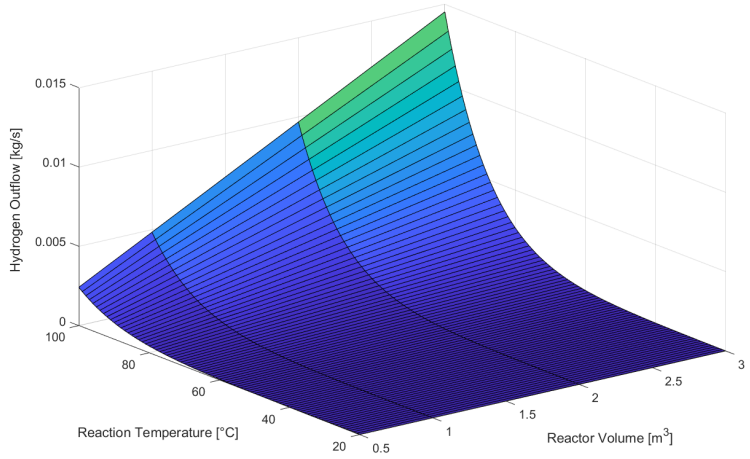

Figure 5.15: Hydrogen Outflow Dependency from Reaction Temperature and Reactor Volume

Table 5.7: FAtH2-Reactor Controller - Fitting Parameters

Parameter	Value
a	3.545
b	-664.5

Finally, Equation 5.53 is rearranged to calculate the reaction temperature directly from the hydrogen demand and the reactor volume. The temperature output is bounded between the ambient temperature and the maximal possible reaction temperature [1]

$$T_{set} = \frac{b}{ln\left(\frac{\dot{m}_{H_2,demand}}{V \cdot a}\right)} \tag{5.54}$$

Providing T_{set} as an input for the FA-to-H2 reactor model allows to control the hydrogen production rate of the reactor.

5.2 Additional Component Models

In this section, additional components for modeling formic acid based hydrogen storage systems are introduced. These models already exists in some form or another, and are either

[1] Note that the the function has a vertical asymptote and negative values could appear at very high hydrogen demands in relation to the reactor volume. By sizing the reactor volume for the concrete use case, the operation of the reactor is far from these areas. However, this issue is assumed in the model by setting the temperature set point to the maximal value, if negative values are calculated.

already described in literature or are available in common simulation tools. For this thesis, the models are either newly implemented to the INSEL simulation environment or are improved and optimized for the targeted application.

5.2.1 PEM-Electrolyzer

In this section the main equations to describe the dynamic behavior of an PEM electrolyzer are introduced. Most of the governing equations and fundamentals for modelling PEM electrolyzers are already described in Section 2.3.3 and Section 3.1. At this point only specific aspects for the PEM water eletrolyzer model is given. For a more detailed description of PEM electrolyzer modeling see Carmo et al. [37].

Thermodynamics The change of Gibbs free energy determines if an electrochemical reaction is spontaneous (galvanic cell: $dG < 0$) or non-spontaneous (electrolytic cell: $dG > 0$). It is the difference between the reaction enthalpy and the product of the reaction entropy and the temperature:

$$dG = dH - T_{cell} \cdot dS \tag{5.55}$$

With dG, the open cell voltage (OCV) of an electrochemical reaction could be calculated:

$$E_{OCV} = \frac{-dG}{zF} \tag{5.56}$$

Under standard conditions, the OCV for water electrolysis 1.23 V. The thermoneutral voltage E_{th} is calculated with the enthalpy instead of the Gibbs free energy.:

$$E_{th} = \frac{-dH}{zF} \tag{5.57}$$

Neglecting the entropic part means that the energy needed to drive the electrolysis must completely supplied by the electric component of the reaction. This rises the cell voltage under standard conditions to 1.48 V.

Voltage losses are modeled according to Section 2.3.3. The modeling approach is both used for the CO_2-electrolyzer and the PEM water electrolyzer, however with changing parameters.

Hydrogen Production Rate The rate of hydrogen formation $\dot{n}_{H_2}$ is proportional to the electrolysis current I, as stated by Faraday's first law of electrolysis (with the Faraday effi-

ciency η_{FA} and the number of cells N).

$$\dot{n}_{H_2} = \frac{I}{zF} \cdot \eta_{FA} \cdot N \tag{5.58}$$

Finally, $\dot{n}_{H_2}$ is converted to the mass flow rate $\dot{m}_{H_2}$ with the molar mass of a hydrogen molecule $M_{H_2} = 2 \times 10^{-3}\,\mathrm{kg\,mol^{-1}}$.

$$0\dot{m}_{H_2} = \dot{n}_{H_2} \cdot M_{H_2} \tag{5.59}$$

Cell Temperature If the cell voltage is higher than the voltage needed to drive the electrolysis process, heat is generated. The amount of heat generated by the stack with a given cell voltage and current is calculated according to the following equation.

$$\dot{Q}_{react} = (V_{cell} - E_{th}) \cdot I \cdot N \tag{5.60}$$

The losses to the environment by convection and radiation could be approximated with two parameters k and m and an exponential equation (see [44]). Both parameters k and m are fitting parameters and must be adapted to experimental data[2].

$$\dot{Q}_{loss} = k \cdot (T_{cell} - T_{amb})^{(1-m)} \tag{5.61}$$

The overall heat balance of the stack is determined by the sum of the heating/ cooling power, the reaction heat, and the heat losses.

$$\dot{Q} = \dot{Q}_{heat} + \dot{Q}_{react} - \dot{Q}_{loss} \tag{5.62}$$

Finally, the cell temperature is calculated with an ordinary differential equation, with a given heat capacity C of the stack[3].

$$T_{cell} = \frac{1}{C} \cdot \int (\dot{Q} \cdot dt) \tag{5.63}$$

5.2.1.1 Electrolyzer Model Validation

The electrical submodel of the electrolyzer is validated against the reported performance range of PEM Electrolyzers at 80 °C according to Carmo et al. [37]. For an exchange current density of $i_{e,an} = 1.5{\cdot}10^{-2}$ and $i_{e,cat} = 1.3{\cdot}10^{-2}$ the performance of the electolyzer model lies

[2] There are other possibilities to model the heat losses based on the stack geometry (surface area) and a heat transfer coefficient which includes effects of radiation and natural convection. However the heat transfer coefficient must also be estimated or determined from experiments

[3] The heat capacity could either be evaluated from experimental data or estimated by taking the mass and specific heat capacity of the electrolyzer parts (end plates, bibpolar plates, MEA) into account

within the reported boundaries (see Figure 5.16a). However, as the Butler-Volmers equations determining the activation overpotential is highly sensitive to the exchange current density, this parameter must be adapted with experimental data if any specific electrolyzer system is supposed to be simulated. The thermal submodel of the electrolyzer is also validated against reported data (from [39]). Figure 5.16b shows the curve of the cell temperature in a natural cooling experiment. The stack is cooled down from 50 °C to ambient temperature.

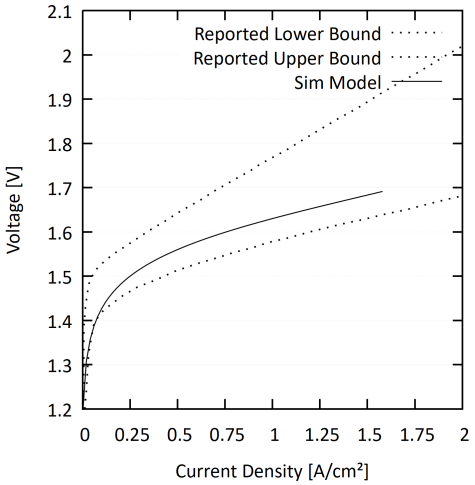

(a) Validation of the PEMEC electrical submodel against reported data

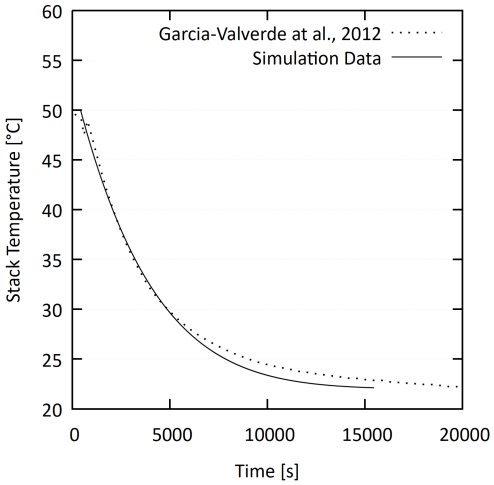

(b) Validation of the PEMEC natural cooling against reported data

Additionally the development of the stack temperature over time at different current setpoints is evaluated. Figure 5.17a shows the attached current setpoint according to an experiment reported by Garcia-Valverde et al. [39] and the consequential simulated stack voltage. The simulated cell temperature in the course of this experiment and the reported experimental data is shown in Figure 5.17b.

The PEM electrolyzer model shows good consistency to the reported experimental data.

5.2.2 Hydrogen Storage Cylinder

To determine the pressure in the storage tank, the net hydrogen mass flow is calculated by the currently occurring inflow from the electrolyzer and outflow requested by the consumer (e.g. a fuel cell):

$$\dot{m}_{H_2} = \dot{m}_{H_{2,inflow}} - \dot{m}_{H_{2,outflow}} \tag{5.64}$$

With the net mass flow and the amount of hydrogen present in the previous time step results

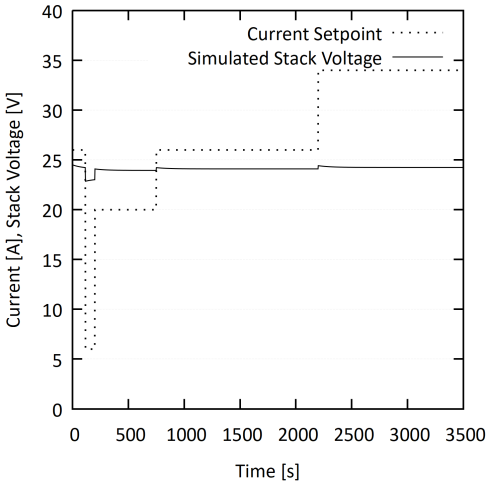

(a) Current Setpoint and simulated Stack Voltage

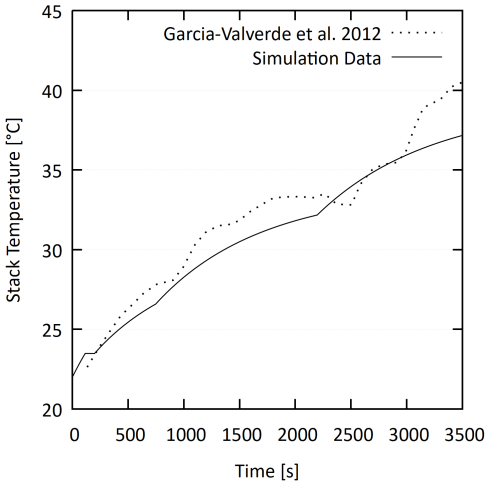

(b) Simulated and experimental Cell Temperature

the overall mass of hydrogen in the storage device:

$$m_{H_2} = \int \dot{m}_{H_2} \cdot dt \tag{5.65}$$

In real compressed gas storage situations, the heating of the gas due to compression and the opposite effect: cooling due to relaxation (Joule-Thomson-Effect) must be considered, as this effect lowers the storage capability. This is especially observed in fast filling processes (e.g. filling of FCV tanks). In this work these effects are neglected ($T_{gas} = T_{amb}$) as the incoming hydrogen mass flow is expected to be low compared to the storage capacity for the use as a seasonal storage system. The pressure in the storage tank (in Pa) is calculated with the ideal gas law. If the maximal storage pressure P_{max} is reached, any additional incoming hydrogen will be purged to the atmosphere in this model.

$$p_{storage}(t) = \frac{m_{H2}(t) \cdot R_S \cdot T_{gas}}{V} \tag{5.66}$$

5.2.3 Hydrogen Compressor

The hydrogen compression process is modeled as iso-thermal (approximately true for multi-stage compressors) and hydrogen treated as an ideal gas which is corrected with a compressibility factor Z (from empirical equations, see [153], [108]) , or interpolated from table data).

Isothermal compression work is calculated as follows:

$$W_{1\to 2} = -\int_{p_1}^{p_2} V \cdot dp \tag{5.67}$$

With the Z corrected ideal gas law:

$$p \cdot V = Z \cdot m \cdot R_s \cdot T \tag{5.68}$$

The power needed for the compression is calculated with the subsequent equation::

$$P_0 = \dot{m} \cdot R_s \cdot T \cdot Z \cdot \ln\left(\frac{P_{storage}}{p_{in}}\right) \tag{5.69}$$

Also the efficiency of the compressor is taken into account to determine the resulting electrical power needed for the compression:

$$P = \frac{P_0}{\eta} \tag{5.70}$$

The efficiency of a single compressor stage η_i depends on the load percentage of the hydrogen flow and is assumed to follow a characteristic as shown in Figure 5.18a (see [154]). For a multi-stage compressor with n symmetric stages, the overall efficiency η calculates according to Equation 5.71.

$$\eta = \eta_i^n \tag{5.71}$$

Figure 5.18b shows the course of the compressor power and the storage pressure for the filling of a 600 L storage cylinder from 1 MPa to 35 MPa at the nominal flow rate of the compressor. For this porcess about 40 kWh of energy are consumed by the compressor resulting in 2.55 kW h kg^{-1}. For a compression to 35 MPa values between 2 and 4 kW h kg^{-1} for the specific energy consumption of the compressor are reported in literature [155].

5.2.4 PEM Fuel Cell

As an electrochemical device with similarities to PEM electrolyzers, the model of the fuel cell is at this point not further described, only fuel cell specific changes are described. A profound introduction into PEM Fuel Cell modeling is e.g. given by C. Spiegel [41].

The Nernst equation for the fuel cell takes the partial pressures of the involved species into account:

$$V_{nernst} = V_{OCV} + \frac{R \cdot T}{zF} \cdot \ln\left(\frac{p_{H_2} \cdot p_{O_2}^{0.5}}{p_{H_2O}}\right) \tag{5.72}$$

Furthermore, the activation losses of the fuel cell are modeled using a logarithmic equation

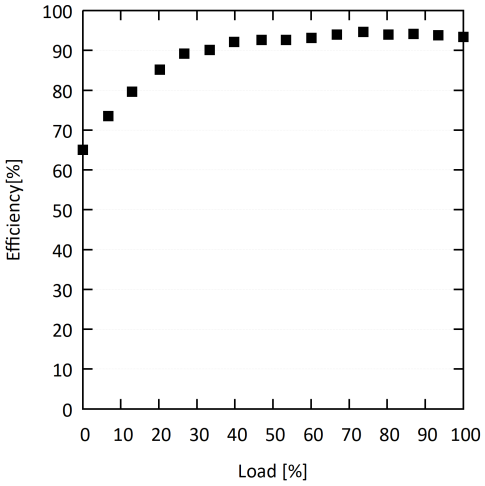

(a) Single Stage Compressor Efficiency over Part Load

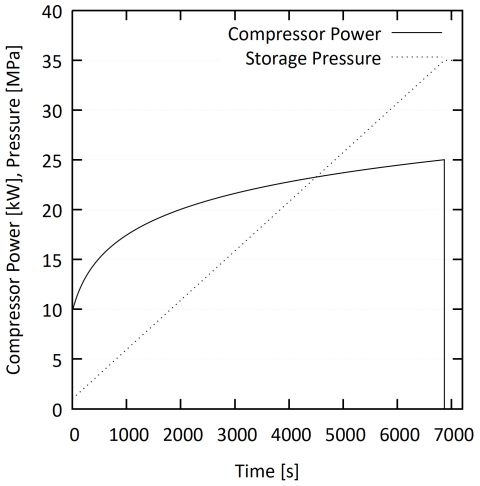

(b) Compressor Power and Storage Pressure for Model Validation

with the exchange current density i_e:

$$V_{act} = -\frac{R \cdot T_{cell}}{\alpha \cdot z \cdot F} \cdot \ln\left(\frac{i}{i_e}\right) \tag{5.73}$$

The mass transportation losses are also modeled differently as described by Spiegel [156]. With the amplification factor $\alpha = 0.085$, the constant $k = 1.1$ and the limit current density i_L:

$$V_{trans} = \alpha_1 \cdot i^k \cdot \ln\left(1 - \frac{i}{i_L}\right) \tag{5.74}$$

Finally, the fuel cell model is validated against experimental data reported by Neto et al. [142] for a PEMFC stack with an electrode area of 250 and 12 cells. The exchange current density was fitted to match the experimental data. Figure 5.19a shows the voltage current characterstitic of the stack at an operation temperature of 41 °C, a hydrogen pressure of 300 mbar and an air pressure of 500 mbar. The electricity and heat output of the stack at 30 °C is shown in Figure 5.19b.

To represent the influence of the power demand of the auxiliary systems (e.g pumps, power electronics), the power output of the fuel cell is lowered according to Equation 5.77.

$$P_{net} = P_{FC} - P_{aux} \tag{5.75}$$

The auxiliary power is modeled with a base load $P_{aux,base}$, which depends on the fuel cell

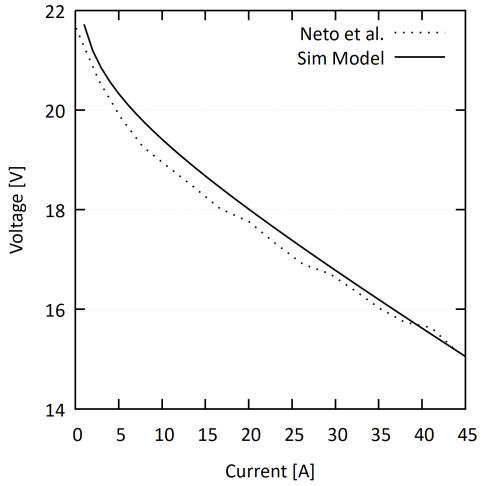

(a) Fuel Cell Current and Voltage for Model Validation

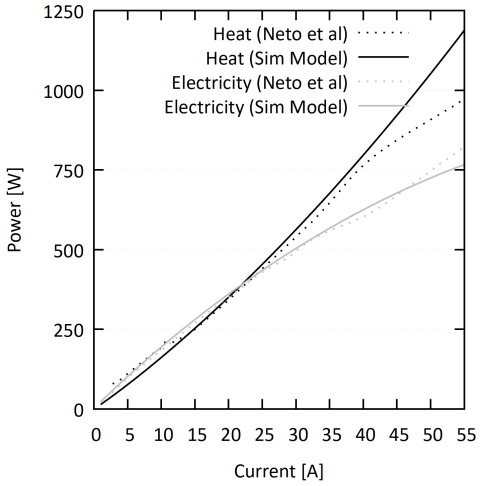

(b) Fuel Cell Heat and Electricity Output for Model Validation

power at the nominal operating point $P_{FC,nominal}$.

$$P_{aux,base} = X_{base} \cdot P_{FC,nominal} \tag{5.76}$$

Finally, P_{aux} consists of $P_{aux,base}$ and a variable share related to the current fuel cell power output P_{FC} with $X_{aux,varaible}$.

$$P_{aux} = P_{aux,base} + X_{aux,variable} \cdot P_{FC} \tag{5.77}$$

Both X_{base} and $X_{aux,variable}$ could be interpreted as the percentage of the fuel cell power needed to operate the auxiliary units. They could chosen as a model parameter. With both values set to zero, the auxiliary system power demand is neglected.

5.2.5 Building Models

The building models used to predict the heat and power demand are simplified white box models. These models are based on the nodal method and require physical information e.g. about the building outlines. The simplifications made in this approach, is that the building consist of a single zone with a homogeneous volume and a lower grade of geometric details are applied. For each wall a one-dimensional heat conduction equation is solved. Also heat transfer by radiation is considered [48].

5.2.6 Energy System Models

PV and Heat Pumps An common approach to model the voltage-current-characteristic of a PV module is a two-diode model with a maximum power point tracking (MPPT) loop. The power demand and heat output of heat pumps could be modeled with characteristic curves from the manufacturer. As the load profiles, which include PV power production and heat pump power consumption, later on used for the simulation of the building cluster are based on the work of Brennenstuhl, more details on PV and heat pump modelling could be derived from [48].

Small Wind Turbines To evaluate the power output of a small wind turbine a given location two kinds of input data are used: measured or simulated wind speeds and a power curve of the wind turbine. For any measured wind speed $v_{measure}$ at height $H_{measure}$, the wind speed in height of the wind turbine hub v_{hub} could be calculated with a simplified law of logarithmic boundary layer profiles:

$$v_{hub} = \left(\frac{H_{hub}}{H_{measure}} \right)^{\alpha} \cdot v_{measure} \tag{5.78}$$

The exponent α refers to the terrain roughness and takes values between 0.16 for open terrains (water, grassland) over 0.28 for terrain with obstacles (forests, villages) to 0.4 for a terrain with big obstacles, such as high-rise buildings. The power output of the wind turbine is than given by using a power curve for the specific wind turbine type with the wind speeds at input data.

5.3 System Models

For all systems introduced in chapter 5, system models were created with the graphical user interface of INSEL. The following features are common to all system models:

- The load profile is read as an input file (.txt) divided into surplus power ($P > 0$) connected to the electrolyzer controller and deficit power ($P < 0$) connected to the fuel cell controller.
- The simulation timestep is one minute. Seconds of the year (SOY) is used as a clock.
- All relevant system design parameters were defined as global variables, so that it is easy to adapt the system to the specific requirements of its application. This approach also allows an automation of the simulation initialization, as the global variables could be accessed with externally, for example by embedding the INSEL simulation execution via templates into Python scripts.

- The most important simulation results are logged into a .csv file at each time step for evaluation purposes
- Generic INSEL Blocks are used, e.g. for unit conversions or to delay inputs for a single time step

5.4 Simulation workflow

The overall workflow of the system simulation consists of several steps (see Figure 5.20). First, the input data must be processed. In this case the accumulated load profiles of a building or building cluster, which includes renewable energy production, household power demand, as well as power demand for the heat pump are used. The load profile is processed in a Python script to determine suitable system parameters, based on simple rules (see Section 6.4.1). These parameters are subsequently passed to a INSEL template of the system model. The actual simulation run is then executed in INSEL. To provide a data transfer, INSEL writes a .csv-File with the simulation results for each time step. Another Python script is used to finally evaluate the results. At this point an optimization loop can be applied, with either a manual adjustment of the system parameters based on the simulation results or by an automatic, stochastical approach with genetic algorithms. Therefor, first a target function must be determined (see Section 6.4.2).

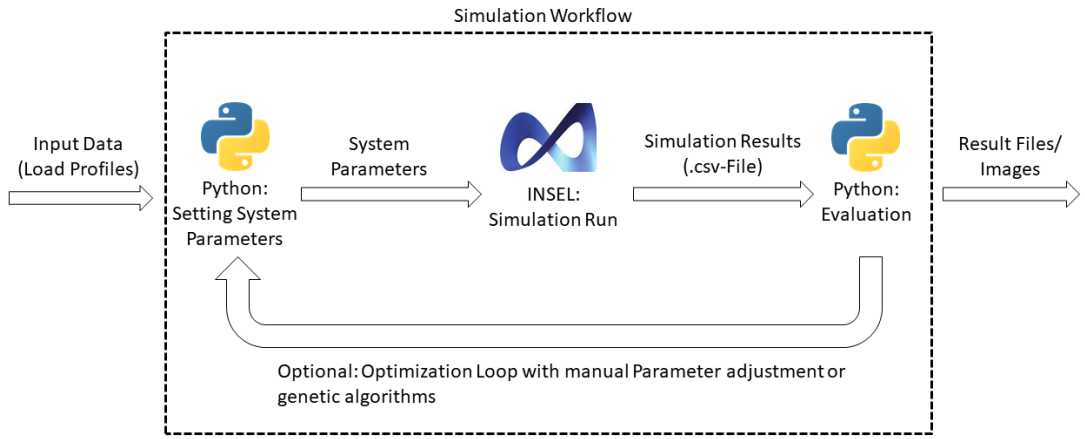

Figure 5.20: Workflow of the simulation

Chapter 6

System Design and Integration

In this chapter three different approaches for a seasonal district storage system with formic acid based hydrogen storage are introduced. Also, a reference system with water electrolysis and high-pressure hydrogen storage is shown. All systems variations include a fuel cell for the reconversion of hydrogen to power and heat. After a detailed description of the energy systems, system integration aspects, such as the electrical and thermal integration into the existing energy system, are more closely examined. Furthermore, different operation modes and control strategies for all system variants are regarded. This chapter finishes with aspects concerning the dimensioning of the systems to their operational environment. Two different approaches for the dimensioning are shown: a rule-based system design and an automatic system design with a cost function and genetic algorithms.

This chapter aims at answering the second research objective: how can formic acid based hydrogen storage systems be dimensioned, controlled and integrated into existing energy systems?

6.1 System Design of a District Storage System with Formic Acid based Hydrogen Storage

System 1 of the proposed energy storage systems is the reference system. It consists of a grid-connected PEM electrolyzer, a multi-stage hydrogen compressor, a high-pressure hydrogen storage tank and a PEM fuel cell (see Figure 6.1). The PEM electrolyzer stack is chosen, because this technology is adaptive to the input power, tolerant to fast load changes and usually shows fast response times. For more information about PEM electrolysis see Section 3.1. Additionally, a buffer battery is used to smooth fast load changes and avoid electrolyzer stand-by times. The PEM Fuel Cell, which is considered for the reconversion of hydrogen to

power and heat, generally is controllable with to different modes:

- Electricity controlled mode: the current setpoint is determined by the electricity demand of the building/ district with heat produced as a by-product. In this mode the whole system could be classified as a seasonal electrical energy storage system.
- Heat controlled mode: the current setpoint is determined by the heat demand of building/ district with electricity as a by-product. In this case the system represents a power-to-heat application.

All components are assumed to be housed in a heating center. For an overall better system efficiency, the waste heat of the electrolyzer and the fuel cell could be used, if a heat network is available. Another possibility would be to use the waste heat for a nearby consumer (e.g. a public building) depending on the location of the heating center.

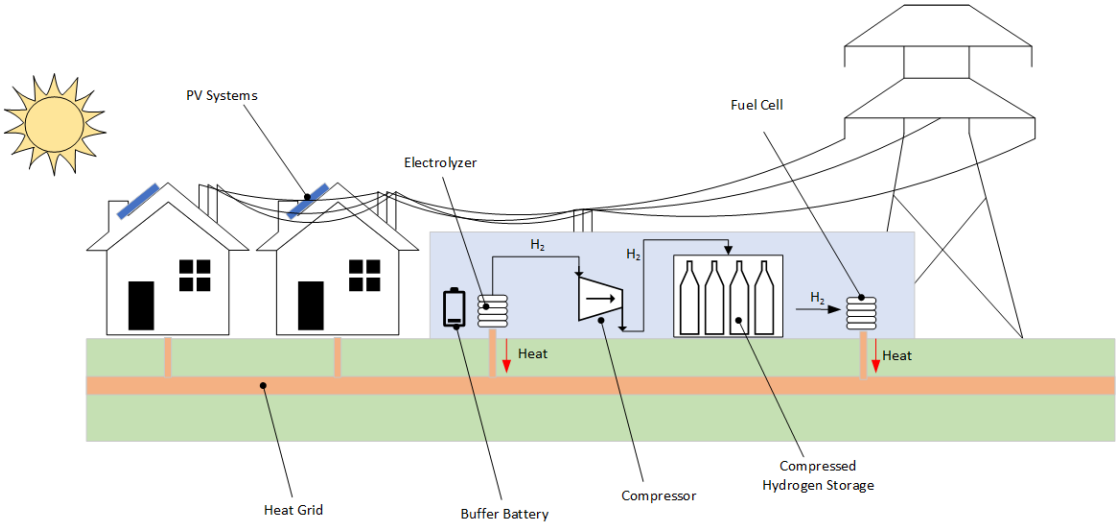

Figure 6.1: System 1: reference system with water electrolysis and compressed hydrogen storage

The first system variant with formic acid based hydrogen storage is based on reversible H_2 batteries. Those reactive batteries directly replace the compressor and the high-pressure storage tank from the reference system (see Figure 6.2), which is advantageous because gaseous hydrogen does not have to be stored at high pressures. All other components remain unchanged, meaning that the released hydrogen from the reversible hydrogen batteries are utilized in a PEM fuel cell for power and heat production
System 3 is based on formic acid synthesis and formic acid decomposition in flow reactors (see Figure 6.3). The first flow reactor is used to synthesize formic acid with hydrogen from water electrolysis and carbon dioxide. An external CO_2 source is therefor needed. Formic

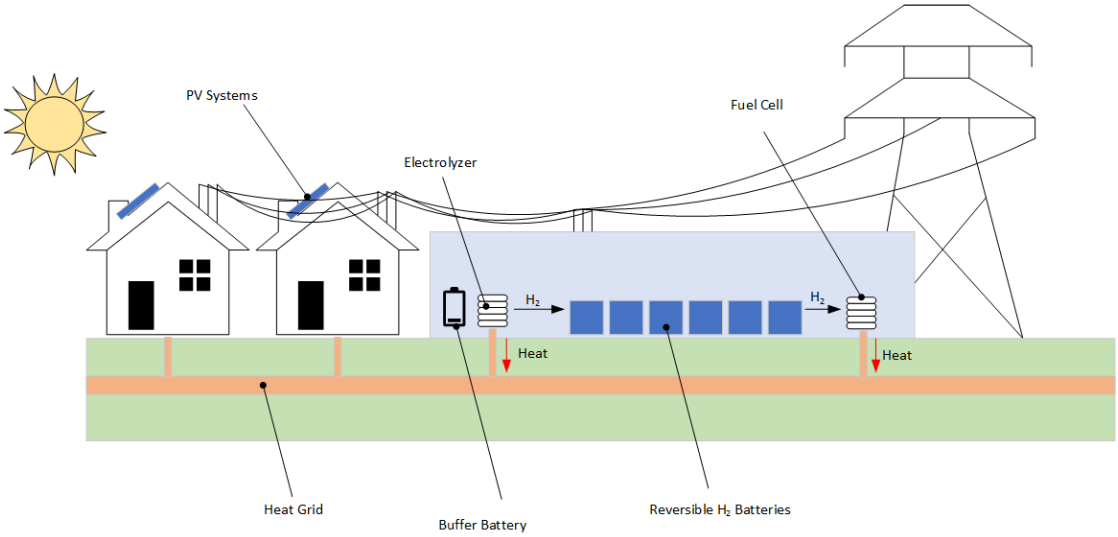

Figure 6.2: System 2: Water Electrolysis and Reversible H_2 Batteries

acid is stored in a storage tank and on demand decomposed to carbon dioxide and hydrogen, which is subsequently utilized in a PEM fuel cell. Due to good material compatibility low-cost polyethylen (PE) tanks could be used for the formic acid storage in this system.

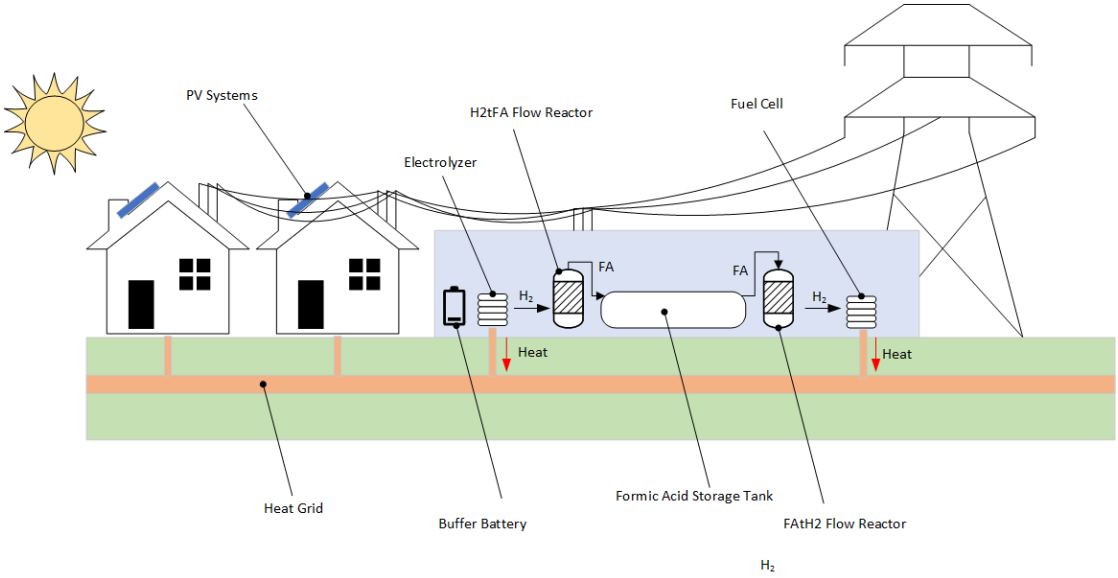

Figure 6.3: System 3: water electrolysis and formic acid based hydrogen storage with flow reactors

System 4 shows the biggest changes with regard to the reference system. The PEM elec-

trolyzer is replaced with a CO_2 electrolyzer, which directly produces formic acid from electrical power, water and carbon dioxide (see Figure 6.4). The carbon dioxide electrolyzer used for System 4 is based on the electrolysis cells described in Section 4.3. Formic acid storage and utilization is similar to system 3, with a storage tank, a flow reactor for formic acid decomposition and a PEM fuel cell for power and heat production.

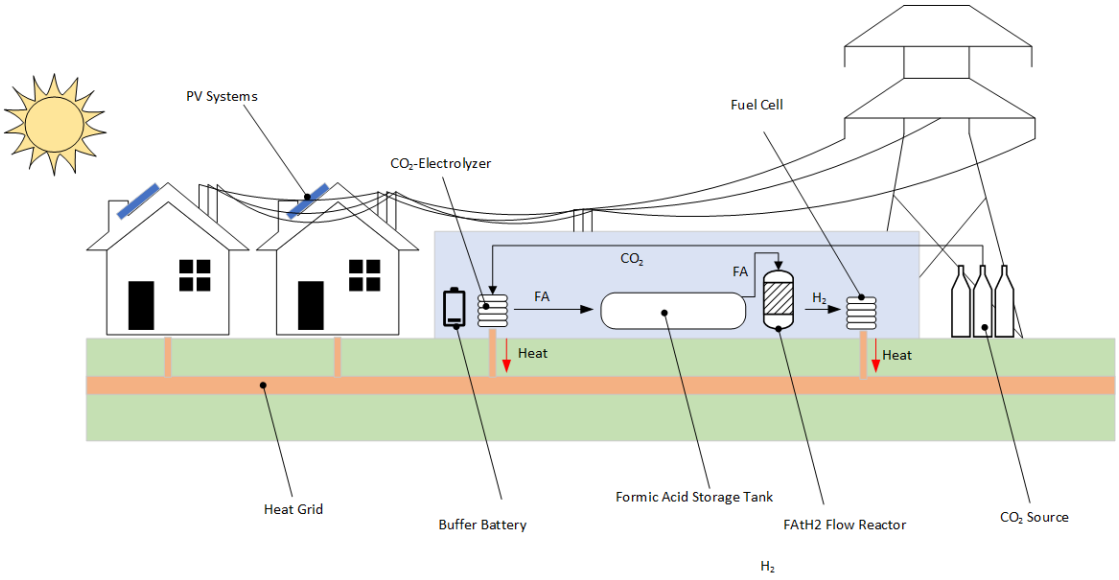

Figure 6.4: System 4: CO_2-electrolysis, formic acid storage tank and formic acid dehydrogenation flow reactor

6.1.1 Energy Systems

The purpose of the above proposed formic acid based hydrogen storage systems is the seasonal storage of electrical energy from renewable energy sources. As this work focuses on the building sector, the main source of energy, which is meant to be stored, are building integrated PV systems. State of the art for PV systems are monocrystalline, polycrystalline and amorphous silicon cells with a combined market share of about 70% [157]. Depending on the cell technology, about 5 m^2 to 8 m^2 area is needed for the installation of 1 kW_p rooftop mounted PV. For southern Germany a annual yield of about 1000 kWh per installed kW_p could be assumed[1]. In order to increase the energy production for the regarded building cluster, additional open space photovoltaic systems or small wind turbines (SWT) could be considered. This form of energy production is more suitable for rural areas with larger area availability. Another measure to increase the system efficiency is to couple the heat demand

[1]Note that this value is only a rule of thumb. The exact PV yield strongly depends on the roof inclination and orientation, as well as on the cell type

of the electrolyzer and the flow reactors with solar thermal reactors. However, this system combination is not further investigated in this work.

6.2 System Integration Aspects

Three different aspects of the integration of formic acid based hydrogen storage systems into existing energy systems are subsequently further investigated:

- The electrical integration into the low-voltage grid
- The thermal integration into a district heating network or thermal storage of a single building
- The demand and outflow of reactants and products

6.2.1 Electrical

All described systems are intended for an integration into the low-voltage grid. In Europe the LV grid usually consists of four conductors (L1, L2, L3 and N). This setup allows a one or three-phase connection of loads and generators. The LV grid has two levels of voltage (230 V and 400 V) and a target frequency of 50 Hz. The one-phase power could be calculated according to Equation 6.1.

$$P = U \cdot I \tag{6.1}$$

For a three-phase connection the power is calculated as follows:

$$P = U \cdot I \cdot \cos\phi \cdot \sqrt{3} \tag{6.2}$$

With the power factor of $\cos\phi \approx 1$. The current limit depends on the grid impedance, which means it could be necessary to connect the storage systems to individual grid branches. Figure 6.5 shows a possible layout of a LV grid with an integrated hydrogen storage system.
There are two possible options of the connection of an electrolyzer and a fuel cell to the LV grid: using a DC bus or the direct connection to the grid. Both options are shown in Figure 6.6a and Figure 6.6b, where the arrows indicate the direction of the power flow. Using a DC bus offers advantages in controllability and allows an easier connection of other DC systems, such as batteries. However, compared to the direct grid connection, additional hardware is necessary. The design of an efficient AC/DC converter is a complex task. A review of suitable AC/DC converters for electrolysis applications is given by Yodwong et al. [158].
If a specific grid segment is defined as a microgrid with the optimization target of zero net power flow through the segment boundary (e.g. transformer station or distribution station),

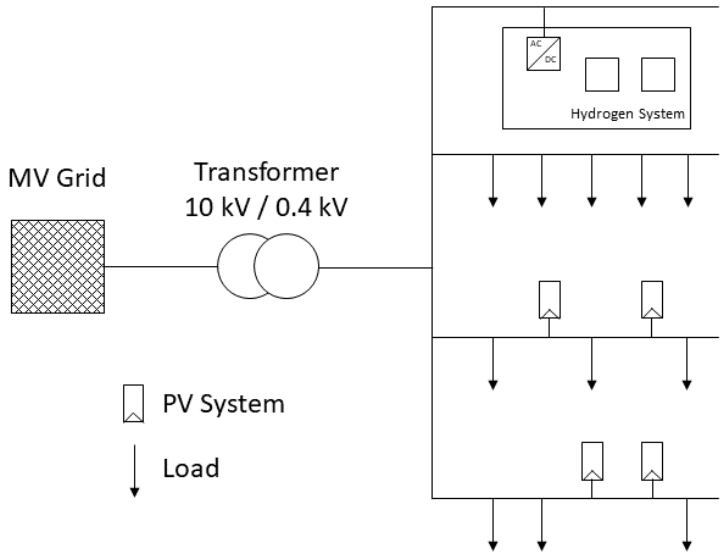

Figure 6.5: Representation of a possible LV grid connection of the proposed hydrogen systems

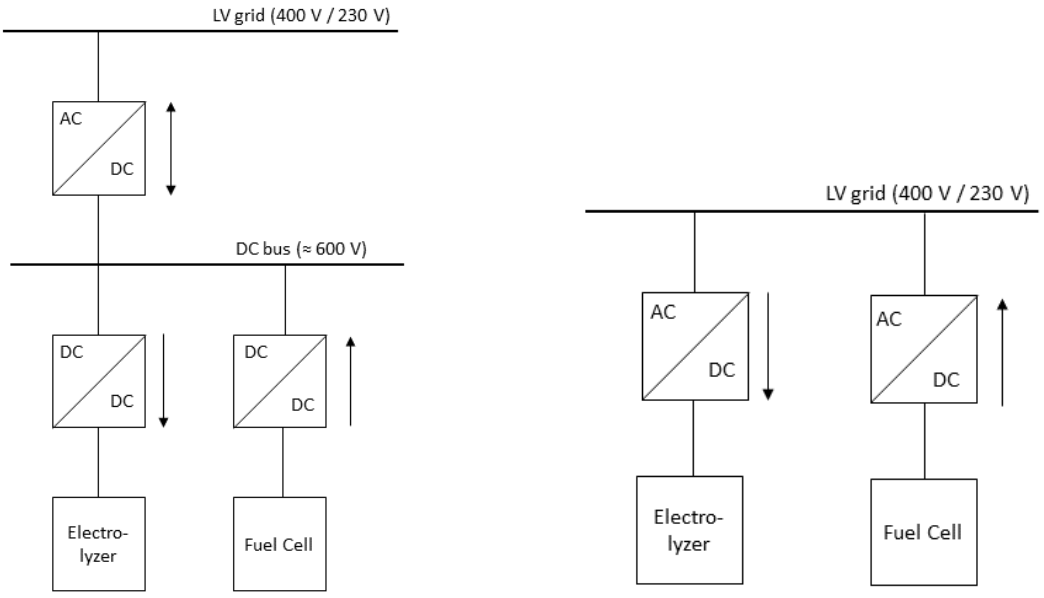

(a) DC bus

(b) AC bus

the hydrogen system must be capable of handling fast load changes. Figure 6.7a and Figure 6.7b show an example for the accumulated electrical load profile of a building cluster for a

summer day and a summer week, respectively. Whereas the rough course of the power curve for a summer week is periodic and therefore predictable, there is more uncertainty on a day scale. Depending of the dynamic capability of the hydrogen system, it could be necessary to add a fast reacting storage system like Li ion batteries to the system in order to smooth the load profile.

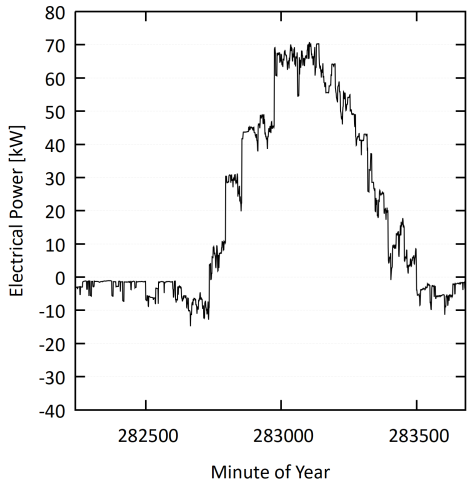

(a) Example for a load profile on a Summer day

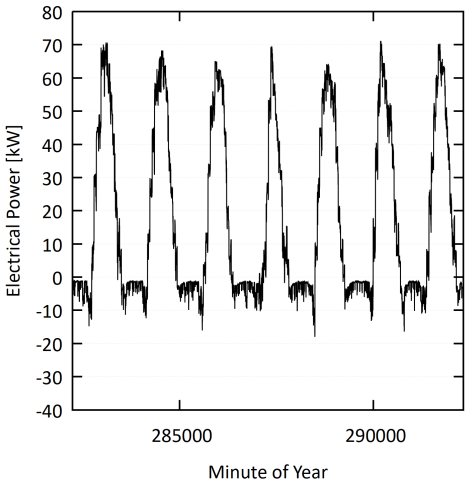

(b) Example for a load profile in a Summer week

A representation of a winter day and week are shown in Figure 6.8a and Figure 6.8b. These profiles show even more fluctuation, compared to the summer case, with a shift towards power deficits. The re-conversion of formic acid to power (formic acid decomposition with subsequent fuel cell) should be able to handle the dynamics or additional buffering subsystems must be applied.

6.2.2 Thermal

The thermal integration of the hydrogen district storage system aims at the utilization of the excess heat produced by the electrolyzer, fuel cell or flow reactors for the heating of buildings. The achieved temperature of the system must be compared to the heating system working temperature. Typical operation temperature of different building heating systems are:

- Heating Network: 70°C to 100°C
- Low-ex Heating Network: 10°C to 30°C
- Household Heating: 30°C (surface heating) to 60°C (radiator)

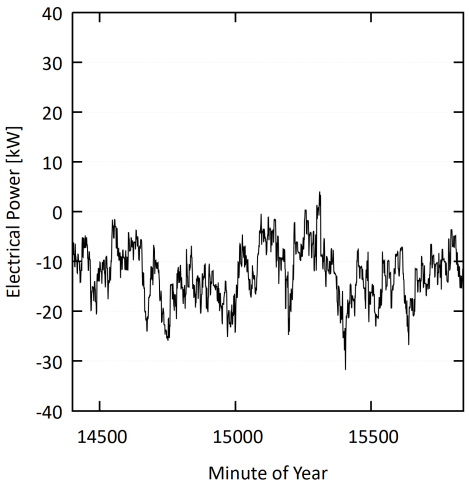

(a) Winter day

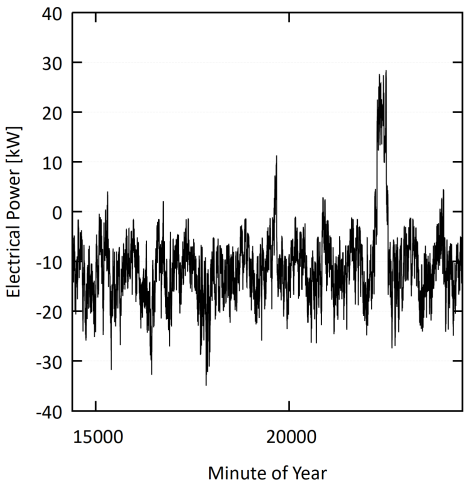

(b) Winter week

In a heat controlled mode of a CHP device, such as a PEM fuel cell, it is mandatory to utilize the heat produced by the fuel cell. This could either be realized by heating up a thermal storage, for example in a building integrated system, or by feeding the heat into a district heating network. In both applications the heat is removed from cooling loop of the fuel cell with a heat exchanger. To further improve the heat output the anode off-gas of the fuel, which still contains hydrogen (about 9 mol.% [159]) could be burned in a combustion chamber. Figure 6.9 illustrates the thermal integration of a fuel cell with anode off-gas combustion.

The utilization of the waste heat from a PEM electrolyzer further increases the overall system performance. Accordingly to the fuel cell system, the waste heat caused by an electrical overpotential, could be derived from a cooling loop via heat exchangers and fed into a heating network. The consideration of the additional system complexity and the expected impact of the electrolyzer waste heat must be evaluated regarding the specific operation environment and heat demands.

The thermal power of the electrolyzer and the fuel cell is calculated with the electrical voltage above the thermo-neutral voltage and the current:

$$\dot{Q}_{heat} = (U - U_{th}) \cdot I \tag{6.3}$$

With the cell temperature T_{cell}, the inflow temperature T_{in} and the specific heat capacity of

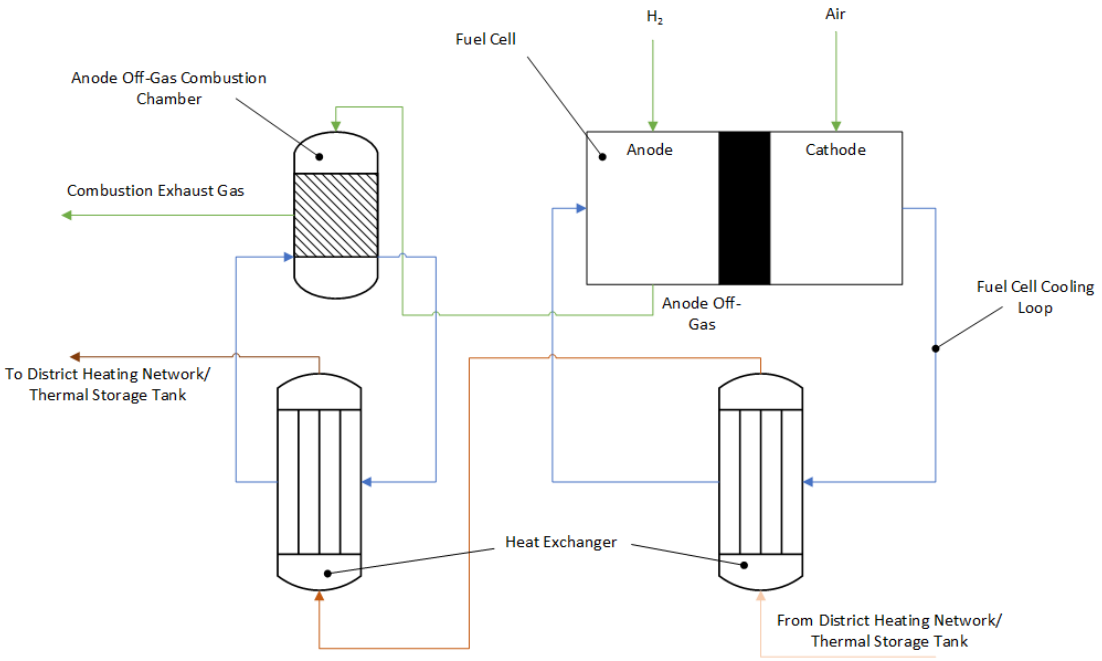

Figure 6.9: Thermal Integration of a Fuel Cell

coolant c_p, the necassary mass flow of the coolant could be evaluated:

$$\dot{m} = \frac{\dot{Q}_{heat}}{c_p \cdot (T_{cell} - T_{in})} \tag{6.4}$$

The waste heat generated (approximately equal to the cooling demand) by a flow reactor, for an exothermic process and isothermal process control, depends on the on the reaction rate r and the enthalpy of the reaction ΔH and could be estimated with Equation 6.5.

$$\dot{Q} = r \cdot \Delta H \tag{6.5}$$

If a reactor with an endothermic reaction (e.g. formic acid decomposition) is integrated into the system, Equation 6.5 can be applied to determine the heating demand.

6.2.3 Substance Inflow and Outflow

Water Demand The water demand of the hydrogen system is determined by reaction equation. Both for water electrolysis and for CO_2 electrolysis, 1 mol of water is needed for the production of 1 mol of hydrogen or 1 mol of formic acid respectively. The specific hourly

water demand per ampere of current and per cell there for is:

$$\dot{m}_{H_2O} = \frac{I}{zF} \cdot M_{H_2O} \cdot 3600s = 3.36 \times 10^{-4}\,\mathrm{kg\,h^{-1}\,A^{-1}} \tag{6.6}$$

This value represents the stoichiometric water demand for the anode reaction. In reality, the water demand is higher due to the necessary water pretreatment. There is an additional water demand for the CO_2-electrolyzer in order to provide water as a solvent for the aqueous formic acid solution.

The requirements for the water quality depends on the electrolyzer type. For acidic water electrolysis, such as PEM electrolysis, usually a higher water purity is required. CO_2 electrolysis demands ultra-pure water with a resistance of 18 MΩ.

Carbon Dioxide Demand The demand of carbon dioxide for CO_2 electrolysis could be calculated like shown in Equation 6.6, as also one mol of carbon dioxide is needed for the production of one mol formic acid. With the molar mass of carbon dioxide $M_{CO_2} = 44.01\,\mathrm{g\,mol^{-1}}$ the hourly carbon dioxide demand per cell is calculated as follows:

$$\dot{m}_{CO_2} = \frac{I}{zF} \cdot M_{CO_2} \cdot 3600s = 8.21 \times 10^{-4}\,\mathrm{kg\,h^{-1}\,A^{-1}} \tag{6.7}$$

As a carbon dioxide source, pressurized gas cylinders could be used. The interval of external carbon dioxide deliveries depend on the installed electrolysis power. For an assumed 10 kW CO_2-electrolyzer with a operating point of 100 A and 4.5 V per cell and and overall amount of 23 cells (stack voltage: 103.5 V), a 30 kg carbon dioxide bottle would reach for about 365 full load-hours, without losses taken into account. Low-temperature direct air capture (LT-DAC) is a promising option for on site carbon dioxide extraction, which avoids the dependency of external deliveries. The following data (Table 6.1) for an estimation of the development of this technology until the year 2030 is derived from Fasihi et al. [63].

Table 6.1: DAC parameters used for further investigations

Parameter	Value
capex	338 €/ t_{CO_2}
opex	4%
el. demand	225 kWh/ t_{CO_2}
therm. demand	1500 kWh/ t_{CO_2}

In order to increase the efficiency with regard to the use of substance, the recycling of carbon dioxide from the formic acid dehydrogenation should be applied as far as possible.

Formic Acid Deliveries Formic acid deliveries could be considered in a scenario with either a high overproduction or a high deficit of renewable energy. System 3 and 4 would easily allow a formic acid transfer, as the produced formic acid solution is accessible in storage tanks. The maximal delivery quantity for a road transportation could be estimated, if the maximal allowed weight of a semitrailer in Germany of 40 t is considered. With an assumed empty weight of 15 t for the tractor plus trailer, a maximal load of 25 t is possible. This load equals 20,500 l of formic acid. Table 6.2 summarizes the maximal delivery volume for the formic acid transportation via road, rail and river.

Table 6.2: Formic acid delivery volume for different transportation types

Transportation Type	Max. Load	Max. FA Volume
Road	25 t	20,500 l
Rail (per tank car)	67.7 t	55,500 l
Ship (European Riverboat Class Type Va)	3.000 t	2,500,000 l

6.3 Operation and control modes

In this section the operation and control modes for the main components of the regarded systems are introduced: the electrolyzer, fuel cell, reversible hydrogen battery and flow reactors.

6.3.1 Electrolyzer Operation and Control

Both systems, the PEM water electrolyzer and the CO_2-electrolyzer are operated with surplus electrical energy in the subsequent case-study. The usage of additional grid energy for the electrolysis is not intended. This means that the electrolyzers must handle fast load changes and stand-by times. An electrolysis controller assigns the surplus electrical power to the following three sinks:

- Buffer battery (if available)
- Electrolyzer
- Power grid

Figure 6.10 shows the developed control algorithm for the surplus utilization with an integrated buffer battery.
If the surplus power of the energy systems exceeds the maximal power of the electrolyzer, the electrolyzer is operated at full power and the remaining power is either used to load the

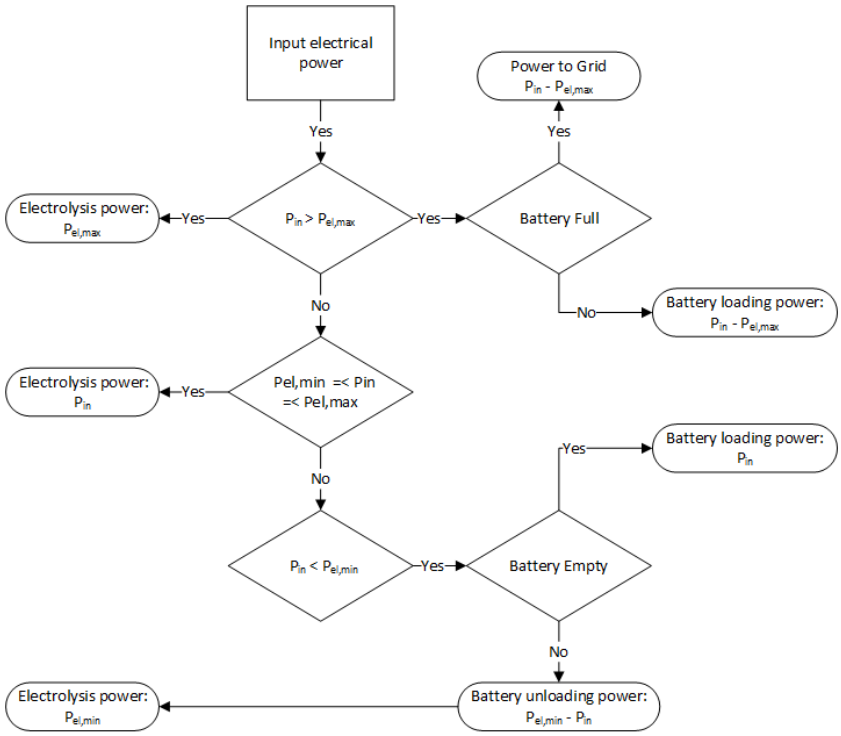

Figure 6.10: Electrolyzer control algorithm

battery or, in case of a full battery, is fed into the power grid. For an input power between the maximum and minimum electrolyzer power, the surplus power is directly assigned to the electrolyzer. In case the input power is below the minimum electrolyzer power, additional power is provided by the battery to match the minimum electrolysis power. If the battery is empty (threshold SOC: 0.1), the loading of the battery, in this case, is prioritized up to a battery SOC of 0.5. The battery loading is implemented with a hysteresis control. This control scheme was applied to both the water electrolyzer of System 1, System 2 and System 3 and the CO_2-electrolyzer of System 4.

6.3.2 Fuel Cell Operation and Control

Depending on the application, fuel cells or CHPs in general could be operated with to different control modes: power controlled or heat controlled.

Power controlled FC operation The current setpoint of a power controlled FC is directly determined by the power demand and the stack voltage.However the setpoint must be limited by the maximal possible current of the fuel cell.

$$I_{FC,set} = min\left(\frac{P_{demand}}{V_{stack}}, I_{max}\right) \tag{6.8}$$

The current $I_{FC,set}$ should be set to zero, if the filling level of the hydrogen or formic acid storage falls below a certain threshold.

Heat controlled FC operation In a heat-controlled mode, the fuel cell current set point is determined with an on-off-controller. The lower and the upper threshold of the controller are defined by the requested temperature level of the thermal storage. Figure 6.11 shows the output of an on-off-controlled FC current (50 A) and the temperature of a thermal storage with a lower threshold of 55°C and an upper threshold of 65°C.

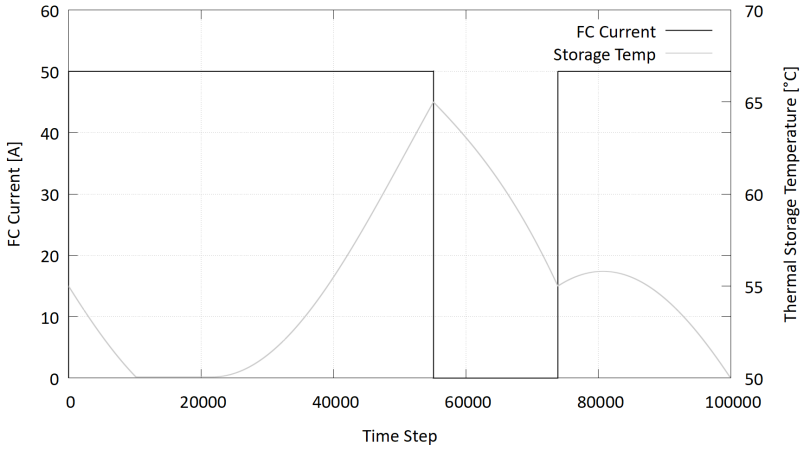

Figure 6.11: On-off-controller for a FC with an attached thermal storage

An on-off control of a CHP device is the must simplest control mode, however in many cases it is inefficient for fuel cells as it does not consider the part load capabilities of PEMFCs. There are more matured methods for heat controlled fuel cells, including PID controller, fuzzy logic or model-based control. Corresponding explanations could be found in literature (see Daud et al. [160] or Zou and Kim [161]).

6.3.3 Reversible Hydrogen Battery Operation and Control

The operation state of the reversible H_2 battery could be controlled by a heater and a purge valve (see Section 5.1.1.2). Depending on the current conditions and requirements, the state of these actors (0/1) is determined by a controller. Therefor the following variables are considered:

- Hydrogen demand of the fuel cell: determines whether hydrogen release is necessary

- Pressure of the battery gas phase: ensures that the maximum pressure in the gas phase is not exceeded through formic acid dehydrogenation[2]. Also a minimum amount of hydrogen is kept in the gas phase for faster response times
- Battery loading state: ensures that the battery is not overloaded

The flow diagram of the control algorithm is shown in Figure 6.12. Overall four different operation states are possible, corresponding to the states defined in Section 5.1.1.2: hydrogenation (heater 1/ valve 0), dehydrogenation (heater 1/ valve 1), hydrogen release (heater 0/ valve 1) and idle/ filling (heater 0/ valve 0).

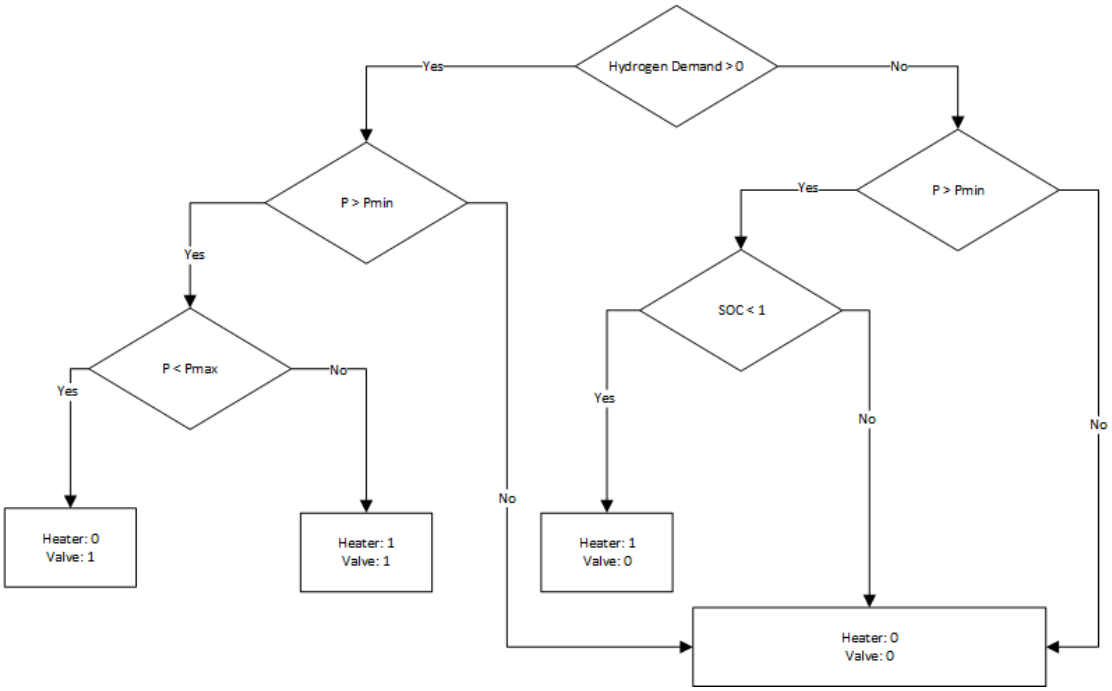

Figure 6.12: Control algorithm for the reversible hydrogen battery

6.3.4 Flow Reactor Operation and Control

Subsequently the operation and control modes for the flow reactor are introduced.

H2-to-FA Reactor Control The inflow of hydrogen for the H2-to-FA reactor is determined by the production rate of the water electrolyzer. In order to provide enough carbon dioxide

[2]Pressure in the battery could still be exceeded through hydrogen inflow. This must be considered by the compressor controller

for the reaction, the carbon dioxide inflow is calculated based on stoichiomentric considerations. At each time step the inflow into the reactor is complemented by the re-circulation of unreacted carbon dioxide and hydrogen. The reactor model does not allow a dynamic control of the reactor at each time step. However, the reactor production rate could be varied before the execution of the simulation by changing the reaction rate slope, the operating pressure and the operating temperature (INSEL Block Paramters).

FA-to-H2 Reactor Control The FA-to-H2 reactor is controlled by changing the reaction temperature. Thereby the temperature setpoint is calculated at each time step as shown in Section 5.1.4.2 with regard to the current hydrogen demand of the fuel cell. An upper and lower bound for the temperature setpoint could be determined as an INSEL Block Parameter.

6.4 System Dimensioning

In this section two different approaches for the system dimensioning to a given load profile are introduced: rule-based dimensioning and automated dimensioning with genetic algorithms.

6.4.1 Rule-based Dimensioning

Dimensioning rules are helpful, whenever complex system simulations are not available. They are also used for rough approximations are as a starting point for dimensioning algorithms. Most often they are derived rules of thumb, which are based on experiences from similar applications. As no empirical data from real applications of the systems regarded in this thesis are available, in the following sections dimensioning rules are set up based on system characteristics.

6.4.1.1 Electrolyzer

For the dimensioning rule of both the PEM water electrolyzer and the CO_2-electrolyzer, the rated power of the electrolyzers is defined by the maximum electrical power of the load profile. This will lead to the maximum production of electrolysis product, however will also have low full load hours as a consequence and should only be applied if no economical constraints prevail.

PEM Water Electrolysis Based on the maximum input power P_{in}, the cell area A_{cell} and the rated cell voltage V_{cell} of the PEM water electrolyzer are determined based on the data presented in Table 3.2. The cell area and rated voltage are shown in Table 6.3.
With the values from Table 6.3 and the maximum current density i_{max} (default value: $3\,\mathrm{A\,cm^{-2}}$), the overall number of needed electrolysis cells are calculated according to Equation

Table 6.3: Dimensioning rule: cell area and voltage of a PEM electrolyzer

Input Power	A_{cell}	V_{cell}
<= 1.5 kW	50 cm^2	1.9 V
> 1.5 kW and <= 150 kW	300 cm^2	1.93 V
>= 150 kW	1250 cm^2	2.01 V

6.9. In order to get an integer for N_{cells}, the result is rounded up.

$$N_{cells} = min\left\{k \in Z \middle| k >= \frac{P_{in}}{A_{cell} \cdot V_{cell} \cdot i_{max}}\right\} \tag{6.9}$$

CO2 Electrolysis The methodology of the PEM electrolyzer is also adopted to the CO_2-electrolyzer, although with different parameters (see Table 6.4). To determine the cell voltage, experiments with the component model have been carried out. The rated current density of the CO_2-electrolyzer is assumed to be 0.8 A cm^{-2}.

Table 6.4: Dimensioning rule: cell area and voltage of a CO_2-electrolyzer

Input Power	A_{cell}	V_{cell}
<= 5 kW	200 cm^2	4.96 V
> 5 kW	400 cm^2	4.96 V

6.4.1.2 Hydrogen Compressor

The maximum hydrogen delivery rate is calculated based on the electrolyzer full load operation, with the parameters determined for the electrolyzer dimensioning.

$$\dot{m}_{H_2,max} = \frac{i_{max} \cdot A_{cell}}{z \cdot F} \cdot N_{cell} \tag{6.10}$$

Based on the hydrogen production rate, the needed compressor power could also be estimated with the compressibility factor Z, the inlet temperature T, the compressor efficiency η, the number of compressor stages N, the ratio of specific heats $\gamma = 1.4$, the inflow pressure P_{in} and the outflow pressure P_{out}, as described by Christensen [162]:

$$P = \dot{m}_{H_2,max} \cdot \frac{Z \cdot T \cdot R}{M_{H_2} \cdot \eta} \cdot \frac{N \cdot \gamma}{\gamma - 1} \cdot \left(\left(\frac{P_{out}}{P_{in}}\right)^{\frac{\gamma-1}{N \cdot \gamma}} - 1\right) \tag{6.11}$$

6.4.1.3 Storage Cylinder

The size of the storage cylinder is calculated with the maximal seasonal surplus energy which could be stored from time 1 to time 2 (e.g. May to October).

$$E = \int_{t_1}^{t_2} P_{surplus} \cdot dt \tag{6.12}$$

From an assumed energy demand for the hydrogen production of $e = 50\,\mathrm{kW\,h\,kg^{-1}}$ and the overall amount of surplus energy E follows the mass of stored hydrogen m_{H_2}:

$$m_{H_2} = \frac{E}{e} \tag{6.13}$$

Finally, with the targeted storage pressure P_{stor}, the needed cylinder volume could be determined:

$$V_{cylinder} = \frac{m_{H_2} \cdot R_s \cdot T}{p} \tag{6.14}$$

6.4.1.4 Reversible H2-Battery

The size of the reversible H2-Battery is dimensioned based on the the energy storage demand. With the assumptions, that the overall battery cell size is ten times that of the liquid phase ($V_{H2bat} = 10 \cdot V_{H2Bat,lqd}$) and that every DBU molecule is capable of binding one formic acid molecule, the volume needed per kWh of stored energy is calculated as follows:

$$V_{H2bat} = 10 \cdot \frac{1}{LHV_{H2} \cdot \chi_{H2} \cdot M_{FA} \cdot c_{DBU}} = 2.5\,\mathrm{kW\,h\,L^{-1}} \tag{6.15}$$

Where $\chi_{H2} = 0.044$ is the weight percentage of hydrogen per formic acid molecule.

In order to match the demanded hydrogen flow rate for the fuel cell, a second design criteria for the reversible hydrogen battery is the achievable hydrogen outflow rate. With the linearized reaction slope of the dehydrogenation reaction $k_2 = 7.88 \times 10^{-5}\,\mathrm{s^{-1}}$ (see Section 5.1.1) the maximum hydrogen flow rate related to the overall battery volume is determined with the following equation:

$$r_{H2,max} = k_2 \cdot c_{DBU} \cdot M_{H_2} \cdot \frac{1}{10} = 9.45 \times 10^{-8}\,\mathrm{kg\,s^{-1}\,L^{-1}} \tag{6.16}$$

The maximum reaction rate therefor could either be affected by the overall battery volume or through the parallel interconnecting of several "battery cells".

6.4.1.5 H2tFA Reactor

This component should be sized based on the requirement that the maximal reaction rate should match the maximal hydrogen production rate of an upstream electrolyzer.

6.4.1.6 FAtH2 Reactor

For the FAtH2 reactor it is assumed that the hydrogen outflow should suffice the maximal power of the downstream fuel cell. With the fuel cell power P_{FC}[3], the lower heating value of hydrogen and the fuel cell efficiency η_{FC}. The required hydrogen outflow could be calculated as follows:

$$\dot{m}_{H_2,max} = \frac{P_{FC}}{LHV_{H_2} \cdot \eta_{FC}} \tag{6.17}$$

Finally, the decisive parameter is the reactor volume $V_{reactor}$, as it affects the averaged reaction rate $\tilde{r}$.

$$V_{reactor} = \frac{\dot{m}_{H_2,max}}{M_{H_2} \cdot \tilde{r}} = \frac{P_{FC}}{M_{H_2} \cdot \tilde{r} \cdot LHV_{H_2} \cdot \eta_{FC}} \tag{6.18}$$

The detailed calculation of $\tilde{r}$ is described in chapter 5. With an assumed reaction temperature of 105°C, the averaged reaction rate $\tilde{r}$ for the dimensioning of the reactor is determined as $\tilde{r}_{105C} = 1.388\,\mathrm{mol\,s^{-1}\,m^{-3}}$ (see [35]). From this, the specific volume $v_{FAtH2-Reactor}$ of the reactor per kW rated power of the electrolyzer could be derived.

Table 6.5: Specific volume for the FAtH2-reactor design

Control Mode	Efficiency	Specific Reactor Volume
Electricity controlled	0.37	$8.11 \times 10^{-3}\,\mathrm{m^3\,kW^{-1}}$
Heat controlled	0.53	$5.66 \times 10^{-3}\,\mathrm{m^3\,kW^{-1}}$

6.4.1.7 Formic Acid Tank

The needed size of the formic acid tank is determined by the energy storage demand E_{demand}. With the density of formic acid ρ_{FA}, the weight percentage of hydrogen in formic acid $\chi_{H2} = 0.044$ and the lower heating value of hydrogen LHV_{H2}, the volume is calculated according to Equation 6.19. E_{demand} could be estimated by the integrating the surplus electrical power during a given period (see Equation 6.12).

[3]The power and efficiency of the fuel cell, in this case, refers to either the electrical or thermal parameter, depending on the requested application

$$V_{FA,tank} = \frac{E_{demand}}{\rho_{FA} \cdot \chi_{H2} \cdot LHV_{H2}} \tag{6.19}$$

The reactor volume calculated this way is only valid for concentrated formic acid. This presupposes that the CO_2-electrolysis product is concentrated in a separate procedure which is not part of the system model.

6.4.1.8 Fuel Cell

The rated power is defined by the minimal electrical power of the load profile (or rather the maximal power deficit). As for the electrolyzer the cell area results from the rated power (see Table 6.6. Values for cell voltage (0.63 V) and the maximal current density (0.4 A cm^{-2}) are derived from [163].

Table 6.6: Dimensioning rule: cell area and voltage of a PEM fuel cell

Input Power	A_{cell}	V_{cell}
$<=$ 5 kW	200 cm^2	0.63 V
$>$ 5 kW	400 cm^2	0.63 V

The number of cells needed for the fuel cell could be calculates according to Equation 6.9.

6.4.2 Automatic System Dimensioning

As an alternative to rule-based dimensioning, optimized dimensioning by a methaheuristic approach using genetic algorithm could be considered. Genetic algorithms are variable and could be adapted to different tasks. The underlying principle is derived from natural selection, as genes (system parameters) are passed on to following generations (next simulation run). Mutations (random variations in the parameters) occur after each generation and finally the fittest parameter set prevails. A major advantage of this approach is that dimensioning rules must not be known, but he algorithms finds a local minimum (or maximum) based on simulated data. This is especially useful for complex systems without a profound basis of measurement data, as it is true for the systems regarded in this work. However for this approach detailed system models must be available and a specific target function must be assigned. Using the Python programming language, genetic algorithms could be applied with the DEAP toolbox[4]. An INSEL simulation execution could be directly triggered from a Python script with the parameter set defined by the genetic algorithm.

[4] `https://pypi.org/project/deap/`

Example: Cost Function of a Hydrogen System The following example shows a possible cost function for a hydrogen system, which calculates the equivalent annual costs (EAC) based on the annualized hardware costs $f_{Hardware}$, and the operating costs consisting of the costs for electricity $f_{Electricity}$, carbon taxes f_{CO2} and hydrogen deliveries f_{H_2}

$$f_{EAC} = f_{Hardware} + f_{Electricity} + f_{CO2} + f_{H_2} \tag{6.20}$$

The costs for hydrogen deliveries could be calculated with the market price for hydrogen c_{H_2}, the number of necessary external storage tank refills N_{REFILL} per year and the hydrogen mass which could be stored within the tank (ideal gas with the specific gas constant for hydrogen $R_{s,H_2} = 4124\ Jkg^{-1}K^{-1}$), as follows:

$$f_{H_2} = c_{H_2} \cdot N_{REFILL} \cdot \frac{V_{tank} \cdot p_{max,tank}}{R_{s,H_2} \cdot T} \tag{6.21}$$

The genetic algorithms tries to find a minimal solution for the cost function defined in Equation 6.20 by varying a defined parameter set.

A study which applied a genetic algorithm with this target function on a hydrogen system comparable to System 1 defined in this work, could be found by Weiler et al. [164]. This methodology was applied for a 2020 and a 2050 scenario with changing economic frameworks. This study also includes a comprehensive comparison between a rule-based dimensioning and automated dimensioning for a heat pump system. It is stated that, under 2020 conditions the automated dimensioning for the heat pump system results in a 27 % lower EAC as for the rule-based dimensioned system. Under 2050 conditions, the hydrogen system designed with the genetic algorithm becomes economical superior to the heat pump system compared with it.

Chapter 7

System Operation, Comparison and Optimization

In this chapter, the use-case on which the developed system models are applied is introduced. For the regarded building cluster, load profiles for the annual surplus and deficit power are derived. Further in this chapter the simulation results of all four proposed formic acid based hydrogen storage systems (see Section 6.1) are evaluated and all systems compared to each other. Different optimization steps for System 4 are shown, as well as the outcome on the system performance if small wind turbines are used for additional power production. A possible heat recovery for the fuel cell is considered. Finally, an economic evaluation of System 4 is carried out.

This chapter aims at answering the third research objective: How can simplified models be used to evaluate the performance of formic acid based hydrogen storage systems in an application scenario? How do these systems perform, if applied to a building cluster with decentral heat pumps, PV systems and small wind turbines? Which system is most promising for an application in the building sector?

7.1 The Plus Energy Settlement

The case-study chosen to demonstrate the feasibility of a formic acid based hydrogen storage system is a plus energy settlement in Wüstenrot called "Vordere Viehweide". Wüstenrot is a rural municipality in southern Germany with about 6,613 residents. The settlement "Vordere Viehweide" is used as a demonstration site. It overall consists of 23 buildings with a high-energy standard. All buildings use decentral heat pumps for heating. The heat pumps are connected to a cold district heating grid with agrothermal collectors (see Figure 7.1).

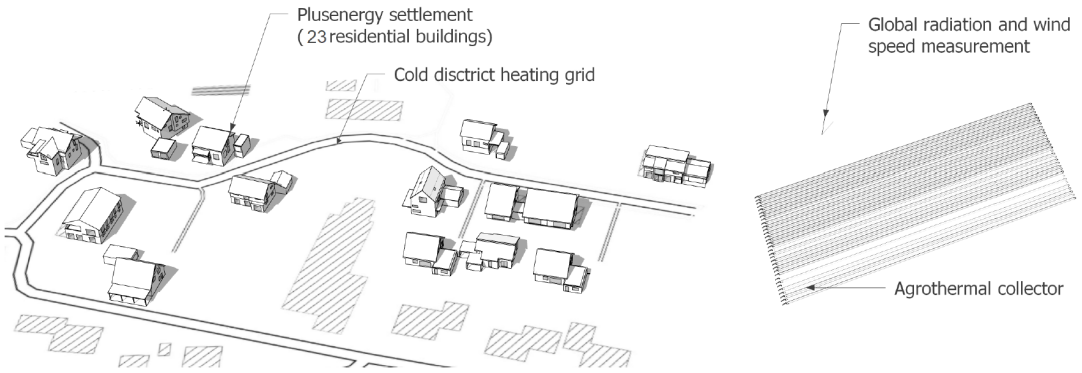

Figure 7.1: The plus energy settlement 'Vordere Viehweide', Source: [48], Author of the illustration: Marcus Brennenstuhl

For more information on the pilot site see Pietruschka et al. [45].

7.1.1 Building Cluster

Ten buildings of the cluster, with sufficient monitoring data, are considered for the evaluation of the formic acid based energy system. Table 7.1 shows the key parameters for those buildings. Each building has a rooftop mounted PV system with an installed power from 3.4 kWp to 28.8 kWp. This results in an overall PV power of 99.75 kWp for the cluster. For heating, each building is equipped with a heat pump with an rated electrical power in the range of 1.3 kW to 4.5 kW. The annual heat demand, including domestic drinking water, and household power demand are based on detailed building simulations and aligned with measured monthly data. Data gaps are filled with historic measurement data or with assumed values, based on the net floor space. For more details on the building models and data validation see Brennenstuhl et al. [48]. The Building IDs in Table 7.1 is chosen to be consistent with other publication using this building cluster as a data basis.

7.1.2 Electrical Load Profile of the Building Cluster

With the data from Table 7.1 an electrical load profile of the cluster in generated for one year with a resolution of one minute. This load profile includes the power generated by the PV system, as well as the household power demand and the power demand of the heat pumps. For its application in the energy system simulation, the load profile is divided into a surplus power curve (see Figure 7.2) and a deficit power curve (see Figure 7.3). As expected, the curves show higher surplus power in the summer months and high deficits in the winter. A maximal surplus power of 77.6 kW is achieved by the cluster. Overall about 78,260 kWh of surplus energy is yielded over the year. The maximum deficit power is about 41 kW

Table 7.1: Key parameters for all buildings of the cluster

Building ID	Net Floor Space	Installed PV Power	Annual Heat Demand	Household Electricity Demand
0001	327 m^2	28.8 kWp	13.577 kWh	4.360 kWh
0002	193 m^2	7.85 kWp	10.466 kWh	3.483 kWh
0009	312 m^2	7.85 kWp	9.293 kWh	2.642 kWh
0010	162 m^2	13.6 kWp	4.505 kWh	4.084 kWh
0012	285 m^2	13.64 kWp	20.005 kWh	4.439 kWh
0019	307 m^2	5.4 kWp	17.270 kWh	4.760 kWh
0020	158 m^2	3.4 kWp	10.886 kWh	2.946 kWh
0022	203 m^2	4.4 kWp	7.366 kWh	1.625 kWh
0024	203 m^2	5.2 kWp	7.694 kWh	2.743 kWh
0025	241 m^2	5.6 kWp	8.128 kWh	2.776 kWh
		95.75 kWp	99.390 kWh	31.115 kWh

with an annual deficit energy of 68,169 kWh. Both load profiles show a distinct seasonality. The surplus energy does to complement the deficit from a temporal view. This justifies the implementation of a seasonal energy storage system.

For a fuel cell system dimensioned at the peak electrical deficit load of 41 kW, an annual hydrogen demand of 2,467 kg occurs. With a weight share of 4.4% the overall annual formic acid demand of the building cluster is calculated as 56,068 kg. All power and energy related parameters of the building cluster are shown in Table 7.2.

Table 7.2: Energy parameters of the building cluster

Parameter	Value	Unit
Peak surplus power	77.6	kW
Annual surplus energy	78,260	kWh
Peak deficit power	41	kW
Annual deficit energy	68,169	kWh
Corresponding hydrogen demand	2,467	kg
Formic acid demand	56,068	kg

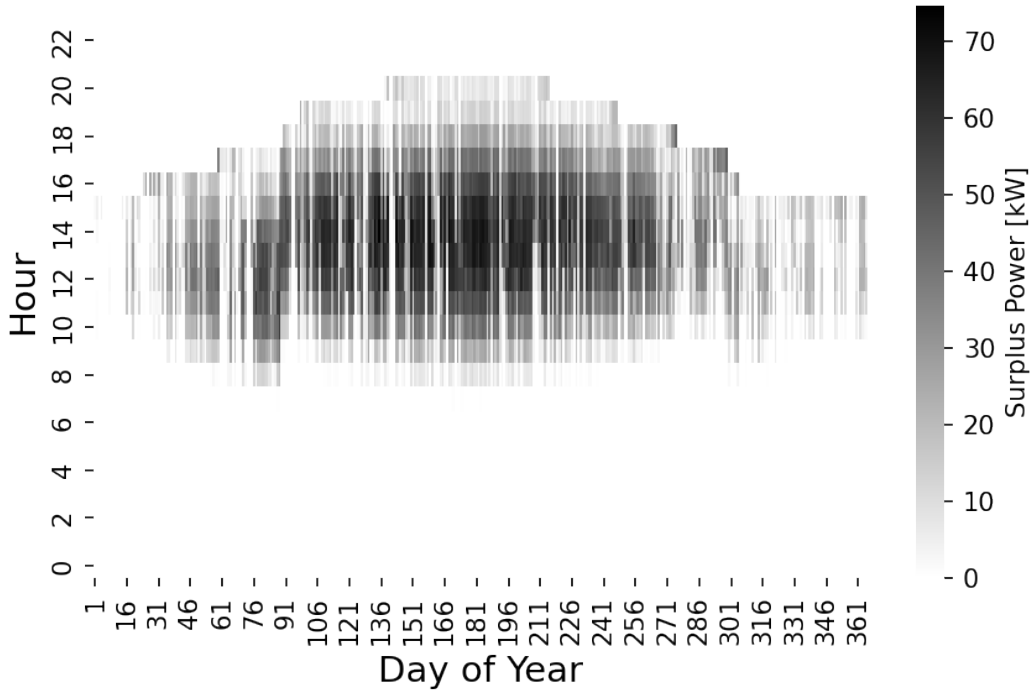

Figure 7.2: Building cluster surplus power

7.2 Implementation of a Formic Acid Based seasonal Energy Storage System

In this section, the developed system models for the proposed formic acid based hydrogen storage systems, are used for an simulation of one year. The load profiles for the surplus and the deficit power of the above described building cluster is therefor used. All systems are designed to fit to this laod profiles by using the dimensioning rules from Section 6.4.1.

7.2.1 System 1: Reference System

System 1, the reference system, consists of state-of-the-art technology. Hydrogen is produced via PEM water electrolysis, compressed and stored in high-pressure storage devices. The stored hydrogen is on demand reconverted to electrical power with an PEM fuel cell. In the following section, the dimensioning rules determined in Section 6.4.1 are applied to System 1 and and the load profiles for the surplus and the deficit power of the building cluster is used to determine the system performance in the course of one year.

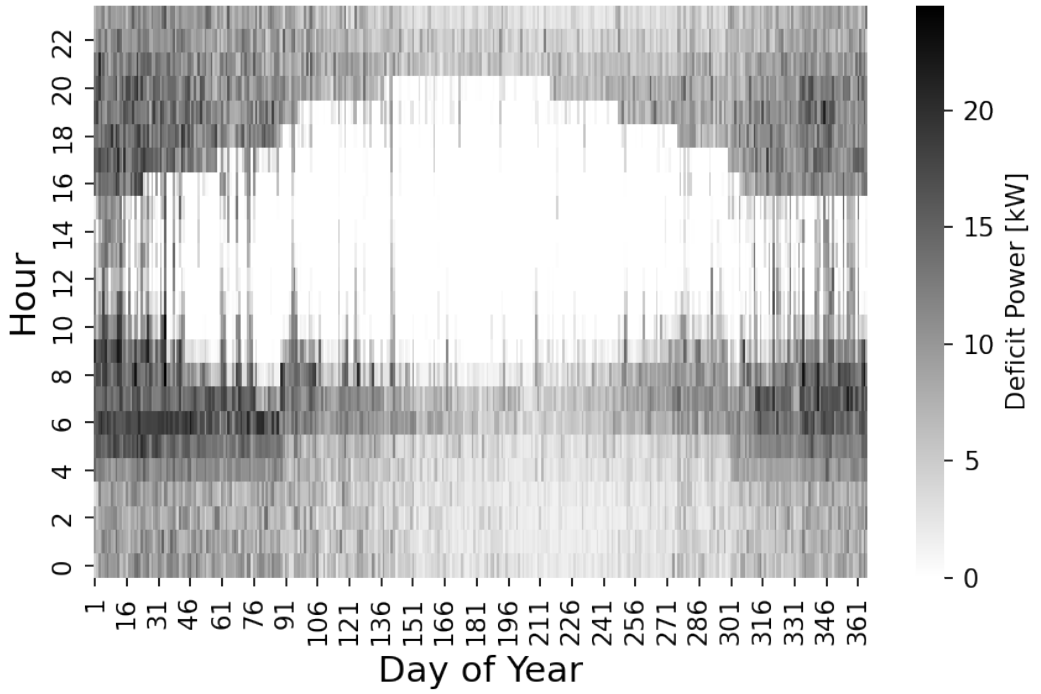

Figure 7.3: Building cluster deficit power

7.2.1.1 System 1: Dimensioning

With the dimensioning rules introduced in Section 6.4.1, the installed power of the electrolyzer and the fuel cell of System 1 were adjusted to the surplus and deficit power of the building cluster. The needed compressor delivery rate can afterwards be matched with the assumed maximum hydrogen production rate of the electrolyzer. As a high compression ratio from ambient pressure to 35 MPa is required, the hydrogen compressor is designed with five compression stages. All design parameters which are afterwards used for the simulation of System 1 are shown in Table 7.3.

7.2.1.2 System 1: Simulation Results

The simulation of System 1 was executed with the design parameters from Table 7.3. From the simulation results (see Table 7.4), it could be seen, that the peak electrolysis power is reached, however with only about 1.4 full load hours per year. This lead to a maximum hydrogen production rate of $3.8 \times 10^{-4}\,\mathrm{kg\,s^{-1}}$. The mean hydrogen production rate throughout the year is lower by a factor of ten around $4.33 \times 10^{-5}\,\mathrm{kg\,s^{-1}}$. Overall 1,379 kg of hydrogen are produced. With the given assumptions and the applied control algorithm,

Table 7.3: System 1: parameter overview

Parameter	Value	Unit
Electrolyzer power	78	kW
Electrolyzer cells	45	-
Electrolyzer cell area	300	cm^2
Compressor stages	5	-
Compressor max delivery rate	1.4	$kg\,h^{-1}$
Storage volume	29.5	m^3
Initial storage tank filling	0.1	MPa
FC power	37.5	kW
FC cells	345	-
FC area	400	cm^2

the electrolyzer is operated with an efficiency of 58 % on average.
Figure 7.4 shows the current and voltage of the electrolyzer in the course of the year. As expected, current peaks are reached in the summer months

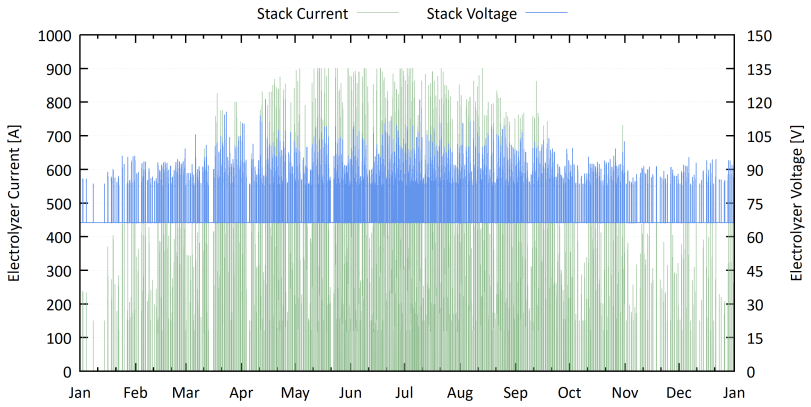

Figure 7.4: Stack current and voltage of the electrolyzer of System 1

The power output of the fuel cell (23,335 kWh) compensates 47 % of the annual power deficit. Additionally, around 14,000 kWh of heat are produced by the fuel cell with a maximum heating power of about 23 kW. Considering the hydrogen storage tank, the resulting hydrogen inflow resulting from the electrolyzer production and the outflow resulting from the hydrogen demand of the fuel cell is shown in Figure 7.5.
Finally, the inflow and outflow rates lead to the pressure in the storage cylinder as shown in Figure 7.6. As the peak cylinder pressure is achieved at the beginning of the heating period, a seasonal charactersitic is cleary visible.
Overall additional electrical energy of nearly 29,000 kWh is needed from the power grid to

Table 7.4: System 1: simulation results

Parameter	Value	Unit
Max electrolysis power	77	kW
Electrolyzer full load hours	1.38	h
Electrolyzer stand by hours	6377	h
Electrolyzer off-on-switches	1519	-
Max H2 production rate	3.8e-4	$kg\,s^{-1}$
Mean H2 production rate	4.33e-5	$kg\,s^{-1}$
Produced hydrogen	1,379	kg
Max electrolysis efficiency	0.63	-
Mean electrolysis efficiency	0.58	-
FC yearly heat production	14,185	kWh
FC yearly power production	23,335	kWh
Power coverage (without compressor power)	0.47	-
Max FC power	30.4	kW
FC heating power	22.6	kW
FC full load hours	0.05	h
Max FC efficiency	0.69	-
Mean FC efficiency	0.54	-
Max storage tank pressure	30.8	MPa
Max storage tank H2 inflow	3.8e-4	$kg\,s^{-1}$
Max storage tank H2 outflow	3.9e-4	$kg\,s^{-1}$
Max compressor power	3.54	kW
Compressor energy consumption	2,976	kWh
Power from grid (including compressor power)	28,947	kWh
CO_2-emissions from grid power	11.6	t

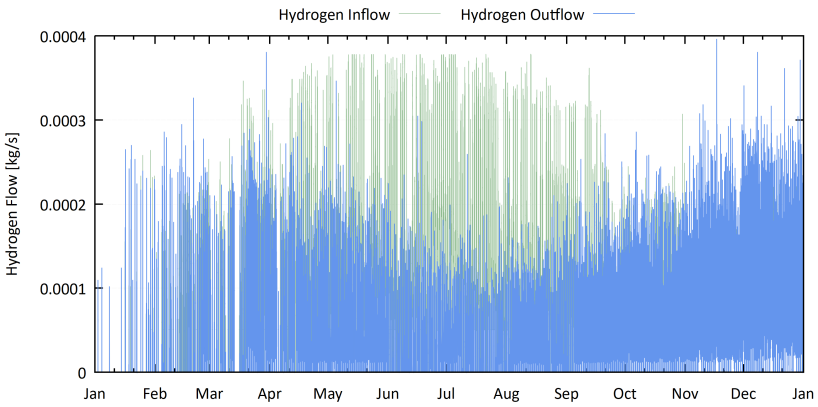

Figure 7.5: Hydrogen inflow and outflow rate of the storage cylinder of System 1

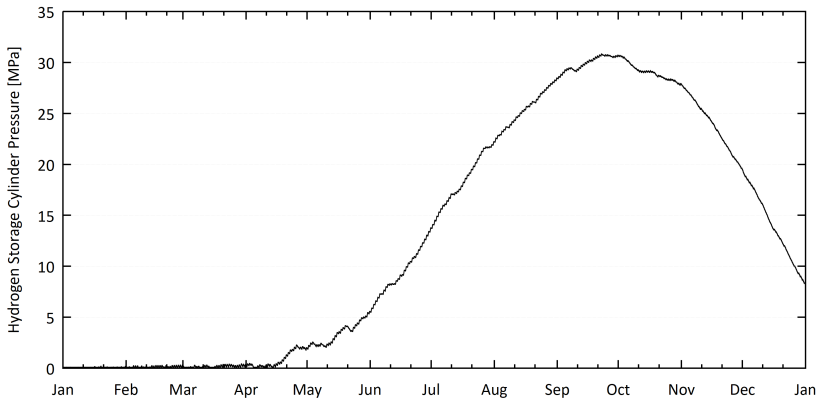

Figure 7.6: Hydrogen storage tank pressure of System 1

meet the power demand of the building cluster. With a CO_2 emission factor of 401 g per kWh, this amount leads to corresponding CO_2 emissions of 11.6 t per year for the building cluster.

7.2.2 System 2: Reversible Hydrogen Battery

In contrast to System 1, the hydrogen produced from water electrolysis, in System 2, is further processed to formic acid in a reversible hydrogen battery. This avoids the necessity to store gaseous hydrogen at high pressures.

7.2.2.1 System 2: Dimensioning

The electrolyzer and the fuel cell of System 2 are designed by using the dimensioning rules defined in Section 6.4.1. For the determination of volume of the reversible hydrogen battery, a simulation based approach is used. From simulation results, a suitable volume for the liquid phase of the battery is derived, so that the all seasonal power surpluses could be stored in the battery. The overall battery volume (gas phase and liquid phase) is 8.5 times the liquid volume according to the laboratory setup described by Hsu et al. [143]. Table 7.5 summarizes the resulting design parameters for System 2.

7.2.2.2 System 2: Simulation Results

The simulation run is executed with the design parameters set in Table 7.5 in the course of one year, starting with an empty hydrogen battery. From the simulation results shown in Table 7.6 it could be seen that the electrolyzer is oversized and has no full load hours. The fuel cell in this setup produces about 23,000 kWh electricity, which covers about 47% of

Table 7.5: System 2: parameter overview

Parameter	Value	Unit
Electrolyzer power	79	kW
Electrolyzer cells	45	-
Electrolyzer cell Area	300	cm^2
FC power	37.5	kW
FC cells	153	-
FC area	400	cm^2
H2 bat liquid volume	6,000	l
H2 bat overall volume	51,000	l

the overall power demand of the building cluster. Additionally, around 14,000 kWh of heat are produced, which could be utilized if the fuel cell is connected to a heating network or a single load. At the peak at late summer, the reversible hydrogen battery is loaded to 86%. This approves the general principle of operation as a seasonal storage system. The course of the battery loading state over the simulated year could be seen in Figure 7.7.

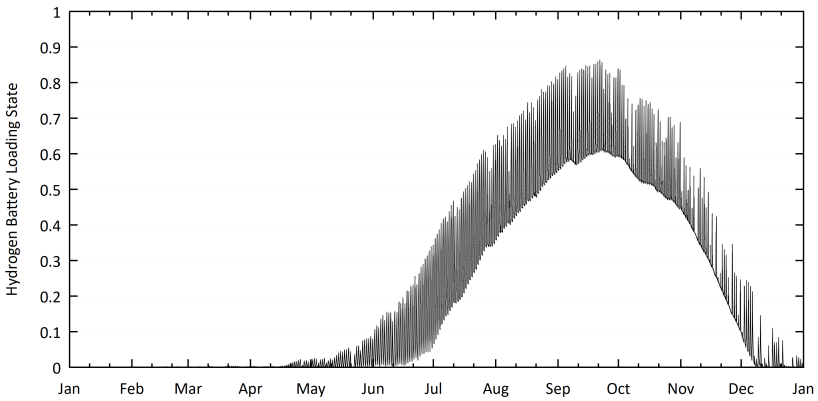

Figure 7.7: Loading State of the reversible Hydrogen Battery over the simulated year

Also changing due to seasonal effects is the gas phase pressure of the hydrogen battery, which can be seen in Figure 7.8. The occurring fluctuations around the pressure setpoint of 14 MPa is caused by the temperature change between the heated mode of the battery and the ambient temperature. Since in some cases a considerable amount of gaseous hydrogen is stored in its gaseous state, the setup of the reversible hydrogen battery in System 2 could be described as a hybrid system with physical and chemical hydrogen storage.
Overall, the reversible hydrogen battery reaches in this setup a hydrogen production rate of up to $4.88 \times 10^{-3}\,kg\,s^{-1}$. The fuel cell, on the other hand, has a maximum hydrogen demand

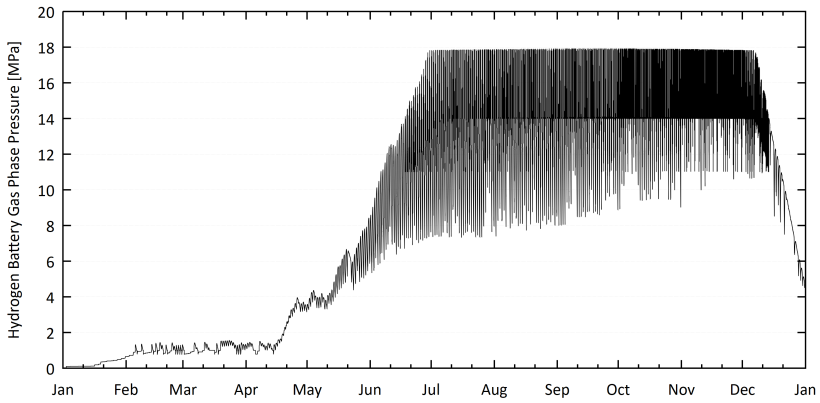

Figure 7.8: Gas Phase Pressure of the reversible Hydrogen Battery over the simulated year

of $3.94 \times 10^{-4}\,\mathrm{kg\,s^{-1}}$ at full load (250 A), which means that the hydrogen battery is capable of delivering sufficient hydrogen on the fly under these assumptions. For an optimization of the battery volume, it therefor could be possible to reduce the gas volume.
With this system setup an additional amount of 28,150 kWh of grid energy is needed, which results in annual carbon dioxide emissions of 11.4 tons.

7.2.3 System 3: H2-to-FA Flow Reactor

For System 3, the reversible hydrogen battery is substituted with a flow reactor for the hydrogenation of gaseous carbon dioxide and hydrogen from water electrolysis to formic acid. A tank is used to store the liquid formic acid. Depending on the hydrogen demand of the fuel cell, the stored formic acid is afterwards dehydrogenated in another flow reactor.

7.2.3.1 System 3: Dimensioning

The same rules for dimensioning the electrolyzer and fuel cell from System 1 and System 2 were also applied to System 3, hence leading to the same results. As the pressure ratio is lower than in System 1, the compressor in this system is designed as two-stage isothermal compressor with a maximum delivery rate of 1.5 kg/h a maximum pressure of 15 MPa. For the H2-to-FA reactor, there were no dimensioning rules defined in Section 6.4.1 due to the complex correlations of the system variables. From the evaluation of the simulation results it is derived that a reactor length of 5 m and a reactor diameter of 0.8 m is sufficient to minimize the effects of the formic acid production time shift on the fuel cell operation. From the simulation results, also a storage volume of 10,000 l could determined. However, this volume refers to pure formic acid. If formic acid in aqueous solution should be stored, the storage volume must be increased depending on the formic acid concentration. For the design

Table 7.6: System 2: simulation results

Parameter	Value	Unit
Max electrolysis power	78.57	kW
Electrolyzer full load hours	0.016	h
Electrolyzer stand By hours	6377	h
Electrolyzer off-on-switches	1522	-
Max H2 production rate	3.8e-4	$kg\,s^{-1}$
Mean H2 production rate	4.33e-5	$kg\,s^{-1}$
Produced hydrogen	1379.47	kg
Max electrolysis efficiency	0.63	-
Mean electrolysis efficiency	0.4	-
FC yearly heat production	14,025	kWh
FC yearly power production	23,063	kWh
Power coverage (without compressor power)	0.47	-
Max FC power	30.4	kW
FC heating power	22.6	kW
FC full load hours	0.03	h
Max FC efficiency	0.69	-
Mean FC efficiency	0.54	-
H2 Bat max FA concentration	5.18	$mol\,l^{-1}$
H2 Bat max loading state	0.86	-
Max compressor power	3.12	kW
Compressor energy consumption	2,667	kWh
Power from grid (including compressor power)	28,510	kWh
CO_2-emissions from grid power	11.4	t

of the FA-to-H2 reactor, the application rule from Section 6.4.1 was applied. This leads to a reactor volume of $0.2\,m^3$. The resulting design parameters of System 3 are summarized in Table 7.7.

7.2.3.2 System 3: Simulation Results

The load profiles for the surplus and the deficit power of the building cluster was applied to System 3. Table 7.8 shows the simulation results for System 3. All results concerning the electrolyzer are identical with System 1 and System 2, as no changes in the electrolyzer design were applied in System 3. Overall, in this setup, the fuel cell produces 22,443 kWh of electrical energy and 13,679 kWh of heat. The produced electrical energy covers about 46 % of the annual power deficit of the building cluster. If the energy needed for the compressor is taken into account, an additional amount of 29,713 kWh of grid energy is needed to cover the power demand of the cluster, resulting in CO_2 emissions of 11.9 tons per year.

Table 7.7: System 3: parameter overview

Parameter	Value	Unit
Electrolyzer power	79	kW
Electrolyzer cells	45	-
Electrolyzer cell area	300	cm^2
FC power	37.5	kW
FC cells	153	-
FC area	400	cm^2
Compressor stages	2	-
Compressor max delivery rate	1.5	$kg\,h^{-1}$
H2-to-FA reactor length	5	m
H2-to-FA reactor diameter	0.8	m
FA Storage tank volume	10,000	l
FA-to-H2 reactor volume	0.2	m^3

The comparison of the amount of hydrogen produced with the electrolyzer with the amount of formic acid produced for the flow reactor shows that all hydrogen is converted into formic acid. An maximum formic acid outflow rate of $0.003\,kg\,s^{-1}$ could be achieved with the H2-to-FA flow reactor. Figure 7.9 shows the filling level of the formic acid storage tank over the course of the year. A clear seasonal effect could be seen.

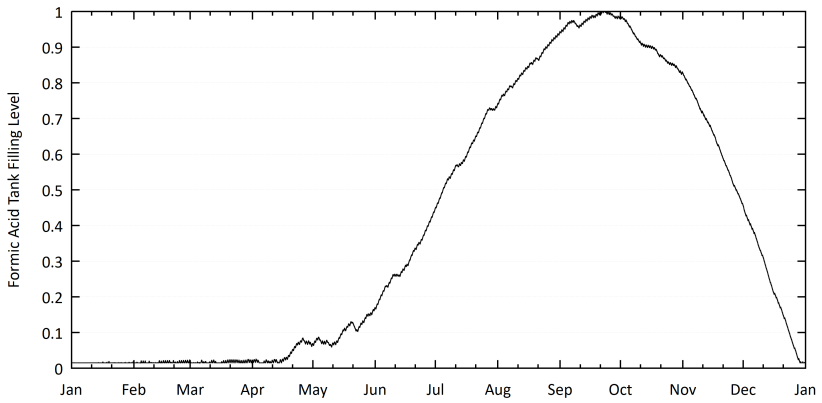

Figure 7.9: Formic acid storage tank filling level of System 3

As a maximal hydrogen outflow of the FA-to-H2 flow reactor is achieved, the hydrogen demand of the fuel cell corresponding to the maximum fuel cell current of 250 A could be matched.

Table 7.8: System 3: simulation results

Parameter	Value	Unit
Max electrolysis power	78.57	kW
Electrolyzer full load hours	0.016	h
Electrolyzer stand by hours	6377	h
Electrolyzer off-on-switches	1522	-
Max H2 production rate	3.8e-4	$kg\,s^{-1}$
Mean H2 production rate	4.33e-5	$kg\,s^{-1}$
Produced hydrogen	1,379.47	kg
Max electrolysis efficiency	0.63	-
Mean electrolysis efficiency	0.58	-
FC yearly heat production	13,679	kWh
FC yearly power production	22,443	kWh
Power coverage (without compressor power)	0.46	-
Max FC power	30.4	kW
FC heating power	22.6	kW
FC full load hours	0.033	h
Mean FC efficiency	0.54	-
Max compressor power	2.64 kW	
Compressor energy consumption	2,850	kWh
H2-to-FA reactor max FA outflow	0.003	$kg\,s^{-1}$
H2-to-FA reactor produced FA	31,728	kg
FA Storage tank max filling level	1	-
FA-to-H2 reactor max H2 outflow	3.77e-4	$kg\,s^{-1}$
Power from grid (including compressor power)	29,713	kWh
CO_2-Emissions from grid power	11.9	t

7.2.4 System 4: Electrochemical Formic Acid Production

System 4 features major changes compared to the previous investigated systems. The PEM water electrolyzer is substituted with a CO_2 electrolyzer for the direct electrolysis of carbon dioxide and water to formic acid under moderate conditions. Formic acid could afterwards be stored as a liquid and the containing hydrogen released on demand in a flow reactor.

7.2.4.1 System 4: Dimensioning

Again, the dimensioning rules introduced in Section 6.4.1 were applied for System 4. This results in a rated power for the CO_2 electrolyzer of 78 kW, which requires 50 cells with an area of each 400 cm^2. A storage tank volume of 8820 l is determined[1]. The FA-to-H2

[1] note that the storage tank volume refers to pure formic acid. For an aqueous formic acid solution higher storage capacities are necessary

reactor volume is set to 0.3 m^3. All parameters concerning the fuel cell do not deviate from the other systems. Table 7.9 summarizes the parameters used for the simulation of System 4.

Table 7.9: System 4: system parameters

Parameter	Value	Unit
CO_2 electrolyzer power	78	kW
CO_2 electrolyzer cells	50	-
CO_2 electrolyzer cell area	400	cm^2
FA dtorage tank volume	8820	l
FC power	37.5	kW
FC cells	153	-
FC area	400	cm^2
FAtH2-reactor volume	0.3	m^3

7.2.4.2 System 4: Simulation Results

With the parameter set defined in the previous section, a maximum electrolysis power of 77.62 kW is achieved. As expected, no full load hours are achieved with this setup (see Table 7.10). The maximum formic acid production rate of the CO_2 electrolyzer is 0.0029 $kg\,s^{-1}$ and an overall amount of 10,581 kg of formic acid is produced throughout the simulated year. Considering the total electrical energy generated with the fuel cell in this system (6,268 kWh), a power coverage of 12 % is reached, which is the lowest value of the investigated systems. A additional amount of 45,372 kWh of electrical energy is needed from the power grid, resulting in annual CO_2 emissions of 18.2 t for the building cluster. The simulation results from Table 7.10 show that more hydrogen is produced by the FA-to-H2 reactor, than required by the fuel cell. A more advanced controller for the reactor will contribute to the reduction of wasted hydrogen.
The CO_2-electrolyzer is operated with a low efficiency of 19 % compared to the efficiency of the PEM electrolyzer used in the other systems. High voltage losses are the reason for the low efficiency of the CO_2 electrolyzer. For a representative summer day, the cell voltage of the CO_2 electrolyzer and the PEM electrolyzer is shown in Figure 7.10. The cell voltage of the CO_2-electrolyzer is at all times about 2.5 times higher than the cell voltage of the PEM electrolyzer. This results in lower currents at the same power input and hence lower production rates according to Farraday's Law. Figure 7.11 shows the loading state of the formic acid tank in the course of the year. Like in the other systems, a seasonal dependency could be seen. The low maximum tank filling level points to an inaccurate sizing of the tank volume.

Table 7.10: System 4: simulation results

Parameter	Value	Unit
Max electrolysis power	77.62	kW
Electrolyzer full load hours	0.017	h
Electrolyzer stand by hours	6385	h
Electrolyzer off-on-switches	1571	-
Max FA production rate	0.0029	$kg\,s^{-1}$
Mean FA production rate	0.0003	$kg\,s^{-1}$
Produced formic acid	10,581	kg
Max electrolysis efficiency	0.21	-
Mean electrolysis efficiency	0.19	-
FC yearly heat production	3,866	kWh
FC yearly power production	6,268	kWh
Power coverage	0.12	-
Max FC power	28.6	kW
FC heating power	20.4	kW
FC full load hours	0.017	h
Max FC efficiency	0.69	-
Mean FC efficiency	0.47	-
Hydrogen demand by FC	337	kg
FAtH2-reactor H2 outflow	478	kg
Power from grid	45,372	kWh
CO_2-emissions from grid power	18.2	t

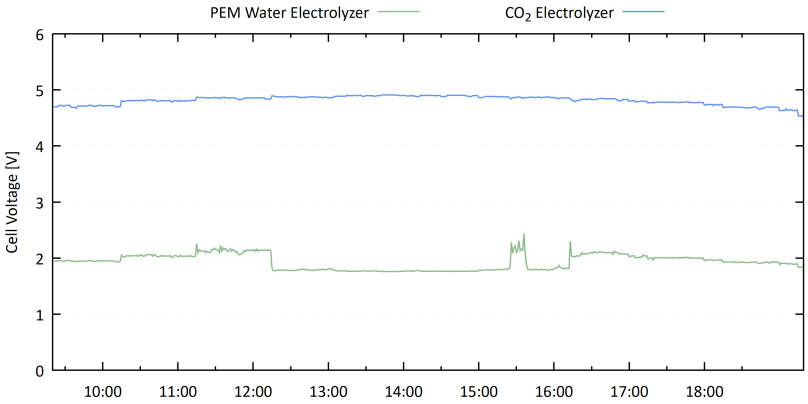

Figure 7.10: Cell Voltage of the CO_2 electrolyzer and the PEM water electrolyzer in a representative summer day

7.3 System Comparison

Based on the simulation results from the previous sections and more general considerations, all investigated system are subsequently compared to each other. Five parameters were used

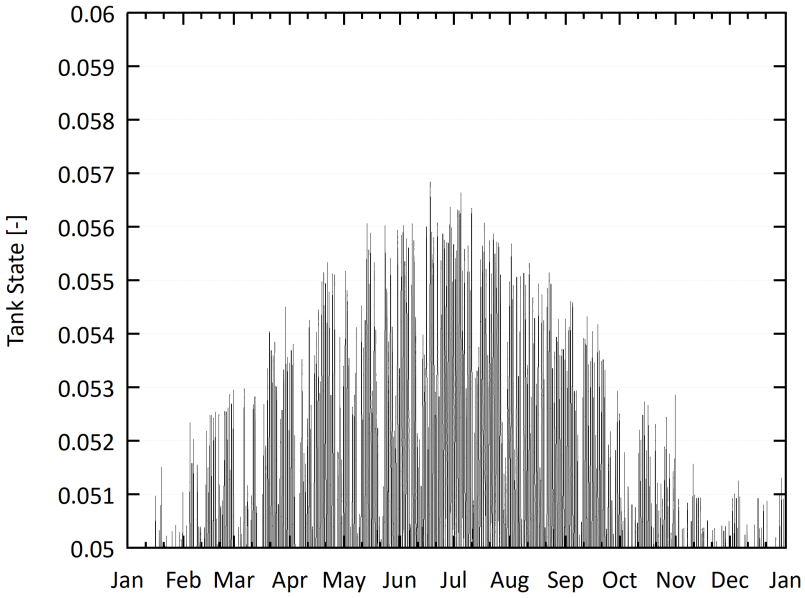

Figure 7.11: Annual Tank State Curve of System 4

as a basis for the comparison: the power-to-power efficiency, land use, technology readiness, transportability of the energy carrier and system complexity.

Power-to-Power Efficiency The simulation results are considered to calculate the power-to-power (P2P) efficiency of the formic acid based energy storage systems. With the annual surplus energy $E_{surplus}$ and the power output of the fuel cell $E_{FC,out}$ as well as the energy demand of a possible compressor E_{comp}, the P2P efficiency is calculated as follows:

$$\eta_{p2p} = \frac{E_{surplus}}{E_{FC,out} - E_{comp}} \tag{7.1}$$

All systems show similarly low efficiencies between 25.7 % for System 1 and System 2 and 7.3 % for System 4. The efficiency is mainly determined by the efficiency of the electrolyzer and the fuel cell. Although no compressor is needed for System 4, this systems shows the by far lowest P2P efficiency. This can be attributed to the fact that the CO_2 electrolyzer has a significantly lower efficiency compared to a PEM water electrolyzer. The efficiencies of System 2 and System 3 may be lower in a real application, as the simulation model does not regard the power demand for the heating and cooling of the flow reactors or reversible hydrogen battery. Figure 7.12 shows the P2P efficiency for all four Systems.

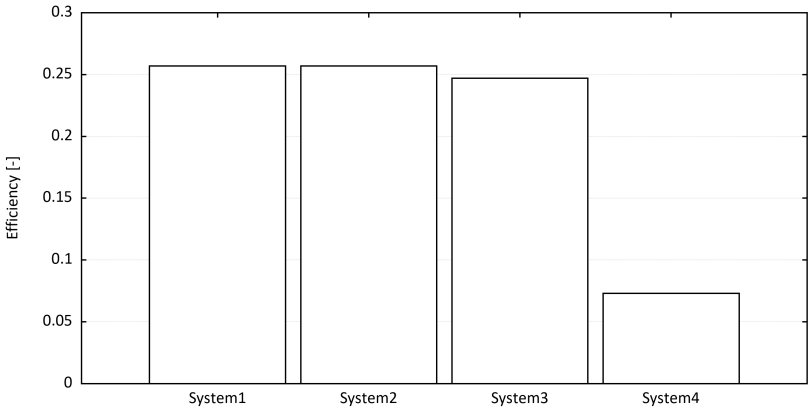

Figure 7.12: Power-to-power efficiency of the proposed formic acid based storage systems

Land use The next parameters which is evaluated is the land use of the systems. As all system proposed are supposed to be alternatives for local energy storage in urban areas, the overall area demand of the system is an important parameter. A high footprint may lead to exorbitant system costs, especially in high dense urban areas. The following assumptions for the area footprint are applied:

- Water electrolyzer and CO_2-electrolyzer: 20 foot ISO container with in a footprint of $15\,m^2$
- High pressure storage tank: bundle of bottle with a volume of $0.6\,m^3$ has a footprint of $0.77\,m^2$
- Formic acid storage tank: IBC tank ($1\,m^3$) has a footprint of $1.44\,m^2$. Formic acid is stored with a concentration of 10 mol per liter.
- Compressor: 20 foot ISO container with in a footprint of $15\,m^2$
- Fuel cell: 20 foot ISO container with in a footprint of $15\,m^2$
- Flow reactor: both reactors fit into 20 foot ISO container with in a footprint of $15\,m^2$

The resulting footprints for each system and the normalized land use parameter are shown in Table 7.11.
Finally, the estimated land use of all systems are compared in Figure 7.13.

Technology Readiness Level (TRL) For an real application of the proposed systems, the readiness of the technology is an important parameters. PEM water electrolysis and PEM fuel cells are proven technologies which are in operation worldwide (TRL 8 - 9). The concept

Table 7.11: Land Use

System	Footprint	Normalized Land Use
System 1	83.5 m^2	0.95
System 2	96 m^2	0.83
System 3	98.88 m^2	0.80
System 4	79.56 m^2	1

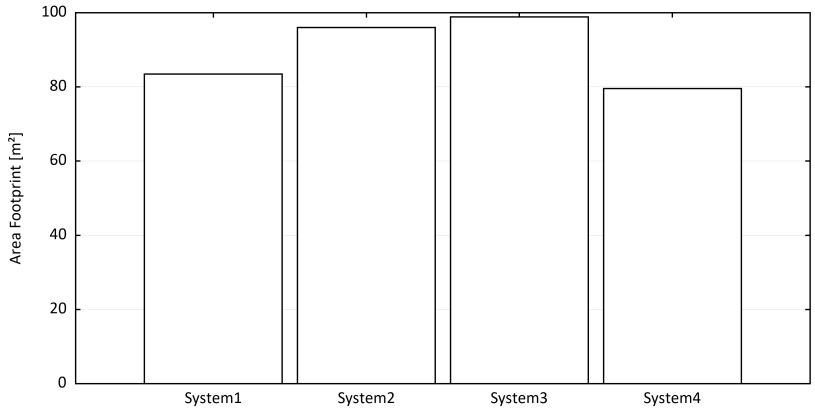

Figure 7.13: Estimated land use of the proposed formic acid based storage systems

of a reversible hydrogen battery was experimentally shown in lab scales which corresponds to a TRL of 3. Flow reactors, as used in System 3 and System 4, are generally reliable technologies. It is assumed that existing flow reactors could be redesinged for the hydrogenation of carbon dioxide to formic acid and the dehydrogenation of formic acid to hydrogen without major hurdles, if the suitable catalysts are available. From this point of view the TRL for the flow reactor was set to 6. Finally, the TRL of carbon dioxide electrolysis is assumed to be between 4 to 6. Figure 7.14 summarizes the estimated lowest TRL of all propsed systems.

Transportability The ability to be easily transported over long distances is an decisive property of an energy carrier. Disparities between areas of high renewable energy production potential and low consumption and locations of high energy consumption and lower renewable energy production potential must be equalized. However the transportability of an energy carrier is hard to quantify. For the system comparison three different scores in transportability were defined:

- Best case (score: 1 of 1): the energy carrier is liquid under ambient conditions, e.g. pure or diluted formic acid. This requires only minor adjustments to existing transportation possibilities such as road, rail or ship transportation

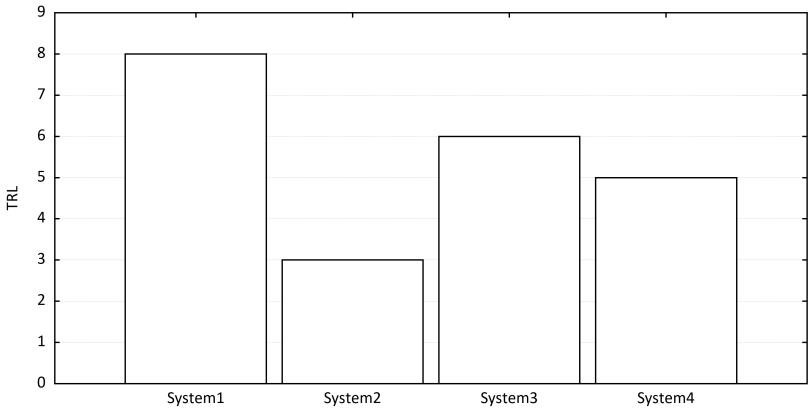

Figure 7.14: Lowest TRL of the proposed formic acid based storage systems

- Medium case (score 0.5 of 1): the energy carrier is gaseous under ambient conditions and no complete infrastructure exists, which is e.g. true for hydrogen. Major adjustments to existing systems are therefor necessary (e.g. H2-ready gas pipelines, newly developed and certified transport containers)
- Worst case (score 0.1 of 1): the energy carrier is not directly accessibly and could only be transported with surrounding hardware. This is especially true for different kinds of batteries.

Based on this classification, the resulting score for the proposed systems are shown in Table 7.12.

Table 7.12: Transportablity

System	Storage Medium	Transportablity Score
System 1	gaseous hydrogen	0.5
System 2	formic acid/ DBU in battery	0.1
System 3	lqd formic acid	1
System 4	lqd formic acid	1

System complexity Another important parameter for the comparison of the formic acid based energy storage systems is the complexity of the system. Higher system complexity usually comes with higher investment and operation costs, as well as more malfunctions and shorter maintenance intervals. Besides the amount of main components, also the highest process temperature and the highest process pressure is taken into account to evaluate the complexity of the system. Different weights are applied to calculate the system complexity:

- Number of main system components (weight: 0.6)
- Highest process temperature (weight: 0.3)
- Highest process pressure (weight: 0.1)

Table 7.13 shows the parameters for all systems as well as the calculated system complexity score and the normalized system simplicity.

Table 7.13: System Simplicity

System	Number of Systems	Highest Temperature	Highest Pressure	System Complexity Score	Normalized System Simplicity
System 1	4	70 °C	35 MPa	26.9	0.65
System 2	4	100 °C	14 MPa	33.8	0.52
System 3	5	110 °C	14 MPa	37.4	0.46
System 4	4	50 °C	0.1 MPA	17.41	1

System Comparison Summery With all evaluated parameters for the comparison of all four system a spyder plot could be drawn (see Figure 7.15).

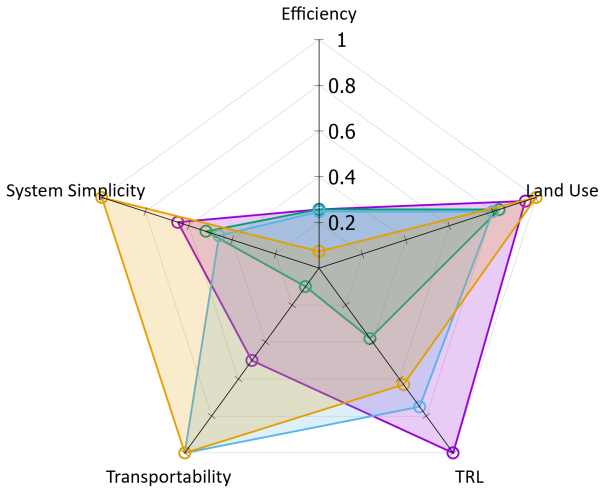

Figure 7.15: System comparison spyder plot: System 1 (purple), System 2 (green), System 3 (blue), System 3 (yellow)

With the underlying assumptions, it could be seen from Figure 7.15, that System 2 and System 3 are not competitive, as they do not show any outstanding characteristics. System 1

stands out for its high TRL and could be applied without the need of further research. However, the most promising option is system 4, the electrochemical carbon dioxide reduction, as it combines the easy transportability of liquid formic acid with a low system complexity. The low area footprint in combinations with a low process temperature and pressure and the avoidance of having to store gaseous hydrogen, makes System 4 attractive for an application in densely populated urban areas. For an real application of this system, still major research activities are necessary to increase the system efficiency.

7.4 Optimization of System 4

As System 4 was previously identified of being a promising option for are seasonal energy storage application, the following section deals with the optimization of System 4.

7.4.1 Varying the Number of Electrolysis Cells

As sizing the electrolyzer to the maximal surplus power of the building cluster comes with some disadvantages, such as low full load hours and high load fluctuations, the number of cells are reduced in this section and the overall formic acid coverage determined. Table 7.14 summarizes the simulation results for an adaption of the electrolyzer power to 100%, 50%, 25% and 10% of the maximal surplus power. The rated power of the electrolyzer ranges from 77.62 kW to 7.9 kW.

Table 7.14: System 4: varying the number of electrolysis cells

Parameter	**100%** P_{max}	**50%** P_{max}	**25%** P_{max}	**10%** P_{max}
Number of cells	50	25	12	5
Max power	77.62 kW	39.68 kW	19 kW	7.9 kW
Full load hours	0.017	863	1655	2233
Stand by hours	6366	6868	6399	5962
Off-on-switches	4678	1641	921	1078
Max FA prod rate	$0.003\,kg\,s^{-1}$	$0.0014\,kg\,s^{-1}$	$0.000\,69\,kg\,s^{-1}$	$0.000\,29\,kg\,s^{-1}$
Max efficiency	0.21	0.19	0.19	0.19
Mean efficiency	0.198	0.19	0.19	0.19
Produced FA	10,738 kg	8764 kg	5547 kg	2825 kg
FA coverage	0.19	0.15	0.1	0.05

As expected, the full load hours of the electrolyzer increases with decreasing power. Although the maximal formic acid production rate scales linearly with the power, the annual mean formic acid production rate does not, as shown in Figure 7.16a. This behavior could be traced back to the circumstance that peak surplus power only occurs at very short periods

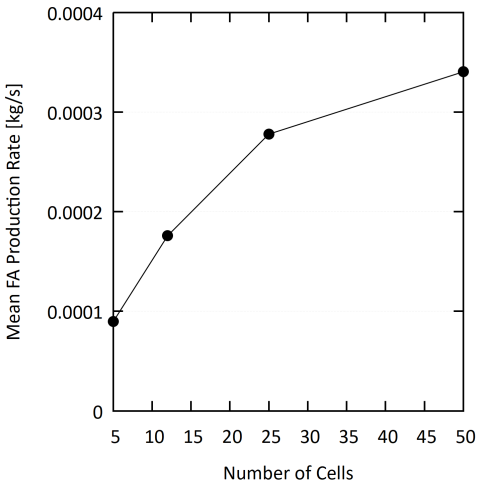

(a) Annual mean FA production rate depending over the number of cells

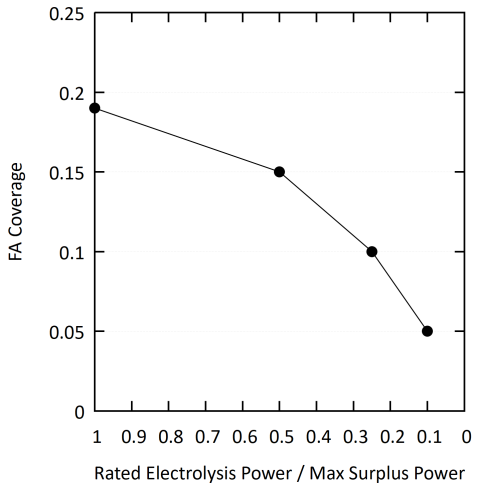

(b) Influence of the rated electrolysis power on the overall formic acid coverage

Figure 7.16: FA coverage and mean production rate of System 4 with a changing number of electrolysis cells

over the year. With this system, the overall coverage of the formic acid demand lays between 19% for an electrolyzer dimensioned at 100% peak load to 5% for a rated power of 10% of the peak load (see Figure 7.16b).
Between 100% and 50% peak load the FA coverage only decreases slightly. Therefor, for this system, a system size of 50% of the peak load, leading to 25 electrolysis cells and a rated power of about 40 kW, is further chosen as the optimal design point. This design point and its corresponding full load hours are illustrated in the annual load duration curve of the surplus power shown in Figure 7.17.

7.4.2 Adjusting the Battery Power and Capacity

In the next optimization step, the power and the capacity of the buffer battery is optimized for an electrolyzer with a rated power of 40 kW, as determined in the previous section. Figure 7.18a shows the annually amount of produced formic acid by this system with varying battery power. It is clearly visible that a optimum exists for a battery power of 50% of the rated electrolysis power. This results in a rated battery power of 20 kW for this use case. Further increasing the battery power does not lead to a higher formic acid production, as a too high share of electrical surplus power is used for battery charging. After the battery power is determined to 20 kW, the next step is the optimization of the battery capacity. This process aims at reducing the stand-by hours of the electrolyzer. From Figure 7.18b it is visible that the stand-by hours are reduced linearly between 10 kWh (C-rate: 2) and 80

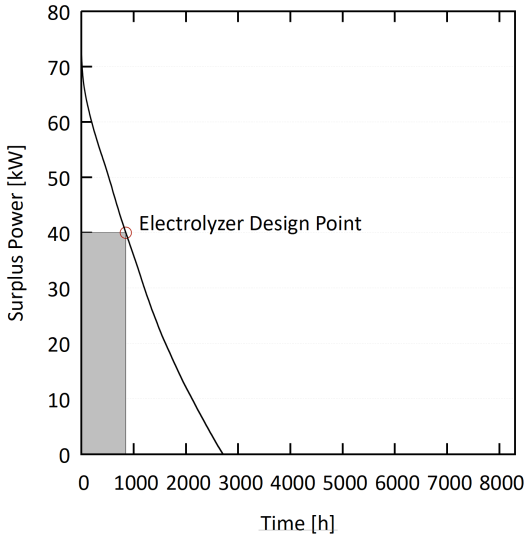

Figure 7.17: Load duration curve of surplus power and electrolyzer design point of system 4

kWh (C-rate: 0.25). Within this range, economical factors may have the final impact on the selected battery capacity. As the curve flattens at higher capacities, it is assumed that an increase over 80 kWh is not useful.

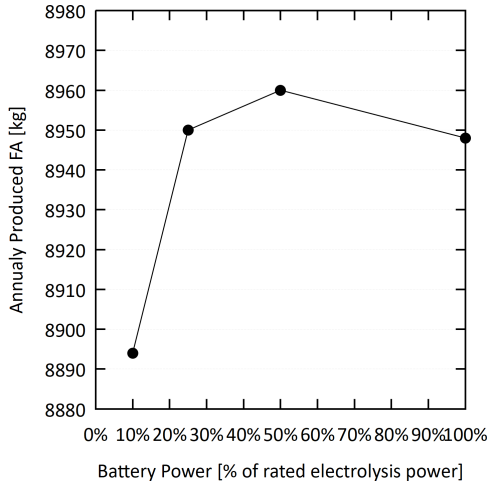

(a) Produced formic acid depending on the battery power

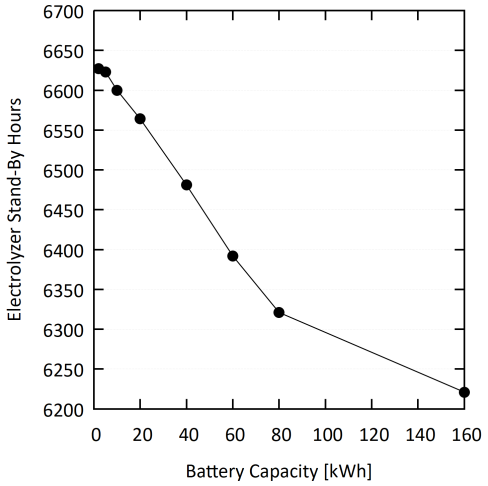

(b) Electrolyzer stand-by hours depending on the battery capacity

Figure 7.18: System 4: optimization of the buffer battery power and capacity

Finally, from the investigations of this section, the following update on the buffer battery

Table 7.15: System 4: adjusting the battery capacity for a power output of 20 kW

Parameter	10 kWh	20 kWh	80 kWh	160 kWh
Full load hours	863	863	863	863
Stand-by hours	6600	6564	6320	6220
Off-on-switches	1227	938	1241	1387
Produced FA	8876 kg	8960 kg	9625 kg	9898 kg

design rules are derived:

- Battery Power: 50% of the rated electrolysis power
- Battery Capacity: C-rate in the range of 0.25 to 2

For the further optimization process a C-rate of 1 (20 kWh) for the buffer battery was applied.

7.4.3 Optimization of the Tank Volume

In a real application of system 4 the maximal volume of the tank is only limited by the available space and the project budget. However, as Figure 7.11 shows, a formic acid tank designed with a rough estimation of the formic acid production is only filled to under 6% at its peak. Hence it is possible to consider a significantly smaller tank volume.

From the produced amount of formic acid it could be derived that a specific storage volume of 1.5 liter per installed electrolysis power may be sufficient. The application of this rule results in the peak tank usage shown in Table 7.16.

Table 7.16: System 4: adjusting the tank volume

Installed Electrolysis Power	77.62 kW	39.68 kW	7.9 kW
Peak tank filling level	58%	80%	92%

It must be noted, that the exact amount of produced formic acid with a simultaneous demand of the fuel cell must be determined with a detailed system simulation. However the following rule of thumb for the formic acid tank could be applied for an on grid operation of the system:

- Formic Acid Tank Volume: 1.5 liter per installed kW of electrolysis power

7.4.4 Application of the Optimization Steps on System 4

With the optimized system parameters determined in the sections above, the simulation of System 4 was executed again. Table 7.17 shows the simulation results of the base system in comparison to the optimized system. The key parameters are further shown in Figure 7.19.

Table 7.17: System 4: simulation results of the base system and optimized system

Parameter	Base System	Optimized System
Max electrolysis power	77.62 kW	40 kW
Electrolyzer full load hours	0.017	872
Electrolyzer stand-by hours	7699	7025
Electrolyzer off-on-switches	1051	751
Battery power	70 kW	40 kW
Battery capacity	70 kWh	40 kWh
Max FA production rate	$0.0029\,\mathrm{kg\,s^{-1}}$	$0.0014\,\mathrm{kg\,s^{-1}}$
Mean FA production rate	$0.0003\,\mathrm{kg\,s^{-1}}$	$0.000\,28\,\mathrm{kg\,s^{-1}}$
Produced formic acid	9746.12 kg	8948 kg
FA tank volume	8820 l	60 l
FC yearly heat production	3566 kWh	3285 kWh
FC yearly power production	5804 kWh	5331 kWh
Power coverage	0.11	0.10
Power from grid	45,564 kWh	45,796 kWh
CO_2-emissions from grid power	18.27 t	18.36 t

Although the rated power of the electrolyzer is nearly halved, the additional power needed from the grid and hence the assigned carbon dioxide emissions of the building cluster do not change. The full load hours of the electrolyzer are significantly increased with the optimized electrolyzer size. As it turns out, the original design rule for the tank size is not suitable for the formic acid tank. The tank size could either be evaluated from simulation results or more advanced methods for the calculation of the storage demand from load profiles must be applied.

The results of the optimization show, that if CO_2 electrolyzers are used for a stationary energy storage application with fluctuating load, the design of the system must carefully evaluated for the local conditions. Rules of thumb although are helpful as a starting point for the system design.

7.5 Additional Aspects to improve the Output of System 4

In this section two different measure to increase the performance of System 4 are evaluated: the adding of small wind turbines to increase the power production of the building cluster

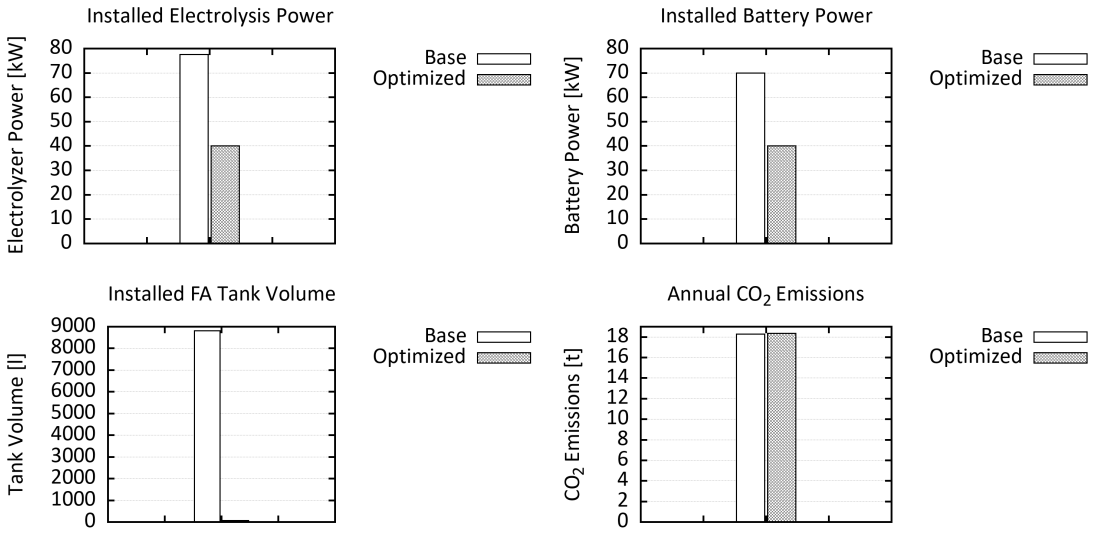

Figure 7.19: System 4: comparison of key parameters for the base system and optimized system

and the utilization of waste heat of the fuel cell.

7.5.1 Adding of Small Wind Turbines

A generic vertical-axis SWT with a rated power output of 5.3 kW at a wind speed of 14 m s^{-1} was assumed for the evaluation of the system performance with added wind turbines. The power output of the SWT depending on the wind speed is shown in Figure 7.20a. At wind speeds above 14 m s^{-1} the wind turbine is shut down to prevent mechanical stress.
The wind speed data is based on hourly data from a nearby measuring station, which was re-sampled to a resolution of one minute using an interpolation algorithm. By using Equation 5.78 the wind speed at hub height with a terrain roughness of 0.28 was calculated. Figure 7.20b shows the resulting wind speeds at hub height over the course of one year.

Table 7.18: Small wind turbine: system parameters

Parameter	Value	Unit
SWT rated power at 14 m s^{-1}	5.3	kW
SWT hub height	14	m
Terrain roughness	0.28	-
Number of SWTs	5	-

The power output of a wind turbine field of five SWTs (see Table 7.18) was calculated and

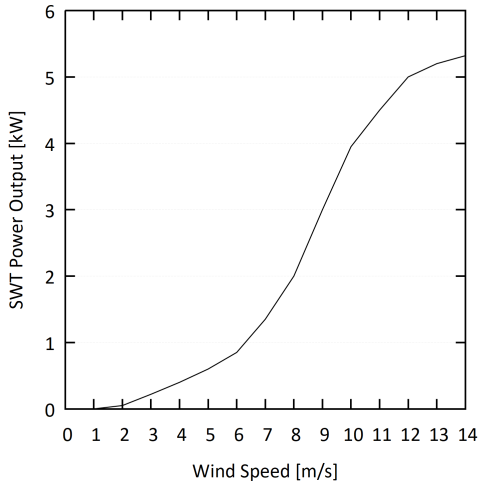

(a) Wind turbine power output

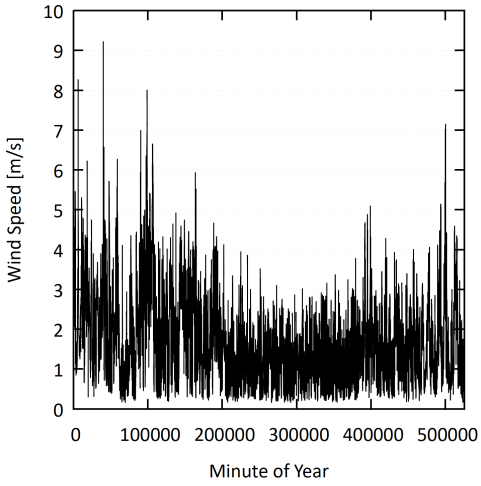

(b) Wind speed at hub height

added to the surplus power of the building cluster[2]. Table 7.19 shows the calculated output of the wind turbines. The median wind speed at hub height is 2.38 $m\,s^{-1}$, which results in a median power output of 0.11 kW per wind turbine. Overall, the wind turbine fields contributes to the energy surplus of the building cluster with 11,673 kWh per year.

Table 7.19: Small wind turbine: power output

Parameter	Value	Unit
Max wind speed at hub height	15.24	$m\,s^{-1}$
Median wind speed at hub height	2.38	$m\,s^{-1}$
Max power output per turbine	5.3	kW
Median power output per turbine	0.11	kW
Annual Energy Yield of the turbine field	11,673	kWh

Figure 7.21 shows the power output of the building cluster with the added wind turbines as a heatmap. Compared with the illustration without wind power (see Figure 7.2), the central dot of power surpluses is blurred, as, however rather low, surplus power is available at winter month and at night.

The new load profile of the building cluster, including the power generation of the wind turbine field is applied to the optimized System 4. A simulation run over one year was executed. The simulation results show only a minor increase in the system performance (see Table 7.20). With the adding of the small wind turbines the full load hours of the CO_2-electrolyzer are further increased to 1,053 h. The overall produced formic acid rises

[2]This assumes that the generated power of the SWTs is solely utilized by the CO_2-electrolyzer

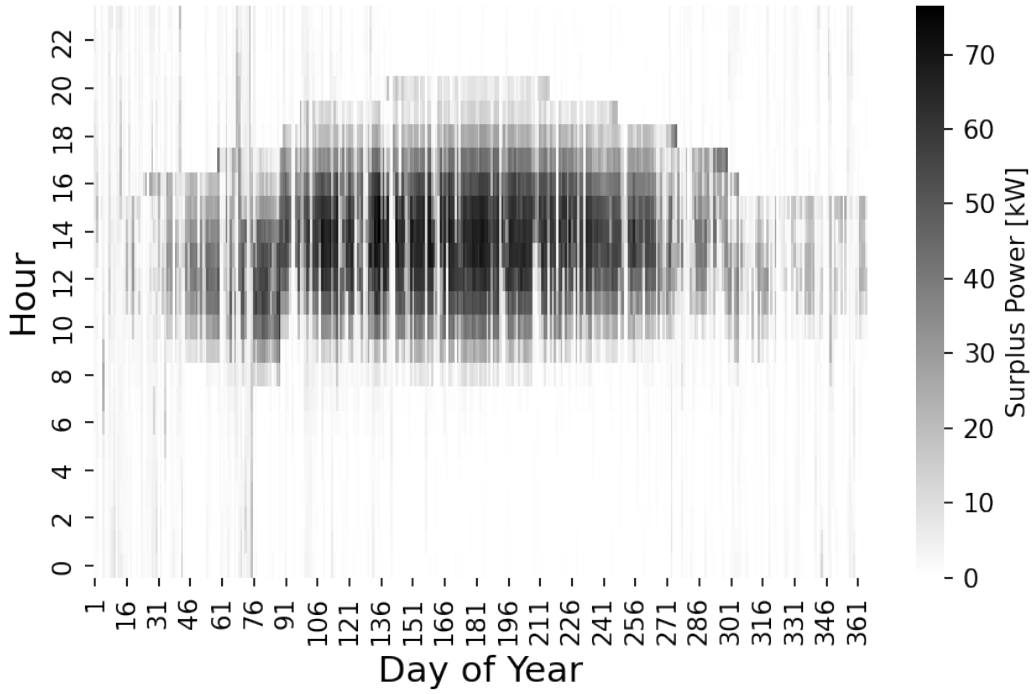

Figure 7.21: Building cluster surplus power with five added SWTs

Table 7.20: System 4: key parameters from the simulation results with wind turbines

Parameter	**System 4 (opt)**	**System 4 (opt+wind)**	**Performance**
EL full load hours	872	1,053	+27 %
Produced FA	8,948 kg	10,196 kg	+14 %
FC heat production	3,566 kWh	3,620 kWh	+1.5 %
FC power production	5,804 kWh	5,901 kWh	+1.7 %
Power coverage	10.4 %	11.5 %	+10 %
Power from grid	45,796 kWh	45,699 kWh	-0.2 %
CO_2-emissions	18.36 t	18.33 t	-0.16 %

to 10,196 kg, which represents an increase of 14% compared to the system without wind turbines. This results on a increase power production of the fuel cell of 1.7 %, which reduces the needed power from the grid and hence the assigned carbon dioxide emissions for the building cluster. It is doubtful whether the outlined performance increase would justify the installation of a wind turbine field. However, it must be said that the wind yield depends strongly on the local conditions. Another option to increase the system performance could be the installation of more PV power.

7.5.2 Heat Recovery

The heat produced of fuel cell of the optimized System 4 without additional wind turbines is 3,566 kWh, which is not enough to directly supply the building with the least heating demand (4,505 kWh for ID 0010, see Table 7.1) within the building cluster. And possible heat losses had not yet been taken into account. Also, a feed in to a hypothetical heating network is not beneficial because of the low operating temperature of the fuel cell (30 °C in this scenario). Possible, however, would be a feed into a low-ex heating network as it exists in the area of this case-study. Such a measure would increase the performance of the heat pumps and as a result, the power demand of the fuel cell would decrease. Hence, a heat recovery system purely for the fuel cell of System 4 is only suitable if a low-ex heating network is available in the regarded location. This assessment may change if a heat recovery system is also applied to the CO_2-electrolyzer. With the underlying assumptions of the used model, an overall annual heat production of 46,176 kWh with a peak heating power of 27 kW is calculated for the electrolyzer. As the electrolyzer is operated at 70 °C this heat could be used for the direct supply of nearby buildings or for feeding into a district heating network. However, as the peak heat production of the electrolyzer correlates to the peak electrical power in the summer months, the seasonal shift of the heat production must be considered.

7.6 Economic Aspects of System 4

In this section economic aspects of the CO_2-electrolyzer of System 4 are regarded. The maximum feasible investigation cost of local CO_2 electrolysis are determined with regard to a comparable system with external formic acid deliveries. Table 7.21 shows the market prices for the carbon dioxide, demineralized water, formic acid and electrical energy which are used for the following calculations.

Table 7.21: System 4: Variable Costs Parameters

Item	Symbol	Price	Unit	Source
CO_2	p_{CO_2}	20 €	t	[165]
Demin·Water	p_{H_2O}	2 €	t	[165]
PureFormicAcid	p_{FA}	20 €	kg	current market price
Electrical Energy (from PV)	p_{power}	0.11 €	kWh	[166]

The conversion factor k_{CO2EL} determines how much energy is needed for the electrolyzer per kg product. Values for the maximum electrolysis power P_{max} and the maximum formic acid production rate $\dot{m}_{FAout,max}$ were taken from the simulation results of the optimized

System 4 (see Table 7.17):

$$k_{CO2EL} = \frac{P_{max}}{\dot{m}_{FAout,max}} = 9.23\,\text{kW h kg}^{-1} \tag{7.2}$$

With k_{CO2EL} the specific variable production costs $k_{var,CO2EL}$ of one kg formic acid produced via CO_2 electrolysis could be calculated, if the costs for the needed water and dioxide, as well as the electrical power, is taken into account. From the reaction equation of carbon dioxide reduction to formic acid follows that 1 kg of carbon dioxide and 0.39 kg of water is needed for the production of one kilogram formic acid. Finally, $k_{var,CO2EL}$ is calculated according to the following equation:

$$k_{var,CO2EL} = p_{CO_2} \cdot \cdot m_{CO_2} + p_{water} \cdot m_{water} + p_{power} \cdot k_{CO2EL} = 1.04\,€\,\text{kg}^{-1} \tag{7.3}$$

If the hydrogen content of formic acid (4.4 wt.-%) is taken into account, the production costs for hydrogen via CO_2 electrolysis is calculated as $23.55\,€\,\text{kg}^{-1}$ or, based on the energy content, as $0.71\,€\,\text{kW}^{-1}\,\text{h}$. As the production costs for hydrogen with System 4 are far above the prevailing market price and hence no economic operation is possible with the underlying assumptions, the following economic considerations aim at selling formic acid as a chemical product. In addition to the variable costs, there are also annual fixed costs for the operation of the CO_2-electrolyzer. The fixed costs consist of maintenance costs and annualized costs for the exchange of the stack. With the specific maintenance costs $c_{maintenance}$, the lifetime of the stack a_{stack} and the system a_{system} and the percentage of the stack exchange with regard to the system CAPEX p_{CAPEX}, the fixed costs can be calculated as follows:

$$k_{fix} = c_{maintenance} \cdot P_{max} + \left(1 - \frac{a_{stack}}{a_{system}}\right) \cdot p_{CAPEX} \cdot CAPEX \tag{7.4}$$

The parameters for the calculation of $k_{var,CO2EL}$ and k_{fix} can be found in Table 7.22.

Table 7.22: System 4: Fixed Costs Parameters

Item	Symbol	Value
Specific maintenance costs	$c_{maintenance}$	$30\,€\,\text{kW}^{-1}$
Stack Lifetime	a_{stack}	5
System Lifetime	a_{system}	25
Costs for stack exchange	p_{CAPEX}	60 % of system CAPEX
Interest rate	i	10 %

Figure 7.22 shows the composition of the annual operation costs of the CO_2-electrolyzer. The cost for the substances carbon dioxide and water are negligible in this context, as the

operation costs are dominated by the costs for the electrical energy.

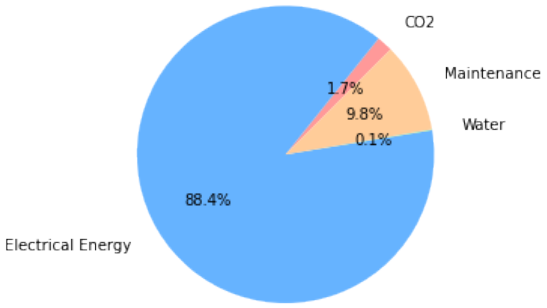

Figure 7.22: System 4: Composition of the annual operation costs of System 4 (without costs for a possible stack exchange)

The annual income I is calculated with the amount of produced formic acid from the simulation results of the non-optimized system and the assumed market price of one kilogram formic acid (see Table 7.21).

$$I_t = p_{FA} \cdot m_{FA,prod} \tag{7.5}$$

The annual expenses E_t are composed of the variable costs $k_{var,CO2EL}$ and the fixed costs k_{fix}:

$$E_t = k_{fix} + k_{var,CO2EL} \tag{7.6}$$

With the annual income and expenses, the capital value of the CO_2 electrolyzer could be calculated as follows:

$$K_0 = -CAPEX_{CO2EL} + \sum_{t}^{n_{CO2EL}} \frac{I_t - E_t}{(1+i)^t} \tag{7.7}$$

Figure 7.23 shows the capital value of the electrolyzer depending on the CAPEX of the electrolyzer.
The line of the capital costs has a zero point at a CAPEX of 332,000 €, which define the maximum possible investment costs for an economical viable operation. With regard to to the rated power of the electrolyzer (in this scenario: 40 kW), the maximum specific investment costs are 8367 € kW^{-1}.

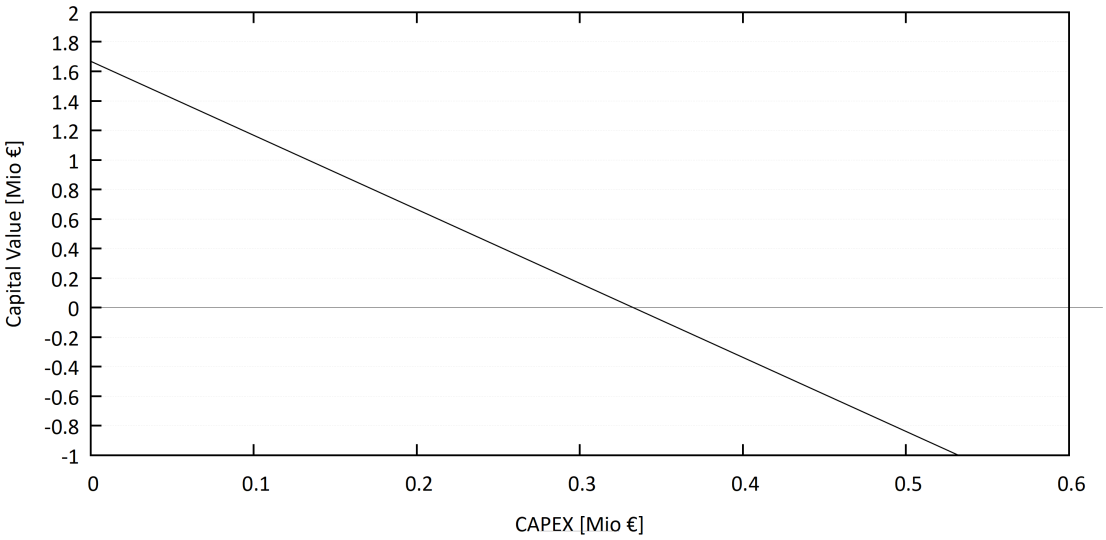

Figure 7.23: System 4: Capital Value vs CAPEX

Chapter 8

Conclusions and Recommendations

The main aspects of this thesis are summarized in this chapter and conclusions are made. Furthermore, recommendations for future research activities in the fields of this thesis are given.

8.1 Conclusions

The supplement of fossil energy carriers with renewable alternatives is an urgent challenge. Many sectors that nowadays depend on fossil fuels could be electrified. However, as most renewable energy sources show a fluctuating characteristic, the need for large-scale energy storage increases. As presented in this thesis, the utilization of carbon dioxide as a raw product is a promising option for energy storage and the synthesizing of energy carriers. Also hydrogen will play a growing role in future energy systems due to its versatility and the possibility to produce hydrogen locally with seasonal surplus power. However, large-scale and long-term hydrogen storage is still a technological challenge. It is shown in this work, that the reduction of carbon dioxide to formic acid is a possibility to address some issues concerning hydrogen storage. In this context, formic acid is considered as a hydrogen carrier. At a concentration of 10 mol per liter (46 wt.% an aqueous formic acid solution shows a comparable energy density than compressed hydrogen at 250 bar combined with all the advantages coming with its liquid state under ambient conditions, namely low safety concerns and good transportability. This work presents different process routes for formic acid utilization in an energy storage context: a reversible hydrogen battery, flow reactors and an electrochemcial process. Suitable catalysts were identified and reactor design were pointed out. After the modelling of these processes and the simulated application on a building cluster, it could be stated, that especially the electrochemical process route for formic acid production is a promising technology for energy storage applications. However

further research to improve the system efficiency and the control with fluctuating loads is needed. Subsequently, further conclusions are given for the main aspects of this work.

8.1.1 Modelling of Formic Acid based Hydrogen Storage Systems

On main aspect of this thesis was the development of models, which could be used to simulate formic acid based hydrogen storage systems. The following novel component models where developed using C++ code and the INSEL simulation environment:

- A reversible hydrogen battery
- A hydrogen to formic acid flow reactor
- A formic acid to hydrogen flow reactor
- A CO_2-electrolyzer for the electrochemical reduction of carbon dioxide to formic acid

Further, several additional model for hydrogen based energy storage systems where developed, revised or transferred to the INSEL environment, namely a PEM water electrolyzer, a hydrogen compressor, a high-pressure storage cylinder and a PEM fuel cell. All components could be combined to complete energy systems with hydrogen or formic acid production, storage and reconversion to heat and power by using the graphical user interface of INSEL. Within this work, four system models are created from the modeled components. The development of auxiliary component models, such as controllers, was carried out to complete the usability of the system models. If possible, the component models were validated with reported data. It is intended that the developed models are part of future INSEL releases and will therefor be available for a larger amount of users.

8.1.2 System Integration, Control and Dimensioning

Another main aspect of this thesis was the investigation of the possibilities for the system integration of the formic acid based hydrogen storage system. Four different systems with hydrogen or formic acid as an energy storage medium were defined:

- System 1 is considered as a reference system. It consists of state-of-the-art technology: a PEM water electrolyzer, a hydrogen compressor, a high-pressure storage cylinder and a PEM fuel cell
- System 2 uses a reversible hydrogen battery to store the hydrogen produced from a PEM water electrolyzer as formate-DBU. It is able to release the stored hydrogen on demand, which could afterwards be utilized in PEM fuel cell

- System 3 uses flow reactors to convert hydrogen to formic acid and vice versa. Formic acid is stored as a liquid.
- System 4 replaces the water electrolyzer with a CO_2-electrolyzer for a direct electrochemical formic acid production. Formic acid is stored as a liquid and on demand reconverted to hydrogen in a flow reactor.

All defined systems show sufficient interfaces for the integration into existing energy systems. The electrical integration into the low-voltage grid was investigated, which could be realized either by a direct connection of the electrolyzer and the fuel cells with AC/DC connections or by using a DC bus. For using the produced heat of the fuel cell or the electrolyzer, the system must be connected either directly to a thermal load or to a district heating network. A thermal integration of the flow reactors was also discussed. Both the electrical and thermal integration are considered as non-critical for a application of these systems. In order to provide the CO_2 demand of System 3 and System 4, a low-temperature direct air capture (DAC) system was identified as most promising for the near future. One of the most outstanding advantages of using formic acid as an energy carrier is its liquid characteristic under ambient conditions. Taking the common transport capacities of different methods into account, it was calculated that the transportable volume via road is 20,500 l, 55,500 l per rail tank car or 2,500,000 l per riverboat. This allows the balancing of local inequalities of energy production and demand with existing infrastructure.
Further, a control algorithm for the operation of a grid connected electrolyzer (for both the PEM water electrolyzer and the CO_2-electrolyzer) with fluctuating electrical loads and a buffer battery was developed. The electrolyzer power is determined based on the current surplus power of the connected energy systems and the battery loading state with the aim to minimize the stand-by times of the electrolyzer. For the fuel cell two different operation modes are proposed: a power controlled mode and a heat controlled mode. The operation of the reversible hydrogen battery requires a profound control strategy. Four different states are defined for this system: hydrogenation, dehydrogenation, hydrogen release and idle/ filling. Depending on the current conditions the developed control algorithm determines the mode by switching the state of a heater and a purge valve.
Rules for the dimensioning of the major system components were defined. As it turned out, the dimensioning rules are for many cases insufficient. This is attributed to the high level of system complexity. However, these rule of thumb could be used for a rough approximation or as a starting point for more detailed analysis. A more sophisticated approach is the automated system dimensioning based on genetic algorithms and the evaluation of simulation results. For this approach it is elementary, to define a target function, e.g. based on economic considerations. For all cases it could be said, that the exact system design must be done carefully based on the local conditions.

8.1.3 System Operation

The third main aspect of this work was the evaluation of the system performance of all four proposed systems in a use-case. The plus-energy settlement "Vordere Viehweide" in Wüstenrot, Germany was chosen as a test facility. The regarded building cluster consists of ten buildings with rooftop mounted PV systems and heat pumps. Load profiles for the surplus and deficit power of the cluster in course of one year were determined. For this use-case all four proposed systems were applied as an electrical energy storage systems with the aim to store seasonal surpluses, which could be reconverted to electrical energy on demand to supplement the power supply of the heat pumps. Hence, all systems were operated in a power controlled mode.
The simulation results show that the power coverage of the systems vary between 47 % for System 1 and System 2, 46 % for System 3 and 12 % for System 4. Using the simulation results and additional considerations, the proposed systems were compared using five parameters from efficiency to system complexity. It turned out that System 2 and System 3 are not competitive in this context. System 1 stands out due to its high TRL and could be implemented without the need of further research. System 4 is a promising option as it combines low system complexity and a low areal footprint with the advantage of avoiding gaseous hydrogen in the production path. This means a gain in safety and therefor acceptance of the system. Under the assumed conditions, however, System 4 shows the by far lowest efficiency of the investigated systems. To increase the performance, several optimization steps were applied to System 4. First, the number of electrolysis cells was varied, following by an adjustment of the power and capacity of the buffer battery and finally the tank volume was adjusted to the needed capacity. With the optimized system design, the electrolysis power could be reduced from 78 kW to 40 kW without impairing the annual power coverage. Furthermore, two additional measures were evaluated to improve the performance of System 4: the addition of five small wind turbines to increase the power input, especially in the winter and transition periods, did not show the targeted improvement, as the median wind speeds at the hub height of the turbines (15 m) at the investigated lactation is as low as $2.88\,\mathrm{m\,s^{-1}}$ which results in an energy yield of 2,335 kWh per wind turbine. Overall, the amount of produced formic acid rises by 14 % through this measure. The utilization of the waste heat of the fuel cell is also not suitable for this use-case as the produced heat of 3,566 kWh is lower that the heat demand of the smallest building in the cluster (4,505 kWh). Also, a feeding into a heating network is not appropriate due to the low operation temperature of the fuel cell.
Furthermore, economic aspects of the CO_2-electrolyzer of System 4 were investigated. An energy demand of $9.23\,\mathrm{kW\,h\,kg^{-1}}$ for the formic acid production was calculated from the simulation results of the optimized system. This results in specific production costs of 1.04

€ per kilogram formic acid. With regard to the hydrogen content of formic acid (4.4 wt.-%) and the energy content of hydrogen (33 kWh per kg) this results in production costs of 23.55 € per kg hydrogen or 0.71 € per kWh respectively. It follows that no positive business case is possible for the CO_2-electrolyzer in case of an energy storage system. This assessment changes if the business case is transferred to the production of formic acid as a chemical raw product. With an assumed market price of 20 € per kg pure formic acid, a specific investment of 8,367 € per kW installed electrolysis power for the optimized system is possible in order to generate a positive cash flow.

8.2 Summarized Answers to the Research Objectives

This section summarizes the answers to the research objectives for this thesis presented in Section 1.3.

Objective 1 A modelling approach with dynamic models for all main components of the introduced systems was presented. The models show a good accuracy, if compared to reported data or measurement data (e.g. MAPE for the voltage-current characteristic of the CO_2 electrolyzer is below 2 %). However, some simplifications were made as e.g. thermal characteristics were neglected. Some simplifications were necessary due to the lack of available measurement data. Carrying out experiments with the components allows further improvements of the models. The application of C++ for the component models and INSEL for graphically design of system models has proven to be useful. This approach allows the extension of the systems with additional energy sources, loads and energy conversion devices. The overall computation time, even for complex systems and a simulation period of one year is within a usable range[1]. This is especially important for automated system dimensioning as several simulation runs must be executed consecutively.

Objective 2 Three different system with formic acid based hydrogen storage were presented. All system could be integrated into existing energy systems and applied as a seasonal energy storage system. The waste heat of the system could be utilized by connecting the systems to a heat grid or a single heat load. For handling fluctuating loads of renewable energy sources, a buffer battery was applied to the PEM water electrolyzer and the CO_2 electrolyzer. A control algorithm to distribute surplus power between the battery, the electrolyzer and the power grid was presented. Furthermore, a controller for the reversible hydrogen battery and the FA-to-H2 reactor was developed. Formic acid based hydrogen storage system can be dimensioned based on rules. However, these rules turned out to be

[1] Approximately 25s per run; System setup: i5-1145G7, 16 GB RAM, Win 10

inaccurate and more be seen as a rough approximation or a starting point for a more detailed analysis. Automated system dimensioning as already presented for the reference system (see Weiler et al. [164]) promises to be a good alternative for the system dimensioning. However, its accuracy depends on the parameters for the target function (e.g. system costs).

Objective 3 The developed system models were applied to a use-case of a building cluster. Based on the assumptions and simplifications made, all systems could be used as a seasonal energy storage system. However, the utilization of the systems do not lead to full autarky of the building cluster. The CO_2 electrolyzer system (System 4) shows the least coverage of the deficit power demand, as high overpotentials lead to a low efficiency. A system comparison based on several parameters however, leads to the assessment, that System 4 is the most promising system for this kind of use-case.

8.3 Recommendations

In this section recommendations for future research in the main aspects of this work are given.

8.3.1 Modelling and experimental validation

As the at some point insufficient data basis was a major hurdle for the development of the component models, the next steps for the improvement of the models should include laboratory setups for all components to gain profound validation data. In case of the CO_2-electrolyzer this planned with an already funded research project[2]. This project includes long-term experiments with the electrolyzer and the improvement of the model with monitoring data, e.g. concerning pH values of the product solution, electrical overpotential, heat production and product composition (formic acid and side products). Still all models should be extended with detailed thermal calculations. This allows to evaluate the heating or cooling demand or production of the systems and is needed for a more detailed consideration of the thermal integration. Whenever liquid substances and products occur, it should be provided that also a hydraulic considerations are included in these models. These calculations should include the energy demand of pumps based on the pressure losses of the pipes and tubes. This will allow a more profound estimation of the system efficiency.
The development of new models should also be considered to supplement the possible system combinations and improve the depth of detail. Possible new models should include direct air capture (DAC) systems for the carbon dioxide providing, gas processing units, gas boilers for

[2] https://www.hft-stuttgart.com/research/projects/current/p2fa4city-project

hydrogen rich gases from formic acid decomposition and high-temperature solid-oxide fuel cells (SOFC).

8.3.2 System Design, Control and Dimensioning

Concerning the system design it is recommended to investigate thermal symbiosis of all systems. This should be done, after all models include detailed thermal calculations. One possible option could be the thermal coupling of a DAC system with an electrolyzer or flow reactor. The combustion of the decomposition products of formic acid should also be considered. This could address applications with high heat demands and simultaneously bypass the carbon monoxide intolerance of PEM fuel cells. Another promising option, specifically for System 4 is the utilization of the side-products carbon monoxide and hydrogen as syngas. This allows further system integration options, e.g. the combination with FT-reactors.
As it turns out in the course of this work, the control of complex systems is challenging. In order to improve the efficiency of the proposed systems regarding electrical energy as well as substance usage, more advanced control methods, e.g. PID controllers or fuzzy logic, should be developed and applied to the systems.
With regard to the dimensioning of the system, it is recommended to improve the automated system dimensioning based on simulations. Due to the high system complexity, rules of thumb often show insufficient accuracy. For the automated dimensioning with genetic algorithms, detailed target functions e.g. with the aim to reduce system costs or carbon dioxide emissions should be defined and applied.

8.3.3 System Operation

If all the above mentioned recommendations for the model and system improvements are addressed, all systems should be tested in many, preferably different, case studies. These case studies should include high-dense urban areas as well as more rural areas. Furthermore all systems should be investigated in heat controlled and power controlled modes for all case studies.

In the long-term it should be considered to develop all components and systems towards the possibility to utilize other energy carriers than formic acid, such as methanol. This will allow to not only evaluate the best system composition but also the most suitable energy carrier for the given application.

Bibliography

[1] Umweltbundesamt, "Renewable energies in figures."

[2] Die Bundesregierung, "Erneuerbare Energien - Ein neues Zeitalter," 2021.

[3] M. Sterner and I. Stadler, *Energiespeicher*. Berlin Heidelberg: Springer Vieweg, 2014.

[4] U. Albrecht, U. Bünger, J. Michalski, T. Raksha, R. Wurster, and J. Zerhusen, "International Hydrogen Strategies - A study commissioned by and in cooperation with the World Energy Council Germany," Tech. Rep. September, 2020.

[5] D. Bothe and M. Janssen, "Die Rolle von Wasserstoff im Wärmemarkt," Tech. Rep. April, 2021.

[6] R. Williams, R. S. Crandall, and A. Bloom, "Use of carbon dioxide in energy storage," *Applied Physics Letters*, vol. 33, no. 5, pp. 381–383, 1978.

[7] S. Enthaler, J. von Langermann, and T. Schmidt, "Carbon dioxide and formic acid—the couple for environmental-friendly hydrogen storage?," *Energy & Environmental Science*, vol. 3, no. 9, p. 1207, 2010.

[8] J. Eppinger and K.-W. Huang, "Formic Acid as a Hydrogen Energy Carrier," *ACS Energy Letters*, vol. 2, no. 1, pp. 188–195, 2017.

[9] K. Müller, K. Brooks, and T. Autrey, "Hydrogen Storage in Formic Acid: A Comparison of Process Options," *energyfuels*, vol. 31, pp. 12603–12611, 2017.

[10] B. Zaidman, H. Wiener, and Y. Sasson, "Formate salts as chemical carriers in hydrogen storage and transportation," *International Journal of Hydrogen Energy*, vol. 11, no. 5, pp. 341–347, 1986.

[11] D. Lust, P. Rößner, M. Brennenstuhl, E. Klemm, B. Plietker, and U. Eicker, "Decentralized city district hydrogen storage system based on the electrochemical reduction of carbon dioxide to formate," vol. 4, no. IRES, pp. 137–144, 2019.

[12] F. Bienen, D. Kopljar, A. Löwe, P. Aßmann, M. Stoll, P. Rößner, N. Wagner, A. Friedrich, and E. Klemm, "Utilizing Formate as an Energy Carrier by Coupling CO2 Electrolysis with Fuel Cell Devices," *Chemie-Ingenieur-Technik*, vol. 91, no. 6, pp. 872–882, 2019.

[13] Y. Y. Gao, C. H. Tan, Y. P. Li, J. Guo, and S. Y. Zhang, "Formic acid-Formate blended solution: A new fuel system with high oxidation activity," *International Journal of Hydrogen Energy*, vol. 37, no. 4, pp. 3433–3437, 2012.

[14] A. F. Dalebrook, W. Gan, M. Grasemann, S. Moret, and G. Laurenczy, "Hydrogen storage: beyond conventional methods.," *Chemical communications (Cambridge, England)*, vol. 49, pp. 8735–8751, 2013.

[15] J. Andersson and S. Grönkvist, "Large-scale storage of hydrogen," *International Journal of Hydrogen Energy*, vol. 44, no. 23, pp. 11901–11919, 2019.

[16] Z. Zhang, S. Liu, M. Hou, G. Yang, and B. Han, "Continuous-flow formic acid production from the hydrogenation of CO2without any base," *Green Chemistry*, vol. 23, no. 5, pp. 1978–1982, 2021.

[17] A. Weilhard, S. P. Argent, and V. Sans, "Efficient carbon dioxide hydrogenation to formic acid with buffering ionic liquids," *Nature Communications*, vol. 12, no. 1, pp. 1–7, 2021.

[18] H. Reymond, J. J. Corral-Pérez, A. Urakawa, and P. Rudolf Von Rohr, "Towards a continuous formic acid synthesis: A two-step carbon dioxide hydrogenation in flow," *Reaction Chemistry and Engineering*, vol. 3, no. 6, pp. 912–919, 2018.

[19] Q. Sun, B. W. J. Chen, N. Wang, Q. He, A. Chang, C. Yang, H. Asakura, T. Tanaka, M. J. Hülsey, C. Wang, J. Yu, and N. Yan, " Zeolite-Encaged Pd–Mn Nanocatalysts for CO 2 Hydrogenation and Formic Acid Dehydrogenation ," *Angewandte Chemie*, vol. 132, no. 45, pp. 20358–20366, 2020.

[20] J. Klankermayer, S. Wesselbaum, K. Beydoun, and W. Leitner, "Selective Catalytic Synthesis Using the Combination of Carbon Dioxide and Hydrogen: Catalytic Chess at the Interface of Energy and Chemistry," *Angewandte Chemie - International Edition*, vol. 55, no. 26, pp. 7296–7343, 2016.

[21] A. Álvarez, A. Bansode, A. Urakawa, A. V. Bavykina, T. A. Wezendonk, M. Makkee, J. Gascon, and F. Kapteijn, "Challenges in the Greener Production of Formates/-Formic Acid, Methanol, and DME by Heterogeneously Catalyzed CO2 Hydrogenation Processes," *Chemical Reviews*, vol. 117, no. 14, pp. 9804–9838, 2017.

[22] D. Kopljar, A. Inan, P. Vindayer, R. Scholz, N. Frangos, N. Wagner, and E. Klemm, "Entwicklung und Einsatz von Gasdiffusionselektroden zur elektrochemischen Reduktion von CO2," *Chemie-Ingenieur-Technik*, vol. 87, no. 6, pp. 855–859, 2015.

[23] D. Kopljar, N. Wagner, and E. Klemm, "Transferring Electrochemical CO2Reduction from Semi-Batch into Continuous Operation Mode Using Gas Diffusion Electrodes," *Chemical Engineering and Technology*, vol. 39, no. 11, pp. 2042–2050, 2016.

[24] A. Löwe, C. Rieg, T. Hierlemann, N. Salas, D. Kopljar, N. Wagner, and E. Klemm, "Influence of Temperature on the Performance of Gas Diffusion Electrodes in the CO2 Reduction Reaction," *ChemElectroChem*, vol. 6, no. 17, pp. 4497–4506, 2019.

[25] A. Löwe, M. Schmidt, F. Bienen, D. Kopljar, N. Wagner, and E. Klemm, "Optimizing reaction conditions and gas diffusion electrodes applied in the co2 reduction reaction to formate to reach current densities up to 1.8 a cm–2," *ACS Sustainable Chemistry & Engineering*, vol. 9, no. 11, pp. 4213–4223, 2021.

[26] H. Yang, J. J. Kaczur, S. D. Sajjad, and R. I. Masel, "Electrochemical conversion of CO2 to formic acid utilizing Sustainion™ membranes," *Journal of CO2 Utilization*, vol. 20, no. April, pp. 208–217, 2017.

[27] H. Yang, J. J. Kaczur, S. D. Sajjad, and R. I. Masel, "Performance and long-term stability of CO2conversion to formic acid using a three-compartment electrolyzer design," *Journal of CO2 Utilization*, vol. 42, no. August, p. 101349, 2020.

[28] M. Osskopp, A. Loewe, C. M. S. Lobo, S. Baranyai, T. Khoza, M. Auinger, and E. Klemm, "Producing formic acid at low pH values by electrochemical CO 2 reduction," no. September, 2021.

[29] N. W. Kinzel, C. Werlé, and W. Leitner, "Transition Metal Complexes as Catalysts for the Electroconversion of CO2: An Organometallic Perspective," *Angewandte Chemie - International Edition*, vol. 60, no. 21, pp. 11628–11686, 2021.

[30] X. Lu, D. Y. C. Leung, H. Wang, M. K. H. Leung, and J. Xuan, "Electrochemical Reduction of Carbon Dioxide to Formic Acid," *ChemElectroChem*, vol. 1, no. 5, pp. 836–849, 2014.

[31] M. Caiti, D. Padovan, and C. Hammond, "Continuous Production of Hydrogen from Formic Acid Decomposition over Heterogeneous Nanoparticle Catalysts: From Batch to Continuous Flow," *ACS Catalysis*, vol. 9, no. 10, pp. 9188–9198, 2019.

[32] D. A. Bulushev, S. Beloshapkin, and J. R. Ross, "Hydrogen from formic acid decomposition over Pd and Au catalysts," *Catalysis Today*, vol. 154, no. 1-2, pp. 7–12, 2010.

[33] M. Mihet, M. Dan, L. Barbu-Tudoran, M. D. Lazar, and G. Blanita, "Controllable H2 Generation by Formic Acid Decomposition on a Novel Pd/Templated Carbon Catalyst," *Hydrogen*, vol. 1, no. 1, pp. 22–37, 2020.

[34] C. Hu, S. W. Ting, J. Tsui, and K. Y. Chan, "Formic acid dehydrogenation over PtRuBiOx/C catalyst for generation of CO-free hydrogen in a continuous-flow reactor," *International Journal of Hydrogen Energy*, vol. 37, no. 8, pp. 6372–6380, 2012.

[35] I. Yuranov, N. Autissier, K. Sordakis, A. F. Dalebrook, M. Grasemann, V. Orava, P. Cendula, L. Gubler, and G. Laurenczy, "Heterogeneous Catalytic Reactor for Hydrogen Production from Formic Acid and Its Use in Polymer Electrolyte Fuel Cells," *ACS Sustainable Chemistry and Engineering*, vol. 6, no. 5, pp. 6635–6643, 2018.

[36] C. Guan, Y. Pan, T. Zhang, M. J. Ajitha, and K. W. Huang, "An Update on Formic Acid Dehydrogenation by Homogeneous Catalysis," *Chemistry - An Asian Journal*, vol. 15, no. 7, pp. 937–946, 2020.

[37] M. Carmo, D. L. Fritz, J. Mergel, and D. Stolten, "A comprehensive review on PEM water electrolysis," *International Journal of Hydrogen Energy*, vol. 38, no. 12, pp. 4901–4934, 2013.

[38] H. Görgün, "Dynamic modelling of a proton exchange membrane (PEM) electrolyzer," *International Journal of Hydrogen Energy*, vol. 31, no. 1, pp. 29–38, 2006.

[39] R. García-Valverde, N. Espinosa, and A. Urbina, "Simple PEM water electrolyser model and experimental validation," *International Journal of Hydrogen Energy*, vol. 37, no. 2, pp. 1927–1938, 2012.

[40] T. Yigit and O. F. Selamet, "Mathematical modeling and dynamic Simulink simulation of high-pressure PEM electrolyzer system," *International Journal of Hydrogen Energy*, vol. 41, no. 32, pp. 13901–13914, 2016.

[41] C. Spiegel, *PEM Fuel Cell Modeling and Simulation using MATLAB*. Elsevier, 2008.

[42] G. Emig and E. Klemm, *Chemische Reaktionstechnik*. Springer Vieweg, 6. ed., 2017.

[43] V. Orava, O. Souček, and P. Cendula, "Multi-phase modeling of non-isothermal reactive flow in fluidized bed reactors," *Journal of Computational and Applied Mathematics*, vol. 289, pp. 282–295, 2015.

[44] J. Schumacher, "Digitale Simulation regenerativer elektrischer Energieversorgungssysteme," *Dissertation, Universität Oldenburg*, 1991.

[45] D. Pietruschka, U. Pietzsch, and D. Monien, *Vision 2020 Die Plusenergiegemeinde Wüstenrot*. Stuttgart: Fraunhofer IRB Verlag, 2017.

[46] M. Brennenstuhl, D. Lust, P. Boch, M. Yadack, and U. Eicker, "The potential of small wind turbine integration in residential buildings complementing pv and heat pump operation," in *Proceedings of the ISEC Conference Renewable Heating Cooling Integrated Urban Industrial Energy Systems, Graz, Austria*, pp. 331–339, 2018.

[47] M. Brennenstuhl, R. Zeh, R. Otto, R. Pesch, V. Stockinger, and D. Pietruschka, "Report on a plus-energy district with low-temperature dhc network, novel agrothermal heat source, and applied demand response," *Applied Sciences (Switzerland)*, vol. 9, no. 23, 2019.

[48] M. Brennenstuhl, D. Lust, D. Pietruschka, and D. Schneider, "Demand side management based power-to-heat and power-to-gas optimization strategies for pv and wind self-consumption in a residential building cluster," *Energies*, vol. 14, no. 20, 2021.

[49] R. W. Howarth and M. Z. Jacobson, "How green is blue hydrogen?," *Energy Science Engineering*, no. July, pp. 1–12, 2021.

[50] N. Sánchez-Bastardo, R. Schlögl, and H. Ruland, "Methane Pyrolysis for Zero-Emission Hydrogen Production: A Potential Bridge Technology from Fossil Fuels to a Renewable and Sustainable Hydrogen Economy," *Industrial Engineering Chemistry Research*, vol. 60, no. 32, pp. 11855–11881, 2021.

[51] Y. S. Najjar, "Hydrogen safety: The road toward green technology," *International Journal of Hydrogen Energy*, vol. 38, pp. 10716–10728, 2013.

[52] M. Binnewies, M. Finze, M. Jackel, P. Schmidt, H. Willner, and G. Rayner-Canham, *Allgemeine und Anorganische Chemie*. 2016.

[53] NASA, "Global Climate Change: Vital Signs of the Planet."

[54] NASA, "Hubble Finds Carbon Dioxide on an Extrasolar Planet," 2008.

[55] C. Breyer, M. Fasihi, C. Bajamundi, F. Creutzig, S. P. Oy, and C. Change, "Commentary: Direct Air Capture of CO 2 : A key technology for ambitious climate change mitigation," no. September, pp. 4–10, 2019.

[56] D. Y. C. Leung, G. Caramanna, and M. M. Maroto-Valer, "An overview of current status of carbon dioxide capture and storage technologies," *Renewable and Sustainable Energy Reviews*, vol. 39, pp. 426–443, 2014.

[57] R. M. Cuéllar-Franca and A. Azapagic, "Carbon capture, storage and utilisation technologies: A critical analysis and comparison of their life cycle environmental impacts," *Journal of CO2 Utilization*, vol. 9, pp. 82–102, mar 2015.

[58] A. Rieder, "CO2-Abscheidung aus Kraftwerksrauchgasen mit wässriger MEA-Lösung - Waschmitteldegradation und Aufbereitungsverfahren," 2016.

[59] X. Li, S. Wang, and C. Chen, "Experimental study of energy requirement of CO2desorption from rich solvent," *Energy Procedia*, vol. 37, pp. 1836–1843, 2013.

[60] J. Tollefson, "Innovative zero-emissions power plant begins battery of tests," *Nature*, vol. 557, pp. 622–623, may 2018.

[61] R. Service, "Goodbye smokestacks: Startup invents zero-emission fossil fuel power," *Science*, may 2017.

[62] J. Wilcox, "A new way to remove CO2 from the atmosphere," 2018.

[63] M. Fasihi, O. Efimova, and C. Breyer, "Techno-economic assessment of CO 2 direct air capture plants," *Journal of Cleaner Production*, 2019.

[64] D. W. Keith, G. Holmes, D. St. Angelo, and K. Heidel, "A Process for Capturing CO2 from the Atmosphere," 2018.

[65] Climeworks, "Our Technology — Climeworks – Capturing CO2 from Air."

[66] E. E. Benson, C. P. Kubiak, A. J. Sathrum, and J. M. Smieja, "Electrocatalytic and homogeneous approaches to conversion of CO2to liquid fuels," *Chemical Society Reviews*, vol. 38, no. 1, pp. 89–99, 2009.

[67] R. Guidelli, R. G. Compton, J. M. Feliu, E. Gileadi, J. Lipkowski, W. Schmickler, and S. Trasatti, "Defining the transfer coefficient in electrochemistry: An assessment (IUPAC Technical Report)," *Pure and Applied Chemistry*, vol. 86, no. 2, pp. 245–258, 2014.

[68] F. Marangio, M. Santarelli, and M. Calì, "Theoretical model and experimental analysis of a high pressure PEM water electrolyser for hydrogen production," *International Journal of Hydrogen Energy*, vol. 34, pp. 1143–1158, feb 2009.

[69] M. Lebbal and S. Lecœuche, "Identification and monitoring of a PEM electrolyser based on dynamical modelling," *International Journal of Hydrogen Energy*, vol. 34, pp. 5992–5999, jul 2009.

[70] J. Milewski, G. Guandalini, and S. Campanari, "Modeling an alkaline electrolysis cell through reduced-order and loss-estimate approaches," *Journal of Power Sources*, vol. 269, pp. 203–211, dec 2014.

[71] D. Guilbert and Gianpaolo Vitale, "Dynamic Emulation of a PEM Electrolyzer by Time Constant Based Exponential Model," *energies*, vol. 12, no. 750, 2019.

[72] J. Udagawa, P. Aguiar, and N. P. Brandon, "Hydrogen production through steam electrolysis : Model-based steady state performance of a cathode-supported intermediate temperature solid oxide electrolysis cell," vol. 166, pp. 127–136, 2007.

[73] M. Ni, "Modeling of a solid oxide electrolysis cell for carbon dioxide electrolysis," *Chemical Engineering Journal*, vol. 164, pp. 246–254, oct 2010.

[74] O. Schmidt, A. Gambhir, I. Staffell, A. Hawkes, J. Nelson, and S. Few, "Future cost and performance of water electrolysis: An expert elicitation study," *International Journal of Hydrogen Energy*, vol. 42, pp. 30470–30492, dec 2017.

[75] M. Götz, J. Lefebvre, F. Mörs, A. McDaniel Koch, F. Graf, S. Bajohr, R. Reimert, and T. Kolb, "Renewable Power-to-Gas: A technological and economic review," 2016.

[76] S. Shiva Kumar and V. Himabindu, "Hydrogen production by PEM water electrolysis – A review," *Materials Science for Energy Technologies*, vol. 2, pp. 442–454, dec 2019.

[77] V. Papadopoulos, J. Desmet, J. Knockaert, and C. Develder, "Improving the utilization factor of a PEM electrolyzer powered by a 15 MW PV park by combining wind power and battery storage - Feasibility study," 2018.

[78] H2 Agentur, "PEM Electrolysis Stacks."

[79] C. Wulf, J. Linßen, and P. Zapp, "Review of Power-to-Gas Projects in Europe," *Energy Procedia*, vol. 155, pp. 367–378, nov 2018.

[80] T. Smolinka, N. Wiebe, P. Sterchele, and A. Palzer, "Study IndWEDe – Brief Overview," 2018.

[81] Y. Zheng, J. Wang, B. Yu, W. Zhang, J. Chen, J. Qiao, and J. Zhang, "A review of high temperature co-electrolysis of H 2 O and CO 2 to produce sustainable fuels using solid oxide electrolysis cells (SOECs): advanced materials and technology," *Chemical Society Reviews*, vol. 46, no. 5, pp. 1427–1463, 2017.

[82] C. Graves, S. D. Ebbesen, and M. Mogensen, "Co-electrolysis of CO2 and H2O in solid oxide cells: Performance and durability," *Solid State Ionics*, vol. 192, no. 1, pp. 398–403, 2011.

[83] L. Wang, M. Rao, S. Diethelm, T. E. Lin, H. Zhang, A. Hagen, F. Maréchal, and J. Van herle, "Power-to-methane via co-electrolysis of H 2 O and CO 2 : The effects of pressurized operation and internal methanation," *Applied Energy*, 2019.

[84] M. Reytier, S. Di Iorio, A. Chatroux, M. Petitjean, J. Cren, M. De Saint Jean, J. Aicart, and J. Mougin, "Stack performances in high temperature steam electrolysis and co-electrolysis," in *International Journal of Hydrogen Energy*, 2015.

[85] F. Alenazey, Y. Alyousef, O. Almisned, G. Almutairi, M. Ghouse, D. Montinaro, and F. Ghigliazza, "Production of synthesis gas (H2 and CO) by high-temperature Co-electrolysis of H2O and CO2," *International Journal of Hydrogen Energy*, 2015.

[86] Sunfire GmbH, "BREAKTHROUGH FOR POWER-TO-X: SUNFIRE PUTS FIRST Co-ELECTROLYSIS INTO OPERATION AND STARTS SCALING," pp. 20–22, 2019.

[87] Karlsruhe Institute of Technology, "Carbon-neutral Fuels from Air and Green Power," 2019.

[88] T. Haas, R. Krause, R. Weber, M. Demler, and G. Schmid, "Technical photosynthesis involving CO2 electrolysis and fermentation," *Nature Catalysis*, vol. 1, no. 1, pp. 32–39, 2018.

[89] J. Xu and G. F. Froment, "Methane steam reforming: II. Diffusional limitations and reactor simulation," *AIChE Journal*, vol. 35, no. 1, pp. 97–103, 1989.

[90] J. G. Xu and G. F. Froment, "Methane Steam Reforming, Methanation and Water-Gas Shift .1. Intrinsic Kinetics," *Aiche Journal*, vol. 35, no. 1, pp. 88–96, 1989.

[91] S. Rönsch, J. Schneider, S. Matthischke, M. Schlüter, M. Götz, J. Lefebvre, P. Prabhakaran, and S. Bajohr, "Review on methanation – From fundamentals to current projects," *Fuel*, vol. 166, pp. 276–296, 2016.

[92] M. Thema, F. Bauer, and M. Sterner, "Power-to-Gas: Electrolysis and methanation status review," *Renewable and Sustainable Energy Reviews*, vol. 112, no. June, pp. 775–787, 2019.

[93] M. Grünewald, "MAN Power to Gas for Augsburg – a Showcase," pp. 1–13, 2018.

[94] ExxonMobil, "Synthetic Fuel Process,"

[95] M. Huš, V. D. Dasireddy, N. Strah Štefančič, and B. Likozar, "Mechanism, kinetics and thermodynamics of carbon dioxide hydrogenation to methanol on Cu/ZnAl2O4 spinel-type heterogeneous catalysts," *Applied Catalysis B: Environmental*, 2017.

[96] S. Arab, J.-M. Commenge, J.-F. Portha, and L. Falk, "Methanol synthesis from CO2 and H2 in multi-tubular fixed-bed reactor and multi-tubular reactor filled with monoliths," *Chemical Engineering Research and Design*, vol. 92, pp. 2598–2608, nov 2014.

[97] B. S. Adji, Y. Muharam, and S. Kartohardjono, "Simulation of methanol synthesis in packed bed reactor for utilization of CO 2 from acid gas removal unit," *E3S Web of Conferences*, vol. 67, pp. 1–5, 2018.

[98] J. Toyir, R. Miloua, N. E. Elkadri, M. Nawdali, H. Toufik, F. Miloua, and M. Saito, "Sustainable process for the production of methanol from CO2 and H2 using Cu/ZnO-based multicomponent catalyst," *Physics Procedia*, vol. 2, no. 3, pp. 1075–1079, 2009.

[99] J. Albo, M. Alvarez-Guerra, P. Castaño, and A. Irabien, "Towards the electrochemical conversion of carbon dioxide into methanol," *Green Chemistry*, vol. 17, no. 4, pp. 2304–2324, 2015.

[100] P. Kaiser, R. B. Unde, C. Kern, and A. Jess, "Production of liquid hydrocarbons with CO2 as carbon source based on reverse water-gas shift and fischer-tropsch synthesis," *Chemie-Ingenieur-Technik*, vol. 85, no. 4, pp. 489–499, 2013.

[101] S. S. Ail and S. Dasappa, "Biomass to liquid transportation fuel via Fischer Tropsch synthesis – Technology review and current scenario," *Renewable and Sustainable Energy Reviews*, vol. 58, pp. 267–286, may 2016.

[102] J. Dodaro and Stanford University, "Fischer-Tropsch Process," 2015.

[103] R. Guettel, U. Kunz, and T. Turek, "Reactors for Fischer-Tropsch Synthesis," *Chemical Engineering & Technology*, vol. 31, pp. 746–754, may 2008.

[104] W. Becker, R. Braun, M. Penev, and M. Melaina, "Production of Fischer–Tropsch liquid fuels from high temperature solid oxide co-electrolysis units," *Energy*, vol. 47, pp. 99–115, nov 2012.

[105] Y. Song, R. Peng, D. K. Hensley, P. V. Bonnesen, L. Liang, Z. Wu, H. M. Meyer, M. Chi, C. Ma, B. G. Sumpter, and A. J. Rondinone, "High-Selectivity Electrochemical Conversion of CO 2 to Ethanol using a Copper Nanoparticle/N-Doped Graphene Electrode," *ChemistrySelect*, vol. 1, no. 19, pp. 6055–6061, 2016.

[106] E. Catizzone, G. Bonura, M. Migliori, F. Frusteri, and G. Giordano, "CO2 recycling to dimethyl ether: State-of-the-art and perspectives," *Molecules*, vol. 23, no. 1, pp. 1–28, 2018.

[107] H. Dagdougui, R. Sacile, C. Bersani, A. Ouammi, H. Dagdougui, R. Sacile, C. Bersani, and A. Ouammi, "Hydrogen Storage and Distribution: Implementation Scenarios," *Hydrogen Infrastructure for Energy Applications*, pp. 37–52, jan 2018.

[108] J. Zheng, X. Zhang, P. Xu, C. Gu, B. Wu, and Y. Hou, "Standardized equation for hydrogen gas compressibility factor for fuel consumption applications," *International Journal of Hydrogen Energy*, 2016.

[109] Hydrogen Europe, "Refueling stations — Hydrogen."

[110] J. Zheng, X. Liu, P. Xu, P. Liu, Y. Zhao, and J. Yang, "Development of high pressure gaseous hydrogen storage technologies," *International Journal of Hydrogen Energy*, vol. 37, pp. 1048–1057, jan 2012.

[111] Linde, "Hydrogen technologies. The Ionic Compressor 90 MPa - IC90," vol. 90, p. 2, 2014.

[112] P. Bouwman, "Electrochemical Hydrogen Compression (EHC) solutions for hydrogen infrastructure," *Fuel Cells Bulletin*, 2014.

[113] M. Nordio, F. Rizzi, G. Manzolini, M. Mulder, L. Raymakers, M. Van Sint Annaland, and F. Gallucci, "Experimental and modelling study of an electrochemical hydrogen compressor," *Chemical Engineering Journal*, 2019.

[114] M. Aasadnia and M. Mehrpooya, "Large-scale liquid hydrogen production methods and approaches: A review," *Applied Energy*, vol. 212, no. September 2017, pp. 57–83, 2018.

[115] J. Bellosta von Colbe, J. R. Ares, J. Barale, M. Baricco, C. Buckley, G. Capurso, N. Gallandat, D. M. Grant, M. N. Guzik, I. Jacob, E. H. Jensen, T. Jensen, J. Jepsen, T. Klassen, M. V. Lototskyy, K. Manickam, A. Montone, J. Puszkiel, S. Sartori, D. A. Sheppard, A. Stuart, G. Walker, C. J. Webb, H. Yang, V. Yartys, A. Züttel, and M. Dornheim, "Application of hydrides in hydrogen storage and compression: Achievements, outlook and perspectives," *International Journal of Hydrogen Energy*, 2019.

[116] A. Fikrt, R. Brehmer, V. O. Milella, K. Müller, A. Bösmann, P. Preuster, N. Alt, E. Schlücker, P. Wasserscheid, and W. Arlt, "Dynamic power supply by hydrogen bound to a liquid organic hydrogen carrier," *Applied Energy*, vol. 194, pp. 1–8, 2017.

[117] D. Teichmann, W. Arlt, P. Wasserscheid, and R. Freymann, "A future energy supply based on Liquid Organic Hydrogen Carriers (LOHC)," *Energy and Environmental Science*, vol. 4, no. 8, pp. 2767–2773, 2011.

[118] P. Preuster, C. Papp, and P. Wasserscheid, "Liquid Organic Hydrogen Carriers (LOHCs): Toward a Hydrogen-free Hydrogen Economy," *Accounts of Chemical Research*, vol. 50, pp. 74–85, jan 2017.

[119] P. Wasserscheid, "Chemical Hydrogen Storage."

[120] P. Preuster, Q. Fang, R. Peters, R. Deja, V. N. Nguyen, L. Blum, D. Stolten, and P. Wasserscheid, "Solid oxide fuel cell operating on liquid organic hydrogen carrier-based hydrogen – making full use of heat integration potentials," *International Journal of Hydrogen Energy*, vol. 43, no. 3, pp. 1758–1768, 2018.

[121] VNG, "Gasinfrastruktur."

[122] M. W. Melaina, O. Antonia, and M. Penev, "Blending Hydrogen into Natural Gas Pipeline Networks : A Review of Key Issues Blending Hydrogen into Natural Gas Pipeline Networks : A Review of Key Issues," no. March, 2013.

[123] Wissenschaftliche Dienste des Bundestages, "Sachstand Grenzwerte für Wasserstoff (H 2) in der Erdgasinfrastruktur," 2019.

[124] Hydrogen Europe, "Hydrogen Europe Vision on the Role of Hydrogen and Gas Infrastructure on the Road Toward a Climate Neutral Economy - A Contribution to the Transition of the Gas Market," 2019.

[125] C. J. Quarton and S. Samsatli, "Power-to-gas for injection into the gas grid: What can we learn from real-life projects, economic assessments and systems modelling?," *Renewable and Sustainable Energy Reviews*, vol. 98, no. September, pp. 302–316, 2018.

[126] D. Pankratov, L. Ohlsson, P. Gudmundsson, S. Halak, L. Ljunggren, Z. Blum, and S. Shleev, "Ex vivo electric power generation in human blood using an enzymatic fuel cell in a vein replica," *RSC Advances*, vol. 6, no. 74, pp. 70215–70220, 2016.

[127] A. Dector, R. Escalona-Villalpando, D. Dector, V. Vallejo-Becerra, A. Chávez-Ramírez, L. Arriaga, and J. Ledesma-García, "Perspective use of direct human blood as an energy source in air-breathing hybrid microfluidic fuel cells," *Journal of Power Sources*, vol. 288, pp. 70–75, aug 2015.

[128] B. Ong, S. Kamarudin, and S. Basri, "Direct liquid fuel cells: A review," *International Journal of Hydrogen Energy*, vol. 42, no. 15, pp. 10142–10157, 2017.

[129] U. B. Demirci, "Direct liquid-feed fuel cells: Thermodynamic and environmental concerns," *Journal of Power Sources*, vol. 169, no. 2, pp. 239–246, 2007.

[130] D. S. Falcão, V. B. Oliveira, C. M. Rangel, and A. M. Pinto, "Review on micro-direct methanol fuel cells," *Renewable and Sustainable Energy Reviews*, vol. 34, pp. 58–70, 2014.

[131] X. Yu and P. G. Pickup, "Recent advances in direct formic acid fuel cells (DFAFC)," *Journal of Power Sources*, vol. 182, no. 1, pp. 124–132, 2008.

[132] C. Rice, S. Ha, R. Masel, and A. Wieckowski, "Catalysts for direct formic acid fuel cells," *Journal of Power Sources*, vol. 115, no. 2, pp. 229–235, 2003.

[133] C. Rice, S. Ha, R. Masel, P. Waszczuk, A. Wieckowski, and T. Barnard, "Direct formic acid fuel cells," *Journal of Power Sources*, vol. 111, no. 1, pp. 83–89, 2002.

[134] N. Aslam, M. Masdar, S. Kamarudin, and W. Daud, "Overview on Direct Formic Acid Fuel Cells (DFAFCs) as an Energy Sources," *APCBEE Procedia*, vol. 3, pp. 33–39, 2012.

[135] L. An and R. Chen, "Direct formate fuel cells: A review," *Journal of Power Sources*, vol. 320, pp. 127–139, 2016.

[136] A. M. Bartrom and J. L. Haan, "The direct formate fuel cell with an alkaline anion exchange membrane," *Journal of Power Sources*, vol. 214, pp. 68–74, 2012.

[137] L. Zeng, Z. K. Tang, and T. S. Zhao, "A high-performance alkaline exchange membrane direct formate fuel cell," *Applied Energy*, vol. 115, pp. 405–410, 2014.

[138] L. Q. Wang, M. Bellini, J. Filippi, M. Folliero, A. Lavacchi, M. Innocenti, A. Marchionni, H. A. Miller, and F. Vizza, "Energy efficiency of platinum-free alkaline direct formate fuel cells," *Applied Energy*, vol. 175, pp. 479–487, 2016.

[139] J. Chang, L. Feng, C. Liu, W. Xing, and X. Hu, "An Effective Pd – Ni 2 P / C Anode Catalyst for Direct Formic Acid Fuel Cells **," pp. 122–126, 2014.

[140] IEEE Spectrum, "This Power Plant Runs on CO2 ," may 2018.

[141] R. H. Moore, K. L. Thornhill, B. Weinzierl, D. Sauer, E. D'Ascoli, J. Kim, M. Lichtenstern, M. Scheibe, B. Beaton, A. J. Beyersdorf, J. Barrick, D. Bulzan, C. A. Corr, E. Crosbie, T. Jurkat, R. Martin, D. Riddick, M. Shook, G. Slover, C. Voigt, R. White,

E. Winstead, R. Yasky, L. D. Ziemba, A. Brown, H. Schlager, and B. E. Anderson, "Biofuel blending reduces particle emissions from aircraft engines at cruise conditions," *Nature*, vol. 543, p. 411, mar 2017.

[142] R. C. Neto, J. C. Teixeira, and J. L. Azevedo, "Thermal and electrical experimental characterisation of a 1 kW PEM fuel cell stack," *International Journal of Hydrogen Energy*, vol. 38, no. 13, pp. 5348–5356, 2013.

[143] S.-F. Hsu, S. Rommel, P. Eversfield, K. Muller, E. Klemm, W. R. Thiel, and B. Plietker, "Eine auf Ru-Katalyse basierende wiederaufladbare Wasserstoffbatterie," *Angewandte Chemie*, vol. 126, no. 27, pp. 7194–7198, 2014.

[144] A. Boddien, C. Federsel, P. Sponholz, D. Orthe Mellmann, R. Jackstell, H. Junge, G. Laurenczy, and M. Beller, "Towards the development of a hydrogen battery," *Energy & Environmental Science*, vol. 5, pp. 8907–8911, 2012.

[145] G. A. Filonenko, R. Van Putten, E. N. Schulpen, E. J. Hensen, and E. A. Pidko, "Highly efficient reversible hydrogenation of carbon dioxide to formates using a ruthenium PNP-pincer catalyst," *ChemCatChem*, vol. 6, no. 6, pp. 1526–1530, 2014.

[146] M. Czaun, A. Goeppert, R. May, R. Haiges, G. K. Prakash, and G. A. Olah, "Hydrogen generation from formic acid decomposition by ruthenium carbonyl complexes. Tetraruthenium dodecacarbonyl tetrahydride as an active intermediate," *ChemSusChem*, vol. 4, no. 9, pp. 1241–1248, 2011.

[147] T. Zell, R. Langer, T. Schaub, M. Trincado, H. Grützmacher, M. Prechtl, M. Vogt, A. Suárez, J. Campos, M. Feller, *et al.*, *Hydrogen Storage: Based on Hydrogenation and Dehydrogenation Reactions of Small Molecules*. De Gruyter, 2019.

[148] S. Lee, H. Ju, R. Machunda, S. Uhm, J. K. Lee, H. J. Lee, and J. Lee, "Sustainable production of formic acid by electrolytic reduction of gaseous carbon dioxide," no. 1, pp. 3029–3034, 2015.

[149] J. T. Feaster, C. Shi, E. R. Cave, T. Hatsukade, D. N. Abram, K. P. Kuhl, C. Hahn, J. K. Nørskov, and T. F. Jaramillo, "Understanding Selectivity for the Electrochemical Reduction of Carbon Dioxide to Formic Acid and Carbon Monoxide on Metal Electrodes," *ACS Catalysis*, vol. 7, no. 7, pp. 4822–4827, 2017.

[150] G. S. Luo, S. Pan, and J. G. Liu, "Use of the electrodialysis process to concentrate a formic acid solution," vol. 150, pp. 227–234, 2002.

[151] B. Mahida, H. Benyounes, and W. Shen, "Process analysis of pressure - swing distillation for the separation of formic acid – water mixture," *Chemical Papers*, vol. 75, no. 2, pp. 599–609, 2021.

[152] J. J. Kaczur, H. Yang, S. D. Sajjd, and R. I. Masel, "Modeling Methods for Concentrating a Formic Acid Product Generated from a Novel Electrochemical Reduction of CO 2 Cell Design," in *AIChE Annual Meeting*, no. October, (Minneapolis, MN), 2017.

[153] E. W. Lemmon, M. L. Huber, and J. W. Leachman, "Revised Standardized Equation for Hydrogen Gas Densities for Fuel Consumption Applications," *Journal of Research of the National Institute of Standards and Technology*, vol. 113, no. 6, pp. 341–350, 2008.

[154] O. Bartholomy, *A Technical, Economic, and Environmental Assessment of the Production of Renewable Hydrogen From Wind in California*. PhD thesis, 11 2008.

[155] M. Gardiner, "Energyrequirements for hydrogen gas compression and liquefaction as related to vehicle storage needs," tech. rep., Department of Energy, 2009.

[156] C. Spiegel, "How to Predict Fuel Cell Performance."

[157] D. Singh, R. Chaudhary, and A. Karthick, *Review on the progress of building-applied/integrated photovoltaic system*, vol. 28. Environmental Science and Pollution Research, 2021.

[158] B. Yodwong, D. Guilbert, M. Phattanasak, W. Kaewmanee, M. Hinaje, and G. Vitale, "AC-DC converters for electrolyzer applications: State of the art and future challenges," *Electronics (Switzerland)*, vol. 9, no. 6, 2020.

[159] J. Meißner, J. Pasel, R. C. Samsun, R. Peters, and D. Stolten, "Start-up and load-change behavior of a catalytic burner for a fuel-cell-based APU for diesel fuel," *Fuel Cells*, vol. 15, no. 1, pp. 15–26, 2015.

[160] W. R. Daud, R. E. Rosli, E. H. Majlan, S. A. Hamid, R. Mohamed, and T. Husaini, "PEM fuel cell system control: A review," *Renewable Energy*, vol. 113, pp. 620–638, 2017.

[161] W. J. Zou and Y. B. Kim, "Temperature Control for a 5 kW Water-Cooled PEM Fuel Cell System for a Household Application," *IEEE Access*, vol. 7, pp. 144826–144835, 2019.

[162] A. Christensen, "Assessment of Hydrogen Production Costs from Electrolysis: United States and Europe," tech. rep., The International Council of Clean Transportation, 2020.

[163] Q. Bai, C. Liu, J. Chen, Y. X. Fan, and H. T. Wang, "Manufacturing Cost Analysis of 100 and 250 kW Fuel Cell Systems for Primary Power and Combined Heat and Power Applications," *Applied Physics B: Lasers and Optics*, vol. 98, no. 4, pp. 681–684, 2010.

[164] V. Weiler, D. Lust, M. Brennenstuhl, K.-H. Brassel, E. Duminil, and U. Eicker, "Automatic dimensioning of energy system components for building cluster simulation," *Applied Energy*, vol. 313, p. 118651, may 2022.

[165] A. Varone and M. Ferrari, "Power to liquid and power to gas: An option for the German Energiewende," *Renewable and Sustainable Energy Reviews*, vol. 45, pp. 207–218, may 2015.

[166] Fraunhofer ISE, "Stromgestehungskosten Erneuerbare Energien," p. 44, 2018.

Appendix A

C++ Code of the developed component models

A.1 CO_2-Electrolyzer

```
/*----------------------------------------------------------------------
  #Begin
  #Block UBCO2TFAELECTROLYZER
  #Description

  #Layout
     #Inputs      4
     #Outputs     4
     #Parameters  6
     #Strings     0
     #Group       S
  #Details
     #Inputs
        #IN[0] Current [A]
        #IN[1] Time
        #IN[2] Amb. Temp. / Temp. Setpoint [ C ]
        #IN[3] Heating/ Cooling Power [W]
     #Outputs
        #OUT[0] Stack Voltage [V]
        #OUT[1] Cell Temp [ C ]
        #OUT[2] Formic Acid Outflow [kg/s]
        #OUT[3] CO2 Demand [kg/s]
     #Parameters
        #BP[0] Cell Area [cm2]
        #BP[1] Number of Cells
        #BP[2] Heat Capacity
        #BP[3] Heat Transfer Exponent
        #BP[4] Heat Transfer Factor
        #BP[5] Timestep
     #Strings
        #None
  #Internals
     #Integers
        #IP[0]  Return code
        #IP[1]  Call mode
                \begin{detaillist}
                   \item[-1] Identification call
                   \item[0]  Standard call
                   \item[1]  Constructor call
                   \item[2]  Destructor call
```

```
41                \end{detaillist}
42          #IP[2]   Operation mode
43          #IP[3]   User defined block number
44          #IP[4]   Number of current block inputs
45          #IP[5]   Jump parameter
46          #IP[6]   Debug level
47          #IP[7..9]   Reserved
48       #Reals
49          #None
50       #Doubles
51          #None
52    #Dependencies
53       #None
54    #Authors
55       INSEL Block Wizard
56    #End
57 ------------------------------------------------------------------------*/
58
59 // Attention: out must not be renamed to OUT (Windows.h conflict)
60
61 #include <vector>
62 #include <cmath>
63
64 using namespace std;
65
66 float interpolateCO2EL( vector<float> &xData, vector<float> &yData, double x, bool extrapolate )
67 {
68    int size = xData.size();
69
70    int i = 0;                                                          // find left end of interval
         for interpolation
71    if ( x >= xData[size - 2] )                                         // special case: beyond right
         end
72    {
73       i = size - 2;
74    }
75    else
76    {
77       while ( x > xData[i+1] ) i++;
78    }
79    double xL = xData[i], yL = yData[i], xR = xData[i+1], yR = yData[i+1];   // points on either side (
         unless beyond ends)
80    if ( !extrapolate )                                                 // if beyond ends of array and
          not extrapolating
81    {
82       if ( x < xL ) yR = yL;
83       if ( x > xR ) yL = yR;
84    }
85
86    double dydx = ( yR - yL ) / ( xR - xL );                            // gradient
87
88    return yL + dydx * ( x - xL );                                      // linear interpolation
89 }
90
91 extern "C" void id (float *in, float *out, int *IP, float *RP, double *DP,
92                     float *BP, char SP[][1024], char BNAMES[1024],
93                     int *OPM, int *INMIN, int *INS, int *OUTS,
94                     int *IPS, int *RPS, int *DPS,
95                     int *BPMIN, int *BPS, int *SPMIN,
96                     int *SPS, int *GROUP);
97
98 extern "C" void ub0105(float *in, float *out, int *IP, float *RP,
99    double *DP, float *BP, char SP[][1024])
100 {
101    char BNAMES[1024] = "UBCO2TFAELECTROLYZER";
102    int  OPM   = 1;
103    int  INMIN = 4;
104    int  INS   = 4;
105    int  OUTS  = 5;
106    int  IPS   = 10;
107    int  RPS   = 1;
```

```
108     int  DPS   = 0;
109     int  BPMIN = 17;
110     int  BPS   = 17;
111     int  SPMIN = 0;
112     int  SPS   = 0;
113     int  GROUP = 3;
114
115     if (IP[1] != 0)
116     {
117        if (IP[1] == -1)
118        {
119            // Identification call
120            id(in, out, IP, RP, DP, BP, SP, BNAMES,
121               &OPM, &INMIN, &INS, &OUTS, &IPS, &RPS, &DPS,
122               &BPMIN, &BPS, &SPMIN, &SPS, &GROUP);
123        }
124        else if(IP[1] == 1)
125        {
126           // Constructor call
127           IP[7] = 0;
128        }
129        else
130        {
131           // Destructor call
132        }
133        return;
134     }
135     // Standard call ---------------------------------------------------
136
137     // static const float Tvalues[] = {298.15,300,350,400,450,500,600,700,800,900,1000,1100};
138     // static const float SCO2values[] = {213.8,214,225.3,234.9,243.3,250.8,257.5,263.6,269.3,274.5};
139     // static const float HCO2values[] =
            {-393.52,-393.45,-389.52,-385.21,-380.61,-375.77,-370.71,-365.49,-360.12,-354.63};
140     // static const float SO2values[] =
            {205.3,209.9,213.87,214.45,220.63,226.451,231.47,235,92,239.93,243.58,246.92};
141     // static const float TH2Ovalues[] = {280,298.15,300,320,340,360,380};
142     // static const float SH2Ovalues[] = {65.22,69.95,70.42,75.28,79.85,84.16,88.27};
143     // static const float HH2Ovalues[] = {-286.41,-285.83,-285.77,-285.14,-284.5,-283.87,-283.24};
144
145     // vector<float> T (Tvalues,Tvalues + sizeof(Tvalues)/ sizeof(Tvalues[0]));
146     // vector<float> SCO2 (SCO2values,SCO2values + sizeof(SCO2values)/ sizeof(SCO2values[0]));
147     // vector<float> HCO2 (HCO2values,HCO2values + sizeof(HCO2values)/ sizeof(HCO2values[0]));
148     // vector<float> SO2 (SO2values,SO2values + sizeof(SO2values)/ sizeof(SO2values[0]));
149     // vector<float> TH2O (TH2Ovalues,TH2Ovalues + sizeof(TH2Ovalues)/ sizeof(TH2Ovalues[0]));
150     // vector<float> SH2O (SH2Ovalues,SH2Ovalues + sizeof(SH2Ovalues)/ sizeof(SH2Ovalues[0]));
151     // vector<float> HH2O (HH2Ovalues,HH2Ovalues + sizeof(HH2Ovalues)/ sizeof(HH2Ovalues[0]));
152
153     float S_FA = 131.84;
154     float H_FA = -425.09;
155
156     float M_FA= 46.03e-3;
157     float M_CO2 = 44.01e-3;
158
159     float Tamb = in[2] + 273.15;
160     float Tcell;
161     float z = 2;
162     float F = 96485;
163     float time = in[1];
164     float QHeat = in[3];
165     float time_old;
166     float I = in[0]; // Current
167     float A = BP[0]; // Cell Area
168     float N = BP[1]; // Number of cells
169     float C = BP[2]*N; // Heat Capacity
170     float k = BP[3]; // Heat Transfer Factor
171     float m = BP[4]; // Heat Transfer Exponent
172     int mode = BP[5]; // Thermodynamic Mode
173     float Rohm = BP[6]; // Ohmic Resitance
174     float alpha_cat = BP[7]; // Cathode Charge Transfer Factor
175     float alpha_an = BP[8]; // Anode Charge Transfer Factor
```

```
176     float i0_ref_cat = BP[9]; // Anode Reference Exchange Current Density
177     float i0_ref_an = BP[10]; // Anode Reference Exchange Current Density
178     float E_a_cat = BP[11]; // Cathode Activation Energy
179     float E_a_an = BP[12]; // Cathode Activation Energy
180     float eta_FA = BP[13];
181     float E0_cat = BP[14];
182     float E0_an = BP[15];
183     float pCO2 = BP[16]*1e6;
184     float pO2 = 1e5;
185
186     float V_cat;
187     float V_an;
188
189     float R = 8.31;
190
191     if (IP[7] == 0)
192     {
193        Tcell = Tamb;
194        time_old = time;
195        IP[7] = 1;
196     }
197     else
198     {
199        Tcell = RP[0];
200        time_old = RP[1];
201     }
202
203     float i = I / A;
204
205     // Open-cell Voltage
206
207     // float dS_Cat = S_FA - interpolateCO2EL(T,SCO2,Tcell,true);
208     // float dH_Cat = H_FA - interpolateCO2EL(T,HCO2,Tcell,true)*1e3;
209     // float dG_Cat = dH_Cat + Tcell*dS_Cat;
210     float E_OCV_Cat = -1*(E0_cat - (R*Tcell)/(z*F)*log(1/pCO2));
211     float E_OCV_An = E0_an - (R*Tcell)/(z*F)*log(pow(pO2,0.5));
212     //float E_th_Cat = dH_Cat/(z*F);
213
214     // float dS_An = 0.5*interpolateCO2EL(T,SO2,Tcell,true)-interpolateCO2EL(T,SH2O,Tcell,true);
215     // float dH_An = -1*interpolateCO2EL(T,HH2O,Tcell,true)*1e3;
216     // float dG_An = dH_An + Tcell*dS_An;
217     //float E_th_An = -dH_An/(z*F);
218
219
220     float Anode_Exchange_currentDensity = i0_ref_an * exp((-E_a_an/R)*((1/Tcell)-(1/293.0)));
221     float Cathode_Exchange_currentDensity = i0_ref_cat * exp((-E_a_cat/R)*((1/Tcell)-(1/353.15)));
222
223     float i_L = 9.965e-3*exp(0.015*Tcell);
224
225
226     // Cathode Potential
227
228     if (1-(i/i_L) > 0)
229     {
230        V_cat = E_OCV_Cat + (R*Tcell)/(alpha_cat*F)*asinhf(i/Cathode_Exchange_currentDensity/(1-(i/i_L))) + i*
              Rohm;
231        V_an = E_OCV_An + (R*Tcell)/(alpha_an*F)*asinhf(i/Anode_Exchange_currentDensity/(1-(i/i_L))) + i*Rohm;
232     }
233
234     else
235     {
236        V_cat = 10*N;
237     }
238
239     float V = V_cat + V_an;
240
241     // Thermal Model
242
243     float Qgen = ((E_OCV_Cat+E_OCV_An)-V)*I*N;
244     float Qloss = k*pow((Tcell-Tamb),(1-m));
```

```
245     float Q = Qgen + QHeat - Qloss;
246
247     if (BP[5] == 0) {
248         Tcell = Tamb;
249     }
250
251     else if (BP[5] == 1) {
252         Tcell = Tcell + (1/C)*Q*(time-time_old);
253     }
254
255     // Formic Acid Production
256     float eta_FA_calc = -719 + 5.228*Tcell -0.08906*i-0.008492*pow(Tcell,2)+0.0003979*Tcell*i - 4.622e-5*pow(i
            ,2);
257     float mdot_FA = I / (z*F) * eta_FA_calc/100 * M_FA;
258     float mdot_CO2 = I / (z*F) * M_CO2;
259
260
261     RP[0] = Tcell;
262     RP[1] = time;
263
264     out[0] = V*N;
265     out[1] = Tcell;
266     out[2] = mdot_FA*N;
267     out[3] = mdot_CO2*N;
268     out[4] = Qgen;
269
270 }
```

A.2 Reversible Hydrogen Battery

```
1  /*----------------------------------------------------------------
2    #Begin
3    #Block UBH2BATTERY
4    #Description
5
6    #Layout
7       #Inputs      5
8       #Outputs     5
9       #Parameters  7
10      #Strings     0
11      #Group       S
12   #Details
13      #Inputs
14         #IN[0] Time
15         #IN[1] Hydrogen Input [kg/s]
16         #IN[2] Heater State [0/1]
17         #IN[3] Ambient Temperature [degree C]
18         #IN[4] Purge Valve State [0/1]
19      #Outputs
20         #OUT[0] Gas Phase Pressure [MPa]
21         #OUT[1] FA concentration [mol/l]
22         #OUT[2] Hydrogen Production Rate [kg/s]
23         #OUT[3] Loading State
24         #OUT[4] Reactor Temperature [degree C]
25      #Parameters
26         #BP[0] Volume [l]
27         #BP[1] Reaction Temperature [degree C]
28         #BP[2] k1 (H2 to FA)
29         #BP[3] k2 (FA to H2)
30         #BP[4] Max. Pressure [MPa]
31         #BP[5] DBU concentration [mol/l]
32         #BP[6] Solvent Volume [l]
33      #Strings
34         #None
35   #Internals
36      #Integers
```

```
37          #IP[0]  Return code
38          #IP[1]  Call mode
39                  \begin{detaillist}
40                     \item[-1] Identification call
41                     \item[0]  Standard call
42                     \item[1]  Constructor call
43                     \item[2]  Destructor call
44                  \end{detaillist}
45          #IP[2]  Operation mode
46          #IP[3]  User defined block number
47          #IP[4]  Number of current block inputs
48          #IP[5]  Jump parameter
49          #IP[6]  Debug level
50          #IP[7..9]  Reserved
51       #Reals
52          #None
53       #Doubles
54          #None
55    #Dependencies
56       #None
57    #Authors
58       Daniel Lust (HFT Stuttgart)
59    #End
60 ----------------------------------------------------------------------*/
61
62 // Attention: out must not be renamed to OUT (Windows.h conflict)
63 #include <cmath>
64
65 extern "C" void id (float *in, float *out, int *IP, float *RP, double *DP,
66                     float *BP, char SP[][1024], char BNAMES[1024],
67                     int *OPM, int *INMIN, int *INS, int *OUTS,
68                     int *IPS, int *RPS, int *DPS,
69                     int *BPMIN, int *BPS, int *SPMIN,
70                     int *SPS, int *GROUP);
71
72 extern "C" void ub0102(float *in, float *out, int *IP, float *RP,
73    double *DP, float *BP, char SP[][1024])
74 {
75    char BNAMES[1024] = "UBH2BATTERY";
76    int  OPM   = 1;
77    int  INMIN = 6;
78    int  INS   = 6;
79    int  OUTS  = 6;
80    int  IPS   = 11;
81    int  RPS   = 6;
82    int  DPS   = 0;
83    int  BPMIN = 7;
84    int  BPS   = 7;
85    int  SPMIN = 0;
86    int  SPS   = 0;
87    int  GROUP = 3;
88
89    if (IP[1] != 0)
90    {
91       if (IP[1] == -1)
92       {
93          // Identification call
94          id(in, out, IP, RP, DP, BP, SP, BNAMES,
95             &OPM, &INMIN, &INS, &OUTS, &IPS, &RPS, &DPS,
96             &BPMIN, &BPS, &SPMIN, &SPS, &GROUP);
97       }
98       else if(IP[1] == 1)
99       {
100         // Constructor call
101         IP[10] = 0;
102      }
103      else
104      {
105         // Destructor call
106      }
```

```
107         return;
108     }
109     // Standard call ------------------------------------------------
110
111     int time_old;
112     float mH2_old;
113     float cH2_old;
114     float cFA_old;
115     float pH2_old;
116     float T_react = BP[1] + 273.15;
117     float R = 8.31;
118     float k1 = BP[2];
119     float k2 = BP[3];
120     float gasPhasePressure;
121     float pH2;
122     float cH2init;
123     float cH2;
124     float cFA;
125     float mH2;
126     int heating = in[2];
127     float cFA_init;
128     float rH2;
129     int mode;
130     int dt;
131     float mdotH2_in = in[1];
132     float dbu_concentration = BP[5];
133     float liquidPhase_volume = BP[6];
134     float loadingState;
135     float T_bat;
136     float T_amb = in[3] + 273.15;
137     int purgeValveState = in[4];
138     float hydrogenOutflowSetpoint = in[5];
139     float hydrogenOutflowRate = 0;
140     float Vgas = (BP[0] - liquidPhase_volume)/1000;
141     float h2in = 0;
142     float maxPressureH2 = 0.5*BP[4]*1e6; // MPa
143     float h2out = 0.0;
144
145     if (IP[10] == 0) {
146         time_old = 0;
147         mH2_old = 0;
148         cH2_old = 0.02;
149         cFA_old = 0;
150         pH2_old = 0;
151         cFA = 0;
152         dt = 0;
153         IP[10] = 1;
154     }
155
156     else {
157         time_old = RP[0];
158         mH2_old = RP[1];
159         cH2_old = RP[2];
160         cFA_old = RP[3];
161         pH2_old = RP[4];
162         dt = in[0] - time_old;
163     }
164
165     if (heating == 0) {
166         T_bat = T_amb;
167     }
168
169     else if (heating == 1) {
170         T_bat = T_react;
171     }
172
173     // Filling
174     if (mdotH2_in > 0 && heating == 0 && purgeValveState == 0) {
175         //mH2 = mH2_old + mdotH2_in*dt;
176         //h2in = mdotH2_in*dt;
```

```
177         cH2 = cH2_old + (mdotH2_in*dt*(1/2e-3))/(BP[0] - liquidPhase_volume);
178         //pH2 = (mH2*4124*T_amb)/Vgas;
179         pH2 = cH2 * 1000 * R * T_bat;
180         cH2init = pH2 / (R*T_amb) / 1000;
181         cH2 = cH2init;
182         rH2 = 0;
183         cFA = cFA_old;
184         RP[5] = cH2init;
185         RP[2] = cH2init;
186         mode = 0;
187         hydrogenOutflowRate = 0;
188      }
189
190      // Hydrogenation
191      else if (heating == 1 && purgeValveState == 0 && pH2_old > 0) {
192         cH2 = cH2_old - k1*pow(cH2_old,2)*dt + (mdotH2_in*dt*(1/2e-3))/(BP[0] - liquidPhase_volume);
193         h2in = (mdotH2_in*dt*(1/2e-3))/(BP[0] - liquidPhase_volume);
194         //cH2 = cH2_old - k1*pow(cH2_old,2)*dt;
195         pH2 = cH2 * 1000 * R * T_bat;
196         cFA = cFA_old + k1*pow(cH2_old,2)*dt;
197         cFA_init = cFA;
198         mH2 = mH2_old;
199         rH2 = 0;
200         mode = 1;
201         hydrogenOutflowRate = 0;
202      }
203
204      // Dehydrogeneation
205      else if (heating == 1 && purgeValveState == 1 && cFA_old > 0) {
206         if (cFA_old > 0)
207         {
208            cFA = cFA_old - cFA_old * k2 * dt;
209            cH2 = cH2_old + (cFA_old - cFA) - (hydrogenOutflowSetpoint*dt*(1/2e-3))/(BP[0] - liquidPhase_volume)
                     ;
210            rH2 = k2*cFA*liquidPhase_volume*2e-3;
211            pH2 = cH2 * 1000 * R * T_bat;
212            mode = 2;
213            hydrogenOutflowRate = hydrogenOutflowSetpoint;
214         }
215
216         else if (cFA_old == 0)
217         {
218            cFA = cFA_old;
219            rH2 = 0;
220            cH2 = cH2_old - (hydrogenOutflowSetpoint*dt*(1/2e-3))/(BP[0] - liquidPhase_volume);
221            pH2 = cH2 * 1000 * R * T_bat;
222            mode = 4;
223            hydrogenOutflowRate = hydrogenOutflowSetpoint;
224         }
225
226      }
227
228      // Hydrogen Release
229      else if (heating == 0 && purgeValveState == 1) {
230         cFA = cFA_old;
231         rH2 = 0;
232         cH2 = cH2_old - (hydrogenOutflowSetpoint*dt*(1/2e-3))/(BP[0] - liquidPhase_volume);
233         pH2 = cH2 * 1000 * R * T_bat;
234         mode = 4;
235         hydrogenOutflowRate = hydrogenOutflowSetpoint;
236      }
237
238
239      // Idle
240      else {
241         cH2 = cH2_old;
242         cFA = cFA_old;
243         mH2 = mH2_old;
244         rH2 = 0;
245         pH2 = pH2_old;
```

```
246         mode = 3;
247         hydrogenOutflowRate = 0;
248     }
249
250     loadingState = cFA / dbu_concentration;
251
252     if (heating == 0) {
253         T_bat = T_amb;
254     }
255
256     else if (heating == 1) {
257         T_bat = T_react;
258     }
259
260     RP[0] = in[0];
261     RP[1] = mH2;
262     RP[2] = cH2;
263     RP[3] = cFA;
264     RP[4] = pH2;
265
266     out[0] = 2*pH2/1e6;
267     out[1] = cFA;
268     out[2] = rH2;
269     out[3] = loadingState;
270     out[4] = T_bat - 273.15;
271     out[5] = hydrogenOutflowRate;
272
273 }
```

A.3 H2-to-FA Reactor

```
1  /*-----------------------------------------------------------------------
2    #Begin
3    #Block UBH2TFAREACTOR
4    #Description
5
6    #Layout
7       #Inputs      1
8       #Outputs     4
9       #Parameters  5
10      #Strings     0
11      #Group       S
12   #Details
13      #Inputs
14         #IN[0] Hydrogen Mass Flow
15      #Outputs
16         #OUT[0] Carbon Dioxide Demand
17      #Parameters
18         #BP[0] Reactor Length
19         #BP[1] Reactor Diameter
20         #BP[2] Operating Pressure
21         #BP[3] Reaction Rate Constant
22         #BP[4] Reaction Temperature
23      #Strings
24         #None
25   #Internals
26      #Integers
27         #IP[0]  Return code
28         #IP[1]  Call mode
29                 \begin{detaillist}
30                    \item[-1] Identification call
31                    \item[0]  Standard call
32                    \item[1]  Constructor call
33                    \item[2]  Destructor call
34                 \end{detaillist}
35         #IP[2]  Operation mode
```

```
36          #IP[3]  User defined block number
37          #IP[4]  Number of current block inputs
38          #IP[5]  Jump parameter
39          #IP[6]  Debug level
40          #IP[7..9]  Reserved
41       #Reals
42          #None
43       #Doubles
44          #None
45    #Dependencies
46       #None
47    #Authors
48       #Daniel Lust (HFT Stuttgart)
49    #End
50 ------------------------------------------------------------------------*/
51
52 // Attention: out must not be renamed to OUT (Windows.h conflict)
53
54 #include <math.h>
55 #include <algorithm>
56
57 extern "C" void id (float *in, float *out, int *IP, float *RP, double *DP,
58                     float *BP, char SP[][1024], char BNAMES[1024],
59                     int *OPM, int *INMIN, int *INS, int *OUTS,
60                     int *IPS, int *RPS, int *DPS,
61                     int *BPMIN, int *BPS, int *SPMIN,
62                     int *SPS, int *GROUP);
63
64 extern "C" void ub0030(float *in, float *out, int *IP, float *RP,
65    double *DP, float *BP, char SP[][1024])
66 {
67    char BNAMES[1024] = "UBH2TFAREACTOR";
68    int  OPM   = 1;
69    int  INMIN = 2;
70    int  INS   = 2;
71    int  OUTS  = 3;
72    int  IPS   = 10;
73    int  RPS   = 0;
74    int  DPS   = 0;
75    int  BPMIN = 5;
76    int  BPS   = 5;
77    int  SPMIN = 0;
78    int  SPS   = 0;
79    int  GROUP = 3;
80
81    if (IP[1] != 0)
82    {
83       if (IP[1] == -1)
84       {
85           // Identification call
86           id(in, out, IP, RP, DP, BP, SP, BNAMES,
87              &OPM, &INMIN, &INS, &OUTS, &IPS, &RPS, &DPS,
88              &BPMIN, &BPS, &SPMIN, &SPS, &GROUP);
89       }
90       else if(IP[1] == 1)
91       {
92          // Constructor call
93       }
94       else
95       {
96          // Destructor call
97       }
98       return;
99    }
100   // Standard call ------------------------------------------------
101   float M_FA= 46.03e-3;
102   float M_H2 = 2e-3;
103   float M_CO2 = 44.01e-3;
104
105   float RsH2 = 4124.2;
```

```
106     float RsCO2 = 188.92;
107
108     float R = 8.31;
109     float L = BP[0];
110     float d = BP[1];
111
112     int dt = 1; // time-step in seconds
113     int N = 100; // Numerical Parts
114
115     float mdotH2 = in[0];
116     float mdotCO2 = in[1];
117     float mdotIn = mdotH2 + mdotCO2;
118     float p1 = BP[2] * 1e6;
119
120     float pi = 3.14159265358979323;
121     float A = pi*pow(d,2)/4;
122
123     float k = BP[3];
124     float T = BP[4] + 273.15;
125
126     float pH2;
127     float pCO2;
128     float pFA;
129     float VdotH2;
130     float VdotCO2;
131     float Vdot;
132     float u;
133     float r;
134
135     float dx = L/N;
136
137     float mdot_CO2_out = 0;
138     float mdot_H2_out = 0;
139     float mdot_FA_out = 0;
140
141     float cFA = 0;
142
143     pH2 = 0.5*p1;
144     pCO2 = 0.5*p1;
145
146     VdotH2 = mdotH2 * RsH2 * T / pH2;
147     VdotCO2 = mdotCO2 * RsCO2 * T / pCO2;
148     Vdot = VdotH2 + VdotCO2;
149     u = Vdot/A;
150
151     float cH2 = pH2 / (R*T);
152     float cCO2 = pCO2 / (R*T);
153
154     for (int i = 0; i < N; i++)
155     {
156        if (pH2 <= 1e-10 || pCO2 <= 1e-10)
157        {
158           r = 0;
159        }
160
161        else
162        {
163           r = k*cH2*cCO2*1e-3;
164        }
165
166        cCO2 = cCO2 - r*dx/u;
167        cH2 = cH2 - r*dx/u;
168     }
169
170     pH2 = std::max((float)1e-10,cH2 * R * T);
171     pCO2 = std::max((float)1e-10,cCO2 * R * T);
172
173     mdot_H2_out = pH2 * VdotH2 / (RsH2 * T);
174     mdot_CO2_out = pCO2 * VdotCO2 / (RsCO2 * T);
175     float mOut = mdot_H2_out + mdot_CO2_out;
```

```
176     mdot_FA_out = mdotIn - mOut;
177
178     out[0] = mdot_H2_out;
179     out[1] = mdot_CO2_out;
180     out[2] = mdot_FA_out;
181
182
183     //RP[1] = cH2;
184     //RP[2] = cCO2;
185
186 }
```

A.4 FA-to-H2 Reactor

```
1  /*----------------------------------------------------------------------
2    #Begin
3    #Block UBFATH2REACTOR
4    #Description
5
6    #Layout
7       #Inputs      1
8       #Outputs     3
9       #Parameters  6
10      #Strings     0
11      #Group       S
12   #Details
13      #Inputs
14         #IN[0] Formic Acid Inflow [kg/s]
15      #Outputs
16         #OUT[0] Hydrogen Outflow [kg/s]
17         #OUT[1] Carbon Dioxide Outflow [kg/s]
18         #OUT[2] Formic Acid Outflow [kg/s]
19      #Parameters
20         #BP[0] Reactor Length [m]
21         #BP[1] Reactor Diameter [m]
22         #BP[2] Pressure [MPa]
23         #BP[3] Reaction Temperature [ C ]
24         #BP[4] Activation Energy [KJ/mol]
25         #BP[5] Frequency Factor [Hz]
26      #Strings
27         #None
28   #Internals
29      #Integers
30         #IP[0]  Return code
31         #IP[1]  Call mode
32                 \begin{detaillist}
33                    \item[-1] Identification call
34                    \item[0]  Standard call
35                    \item[1]  Constructor call
36                    \item[2]  Destructor call
37                 \end{detaillist}
38         #IP[2]  Operation mode
39         #IP[3]  User defined block number
40         #IP[4]  Number of current block inputs
41         #IP[5]  Jump parameter
42         #IP[6]  Debug level
43         #IP[7..9]  Reserved
44      #Reals
45         #None
46      #Doubles
47         #None
48   #Dependencies
49      #None
50   #Authors
51      INSEL Block Wizard
52   #End
```

```
53 ----------------------------------------------------------------------*/
54
55 // Attention: out must not be renamed to OUT (Windows.h conflict)
56
57 #include <math.h>
58 #include <algorithm>
59
60 extern "C" void id (float *in, float *out, int *IP, float *RP, double *DP,
61                     float *BP, char SP[][1024], char BNAMES[1024],
62                     int *OPM, int *INMIN, int *INS, int *OUTS,
63                     int *IPS, int *RPS, int *DPS,
64                     int *BPMIN, int *BPS, int *SPMIN,
65                     int *SPS, int *GROUP);
66
67 extern "C" void ub0104(float *in, float *out, int *IP, float *RP,
68    double *DP, float *BP, char SP[][1024])
69 {
70    char BNAMES[1024] = "UBFATH2REACTOR";
71    int  OPM   = 1;
72    int  INMIN = 1;
73    int  INS   = 1;
74    int  OUTS  = 3;
75    int  IPS   = 10;
76    int  RPS   = 0;
77    int  DPS   = 0;
78    int  BPMIN = 4;
79    int  BPS   = 4;
80    int  SPMIN = 0;
81    int  SPS   = 0;
82    int  GROUP = 3;
83
84    if (IP[1] != 0)
85    {
86       if (IP[1] == -1)
87       {
88           // Identification call
89           id(in, out, IP, RP, DP, BP, SP, BNAMES,
90              &OPM, &INMIN, &INS, &OUTS, &IPS, &RPS, &DPS,
91              &BPMIN, &BPS, &SPMIN, &SPS, &GROUP);
92       }
93       else if(IP[1] == 1)
94       {
95          // Constructor call
96       }
97       else
98       {
99          // Destructor call
100      }
101      return;
102   }
103   // Standard call ------------------------------------------------
104
105   float M_FA= 46.03e-3;
106   float M_H2 = 2e-3;
107   float M_CO2 = 44.01e-3;
108   float rho_FA = 1280;
109   float Tamb = 20 + 273.15;
110
111   float RsH2 = 4124.2;
112   float RsCO2 = 188.92;
113
114   float R = 8.31;
115   float V = BP[0];
116
117   float pi = 3.14159265358979323;
118
119   float T = in[0] + 273.15;
120   float r;
121   float phi_cat = BP[3];
122   float phi_FA = 1 - phi_cat;
```

```
123
124     if (T > Tamb)
125     {
126         r = BP[2]*phi_cat*(rho_FA*phi_FA)/M_FA*exp(-BP[1]*1e3/(R*T)); // mol/(s*m^2)
127     }
128
129     else
130     {
131         r = 0;
132     }
133
134
135     out[0] = r*V*M_H2;
136     out[1] = r*V*M_CO2;
137     out[2] = r*V*M_FA;
138 }
```